

AD-A078 861

SCIENCE APPLICATIONS INC IRVINE CA

F/6 20/4

HYPERSONIC INTERFERENCE FLOW FLIGHT EXPERIMENT DESIGN.(U)

JUN 79 L A CASSEL , T C DUNCAN , E H LAHTI

F33615-77-C-3043

UNCLASSIFIED

SAI-175-80R-008

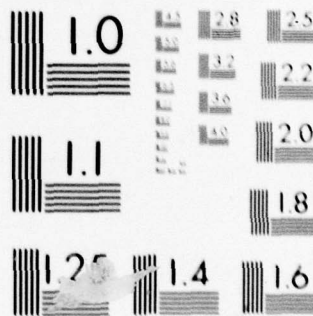
AFFDL-TR-79-3065

NL

1 OF 3

AD  
A078861





MICROCOPY RESOLUTION TEST CHART  
NATIONAL BUREAU OF STANDARDS-1963-A



AFFDL-TR-79-3065

LEVEL

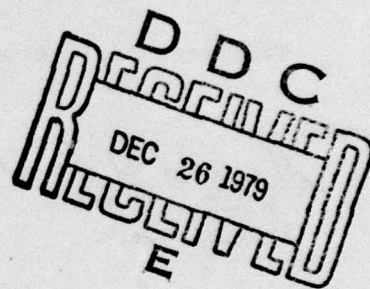
AD A078861

## **HYPERSONIC INTERFERENCE FLOW FLIGHT EXPERIMENT DESIGN**

L. A. CASSEL  
T. C. DUNCAN  
E. H. LAHTI

SCIENCE APPLICATIONS, INC.  
17900 SKYPARK CIRCLE  
SUITE 201  
IRVINE, CALIFORNIA 92714

JUNE 1979



TECHNICAL REPORT AFFDL-TR-79-3065  
Technical Final for the period June 1977 to April 1979

Approved for public release; distribution unlimited.

AIR FORCE FLIGHT DYNAMICS LABORATORY  
AIR FORCE WRIGHT AERONAUTICAL LABORATORIES  
AIR FORCE SYSTEMS COMMAND  
WRIGHT-PATTERSON AIR FORCE BASE, OHIO 45433

79 12 17 159

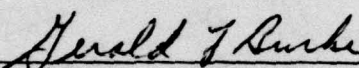
DDC FILE COPY

NOTICE


When Government drawings, specifications, or other data are used for any purpose other than in connection with a definitely related Government procurement operation, the United States Government thereby incurs no responsibility nor any obligation whatsoever; and the fact that the government may have formulated, furnished, or in any way supplied the said drawings, specifications, or other data, is not to be regarded by implication or otherwise as in any manner licensing the holder or any other person or corporation, or conveying any rights or permission to manufacture, use, or sell any patented invention that may in any way be related thereto.

This report has been reviewed by the Information Office (OI) and is releasable to the National Technical Information Service (NTIS). At NTIS, it will be available to the general public, including foreign nations.

This technical report has been reviewed and is approved for publication.

  
GERALD L. BURKE  
Program Monitor

FOR THE COMMANDER

  
PETER J. BUTKEWICZ, Col, USAF  
Chief, Aeromechanics Division

If your address has changed, if you wish to be removed from our mailing list, or if the addressee is no longer employed by your organization please notify AFFDL/FXC, W-PAFB, OH 45433 to help us maintain a current mailing list.

Copies of this report should not be returned unless return is required by security considerations, contractual obligations, or notice on a specific document.



UNCLASSIFIED

SECURITY CLASSIFICATION OF THIS PAGE (When Data Entered)

19 REPORT DOCUMENTATION PAGE		READ INSTRUCTIONS BEFORE COMPLETING FORM								
1. REPORT NUMBER AFFDL-TR-79-3065	2. GOVT ACCESSION NO.	3. RECIPIENT'S CATALOG NUMBER								
4. TITLE (and Subtitle) HYPERSONIC INTERFERENCE FLOW FLIGHT EXPERIMENT DESIGN	5. TYPE OF REPORT & PERIOD COVERED Technical Final Rept. 15 June - 15 April 1979	6. PERFORMING ORG. REPORT NUMBER SAI-175-80R-008								
7. AUTHOR(s) L.A. Cassel, T.C. Duncan, E.H. Lahti	8. CONTRACT OR GRANT NUMBER(s) F33615-77-C-3043									
9. PERFORMING ORGANIZATION NAME AND ADDRESS Science Applications, Inc. 17900 Skypark Circle, Suite 201 Irvine, CA 92714	10. PROGRAM ELEMENT, PROJECT, TASK AREA & WORK UNIT NUMBERS 62201F 2404-07-12									
11. CONTROLLING OFFICE NAME AND ADDRESS Air Force Flight Dynamics Laboratory (FXG) Wright-Patterson A.F.B., OH 45433	12. REPORT DATE June 1979									
14. MONITORING AGENCY NAME & ADDRESS (if different from Controlling Office)	13. NUMBER OF PAGES 209									
	15. SECURITY CLASS. (of this report) UNCLASSIFIED									
	15a. DECLASSIFICATION/DOWNGRADING SCHEDULE									
16. DISTRIBUTION STATEMENT (of this Report) Approved for public release; distribution unlimited.										
17. DISTRIBUTION STATEMENT (of the abstract entered in Block 20, if different from Report)										
18. SUPPLEMENTARY NOTES										
19. KEY WORDS (Continue on reverse side if necessary and identify by block number) <table border="0"> <tr> <td>Aerothermodynamics</td> <td>Flight Testing</td> </tr> <tr> <td>Interference Heating</td> <td>Hypersonic Flow</td> </tr> <tr> <td>Shock Interaction</td> <td>Interference Flow</td> </tr> <tr> <td>Heat Transfer</td> <td>Aerodynamics Testing</td> </tr> </table>			Aerothermodynamics	Flight Testing	Interference Heating	Hypersonic Flow	Shock Interaction	Interference Flow	Heat Transfer	Aerodynamics Testing
Aerothermodynamics	Flight Testing									
Interference Heating	Hypersonic Flow									
Shock Interaction	Interference Flow									
Heat Transfer	Aerodynamics Testing									
20. ABSTRACT (Continue on reverse side if necessary and identify by block number) <p>An experiment has been defined to measure the aeroheating and loads resulting from three dimensional shock wave/boundary layer interference in hypersonic flight. This report describes the definition of this flight experiment, including the instrumentation and electronics required to measure the interference heating and loads and transmit those measurements by telemetry to ground stations. The measurements include quasi-steady heat transfer rates and pressures as well as fluctuating pressures. Additional measurements are</p>										

DD FORM 1 JAN 73 1473

EDITION OF 1 NOV 65 IS OBSOLETE

UNCLASSIFIED  
SECURITY CLASSIFICATION OF THIS PAGE (When Data Entered)

391694

20. Specified for specific definition of the experiment environment. The experiment is configured to investigate the interference flow at the base of a stabilizer on a missile launched from an F-4 aircraft. The missile is to be propelled to hypersonic speed by a solid propellant motor and the measurements are to be made at altitudes between 50 KFT and ground impact. The mechanical, structural, and thermal protection system specifications for the experiment carrier missile are provided in this report. Missile design and fabrication drawings are available under separate cover from the sponsoring agency. The missile is configured within the aircraft compatibility envelope established for a previously conducted flight experiment, called the Fighter Launched Advanced Materials Experiment (FLAME) program, sponsored by the Defense Nuclear Agency.



## PREFACE

This report was prepared by the Flight Technology Division of the Science Applications, Inc. Systems Group, Irvine, California, for the High Speed Aerodynamics Performance Branch of the Aeromechanics Division, Air Force Flight Dynamics Laboratory. SAI conducted this work under contract F33615-77-C-3043.

The Interference Flight Experiment (IFLEX) technical direction was provided by G. L. Burke and R. D. Neumann (AFFDL/FXG).

Significant contributions to the IFLEX definition and vehicle design were made by a number of SAI engineers. L. A. Cassel was the program manager; T. C. Duncan designed the thermal protection system and led the vehicle design analysis effort; E. H. Lahti defined the electronics and telemetry system requirements. Dr. J. E. Craig provided the aeroheating experiment instrumentation requirements and data analyses definition; R. H. Grimes led the mechanical design effort; C. W. Griffing provided the flight operations definition; and S. Taylor provided the trajectory simulations.

Science Applications, Inc. would like to acknowledge the cooperation extended by Aerojet Services Company (AJSC) (formerly Aerojet Liquid Rocket Company) during the IFLEX design program. Information provided by AJSC concerning the FLAME launch vehicle design and flight operations has contributed to both the confidence and efficiency with which the IFLEX design program could be carried out.

Accession For	
NTIS GINA	<input checked="checked" type="checkbox"/>
DDC TAB	<input type="checkbox"/>
Unannounced	<input type="checkbox"/>
Justification	
By _____	
Distribution/	
Availability Codes	
Dist.	Avail and/or special
A	

# TABLE OF CONTENTS

Section	Page
I INTRODUCTION.....	1
II SUMMARY.....	7
III IFLEX LAUNCH AND FLIGHT TRAJECTORIES.....	14
3.1 Aircraft Interface and Launch.....	16
3.2 Aerodynamics.....	22
3.3 IFLEX Trajectory.....	39
3.4 Flight Operations Requirements.....	45
3.5 Flight Range Requirements.....	52
IV INTERFERENCE FLOW EXPERIMENT DEFINITION.....	57
4.1 Interference Flow Measurements.....	64
4.2 Data Interpretation.....	69
4.3 Data Analysis.....	74
4.4 Distribution of Instrumentation.....	80
4.5 Reference Conditions Data Reduction.....	87
4.6 Interference Flow Data Interpretation.....	92
V INSTRUMENTATION, TELEMETRY AND ELECTRONICS.....	96
5.1 Pressure Measurements.....	96
5.2 Heat Transfer/Temperature Measurements.....	110
5.3 Other Measurement and Indicators.....	123
5.4 Data Acquisition System.....	125
5.5 Radar Transponder (C-Band).....	137
5.6 Telemetry and Transponder Antennas.....	139
5.7 Rocket Motor Ignition and Fin Deployment.....	140
5.8 Electrical Power.....	149
VI VEHICLE DESIGN.....	153
6.1 TPS Material Evaluation.....	156
6.2 Forward Conical Section Design.....	172
6.3 Forward Cylindrical Section Design.....	176
6.4 Flare Section Design.....	176
6.5 Conical Frustum Section Design.....	179
6.6 Aft Cylindrical Section Design.....	179
6.7 Fin Design.....	190
6.8 Electronics Components Thermal Protection.....	195
6.9 Mass Properties.....	198
VII PROGRAM PLANNING AND COSTS.....	201
7.1 Program Plan.....	201
7.2 IFLEX Program Schedule.....	204
7.3 IFLEX Program Costs.....	204
REFERENCES.....	207
APPENDIX A.....	A-1
APPENDIX B.....	B-1



## LIST OF ILLUSTRATIONS

<u>Figure</u>	<u>Page</u>
1. FLAME Vehicle Launch Configuration.....	3
2. Oil-Flow Visualization of IFLEX Shock-Boundary Layer Interaction.....	5
3. FLAME/IFLEX Comparison.....	8
4. Typical IFLEX Trajectory.....	9
5. IFLEX Installation On F-4.....	15
6. IFLEX Wind Tunnel Model Geometry.....	23
7. Fin Configuration Influence on Static Stability.....	25
8. Example of Stability Boundaries for X Configuration...	26
9. IFLEX Normal Force Coefficient Data.....	28
10. IFLEX Pitching Moment Coefficient Data.....	29
11. IFLEX Axial Force Coefficient Data.....	30
12. Variation in Normal Force With Mach Number.....	31
13. Components of Zero Alpha Axial Force.....	32
14. IFLEX Pressure Distribution.....	34
15. Prediction Methods for Body Alone Axial Force.....	35
16. Drag Predictions for IFLEX Trajectory Simulations.....	37
17. IFLEX Trajectory Simulation Propulsion Parameters.....	38
18. Launch Angle-Altitude Bounds at Aircraft Separation...	41
19. IFLEX Trajectory A Velocity History.....	42
20. IFLEX Trajectory A Flight Path Angle History.....	43
21. IFLEX Trajectory A Reynolds Number History.....	44
22. Aircraft/IFLEX Post Launch Separation.....	50
23. Estimated IFLEX Footprint.....	54
24. IFLEX Instrumentation Distribution.....	58
25. IFLEX Simulation Compared to Ground Test.....	60
26. Time Variation in Mach Number and Pitch Frequency....	65
27. Time Variation in Wall Temperature and Heating.....	66
28. Time Variation in Pitot and Ambient Pressure.....	67
29. Nominal Interference Flow Pressure Levels.....	70
30. Fin Pressure Levels.....	72

# LIST OF ILLUSTRATIONS (Continued)

<u>Figure</u>	<u>Page</u>
31. Cone Pressure Levels.....	72
32. Fluctuating Pressure in Interference Flows.....	75
33. Heating Rates to be Measured.....	76
34. Surface Temperatures on Aft Cylinder.....	78
35. Surface Temperatures on Fin.....	79
36. Fin Shock and Peak Heating Locus Angles.....	81
37. Distribution of Interference Heating Instrumentation..	83
38. Predicted Heat Transfer and Pressure Augmentation Profiles.....	85
39. Fin Surface Instrumentation Locations.....	86
40. Reference Conditions Measurement Locations.....	88
41. Rosemount Inc. Capacitive Pressure Transducer (Model 1332A).....	100
42. Kulite Diffused Semiconductor Strain Gage.....	103
43. Kulite 36 Transducer Housing.....	104
44. Typical Piezoelectric Pressure Transducer.....	106
45. Typical Diffused Semiconductor Strain Gage.....	107
46. Fluctuating Pressure Transducer Mounting.....	109
47. Selected Heat Transfer Gage.....	113
48. Wiring Diagram of the Chromel-Constantan Calorimeter.....	116
49. Cylinder Plate Instrumentation Schematic.....	117
50. Wall Temperature Thermocouple.....	121
51. Accelerometer Axes.....	124
52. Accelerometer Dimensions.....	129
53. Basic Elements of a PCM System.....	131
54. Aydin Vector MMP-600 PCM System Illustration.....	133
55. Fluctuating Pressure Data Flow Chart.....	134
56. Aydin Vector Frequency Division Multiplexor and Mixer Amplifier.....	135
57. L-Band Transmitter.....	138
58. C-Band Radar Transponder.....	141
59. Quadraloop Radiator.....	142
60. Quadraloop Antenna Assembly.....	144



# LIST OF ILLUSTRATIONS (Continued)

<u>Figure</u>	<u>Page</u>
61. Rocket Ignition Circuit.....	144
62. Fin Deployment Timer Circuit.....	145
63. Mechanical Interval Timer.....	146
64. Command Receiver.....	147
65. UHF Antenna.....	148
66. Battery Schematic.....	150
67. Instrumentation Battery Voltage Vs. Time.....	151
68. IFLEX Design Trajectory No. 1.....	158
69. IFLEX Design Trajectory No. 2.....	159
70. IFLEX Design Trajectory No. 3.....	160
71. IFLEX Design Trajectory No. 4.....	161
72. IFLEX Design Heating Environment, Trajectory 1.....	164
73. Aerodynamic Shear, Effects on $Q_{CW}^*$ , Dyna-Therm DE-350...	164
74. Cold Wall Heat Flux to the Frustum.....	168
75. Frustum Insulation Surface Temperature.....	169
76. Forward Cylinder Insulation Surface Temperature.....	169
77. Forward Cone Design.....	173
78. Forward Cone Surface Temperature Response, Trajectory 1.....	174
79. Forward Cone Wall Temperature Gradient, Trajectory 1.....	174
80. Forward Cone Thermal Stress and Strain.....	175
81. Forward Cylinder Design.....	177
82. Six Degree Flare Design.....	178
83. Conical Frustum Design.....	180
84. Aft Cylinder Design.....	181
85. Aft Cylinder and Fins (Folder).....	183
86. Fin Rotation Mechanism.....	184
87. Fuselage Steel Plate Maximum Temperature Gradient in Undisturbed Flow.....	186
88. Fuselage Steel Plate Maximum Temperature Gradient in Interaction Region.....	186

LIST OF ILLUSTRATIONS (Continued)

<u>Figure</u>	<u>Page</u>
89. Fuselage Steel Plate Maximum Surface Temperature Trajectory 1.....	187
90. Schematic of Steel Plate Thermal Expansion.....	189
91. Thermal Response of Magnesium Skin Insulated from Aft Test Panel.....	191
92. Instrumented Fin Design.....	193
93. Leading Edge Model for Thermal Analysis.....	194
94. Leading Edge Temperature Profile.....	194
95. Leading Edge Stagnation Point Temperature.....	194
96. Fin Plate Maximum Temperature Gradients, Trajectory 1.....	196
97. Fin Plate Surface Temperature.....	196
98. Thickness and Material Influence on Fin Plate Normal Deflection Due to Heating.....	197
99. IFLEX Program Schedule.....	205

# LIST OF TABLES

<u>Table</u>		<u>Page</u>
1	Telemetry Channel Assignments.....	97
2	Comparison of Piezoelectric and DSSG Transducers.....	105
3	Features of the Aydin Vector MMP-600 PCM System.....	130
4	Requirements and Selection of the Frequency Division Multiplex System.....	136
5	Telemetry Transmitter Requirements and Selection.....	137
6	Properties of Dyna-Therm DE-350 and DE-370.....	162
7	Ablation Data for DE-350.....	165
8	TPS Coating Thickness Requirements.....	167
9	Ablation Rate Comparison - Ablation on Frustum.....	170
10	Steel Material Properties.....	171
11	Electrical Component Thermal Requirements.....	199
12	IFLEX Vehicle Mass Properties Summary.....	200
13	IFLEX Program Task Breakdown.....	202
14	IFLEX Program Cost Estimates.....	206



# LIST OF SYMBOLS

$C_A$	Axial force coefficient with base pressure corrected to freestream level
$C_{A_B}$	Axial force coefficient increment due to base pressure drag
$C_{A_t}$	Measured axial force coefficient
$C_D$	Drag coefficient
$c_f$	Skin friction coefficient
$C_M$	Pitching moment coefficient
$C_N$	Normal force coefficient
$C_{N_\alpha}$	Normal force coefficient slope
$C_{Y_\beta}$	Yaw force coefficient slope
$c$	Specific heat
$c_p$	Specific heat at constant pressure
$C_p$	Pressure coefficient
$D$	Diameter
$F$	Frequency
$f_p$	Pitch/yaw frequency
$H$	Enthalpy
$I_{s_p}$	Specific impulse
$k$	Thermal conductivity
$L$	Length
$M$	Mach number
$\dot{m}_a$	Ablation mass removal rate
$\dot{m}_p$	Propellant flow rate
$p$	Pressure

# LIST OF SYMBOLS (Continued)

P1...P9	Pressure taps
$q_{\infty}$	Dynamic pressure
$\dot{q}$	Heat transfer rate
$Q_{cw}^*$	Cold wall heat of ablation
$r$	Radius
$r$	Recovery factor
$R$	Calorimeter foil radius
$Re$	Reynolds number
$S$	Reference area
$s$	Calorimeter foil thickness; surface distance from panel edge (see Figure 38).
$St$	Stanton number
$t$	Time
$T$	Temperature
$T_r$	Recovery temperature
$V$	Velocity
$\bar{V}$	Velocity vector
$w$	Weight
$x$	Vehicle axial coordinate
$X$	Distance
$X_{cg}$	Center of gravity location
$X_{cp}$	Center of pressure location
$y$	Pitch plane coordinate
$z$	Yaw plane coordinate
$\alpha$	Thermal diffusivity
$\alpha$	Angle of attack
$\alpha_0$	Zero angle of attack inclination angle

# LIST OF SYMBOLS (Continued)

$\beta$	Yaw angle
$\gamma$	Ratio of specific heats
$\gamma_L$	Launch angle
$\delta$	Boundary layer thickness
$\epsilon$	Strain
$\eta$	Acceleration factor
$\theta$	Angle
$\lambda_H$	Ray angle defining peak heating region
$\mu$	Dynamic viscosity
$\rho$	Density
$\sigma$	Stress
$\tau_w$	Skin friction
$\tau$	Time constant

## SUBSCRIPTS and SUPERSSCRIPTS

B	Conditions at base
cw	Cold wall
F	Fin
I	Interaction region
X	Length
L	Launch
O	Upstream of flow interference
R	Reference
RMS	Root mean square
S	Shock



# LIST OF SYMBOLS (Continued)

$t$	Stagnation conditions
$w$	Conditions at wall
$\infty$	Freestream conditions
$1, 2, \dots$	Location identifiers for pressure taps

## SECTION I

### INTRODUCTION

A serious aero/thermodynamic design problem facing hypersonic atmospheric flight vehicle designers involves shock wave interactions with boundary layers. These complex flows appear at all flow compression junctions resulting from the flight vehicle external geometry. Typically, these junctions include interfaces between fin and fuselage; wing and fuselage; inlets or pylons, and wings or fuselages; or anywhere a shock from one leading edge intersects a transverse surface. A survey of flows of this class is provided by Korkegi in Reference 1. They are characterized by large local gradients in surface heating and pressures. Both quasi-steady and fluctuating local pressure load amplifications are caused. These result in critical Thermal Protection System (TPS) design points, high localized and buffeting loads, and variations in aerodynamic moments.

The principal concern over shock wave boundary layer interactions, particularly in three-dimensional flows involving turbulent boundary layers, is uncertainties in predictive methodology for design analysis. Computational analysis methods for this class of flows are limited in applicability and extremely expensive in manpower, time, and computing resources when they can be applied. A typical application is described in Reference 2. Some aspects of wind tunnel simulations are possible for small scale vehicles or for high altitude flight. Even these aspects are impossible in application to low altitude hypersonic flight or to large scale hypersonic flight vehicles. The inadequately simulated phenomena are fundamentally related to turbulent viscous flow characteristics. Existing ground test facilities limitations are principally associated with Reynolds number



simulation capability. Simulation of boundary layers on hypersonic atmospheric flight vehicles involving large aircraft scale dimensions or low altitude flight is beyond these limitations.

The Air Force Flight Dynamics Laboratory (AFFDL) has pursued the definition of three-dimensional shock wave/boundary layer interaction phenomena in ground test simulation in a continuing program for several years. Typical results are described in Reference 3. Ground testing and analyses to date have resulted in a number of correlation schemes for predicting the results of shock wave/boundary layer interactions in vehicle design application, such as those in Reference 3. The accuracy of these correlations for flight Reynolds number flows requires substantiation.

Under AFFDL sponsorship, Science Applications, Inc. (SAI) has designed an experiment for measuring the vehicle surface heat transfer and pressure response to three-dimensional, hypersonic shock wave/boundary layer interactions in low altitude flight. A secondary objective of the experiment is to demonstrate the precision with which this type of aero/thermodynamic experiment can be accomplished in a flight environment. The experiment is called the Interference Flow Flight Experiment (IFLEX). It has been designed, according to AFFDL requirements, to use a previously flown basic test vehicle configuration. This vehicle was designed by Aerojet Liquid Rocket Company (AJLRC) under Defense Nuclear Agency sponsorship on the Fighter Launched Advanced Materials Experiment (FLAME) Program. The planned IFLEX program will employ the first stage configuration of the FLAME launch vehicle. The vehicle will be carried to altitude and launched by an F-4 aircraft, in the same manner as the original FLAME test vehicles. This configuration is illustrated, in the carry position on the F-4J employed in the FLAME program, in Figure 1.

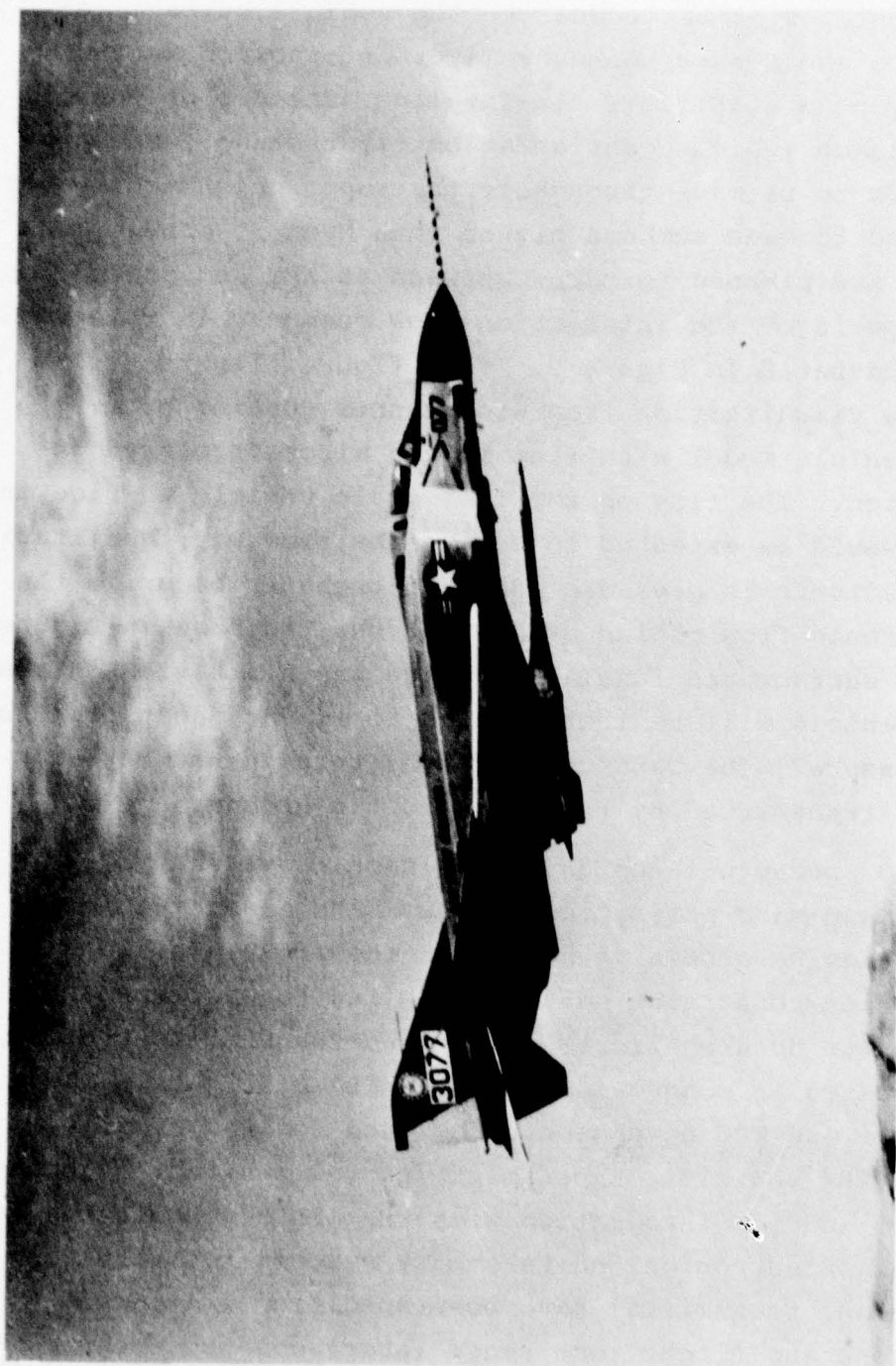


FIGURE 1. FLAME Vehicle Launch Configuration

Following AFFDL specifications, SAI has designed the experiment for IFLEX to measure the vehicle surface response to shock wave/boundary layer interaction in the vicinity of a stabilizer fin-fuselage juncture on the FLAME launch vehicle configuration first stage. Measurements are to be made throughout the supersonic Mach number range and to Mach numbers higher than Mach 5. These Mach numbers are planned to occur between 45 KFT and ground impact. Some aspects of the interaction flow geometry in this region are illustrated in Figure 2. This figure illustrates an oil-flow visualization from wind tunnel testing of an IFLEX vehicle model with fins in the aircraft carry configuration. The flow on the full scale vehicle surface in flight would be expected to behave the same way, qualitatively. High gradients in pressure and heat transfer occur in the interference flow region evident at the fin base in Figure 2. The fin surface and fuselage surface in this region on the IFLEX vehicle will be instrumented to measure heat transfer and pressure. The data collected by this instrumentation will be transmitted by telemetry to the ground.

The conceptual design, propulsion, aerodynamic configuration and mass properties of the FLAME launch vehicle first stage have been retained for the IFLEX vehicle. This significant constraint has been applied to minimize efforts required to assure aircraft carry and launch compatibility demonstrated in connection with the FLAME flights. The structure and TPS have been redesigned for the single stage IFLEX vehicle. Experiment instrumentation has been selected and its integration with the IFLEX vehicle has been defined. Electronics and telemetry systems for data collection and transmittal have been specified. Aircraft operations and flight test range interfaces have been explored to assure IFLEX vehicle design compatibility.



IFLEX INTERFERENCE FLOW  
VISUALIZATION



IFLEX WIND TUNNEL MODEL GEOMETRY

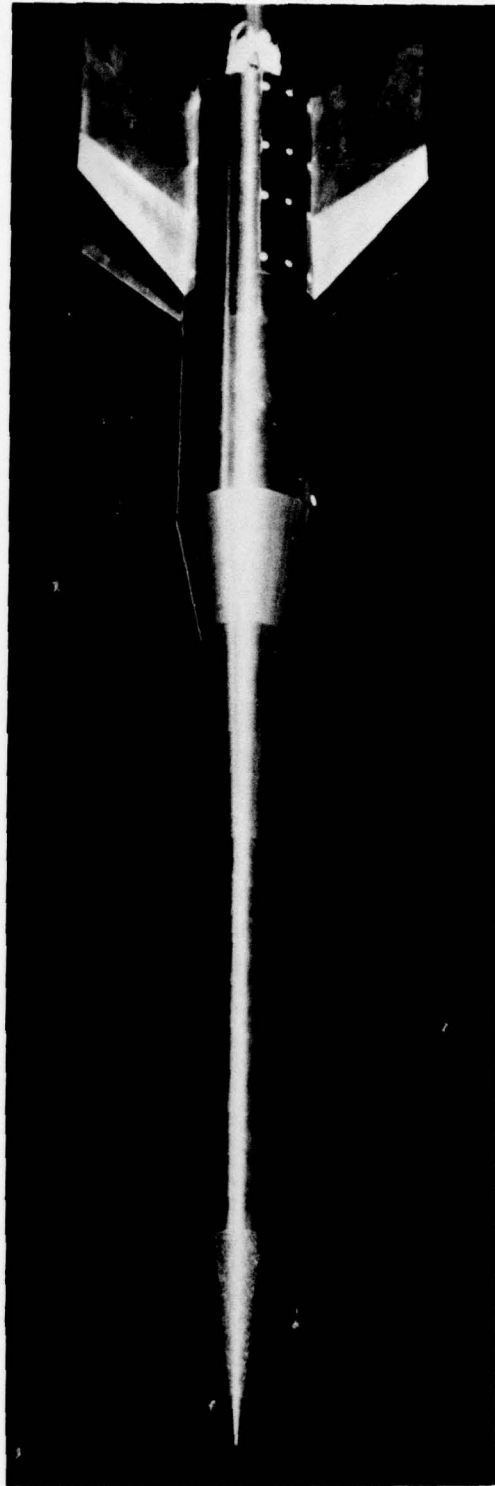


FIGURE 2. Oil-Flow Visualization of IFLEX Shock Wave/Boundary Layer Interaction

The definition and design of the IFLEX program, experiment and vehicle are described in this report. Design drawings and specifications for the vehicle mechanical and electrical systems are listed in Appendix I. They are available from the sponsoring agency.

## SECTION II

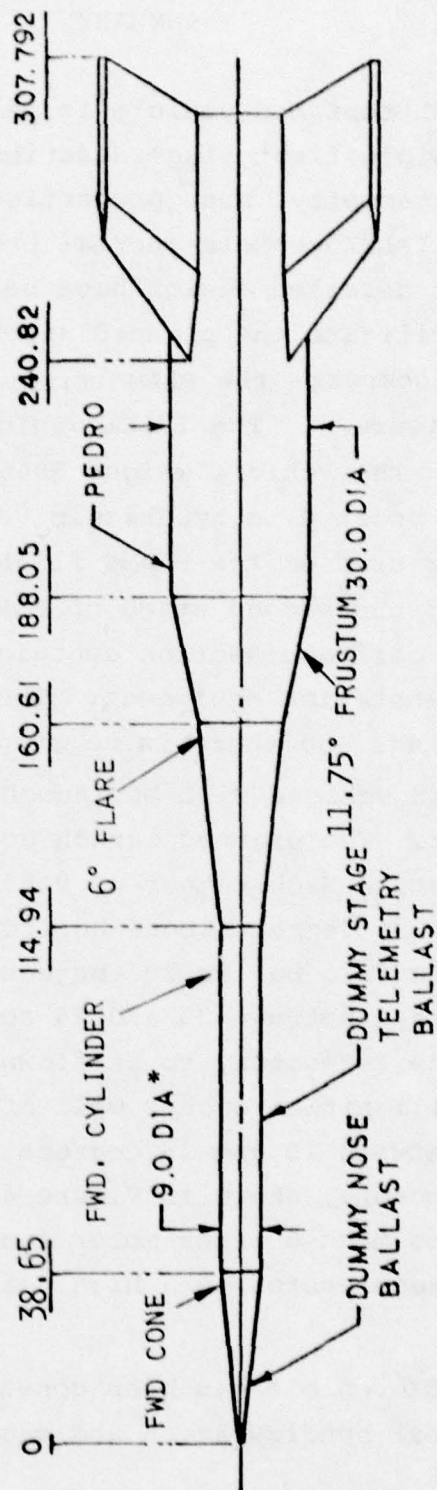
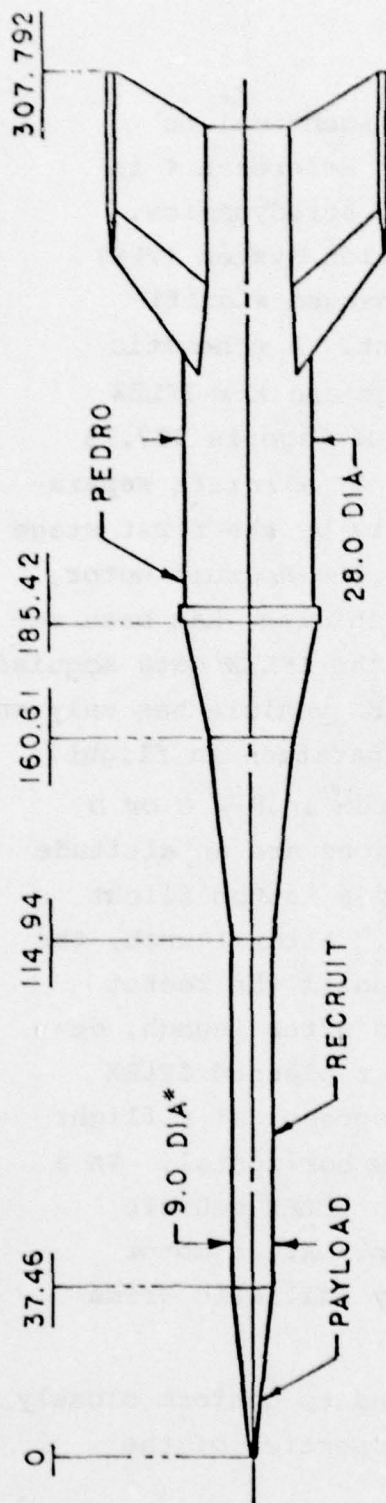
### SUMMARY

The IFLEX test bed vehicle is nearly identical to the FLAME vehicle first stage described in Reference 4 in terms of its geometry, mass properties and aerodynamics. However, the IFLEX vehicle Thermal Protection System (TPS) and component detailed design have been changed significantly to facilitate the planned experiment. A schematic illustration compares the FLAME first stage and the IFLEX vehicle in Figure 3. The IFLEX vehicle fuselage is 297.13 inches long. The vehicle weighs 3966 lbs at aircraft separation. It is boosted to hypersonic velocity by the first stage (Pedro) motor used on the FLAME flights. The Recruit motor, which powered the second stage of FLAME vehicles, has been replaced by an airframe section containing the IFLEX data acquisition and telemetering equipment. The IFLEX vehicle has only one propulsion stage and there is no stage separation in flight.

The IFLEX vehicle will be launched from an F-4 C or D type aircraft. The planned launch conditions are an altitude of 45,000 feet, a Mach number of 0.95, and a launch flight path angle of 30 degrees above horizontal. After launch, the vehicle coasts in a ballistic trajectory until the rocket motor is ignited between 20 and 26 seconds after launch, depending on the trajectory to be flown. For planned IFLEX trajectories, ignition occurs well after apogee, at a flight path angle between 25 and 35 degrees below horizontal. In a typical trajectory, shown in Figure 4, the IFLEX vehicle accelerates to Mach 6 after motor ignition. After motor burnout, it decelerates in a high velocity ballistic glide to impact.

The IFLEX vehicle has been constrained to conform closely to the external configuration and mass properties of the





\* DIAMETERS DO NOT INCLUDE TPS.

FIGURE 3. FLAME/IFLEX Comparison

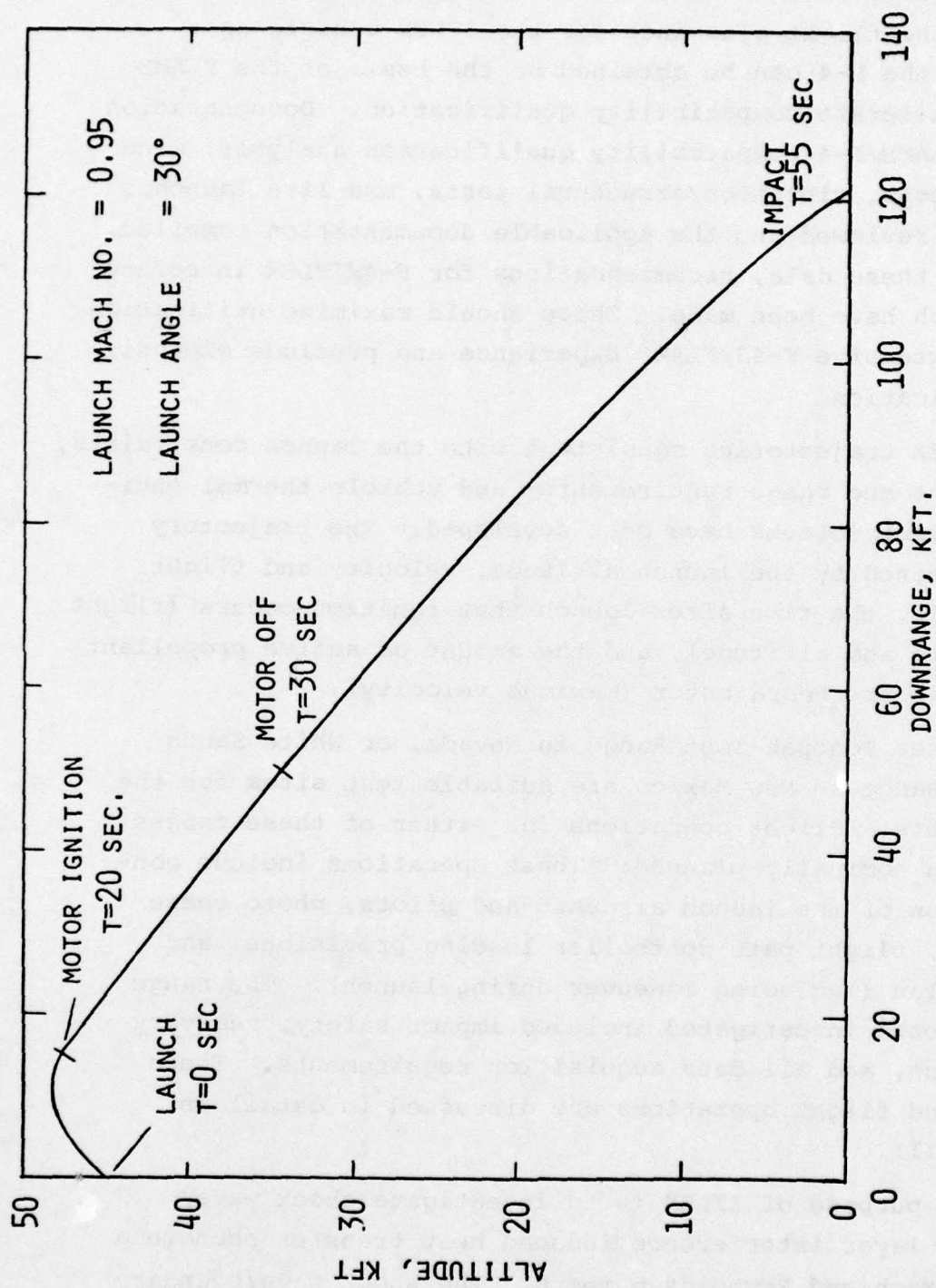


FIGURE 4. Typical IFLEX Trajectory



FLAME vehicle which was flight compatibility qualified and launched from an F-4J aircraft. This constraint was imposed so that the flight clearance for the IFLEX vehicle as a store on the F-4 can be obtained on the basis of the FLAME vehicle aircraft compatibility qualification. Documentation of the FLAME/F-4 compatibility qualification analysis, wind tunnel tests, vibration/structural tests, and live launches has been reviewed and the applicable documentation compiled. Based on these data, recommendations for F-4/IFLEX interface and launch have been made. These should maximize utilization of the extensive F-4J/FLAME experience and preclude expensive regualification.

IFLEX trajectories consistent with the launch constraints, experiment and range requirements, and vehicle thermal environment restrictions have been developed. The trajectory is determined by the launch altitude, velocity and flight path angle, the time after launch that ignition occurs (flight path angle and altitude), and the amount of active propellant loading in the Pedro motor (maximum velocity).

Either Tonopah Test Range in Nevada, or White Sands Missile Range in New Mexico are suitable test sites for the IFLEX tests. Flight operations for either of these ranges have been nominally planned. These operations include consideration of the launch aircraft and pilots, photo chase aircraft, flight path controller loading provisions, and flight plan (including maneuver during launch). The range requirements investigated included impact safety, recovery operations, and all data acquisition requirements. These launch and flight operations are discussed in detail in Section III.

The purpose of IFLEX is to investigate shock wave/boundary layer interference induced heat transfer phenomena at high Mach and Reynolds numbers. The shock wave/boundary

layer interaction experiment will be performed where the fin generated shock wave impinges on the boundary layer on the aft cylinder. The flight environment and scale of IFLEX will provide a Reynolds number more than an order of magnitude larger than that which can be obtained in ground test simulations.

The vehicle will be instrumented to characterize the following:

- 1) Heat transfer in the interference flow area by measuring the quasi-steady wall temperature, heat transfer, and pressure. Fluctuating pressures will also be measured.
- 2) State of the upstream boundary layer by measurements of heat transfer, wall temperature, static pressures, and fluctuating pressures.
- 3) Vehicle flight conditions by continuously measuring the angle of attack, Mach number, and freestream static pressure. This is supported by ground based tracking of the vehicle trajectory, and atmospheric soundings.

The desired flight trajectories have been selected and the test areas of the vehicle have been designed to provide the proper test environment. All necessary instrumentation has been selected and its placement and operation designed into the vehicle. Methodology for reduction of the data and comparison of it with ground test data have been developed. The measurements to be made and the experiment definition are described in Section IV. The instrumentation and electronics required are described in Section V.

Measurements made by instrumentation during the experiment and missile operation will be digitally encoded and telemetered to ground based receivers. Continuously sampled quasi-steady state measurements will include wall heat transfer, skin temperature, pressure, three-axis acceleration,



and missile operation indicators. High frequency data to be processed are limited to fluctuating pressure measurements. All of the quasi-steady state measurements will be time-division multiplexed and then digitally encoded with an eight-bit PCM system. The unsteady measurements will be frequency division multiplexed and transmitted on the L-Band simultaneously with the PCM serial-data stream. In addition to the instrumentation and data processing electronics, a C-Band transponder to aid in radar tracking and a UHF command receiver to initiate the rocket ignition are integrated into the IFLEX vehicle. All instrumentation and electronic equipment have been designed or specified as described in Section V.

The external configuration, stiffness and mass properties of the IFLEX vehicle are nearly identical to those of the FLAME vehicle. However, the detailed design has been changed significantly in order to perform the desired experiments. The basic changes are as follows:

- 1) The FLAME FIREX low temperature ablator TPS has been replaced with a DYNATHERM high temperature insulator with steel inserts in the instrumented regions. The IFLEX objectives require that the amount of ablation products and surface roughness be minimized. The presence of either roughness or ablation products could contaminate the interference flow simulation or instrumentation response.
- 2) The forward cone will be utilized to measure pitot and surface pressures in order to accurately determine the angle of attack and Mach number. This cone has been changed to stainless steel to insure a non-receding surface for these measurements.
- 3) The Recruit motor has been removed and a structurally similar section has been designed to replace it. This

section also houses most of the data processing equipment and the telemetering equipment.

- 4) A thirty-inch diameter insulated magnesium cylinder has been placed around the Pedro motor to provide instrumentation volume and facilitate the experiment. About one-sixth of the circumference of this cylinder is steel, in the regions where the measurements are to be made. The fin support and rotation mechanisms have been redesigned to accommodate this larger diameter.
- 5) One of the fins has been modified to contain an instrumented steel plate for the experiment. Also, stainless steel caps have been placed on the fin leading edges to prevent shape change that could affect the experiment.

Detailed drawings of all modified parts of the IFLEX vehicle, more than 90 percent of the original FLAME vehicle, have been made. Thermal and structural analyses have been accomplished as required to facilitate vehicle redesign to accommodate IFLEX objectives or the flight environment. The results of these analyses are presented in Section VI.

## SECTION III

### IFLEX LAUNCH AND FLIGHT TRAJECTORIES

Two guidelines have been followed in the design of IFLEX which will simplify the experiment and minimize costs. First, the vehicle has been constrained to conform closely to the external configuration and mass properties of the FLAME vehicle which was aircraft compatibility qualified and launched from an F-4J aircraft during 1975. Second, launch aircraft flight operations have been constrained to remain below an altitude of fifty-thousand feet, thus precluding the necessity for full-pressure suit capabilities.

Investigations of test ranges indicates that either the Tonapah Test Range, Nevada, with aircraft operations from Edwards Air Force Base; or White Sands Missile Range, New Mexico, with aircraft operations from Holloman Air Force Base, would be suitable for IFLEX testing. Final determination of the test site is a function under the cognizance of the 3246<sup>th</sup> Test Wing at Eglin Air Force Base, Florida.

#### 3.1 Aircraft Interface and Launch

The Defense Nuclear Agency sponsored programs conducted during 1974 and 1975 to qualify the F-4J for carrying and launching FLAME have been reviewed for applicability to IFLEX. A summary of these programs is outlined below, together with a listing of applicable documentation. This summary is intended to serve as the primary basis for Air Force Armament Test Lab, Eglin A.F.B. (AFATL/DLJC) issuance of flight clearance under AFSCR 80-33 (Class II Modifications).

##### 3.1.1 Aircraft Installation

The basic configuration for carrying IFLEX on F-4C/D aircraft, as shown in Figure 5, is identical to that utilized by FLAME, which was carried and launched from an F-4J. The missile is mounted on a modified LAU-77 launcher which is



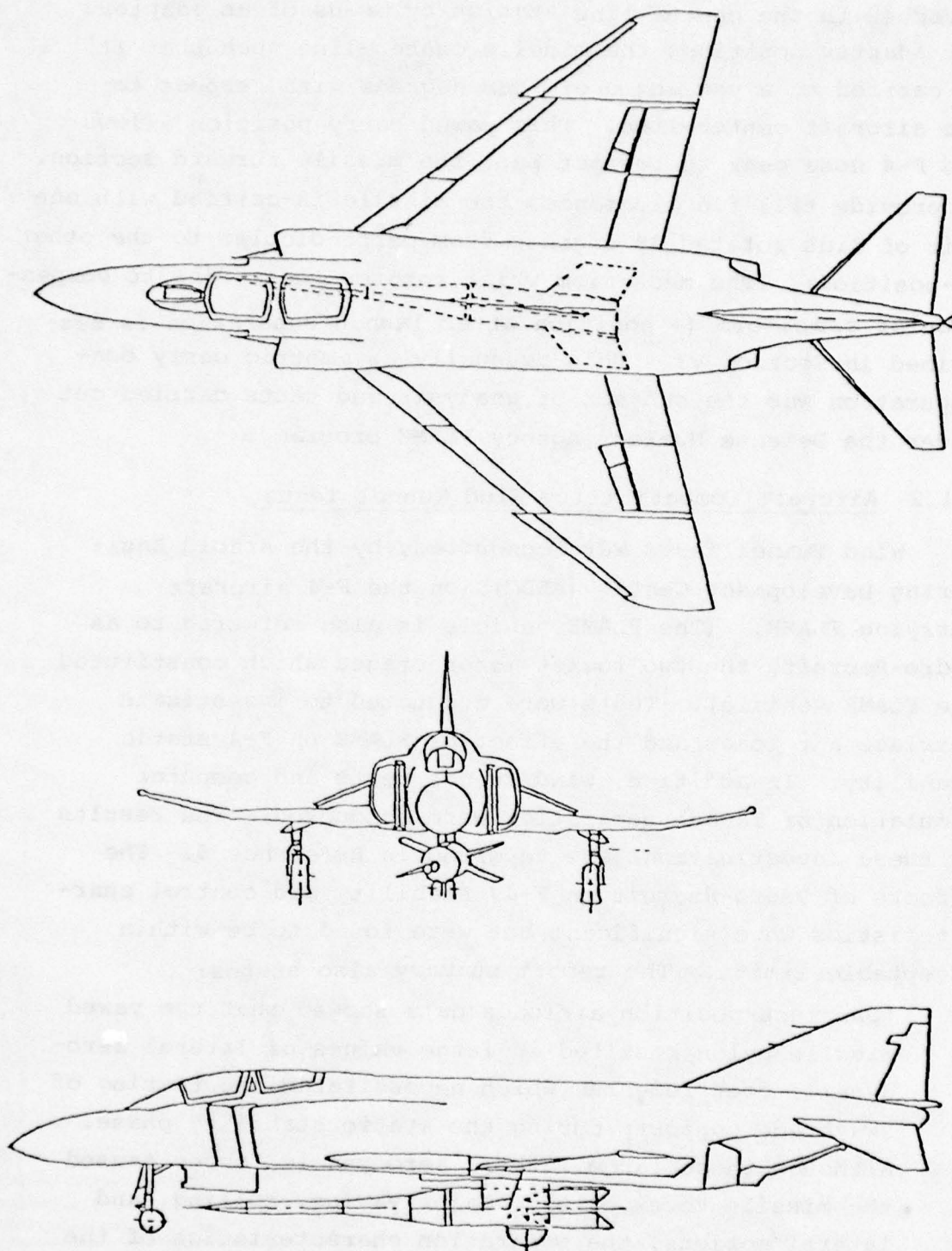


FIGURE 5. IFLEX Installation on F-4

attached to the center-line station by means of an adapter. The adapter positions the missile center-line such that it is carried at a yaw angle of four degrees with respect to the aircraft center-line. This yawed carry position allows the F-4 nose gear to retract past the missile forward section. To provide tail fin clearance, the missile is carried with one pair of fins rotated 48 degrees from perpendicular to the other (X-position). The mechanism which rotates these fins to perpendicular cruciform (+ position after launch separation is described in Section VI. This unusually asymmetric carry configuration was the subject of analysis and tests carried out under the Defense Nuclear Agency FLAME program.

### 3.1.2 Aircraft Compatibility Wind Tunnel Tests

Wind Tunnel Tests were conducted, by the Arnold Engineering Development Center (AEDC), on the F-4 aircraft carrying FLAME. (The FLAME vehicle is also referred to as Pedro-Recruit, the two rocket motor stages which constituted the FLAME vehicle). Tests were conducted to investigate carriage air loads and the effect of FLAME on F-4 static stability. In addition, wind tunnel tests and computer simulation of launch separation were conducted. The results of these investigations are reported in Reference 5. The effects of Pedro-Recruit on F-4J stability and control characteristics were significant but were found to be within acceptable limits. The report summary also states:

"Carriage-position airloads data showed that the yawed missile pylon resulted in large values of lateral aerodynamic coefficients, which necessitated the testing of swaybrace supports during the static stability phase. Although these large lateral aerodynamic forces caused the missile to experience major yawing, rolling, and lateral motions, the separation characteristics of the Pedro-Recruit from the F-4J aircraft were found to be satisfactory for all test conditions."

### 3.1.3 McDonnell Aircraft Company Analysis

The McDonnell Aircraft Company (MCAIR) conducted analyses of the F-4J carrying and launching Pedro-Recruit. The results are reported in Reference 6. Aerodynamic characteristics reported are:

- a) the longitudinal and lateral directional stability characteristics
- b) the Pedro-Recruit installed drag increment
- c) airplane/store separation trajectories for the nominal launch condition.

The structural loads analysis resulted in the following recommended flight envelope with Pedro-Recruit installed:

- a) Speed Placard\*: at altitudes from sea level to 40,000 ft - 450 Knots Calibrated Air Speed (KCAS). At altitudes of 40,000 ft and above- 525 KCAS or  $M=1.8$  (whichever is less).
- b) Maneuvering Envelope: a vertical load factor of  $\eta_z = -1.0$  to 4.0. The stick throw is limited to gradual coordinated turns.
- c) Gust Velocity: lateral gust velocity of 25 fps at 525 KCAS.
- d) Aircraft Trim: as required to maintain zero lateral acceleration.

The Structural Dynamics Analysis results are summarized as follows:

"There is no requirement for flight placards due either to flutter or divergence of the captive vehicle."

### 3.1.4 U.S. Naval Air Test Center, Patuxent River, Tests

Based upon the recommendations of AEDC and MCAIR as outlined above, the U.S. Naval Air Test Center (NAVAIRTESTCEN), after conducting a series of ground tests, air launched one

\*"Placard" is the terminology associated with a performance limitation to be imposed by the pilot.



inert and six live Pedro-Recruit rockets from an F-4J aircraft at the NASA Wallops and DOE Tonapah Test Ranges. The NAVAIRTESTCEN work is reported in Reference 7 and 8. The principal results of the NAVAIRTESTCEN aircraft compatibility testing are summarized in the following excerpts from those reports:

- (a) "... the nose of the aircraft (F-4J) was elevated to the angles where the fin tip just barely cleared the hangar deck. The angle obtained was 11.5 degrees nose-up....Nominal aircraft approach angle is approximately 10 degrees aircraft nose up....It was recommended that all takeoffs be conducted approximately 12 knots faster than normal recommended speeds (7 to 8 degrees nose-up pitch attitude) to avoid ground contact (11.5 degrees nose-up) with the Pedro-Recruit. All takeoffs were accomplished with half flaps and maximum afterburner thrust. The technique for landing was full flaps, 8 knots fast, and no flare."
- (b) "McDonnell personnel on site at NAVAIRTESTCEN conducted a ground vibration test to verify analytical predictions of aeroelastic stability. The values of adapter stiffness and elastic axis location obtained from the Ground Vibration Test (GVT) were used in the divergence analysis. In addition, the GVT established that captive vehicle natural frequencies did not coincide with major airframe structural modes."
- (c) "The only cockpit modification consisted of an easily removable FLAME control panel....The control panel allowed the pilot to arm the rocket and to turn on reentry vehicle telemetry power."

Two warning lights informed the pilot as to which mode the rocket was in, SAFE or ARM. A third light monitored command receiver channels utilized for ground linked rocket motor initiation. The electrical circuits and normal aircraft store jettison circuits were satisfactorily verified during the conduct of the ground tests."

(d) "Based on qualitative pilot opinion, the flying qualities were essentially the same as the basic F-4J aircraft with no external stores. Tests were conducted SAS (Stability Augmentation System) ON and OFF at each of the test conditions. Wind-up Turns were limited to 3g at each test point."

(e) "Following the successful separation of the inert Pedro-Recruit on 9 October 1974, six live rockets were successfully released during the period from 4 February 1975 to 4 June 1975. Release Mach number/calibrated airspeed varied between 1.224/263 KCAS and 1.366/323 KCAS. Release altitude varied between 54,596 feet and 56,031 feet while flight path angle varied between 30 and 33 degrees nose-up."

### 3.1.5 Recommendations for F-4/IFLEX Interface and Launch

In order to make maximum utilization of the extensive F-4J/FLAME experience and preclude expensive requalification, it is recommended that IFLEX interfaces with F-4 launch aircraft be consistent with those which have been previously qualified. Specific recommendations are outlined below:

#### FLAME

F-4J aircraft equipped for pilot - pressure suit operation above 50,000 feet. Launch envelope as recommended by MCAIR.

#### IFLEX

Use USAF F-4C or F-4D aircraft from either Eglin A.F.B. or Edwards A.F.B. Restrict launch



## FLAME

- LAU-77A/A Launcher modified in accordance with MCAIR Dwg. 32-04806. Five MK-9 Mod-0 cartridges give ejection velocity of 8.871 fps. Attachment to F-4 Aero 27A centerline bomb rack in accordance with MCAIR Dwg. 32-04801.

- FLAME aircraft control panel replaced DCU-75/A Special Weapons Control panel. A wiring adapter cable connected FLAME vehicle wiring to aircraft Special Weapons Wiring.

- PEDRO ROCKET  
(1st Stage)

## IFLEX

operation below 50,000 feet. No pressure suit requirement. Otherwise launch envelope as recommended by MCAIR.

- Identical installation. Liaison with Warner Robbins code WR-ALC/MMIMA indicates that action to obtain an Air Force LAU-77B/A-048-0593CH launcher should be initiated at an early date to provide 12 months lead time prior to launcher delivery. Special adapter may be available from the Navy. Otherwise, a new adapter can be fabricated by the test activity from MCAIR drawing.
- Fabricate equivalent special IFLEX aircraft control panel and wiring adapter at the test activity (Eglin or Edwards).
- PEDRO Rocket with equivalent propellant loading or less.



### FLAME

- RECRUIT Rocket  
(2nd Stage)
- FLAME WT & Balance  
WT - 3933 lb.  
CG - 213.5 in.
- Vehicle stiffness. No divergence and no resonant frequencies.
- Ground clearance.  
Fin rotation provides ground clearance to 11.5 degrees nose-up. Landing and take-off conditions planned for maximum nose-up attitude of 8 degrees. Vehicle fins if inadvertently scraped would fail prior to transmitting a damaging load into vehicle body and launcher.

### IFLEX

- Identical external configuration. Inert section carries instrumentation.
- IFLEX WT & Balance  
WT - 3966 lb.  
CG - 212.2 in.
- IFLEX structural design provides equivalent or greater stiffness.
- IFLEX increased diameter reduces ground clearance by 0.9 inches with fins rotated. Ground clearance is provided to 10.6 degrees nose-up. Recommend landing and take-off attitude restriction of 8 degrees as on FLAME. Aluminum fin structure would fail if scraped without endangering safety of flight. Recommend ground observation of take-off run to confirm no fin damage.

## 3.2 AERODYNAMICS

### 3.2.1 Configuration Selection

The requirement to maintain the aircraft compatibility, which was verified for the FLAME program, dictated that the aerodynamic configuration of the IFLEX vehicle be maintained as closely as possible to the FLAME launch vehicle geometry. The degree of freedom left was departure from that configuration after clearing the aircraft. As described in Section VI, except for the small aft body diameter increase, the IFLEX and FLAME launch vehicle external geometries are the same.

During the IFLEX design study, the possibility of flying the IFLEX vehicle with a fin configuration different than that on FLAME, after aircraft separation, was analyzed. The vehicle is carried on the aircraft with one set of opposing fins rotated 48 degrees from perpendicular to the other as illustrated in Figure 6. This is necessary to facilitate ground clearance during aircraft take-off and landing. The possibility of flying the IFLEX mission with the fins in this non-cruciform configuration was examined. A reasonably complex actuator system was employed on the FLAME launch vehicle to rotate one set of the fins to form a cruciform geometry after aircraft separation. Complexity and cost of IFLEX vehicles could be reduced by eliminating the fin rotation requirement. The fin rotation requirement was due to a predicted loss of static stability at high Mach numbers in the plane of the small (42 degrees) included-angle between the fins in the aircraft carry geometry (the x-y' plane in Figure 6). A static stability wind tunnel test was conducted to determine the variation in stability with Mach number and fin configuration. The results of this test are described in detail in Reference 9.

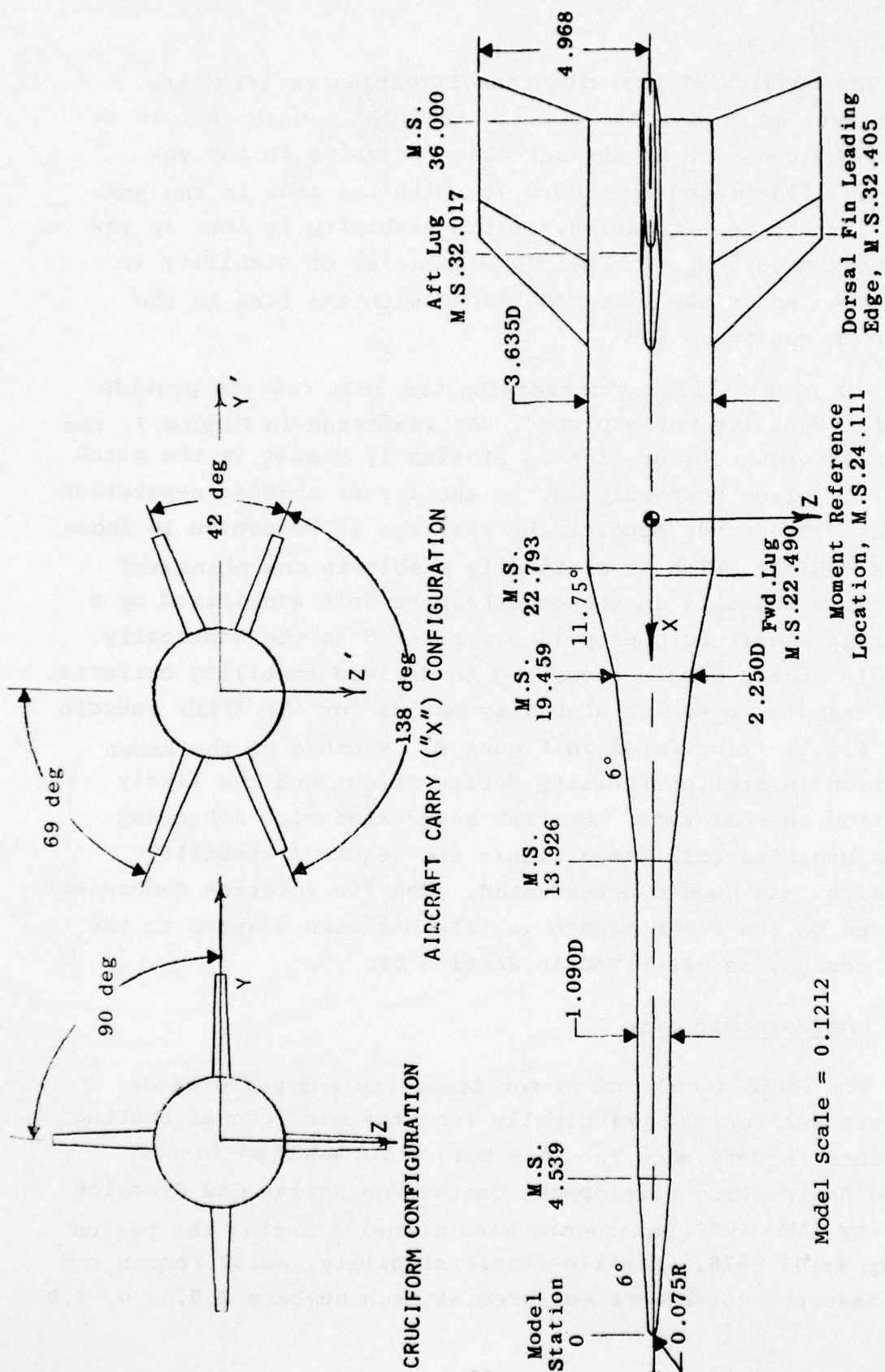


FIGURE 6. IFLEX Wind Tunnel Model Geometry



The results of the wind tunnel testing verified the predictions made by AJLRC during the FLAME launch vehicle design. The behavior of the center of pressure in the yaw plane is illustrated in Figure 7. With the fins in the non-cruciform (X) configuration, static stability is lost in yaw at approximately  $M_\infty = 6$ . Nearly a diameter of stability is maintained, under the same conditions, with the fins in the cruciform configuration.

The possibility of increasing the roll rate to provide dynamic stability was explored. As indicated in Figure 7, the non-cruciform configuration is statically stable in the pitch plane, or plane perpendicular to the larger angular separation of fins. The study reported by Phillips in Reference 10 shows that a vehicle which is statically stable in one plane (and statically unstable in the other) can be spin stabilized by a roll rate magnitude appropriately related to the statically unstable static margin according to derived stability criteria. As an example, a set of stability bounds for the IFLEX vehicle at  $M_\infty = 6.2$  is illustrated in Figure 8. Because of the known variation in static stability during flight and the likely variation in roll rate, the risk associated with achieving and maintaining roll rates within the required stability boundaries was judged unwarranted. The fin rotation mechanism employed on the FLAME launch vehicle has been adapted to the IFLEX design, as described in Section VI.

### 3.2.2 Aerodynamic Data

The IFLEX aerodynamics for stability and performance analysis was derived principally from the wind tunnel testing described in Reference 9. This test was conducted in the Arnold Engineering Development Center-Von Karman Gas Dynamics Facility (AEDC-VKF) Supersonic Wind Tunnel A during the period of May 8-10, 1978. Missile static stability, axial forces and body base pressures were measured at Mach numbers 2.0, 3.0, 4.0

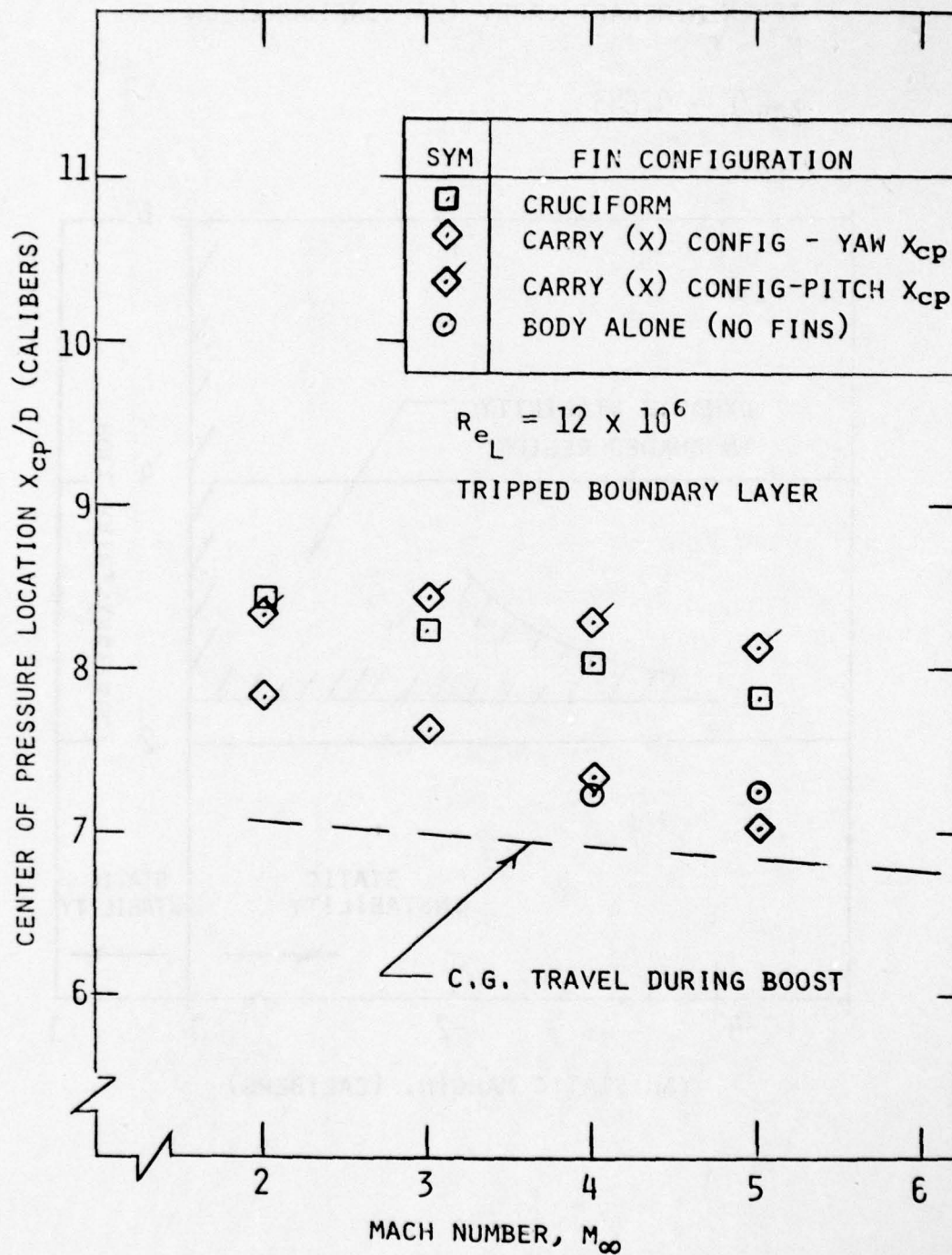


FIGURE 7. Fin Configuration Influence On Static Stability

IFLEX AIRCRAFT CARRY (X) CONFIGURATION

$M_\infty = 6.2$

$x_{cg}/L = 0.633$

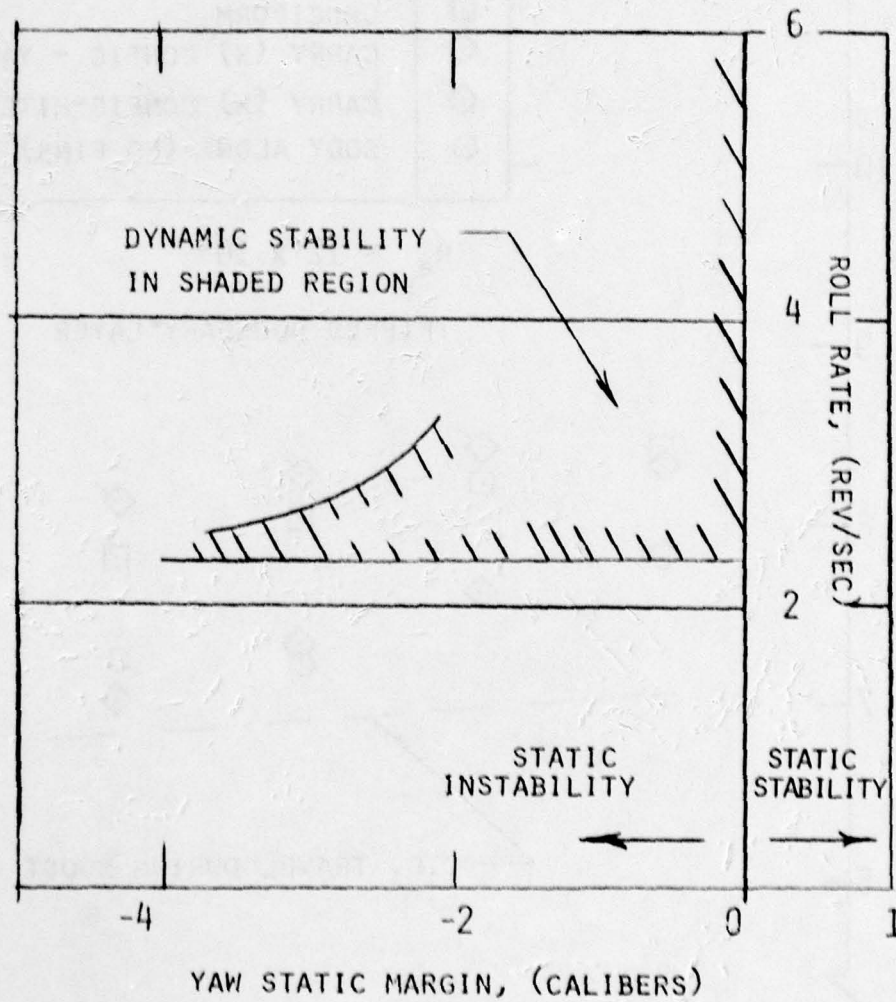


FIGURE 8. Example Of Stability Boundaries For (X) Configuration



and 5.0. Large bands of carborundum grit were applied to the model forecone to assure early boundary layer transition. The testing was conducted at a unit Reynolds number of approximately  $4 \times 10^6$ /foot at all Mach numbers. The fundamental model configuration is shown in Figure 6.

The IFLEX normal force characteristics are illustrated in Figure 9. The pitching moment characteristics measured in the wind tunnel test are shown in Figure 10. The axial force characteristics are shown in Figure 11. The normal force slope at zero angle of attack is shown in Figure 12.

The drag data reported in Reference 9 for the IFLEX configuration at zero angle of attack, is illustrated in Figure 13. Three sets of data were measured. The first is axial force on the body without fins. The second is axial force on the body with fins in position. The third is base pressure in the body base area. The data on the body without fins attached was only reported for  $M_\infty = 4$ . Three sets of axial force coefficients are reported as follows:

$C_{A_t}$  = The measured axial force coefficient

$C_{A_B}$  = The measured base pressure related axial-force coefficient increment defined as

$$C_{A_B} = - \frac{(P_B - P_\infty) S_B}{q_\infty} \quad (1)$$

where  $P_B$  = Measured base pressure

$P_\infty$  = Freestream pressure

$q_\infty$  = Freestream dynamic pressure

$S_B$  = Reference base area

$C_A$  = The axial force coefficient with base pressure corrected to freestream level,

$$C_A = C_{A_t} - C_{A_B} \quad (2)$$

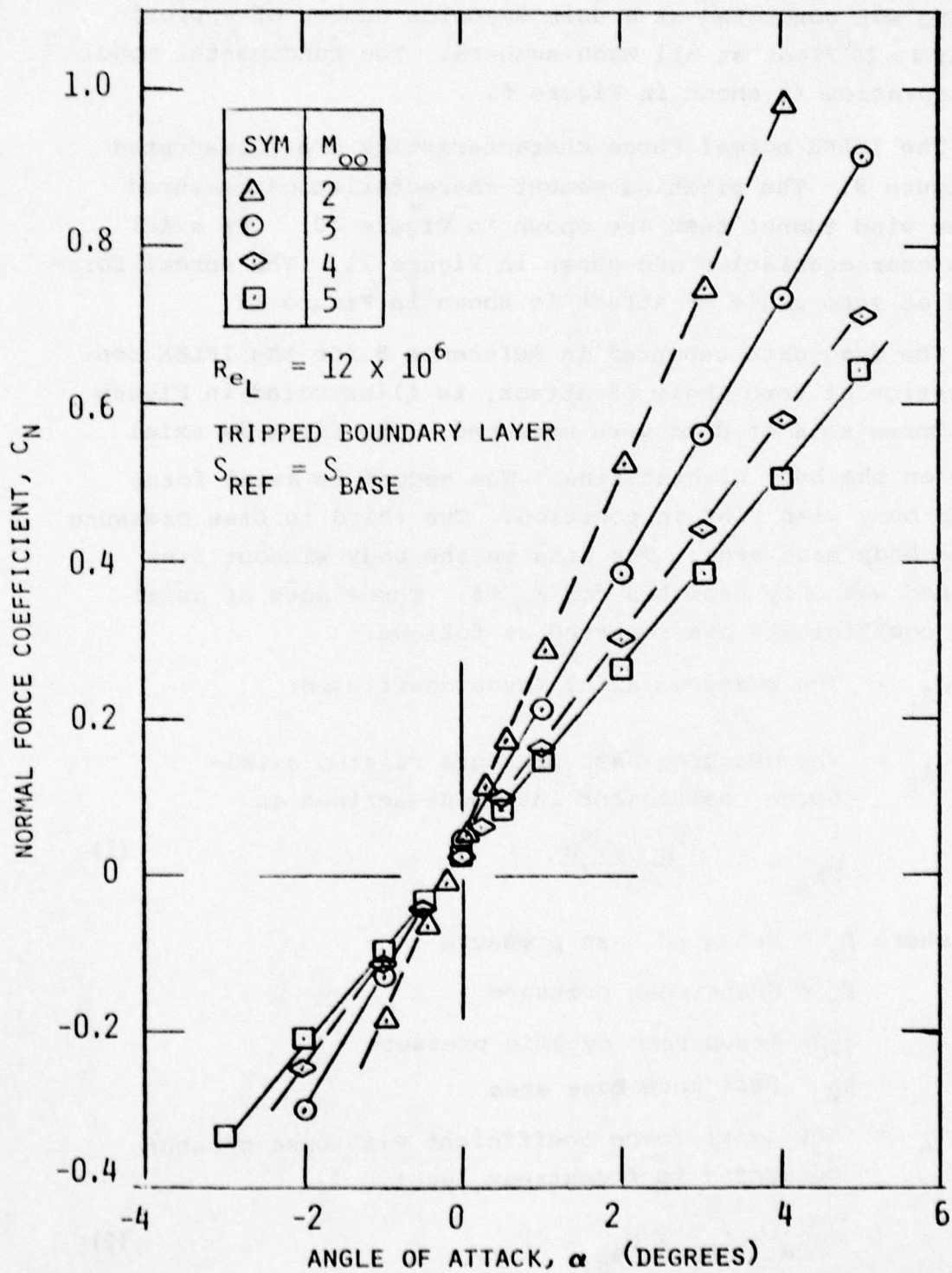


FIGURE 9. IFLEX Normal Force Coefficient Data

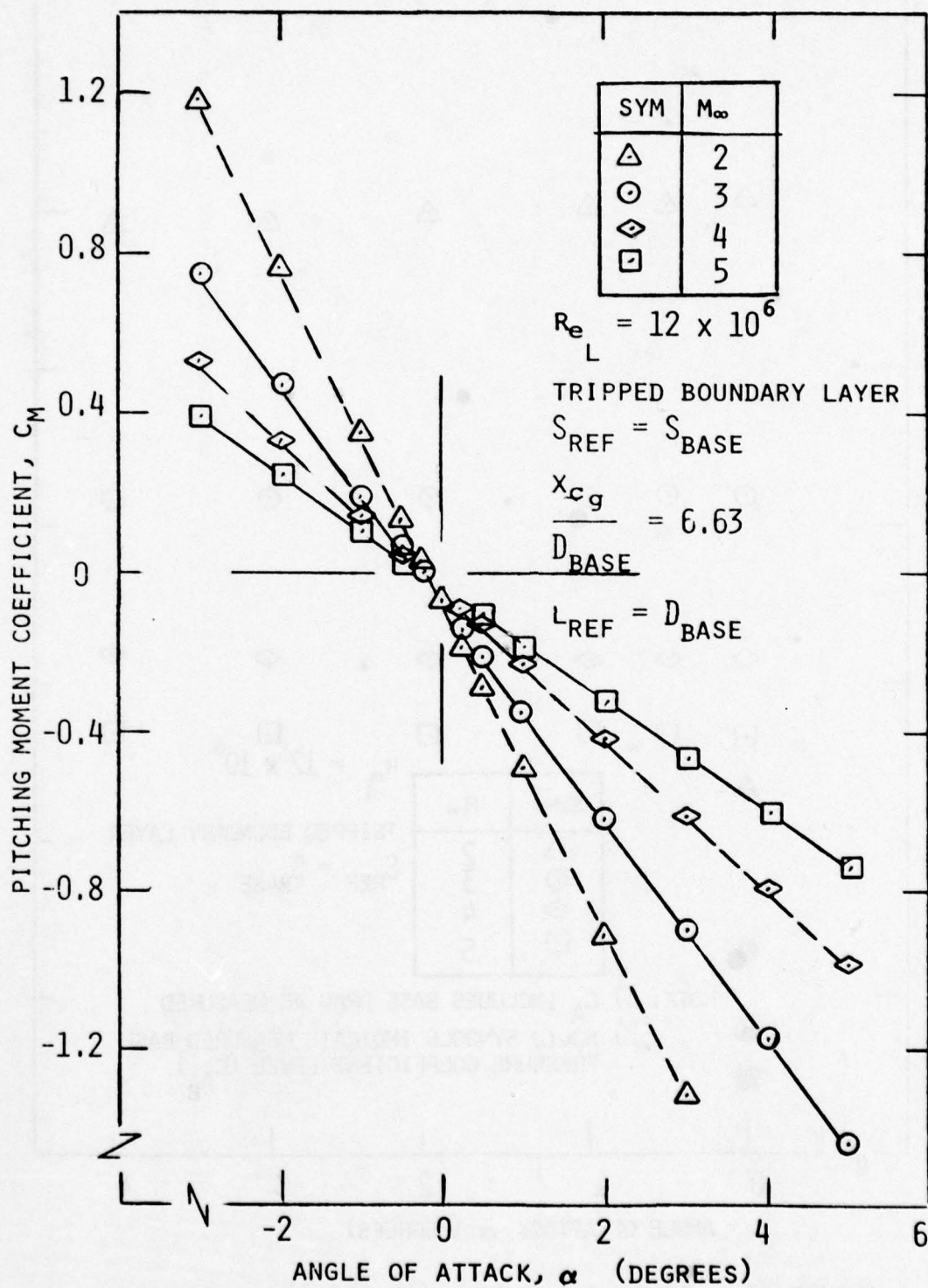


FIGURE 10. IFLEX Pitching Moment Coefficient Data



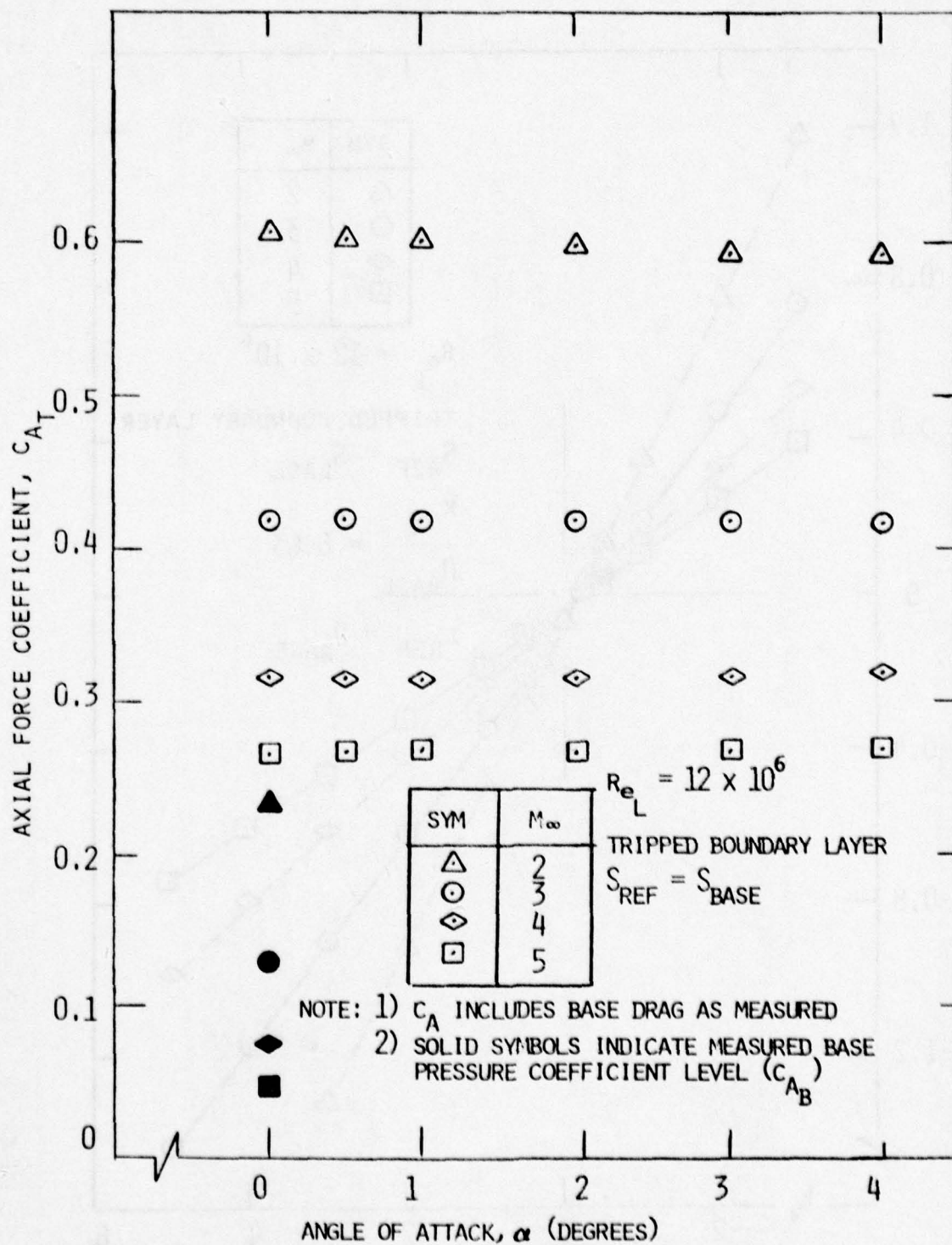


FIGURE 11. IFLEX Axial Force Coefficient Data

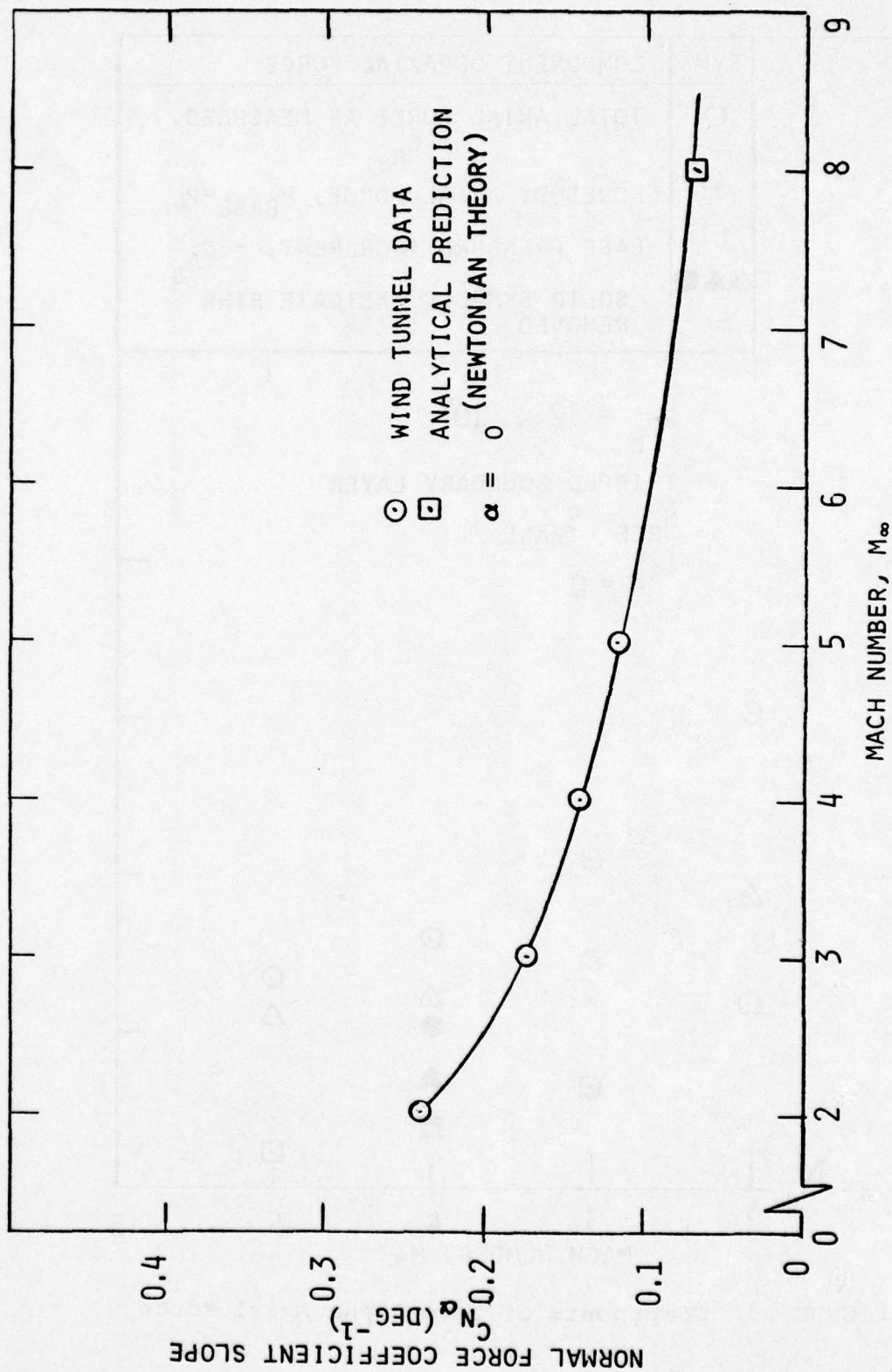


FIGURE 12. Variation in Normal Force Coefficient Slope with Mach Number

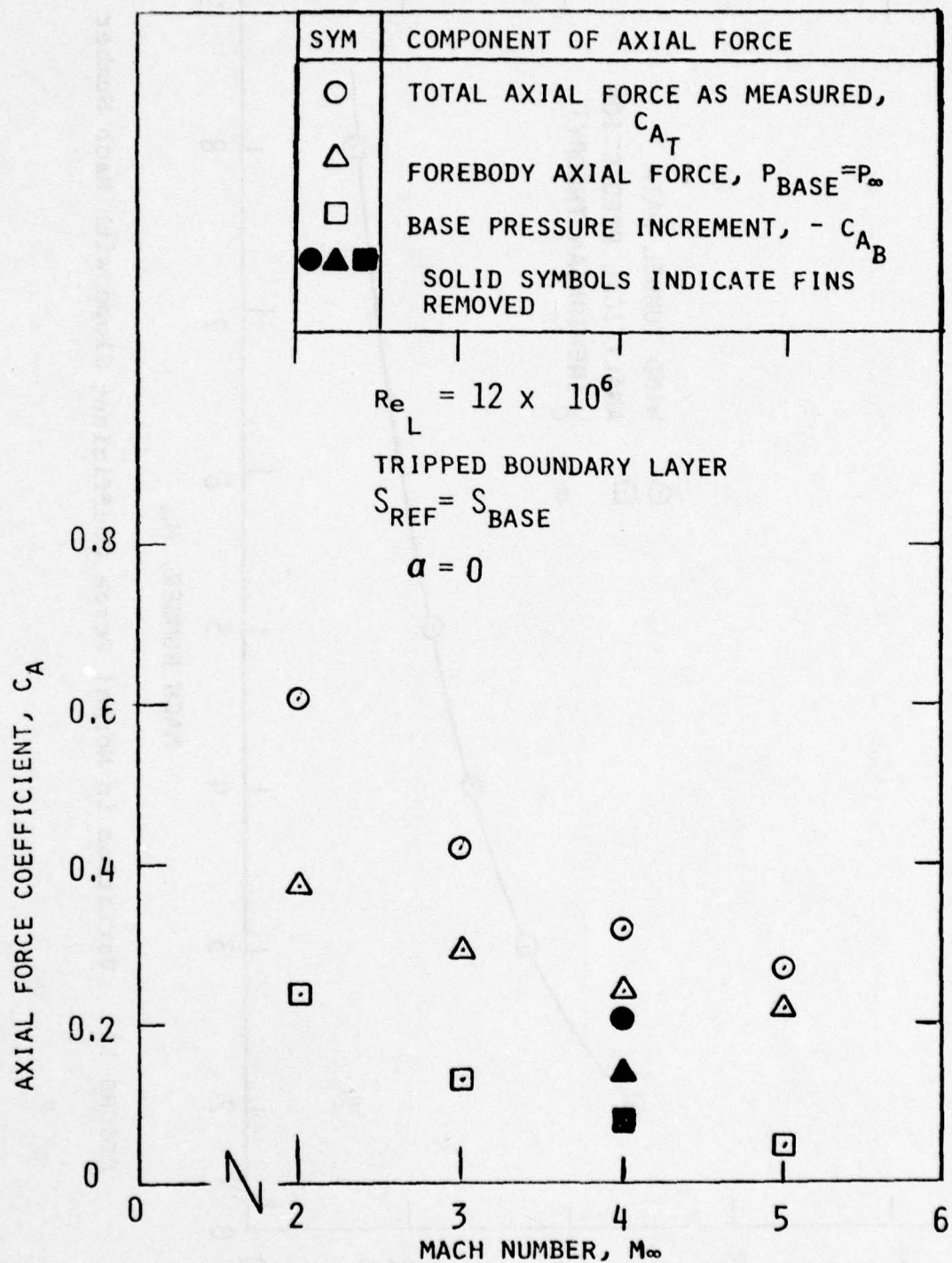


FIGURE 13. Components of Zero Alpha Axial Force



There were no base pressures measured in the fin wakes.

The drag increment build up effects are illustrated in Figure 13 for  $M_\infty = 4$ . It should be noted that the effect of fin base pressure is included in the difference between fin-off and fin-on forebody drag. This may be significant since the total projected fin base area (4 fins) is approximately equal to half the base area (5.15 square inches in model scale).

### 3.2.3 Trajectory Simulation Aerodynamics

Since the IFLEX configuration generates a multishock flowfield, there is uncertainty concerning the adequacy of local slope methods in predicting surface pressures. To investigate the pressure distribution behavior, the flow quantities in the shock layer were calculated by the computer code described in Reference 11, referred to as the NASA/Grumman code. These calculations provided pressure distributions on the surface, shock layer properties, and body alone, inviscid flow aerodynamic coefficients.

A typical pressure distribution predicted by the NASA/Grumman Code is illustrated in Figure 14. The drag coefficient variation with Mach number, for the IFLEX body without fins, is shown in Figure 15. The agreement with the experimental data at  $M_\infty = 4$  is not as good as expected, since some skin friction increment should be present between the two. This may be partly due to fillets (corner rounding) required in the geometry representations employed in the code. The empirical base pressure coefficient representation  $C_{p_B} = -1/M_\infty^2$  appears to be quite accurate for this configuration and flow condition.

To predict the low Mach number drag characteristics of IFLEX for trajectory simulations, tangent-wedge pressures and

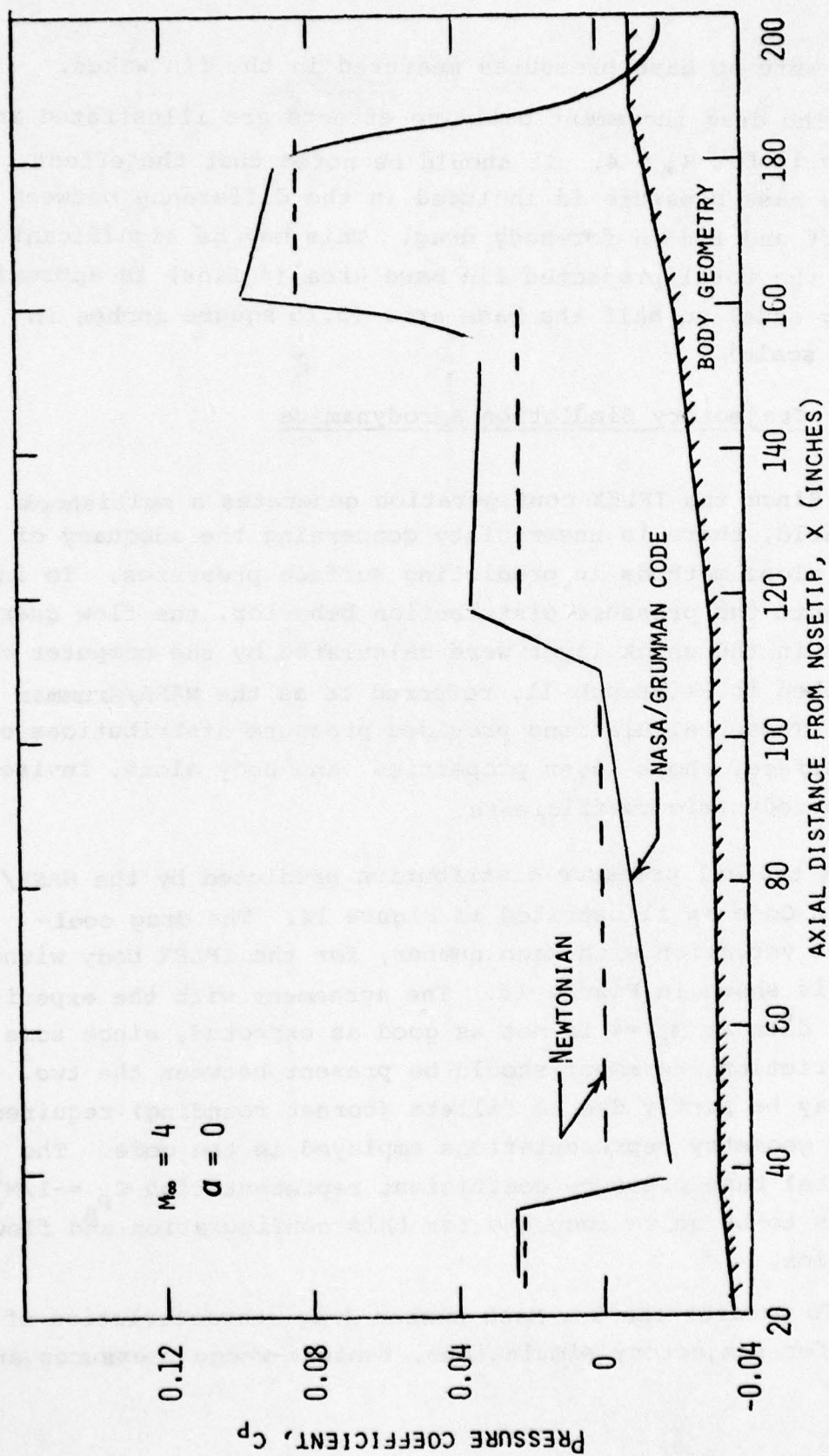


FIGURE 14. IFLEX Pressure Distribution

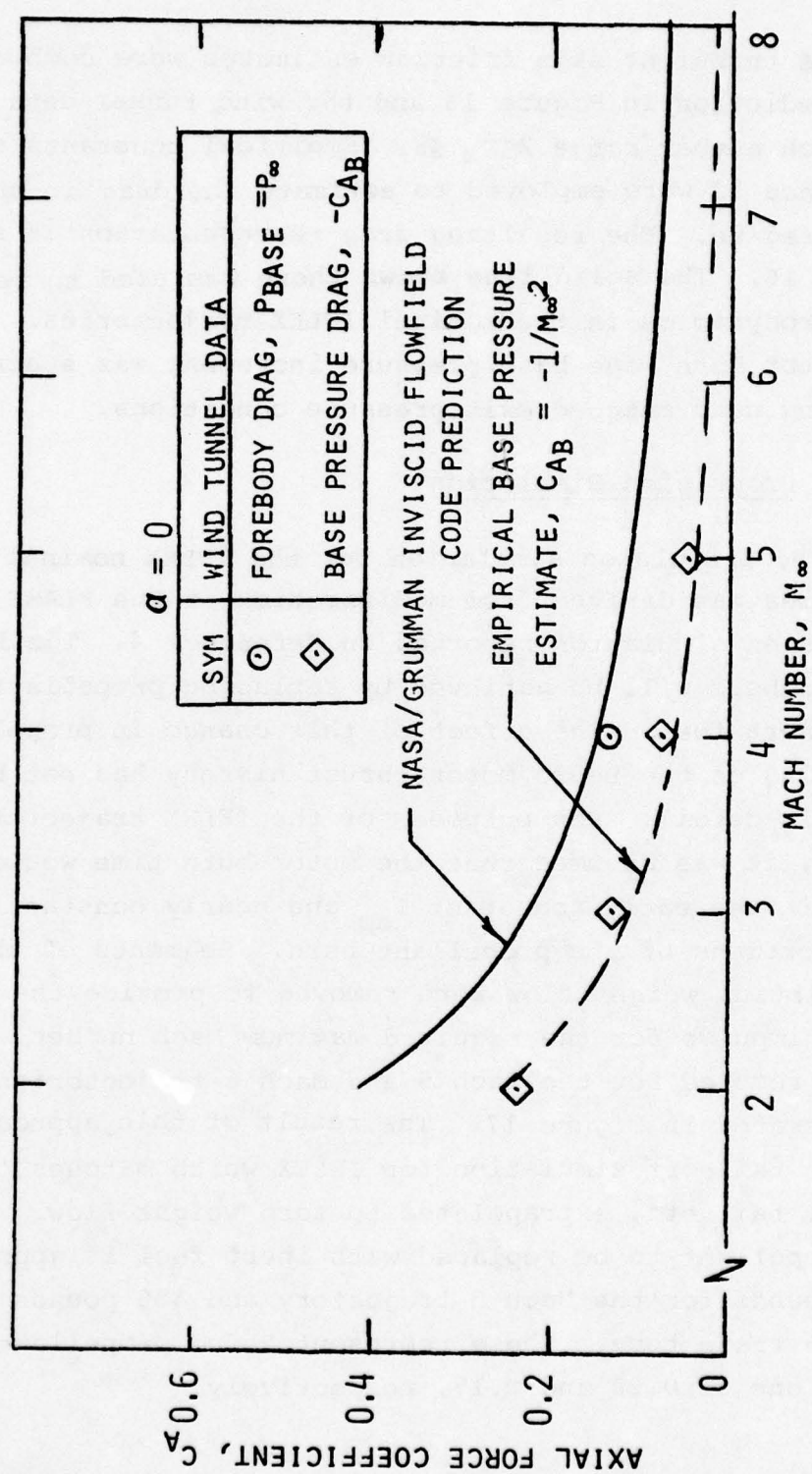


FIGURE 15. Prediction Methods For Body Alone Axial Force



average turbulent skin friction estimates were combined with the prediction in Figure 15 and the wind tunnel data for the Mach number range  $2 \leq M_\infty \leq 8$ . Empirical constants from Reference 12 were employed to estimate the drag in the transonic region. The resulting drag representation is shown in Figure 16. The solid line shown there was used to represent the aerodynamics in the nominal IFLEX trajectories. During the motor burn, the base pressure increment was subtracted, assuming near matched exit pressure conditions.

#### 3.2.4 Propulsion Simulation

The propulsion simulation for the IFLEX nominal trajectories was derived from modification of the FLAME FLT 008 propulsion simulation reported in Reference 4. The lower Mach numbers will be achieved by replacing propellant grain with inert fuel. The effect of this change in propellant packaging on the Pedro motor thrust history has not been analyzed in detail. For purposes of the IFLEX trajectory simulation, it was assumed that the motor burn time would be reduced in the early, constant  $I_{sp}$  and nearly constant weight flow portions of the propellant burn. Segments of the near equilibrium weight flow were removed to provide the required total impulse for the required maximum Mach number. The segments removed for the Mach 5 and Mach 6 trajectories are illustrated in Figure 17. The result of this approach is a thrust tail-off simulation for IFLEX which matches the FLAME thrust tail-off, extrapolated to zero weight flow. The weight of propellant to be replaced with inert fuel is approximately 660 pounds for the Mach 5 trajectory and 380 pounds for the Mach 6 trajectory. These represent Pedro propellant mass fractions of 0.28 and 0.15, respectively.

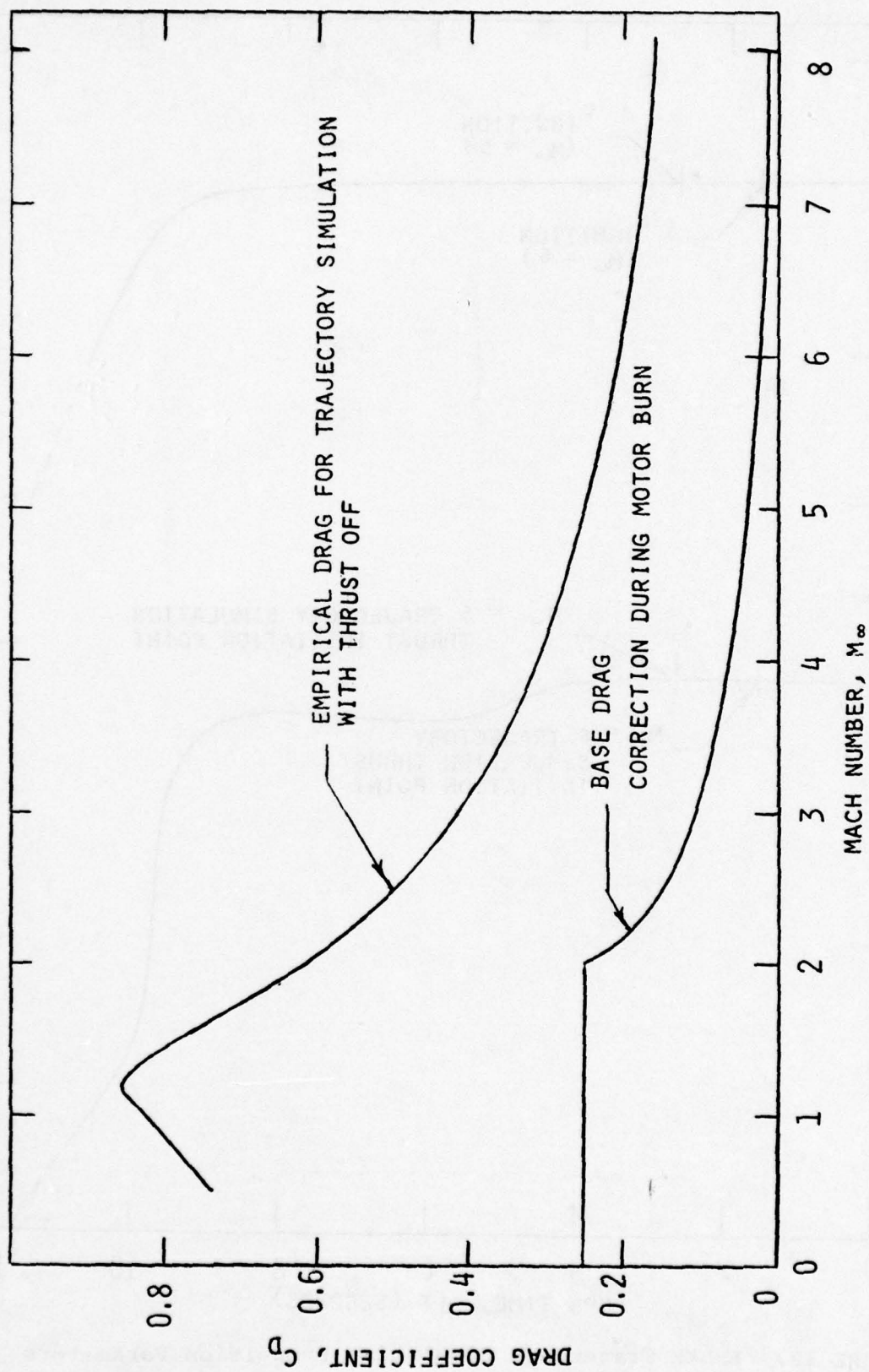


FIGURE 16. Drag Predictions For IFLEX Trajectory Simulation

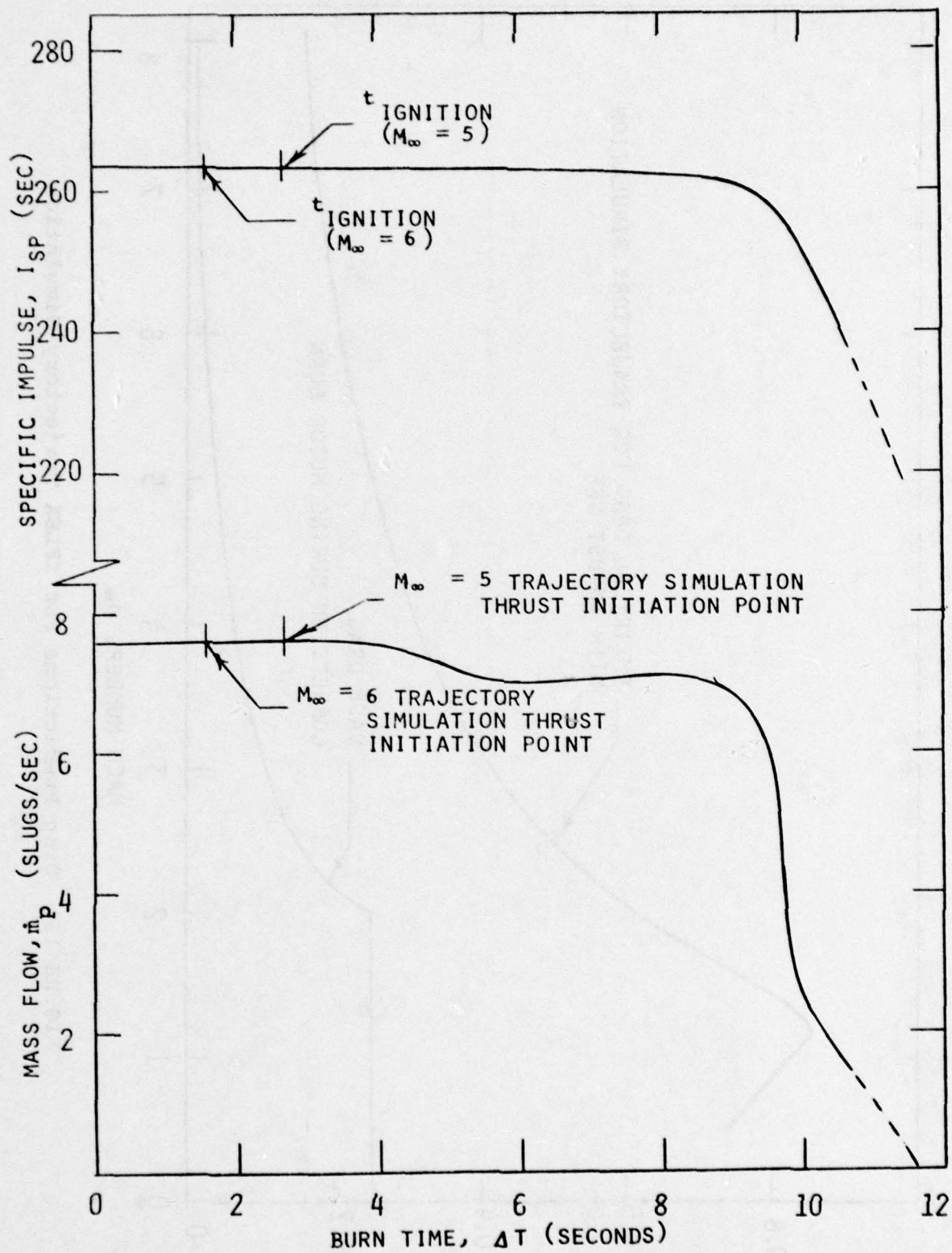


FIGURE 17. IFLEX Trajectory Simulation Propulsion Parameters



### 3.2.5 Lateral Mass Asymmetries

The design of the instrumented region in the vicinity of one of the four IFLEX fins, and the design of the instrumented fin, require the substitution of steel plates for the aluminum or magnesium and Dyna-therm surfaces. The result is a small lateral center of gravity (c.g.) offset relative to the axis of geometry symmetry. This offset has been estimated to be 0.25 inches. An offset of this magnitude is estimated to result in a static trim angle of attack less than 0.02 degrees in the plane of the offset.

### 3.3 IFLEX TRAJECTORY

Since the IFLEX vehicle is uncontrolled, the flight trajectory is determined by a combination of the vehicle state at separation from the carrier aircraft and the timing of the Pedro motor burn. The considerations in determining aircraft separation conditions are principally aircraft performance capability and safety. The considerations governing selection of preset motor ignition conditions are aircraft safety and trajectory shaping. The last degree of freedom in trajectory shaping is the selection of active propellant weight for the Pedro rocket motor, which principally influences maximum velocity and the altitude at which it occurs. These trajectory shaping parameters have been investigated parametrically to select IFLEX trajectories. The impact of trajectory shaping on the TPS is discussed in Section VI.

The vehicle is to be launched from the aircraft in a climbing attitude, with flight path angle approximately 30 degrees above the horizontal, at a Mach number of approximately 0.95. These conditions permit the aircraft to clear the vicinity of the missile while the missile coasts ballistically over a parabolic arc to a downward oriented flight path angle.

The subsequent vehicle trajectory is then determined by selection of the motor ignition time (or initial flight path angle) and propellant loading, or maximum velocity. The launch altitude has been selected as 45 KFT to permit the aircraft to maneuver away from the missile after launch without penetrating a maximum altitude limit of 50 KFT. Lower flight path angles could be selected to allow higher launch altitudes. However, these result in more severe thermal environments and decreased experiment flight times. A profile of maximum allowable launch flight path angles as a function of launch altitude is shown in Figure 18.

Selection of the Pedro rocket ignition time, along the IFLEX parabolic arc coasting trajectory, results in selection of the flight path angle at ignition. The signal for ignition will be a ground command transmitted after an on-board timer has enabled the ignition circuit. Ground based radar observations will provide data on flight path angle as a basis for the ignition time decision. The nominal IFLEX trajectory, designated Trajectory A, has an ignition time 20 seconds after launch and a maximum Mach number of 6 (26.4 seconds was the FLAME ignition time). The corresponding velocity and altitude profiles are shown in Figure 19. The flight path angle profile is shown in Figure 20. The unit Reynolds number-Mach number characteristics are presented in Figure 21.

The parametric thermal protection system design analyses utilized trajectories 1, 2, 3, and 4 of Section VI. These trajectories were based on preliminary aero/propulsion estimates. They differ from trajectory A in that the motor thrust tail-off was not represented and preliminary drag coefficients which were used had values lower than those finally derived for the lower Mach numbers. Because of the lower drag and

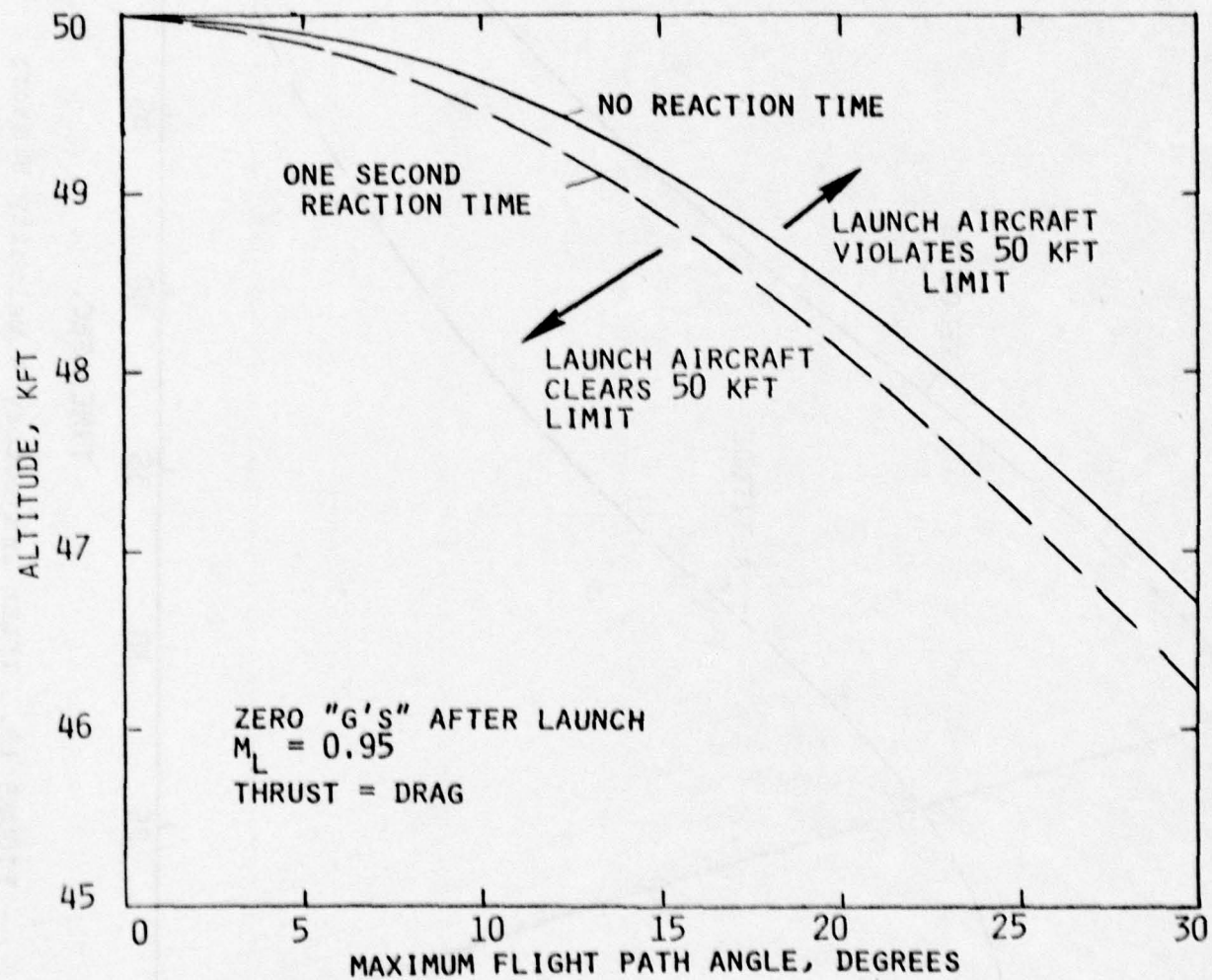


FIGURE 18. Launch Angle-Altitude Bounds At Aircraft Separation



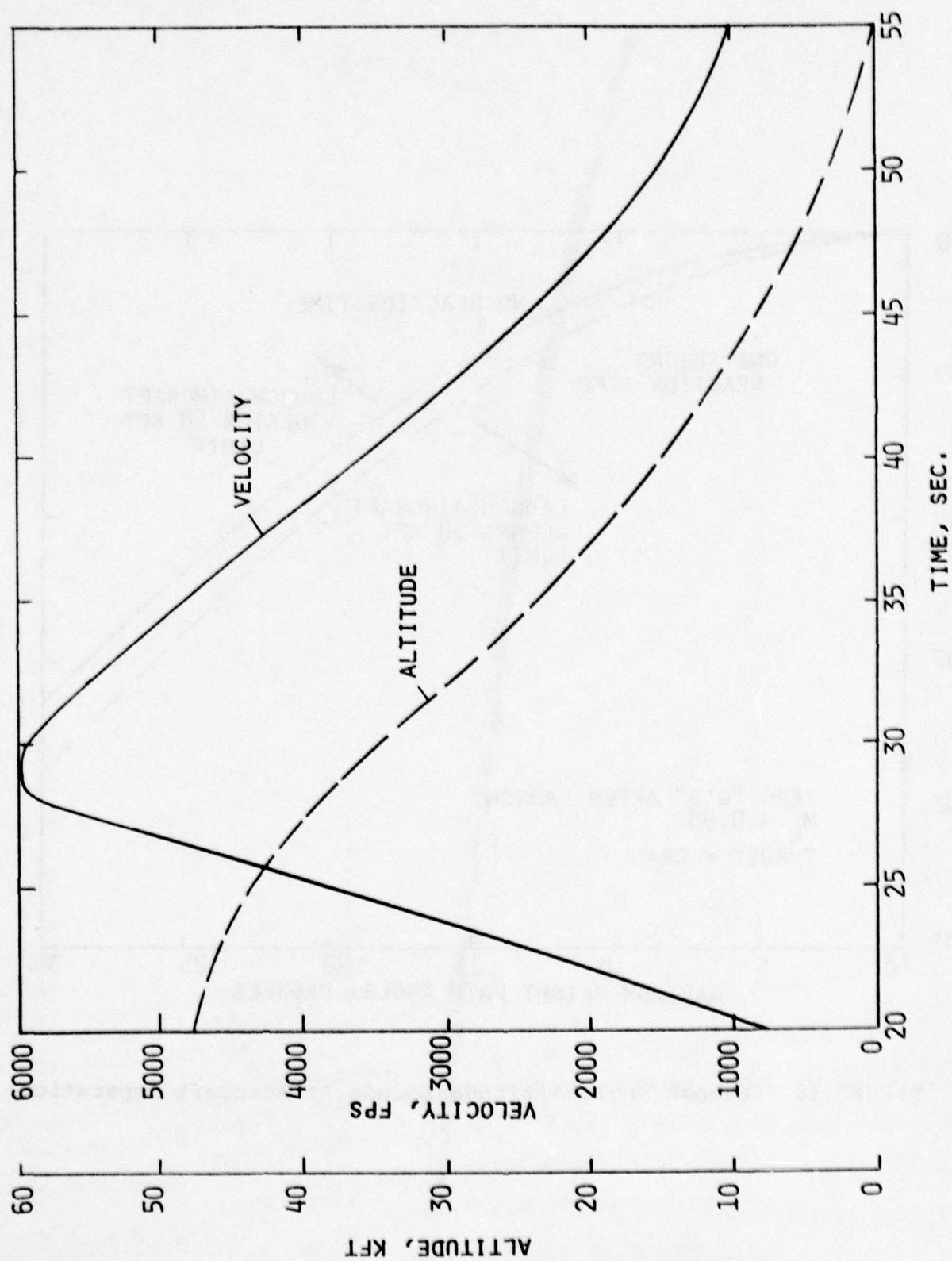


FIGURE 19. IPLEX Trajectory A Velocity History

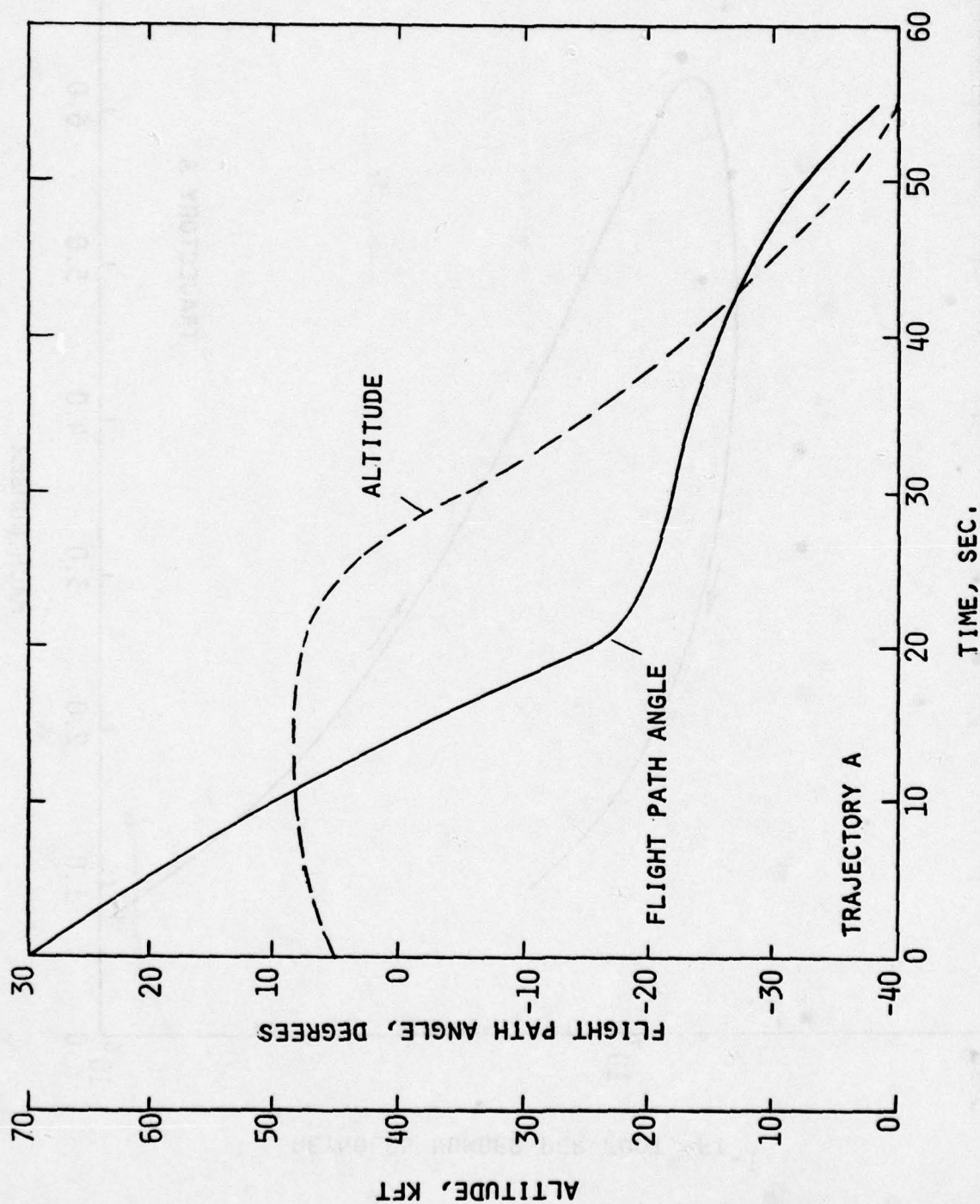


FIGURE 20. Trajectory A Flight Path Angle History

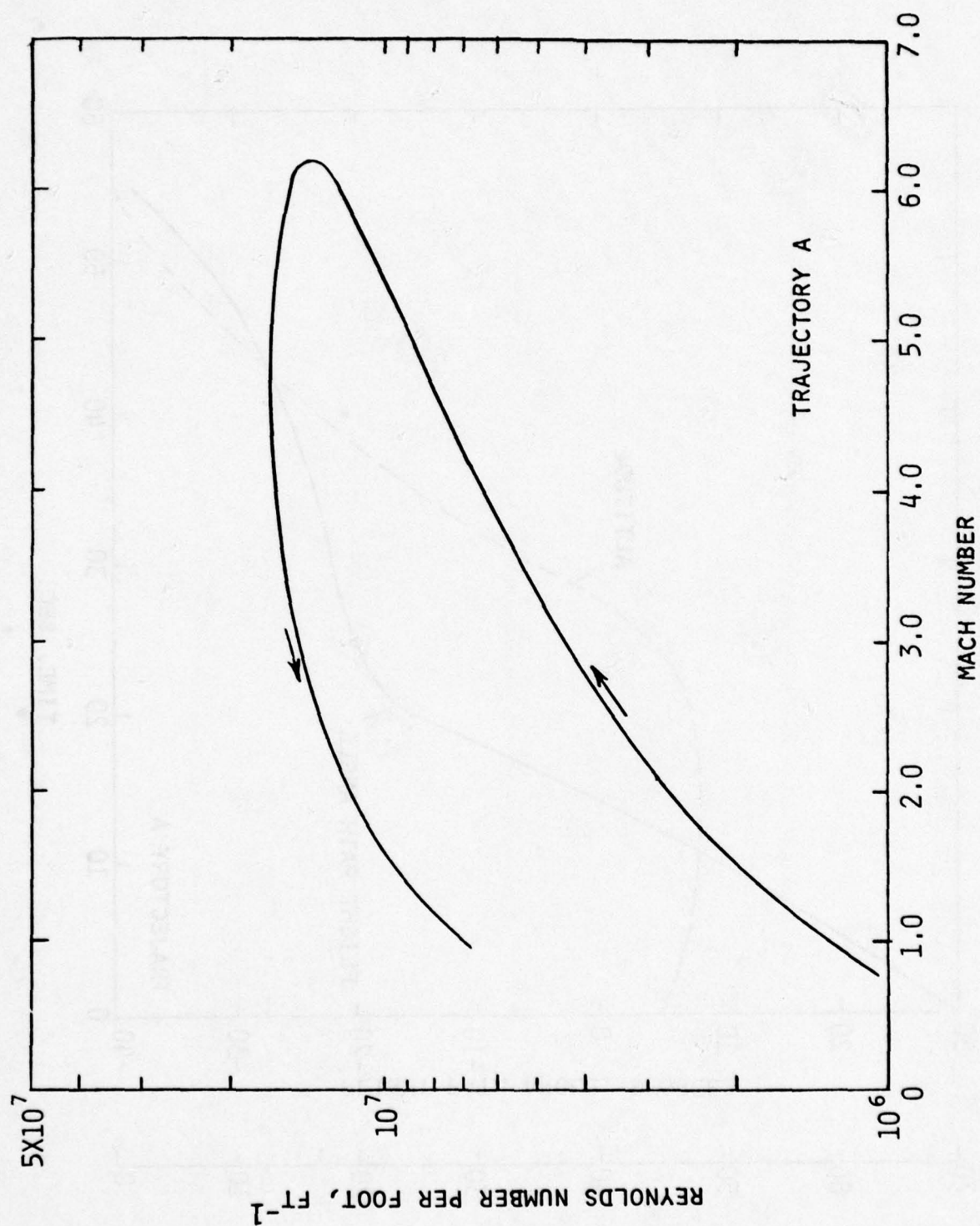


FIGURE 21. IFLEX Trajectory A Reynolds Number History



resulting higher coast velocities, the thermal response predicted is conservative in regard to the thermal design. Trajectory A and variants obtained by using earlier ignition times and appropriately reduced motor propellant loadings are the trajectories employed in the flight and experiment planning.

### 3.4 Flight Operations Requirements

In addition to the actions (outlined in paragraph 3.1) required for issuance of flight clearance by the Air Force for F4/IFLEX, the following recommendations concerning flight operations are outlined.

#### 3.4.1 F-4 C/D Launch Aircraft

Specific Air Force F-4 type aircraft which will be available and suitable for the IFLEX installation should be identified. In addition to the physical form factor compatibility discussed in Section 3.1, the aircraft should be equipped with a C-band transponder for acquisition and precision tracking during dry runs without the IFLEX loaded. It is recommended that compatibility with as many different F-4 aircraft as practicable be retained for operational flexibility of the project. Liaison with both Edwards AFB and Eglin AFB indicates that one or more suitable F-4 type aircraft will be available if requested by the project.

#### 3.4.2 Project Pilots

The achievement of desired IFLEX trajectories is dependent upon a high degree of coordination between the Project Pilot and the Aircraft Flight Path Ground Controller in achieving the planned launch conditions. It is therefore recommended that a single project pilot, backed up by a qualified alternate, perform the training flights, dry runs and IFLEX launches.

#### 3.4.3 Photo Chase Aircraft

A photo chase aircraft having performance capabilities compatible with the planned launch conditions should be planned. Photographic coverage of launch separation and fin rotation is required. The photo chase aircraft should not be required for training operations.

#### 3.4.4 Aircraft Flight Path Controller

The project should furnish an aircraft flight path controller who will work with range personnel during the operational phase of the project in providing precision voice vectoring to the pilot in order to achieve the desired launch separation vector within the range safety and instrumentation constraints. The range personnel would provide to him a suitable radar display or plot, a ground-to-air voice channel, and retain "go-no-go" responsibility for range safety. The approach to launch point will involve pilot/controller team work analogous to that of a final precision Ground Control Approach (GCA) under instrument flight rules (IFR) flight. The Aircraft Flight Path Controller may be provided by the IFLEX contractor or assigned from among qualified military personnel.

#### 3.4.5 Handling and Loading Provisions

It is recommended that assembly of IFLEX at the selected Air Force facility be performed by contractor personnel. Similarly, transport on the base, handling, loading, telemetering ground checks, arming and (if necessary) de-arming would be performed by qualified contractor personnel. Base requirements for handling and loading are:



- Missile assembly and storage building
- Aircraft flight line location suitable for loading large ordnance.
- Runway arming location.
- Post-landing de-arming location.
- Missile transport and loading equipment. The Air-log 4000A trailer which is normally utilized for removing jet engines was utilized satisfactorily during the FLAME program.
- Flight line provisions for tie-in to range telemetry for telemetering ground checks.
- Standard F-4 support for fueling and other flight line support.
- Temporary office space for project personnel.

#### 3.4.6 Flight Plan

The flight plan for IFLEX is described in two separate sections. The aircraft flight plan, from operating base to launch and return, is discussed first. Then the details of aircraft pull-up, launch and post-launch maneuver are described.

##### 3.4.6.1 Aircraft Flight From Base to Launch and Return

A minimal aircraft flight plan has been developed for operations from Edwards AFB and launch at the Tonapah Test Range 162 miles from Edwards. The purpose of this plan was to investigate the amount of fuel reserve available over and above the basic requirements of the flight. An equivalent flight from Holloman AFB, launching IFLEX over the White Sands Missile Range "50-mile range" would be shorter:

	<u>Gross Weight</u>	<u>Fuel Pounds</u>	<u>Distance NM</u>	<u>Time Min.</u>
	48,168			
a) Start Engines, Take-off and Accelerate to 400 KCAS.				
5 MIN SLS* NRT (Normal Rated Thrust)		1303	--	5
1 MIN SLS CRT (Cruise Rated Thrust)		1013	--	1

---

\* Sea level standard conditions



	<u>Gross Weight</u>	<u>Fuel Pounds</u>	<u>Distance NM</u>	<u>Time Min.</u>
	45,852			
MRT (Military Rated Thrust) CLIMB AT 400 KCAS M = 0.9 to 22,500 FT	44,841	1011	32	3.8
c) CRT CLIMB TO 40,000 FT.	44,043	798	13	1.5
d) CRUISE To Launch Point minus 15 miles M = 0.9 (not required at Holloman/WSMR)	42,819	1224	102	12
e) ACCELERATE TO M = 0.95 AND CRT PULL UP TO 30° AT 45,000 FT.	41,874	945	15	1.7
f) LAUNCH	38,004			
g) CRUISE TO EDWARDS AFB, M = 0.9	36,384	1620	162	14
h) FUEL Remaining after Return to Base = 5673 Lbs.				
i) Fuel/Time Available for in-flight holding and delays - approximately 3600 lbs/40 min.				

#### 3.4.6.2 Aircraft Pull-up, Launch and Post-Launch Maneuver

The F-4 aircraft, after climbing to 40,000 ft and receiving confirmation from the range that precision radar acquisition and track are established, is vectored to an initial point from which the run-in, acceleration, final countdown and pull-up are accomplished. During the straight run-in the Aircraft Flight Path Controller issues very frequent vector commands to establish the launch azimuth properly compensated for winds aloft as they affect the entire IFLEX trajectory. Simultaneously, telemetry is checked and rocket launch circuit armed. The pull-up maneuver to 30° at M = 0.95 is initiated

at the command of the Flight Path Controller. The final count-down is initiated from the ground but is turned over to the pilot who continues the last four seconds of count, adjusting the actual release for altitude, compensating for instrument lag. The "fine-tuning" of this launch maneuver will require both training flights and dry-runs on the range. The time of actual launch separation is telemetered to the ground as is the indication of fin rotation. A single fixed correction to ignition time is computed automatically on the ground based upon the radar plot of actual release angle and attitude. The range safety officer enables ignition based upon confirmation of fin rotation and safe missile vector. The actual ignition is then ground commanded automatically. After release of the missile the F-4 executes a roll into a climbing turn to reach and hold a bank angle of approximately 90 degrees until past the point of maximum altitude. The purpose of this post-launch maneuver is to achieve maximum separation between aircraft and missile and to avoid exceeding 50,000 feet aircraft altitude. Figure 22 shows the relative flight paths of F-4 aircraft and IFLEX missile after missile release up to the point of ignition (for a 22 second ignition). The peak altitude reached by the aircraft is 48,306 feet and aircraft-to-missile separation at ignition is approximately 1.15 nautical miles.

#### 3.4.7 Flight Operations

Based upon discussions with test personnel at Edwards AFFTC and Eglin AFAL, an estimate of the types and number of flight operations for the IFLEX program has been made as follows:

- Staging Flights

These flights are for launch aircraft and photo aircraft from Eglin AFB to Holloman AFB. They would not be required for operations out of Edwards AFB at the Tonapah Test Range. Four (4) flights

RELATIVE FLIGHT PATHS  $\gamma = 30^\circ$

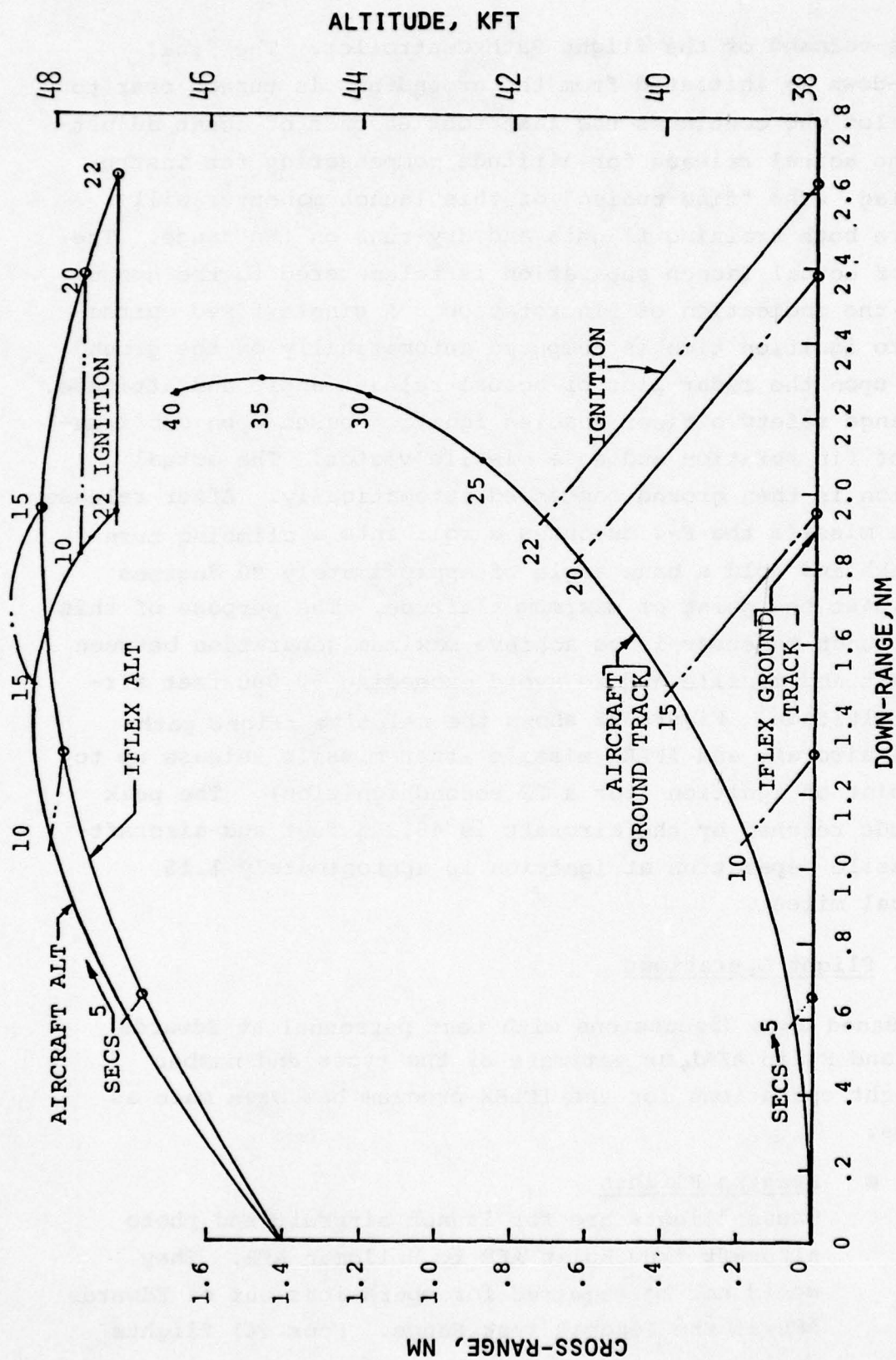


FIGURE 22. Aircraft/IFLEX Post Launch Separation



(2 Flights/2 Aircraft); 3 hours each; 12 hours total.

- Training and Familiarization Flights

These flights are for developing a precision launch maneuver through practice of the Project Pilot and Aircraft Flight Path Controller on the flight test range. Two flights (1 transponder equipped F-4); 2 hours each; 4 hours total.

- Dry Run Flights

One dry run operation is planned for each of the four launches to rehearse all aspects of loading, arming, telemetry and range radar and photo-theodolite acquisition and track. It is possible that a repeat dry run would be required on early launches, however, the dry run may be foregone on the third or fourth launch. Four flights (IFLEX modified F-4 aircraft); 2 hours each; 8 hours total.

- Live Launch Operations

Four live launches are planned. Based upon range experiences, two back-up flight operations are planned with Launch aircraft and Photo Chase. Twelve Flights (6 Flights/2 Aircraft); 1.5 hours each; 18 hours total.

- Summary

The total number of flights planned is 22 (Eglin support) or 18 (Edwards support). The total number of flight hours planned is 42 (Eglin support) or 30 (Edwards support). All dry run and live launch operations require unrestricted visibility from ground to launch altitude. Training flights could be conducted under more restricted visibility conditions at the option of the pilot.

### 3.5 Flight Range Requirements

Based upon liaison conducted by SAI with test personnel at Tonapah Test Range, Nevada, White Sands Missile Range, New Mexico and Air Force Armament Test Lab, Eglin AFB, Florida together with the technical requirements of the IFLEX experiment, the following range requirements for the IFLEX program are outlined. It is believed that the requirements can be realized either at the Tonapah Test Range or White Sands Missile Range. Final determination of the test site is a project function under the cognizance of the 3246<sup>th</sup> Test Wing at Eglin Air Force Base, Florida.

#### 3.5.1 Impact Safety Requirements

The estimated foot print of IFLEX at impact on the range is based upon uncertainties in contributing factors tabulated below and upon the actual launch experience from the FLAME program. It should be noted that dispersion in range is primarily sensitive to variations in aircraft launch speed and direction. Dispersion cross-range is primarily sensitive to aircraft velocity direction and uncompensated cross-wind. Careful training and coordination between the Pilot and Aircraft Flight Path Controller, together with post launch ignition time compensation, should reduce uncertainties below those tabulated. Actual flight experience during FLAME confirms this expectation.

- IFLEX Error Sources Contributing to Impact Dispersion

<u>PARAMETER</u>	<u>STANDARD DEVIATION</u>
Wind	5-Knot Cross Wind Uncompensated
Coast Time	0.2 sec.
Pedro Thrust Misalignment	0.07 deg.
IFLEX Fin Misalignment	0.10 deg.
Pedro Thrust at Constant $I_{sp}$	1.5%
Pedro Burn Time	0.26 sec.

<u>PARAMETER</u>	<u>STANDARD DEVIATION</u>
IFLEX Drag	5%
IFLEX Stage Inert Weight	0.7%

● Estimated IFLEX Dispersion

The one sigma dispersion resulting from IFLEX error sources are tabulated below and plotted on Figure 23.

	<u>STANDARD DEVIATION</u>	
	<u>RANGE (ft)</u>	<u>CROSS (ft)</u>
Position at Beginning of Maneuver	707	707
Response Time Rotating (1 sec)	1,442	-
Position at Release (1.5° Pitch & Yaw)	1,566	783
Altitude at Release (250 ft)	902	-
Aircraft Speed (24.2 fps)	9,257	-
Velocity Direction (0.5° Pitch & Yaw)	4,584	1,809
1.5° Pitch A of A	532	212
1.5° Yaw A of A	1,302	519
Separation Pitch Rate (5 deg/sec)	607	86
Separation Yaw Rate (5 deg/sec)	181	87
.2 sec Coast Time	2,952	-
Pedro Thrust Misalignment	820	327
IFLEX Fin Misalignment	164	65
Pedro Thrust	683	-
Pedro Burn Time	1,060	-
IFLEX Drag	1,399	-
Pedro Inert Weight	153	-
Wind 5 Knot Uncompensated	<u>163</u>	<u>1,112</u>
RSS Dispersion	11,305	2,463

### 3.5.2 Meteorological Data

In order to correlate missile velocity data with Mach number and dynamic pressure, the best attainable data on temperatures, pressures, and humidity from sea level up to 50,000



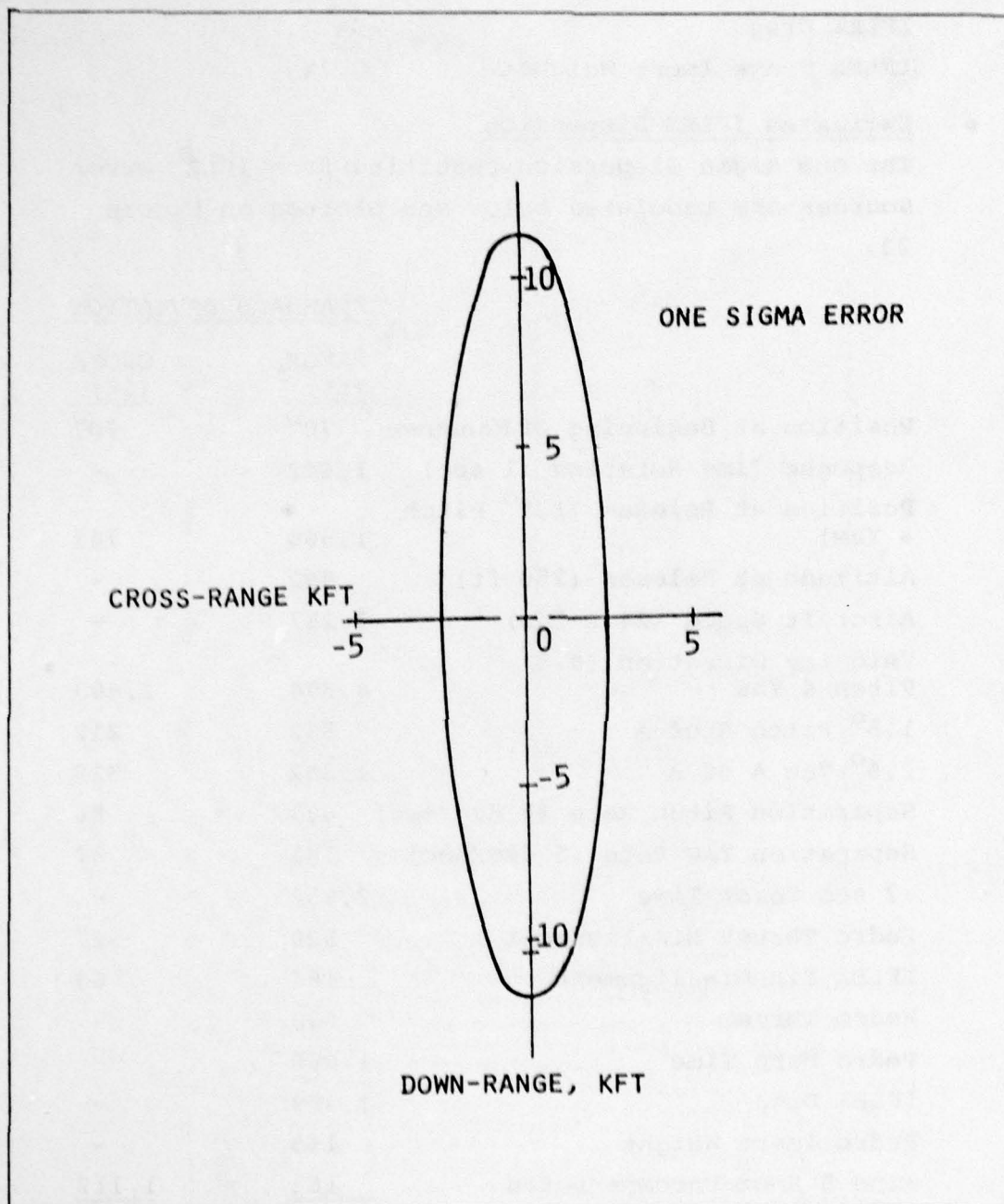


FIGURE 23. Estimated IFLEX Footprint

feet are required. Also, in order to compensate for winds aloft and reduce missile dispersion, accurate wind aloft measurements should be reported to the project prior to missile launch.

#### 3.5.3 Test Range Radar

Real time radar acquisition and track of the launch aircraft is required such that precision voice vectoring to the launch point may be accomplished. A radar plot of the missile trajectory is also required. Both launch aircraft and missile will be equipped with C-Band transponders.

#### 3.5.4 Photo-Theodolite Coverage

Photo-Theodolite coverage of the IFLEX from launch separation throughout the trajectory down to a pressure altitude of 5,000 feet is required as a primary basis for assessing velocity and altitude and a secondary basis for angle of attack and roll rate. Photographic coverage is also required, along with range timing for documentary purposes. The IFLEX missile has a stainless steel nose, and an amber colored body. Paint may be applied to three of the fins. It may be expected to burn-off a few seconds after ignition however.

#### 3.5.5 Range Telemetry

Range telemetry is required in L-Band (1.455-1.540 GHz) for all dry runs and launches. Reliable reception down to an altitude of 5,000 feet is required. In addition, provisions for performing telemetry ground checks is required. This may be a range function, a function of the aircraft support base, or a combination of these. The details of the IFLEX telemetry system are described in Section V.

#### 3.5.6 Recovery Operations

IFLEX will impact the surface at a velocity of approximately 1,500 fps and at an angle of 35 degrees from the

horizontal. Impact point projection and recovery of the broken fragments of the structure is desirable if practicable.

### 3.5.7 Data Requirements

The IFLEX project will require the following data to be delivered by the range:

1) A magnetic tape record of all telemetry data received for all launches. This magnetic tape data will include the telemetry data stream, base stream, base timing, vehicle position coordinates if possible and any audio communication between aircraft and ground control. This data will be recorded on a wide-band magnetic tape recorder.

2) All IFLEX flight telemetry data will be decoded so that the 250 quasi-steady state and three fluctuating pressures are annotated by data source, time, and amplitude (by percentage of full scale). This data will be in the form of a formatted computer compatible digital tape.

3) The trajectory plots with timing require a one sigma accuracy of  $\pm 25$  fps in velocity and  $\pm 50$  feet in altitude. This gives less than a 2 percent change in heating rate. Angle of attack and roll angle accuracy of 5 degrees at a minimum is required. Greater accuracy would be desired if the cost to obtain it does not increase.



## SECTION IV

### INTERFERENCE FLOW EXPERIMENT DEFINITION

The Interference Flow Flight Experiment (IFLEX) will investigate three-dimensional shock wave/boundary layer interference induced heat transfer phenomena at high Mach and Reynolds numbers. Surface heat transfer and pressure measurements will be made on the clockwise side (looking aft) of a stabilizer fin on the IFLEX vehicle. Instrumented panels will be imbedded in the fin and fuselage surfaces, where the shock from the fin leading edge interacts with the boundary layer on the aft body. The approximate geometry of this interference flow region was illustrated by the oil flow photograph in Figure 2. The placement of instrumentation on the IFLEX vehicle is illustrated in Figure 24.

Localized regions of high pressure and high aerodynamic heating in the vicinity of the fin shock intersection with the body have been found in wind tunnel and flight environments. The maximum amplification of pressure and heat transfer on the body have been found to scale with an interaction strength parameter,  $M_\infty \sin \theta_s$ , where  $\theta_s$  is the angle of the fin shock wave. The spatial extent of the interaction depends on the fin shock wave angle and the boundary layer thickness. The peak pressure and peak aerodynamic heating occur along a nearly constant angle ray from the fin leading edge. The ray angle has been correlated to the fin and shock wave angles by Token (Reference 13).

The instrumentation distribution for IFLEX has been selected to provide measurements of pressures and heating rates in the vicinity of the fin shock wave as its angle and location varies during a flight. The locus of peak pressure and heat transfer will sweep across the gauge locations illus-

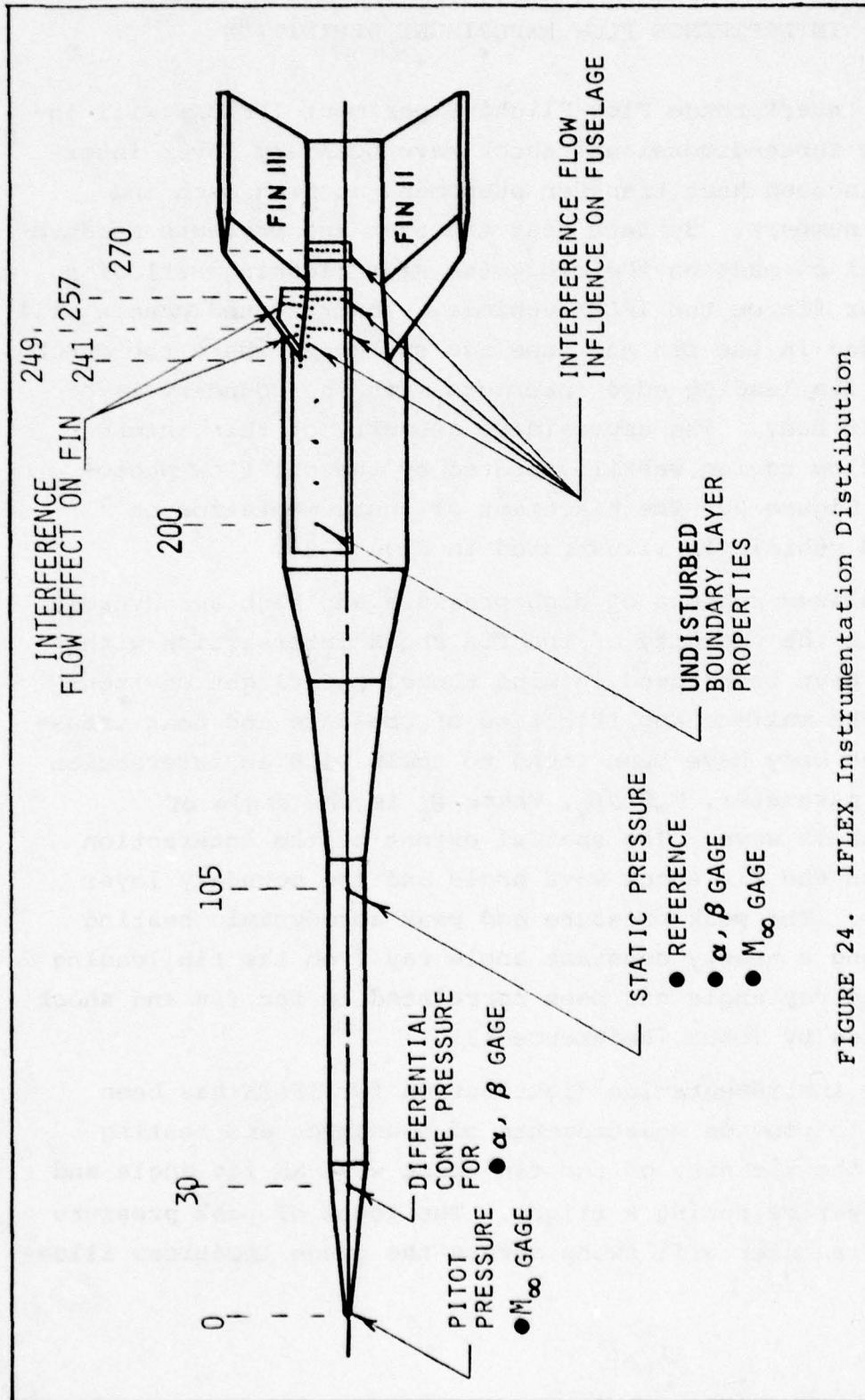


FIGURE 24. IFLEX Instrumentation Distribution

trated in Figure 24 as the shock angle changes during a flight. The measurements illustrated will result in heat transfer and pressure distribution characterization across the interference flow region, over a wide range of Mach numbers in the flight environment.

IFLEX pressure and heat transfer measurements will be made on metallic surfaces which experience variable temperatures during flight. This full-scale, flight environment data will be compared with ground test simulation data and used to extend existing correlations to Reynolds number and wall temperature scales characteristic of flight. The flight performance of IFLEX is compared to the existing ground test data base, described in Reference 3, in Figure 25. The Reynolds number range of IFLEX is seen to exceed the simulation achieved in existing ground test facilities by more than one order of magnitude. Both the wall and recovery temperature vary such that their ratio also varies throughout the flight, as described below in Section 4.3. At launch the temperature ratio is near one. The wall has attained the adiabatic equilibrium temperature while the aircraft delivers IFLEX to its launch altitude. During acceleration, the rate of increase of recovery temperature greatly exceeds the rate of increase of the wall temperature. This results in a minimum temperature ratio of about  $T_w/T_r \approx 0.25$  on a trajectory with a peak Mach number of six. The variation of temperature ratio with time reverses after burnout. The Mach number decreases much faster than the wall temperature decreases. Near ground impact the temperature ratio approaches one. For some of the longer duration and/or higher Mach number flights, the temperature ratio exceeds one near ground impact.

An objective of the IFLEX program is to provide data on interference flow induced aeroheating and loads for use in advanced hypersonic flight vehicle design. Consequently, the measurements made on IFLEX must be adequate to provide for



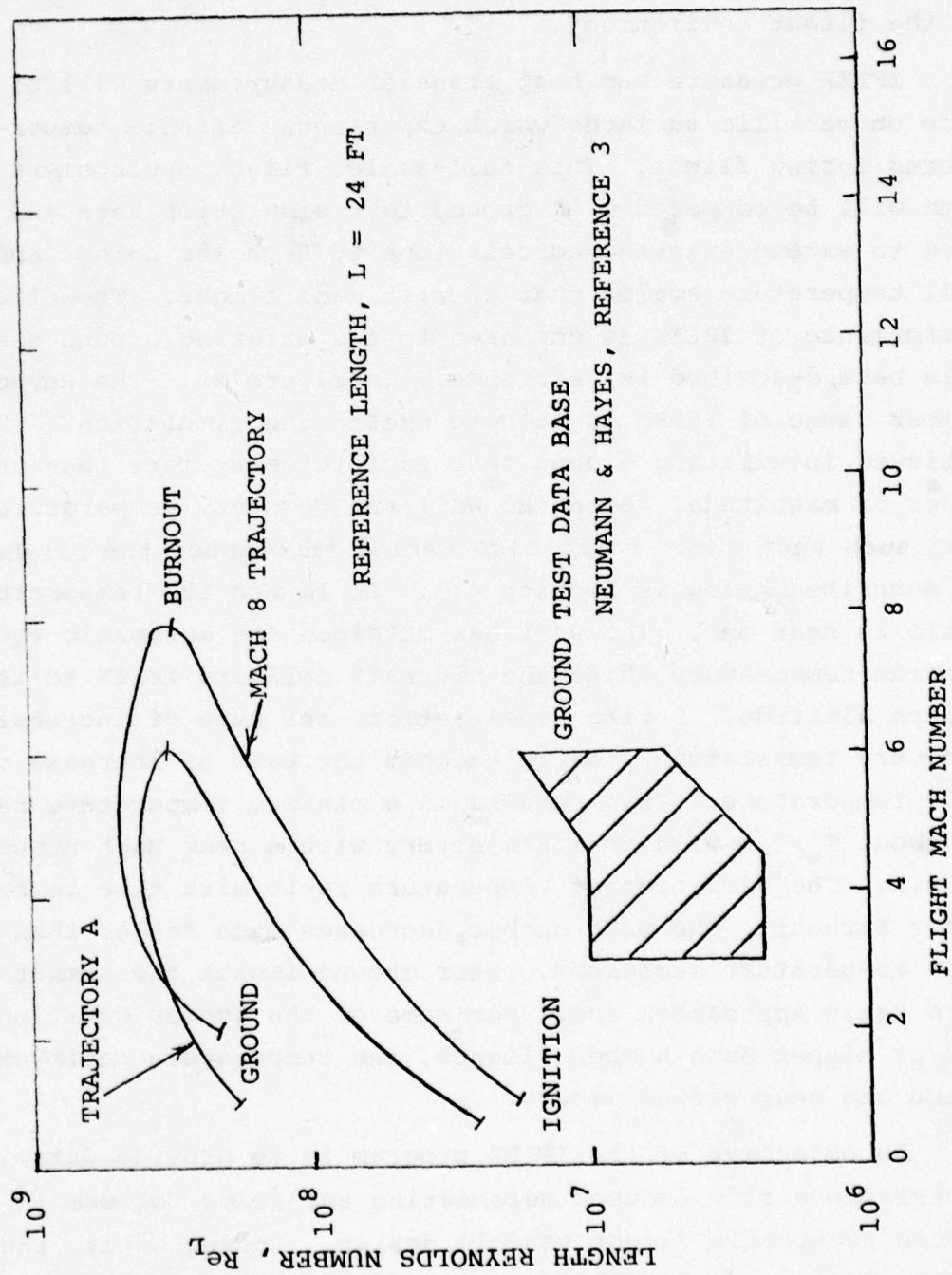


FIGURE 25. IFLEX Flight Test Simulation Regime (Maximum Capability)

scaling aeroheating and pressure distribution parameters to other configurations and similar environments. Fluctuating pressures are of interest since the shock wave induced flowfield variations may be unsteady in time with high energy oscillations of the associated pressure field. This is known to be the case in separated flows and significantly influences aeroelastic and equipment vibration environment specifications in high dynamic pressure environments. In general, this requires the definition of Stanton Number, pressure coefficient, and fluctuating pressure coefficient, with these scaling parameters all normalized by appropriate local flow conditions. The reduced parameters required are:

$$S_{t_o} = \frac{\dot{q}_w}{\rho_o V_o c_p (T_r - T_w)} \quad (3)$$

$$C_{p_o} = \frac{p - p_o}{\frac{1}{2} \rho_o V_o^2} \quad (4)$$

$$C'_{p_o} = \frac{p' - p_o}{\frac{1}{2} \rho_o V_o^2} \quad (5)$$

In each case above, the subscript, o, refers to conditions in the undisturbed flow upstream of the interference phenomena. The axisymmetric geometry of the IFLEX vehicle, upstream of the fin-body interference flow region, provides for reasonably accurate calculation of the reference flow conditions which are not significantly influenced by the boundary layer. Through use of the several available computational solutions of the inviscid flow governing equations, the density,  $\rho_o$ ; velocity,  $V_o$ ; and undisturbed pressure,  $p_o$ , can be calculated. Typical calculation capabilities are those described in References 11 and 14. In order to make these calculations, flight Mach number and angle of attack, as well as free stream pressure and temperature, must be known.

The IFLEX vehicle will carry instrumentation for measuring each of the other quantities, except recovery temperature,

$T_r$ , and specific heat,  $c_p$ , which is a gas property . Continuing consideration has been given to the design of a recovery temperature measurement. However, no method of proven reliability has been devised at this stage in the IFLEX program design. It is generally accepted that recovery temperature, for turbulent boundary layer conditions, can be estimated from the assumption of a recovery factor in the range  $r=0.89\pm0.05$  from the definition

$$T_r = T_o + r \frac{v_o^2}{2c_p} \quad (6)$$

To contribute to the accuracy of the Stanton number derivation, a recovery temperature measurement would have to be more accurate than this estimate.

At each of 50 measurement locations, static pressure, heat transfer rate and wall temperature will be measured on IFLEX. Pressure fluctuations will be measured at three independent locations by high frequency response transducers. The vehicle attitude relative to the velocity vector will be monitored through two measurement methods. On-board accelerations will be measured in three axes and differential pressures on the forecone will provide the independent attitude measurements. Mach number will be determined from a set of on-board pitot and static pressure measurements, as well as from ground based radar and optical velocity and position traces combined with previously sampled and correlated atmospheric temperature data. The pressure and heat transfer rate measurements, in conjunction with the reference quantities deduced as described above, will provide the spatial distribution of  $S_{t_o}$ ,  $C_{p_o}$ , and  $C'_{p_o}$  in the interference flow region, as well as in control locations outside the interference flow region.

As described in Section VI, the IFLEX vehicle heatshield is an epoxy based insulator material which undergoes phase change resulting in outgassing and some surface flow at



very high enthalpy and shear levels. Estimates of ablation products concentration for the nominal IFLEX Trajectory A, with a maximum Mach number slightly higher than  $M_\infty=6$  have been made. These indicate order of one percent ablation products mass concentration in the boundary layer at peak heating. Some surface roughness might also be expected to result from ablation. To minimize these heatshield effects on the interference flow measurements, the measurements will be made on three steel plates imbedded in the heatshield. Two of these plates are located on the aft cylinder and one is located on the fin, as illustrated above in Figure 24.

An objective of integrating the metallic plates in the heatshield is to provide sufficient running length upstream of the instrumentation to allow the boundary layer flow properties profile to adjust to the metallic plate wall temperature. Ideally, the length of the plate upstream of the experiment should be sufficient for the thermal and velocity profiles to relax from the hotter and relatively rough insulator skin boundary condition to the steel skin which is cooler and relatively smooth. There is some controversy in the literature over the required relaxation length. Experiments described in Reference 16 indicate that 10 times the boundary layer thickness is adequate. In opposition, data and calculations described in Reference 17 indicate that a length of 40 to 60 times the boundary layer thickness is required, and some residual influence may exist at twice that distance. On the IFLEX vehicle, the forward plate on the cylinder extends more than 20 times the boundary layer thickness upstream of the interaction. Forward of this, the boundary layer is not in dynamic equilibrium because of the rapid compressions and expansion experienced in the conical frustum region, illustrated above in Figure 24. Measurements on the aft plate will undoubtedly be influenced by the variations in wall properties upstream. A quantitative analysis of this influence will be required in flight data analysis.

During the IFLEX design study, consideration was given to more direct measurements for characterizing the boundary layer. These included boundary layer pitot-pressure surveys, recovery temperature measurements and skin friction measurements. However, the incorporation of apparatus for making these measurements introduces additional potential failure modes for the TPS. The additional design analysis and ground test required to reduce the associated failure probabilities is beyond the scope of the planned IFLEX program.

The measurement requirements employed to select and integrate the IFLEX instrumentation are described in the following paragraphs. This section is concluded with a discussion of approaches to data interpretation. The selection and definition of instrumentation and electronics, required to make the measurements in flight and recover the data, are described in Section V.

#### 4.1 INSTRUMENTATION RESPONSE REQUIREMENTS

The measurement requirements for IFLEX flights are similar to those in wind tunnel testing under transient conditions such as in a shock tube or hot shot tunnel. The measurements include those required to monitor flight conditions, which are analogous to flow conditions and model attitude in the wind tunnel. The transient nature of the IFLEX simulation has several time scales. Reynolds number is changing at a relatively slow rate during the experiment, due to velocity and altitude variations. The rate of variation in Mach number during the flight reaches a peak during boost acceleration as illustrated in Figure 26. The rate of change in heat transfer rate follows this profile as illustrated in Figure 27. The wall temperature variation, indicated in Figure 27, is slower due to conduction effects. The pitot pressure history, indicated in Figure 28, follows the Mach number profile. The histories of these parameters are shown



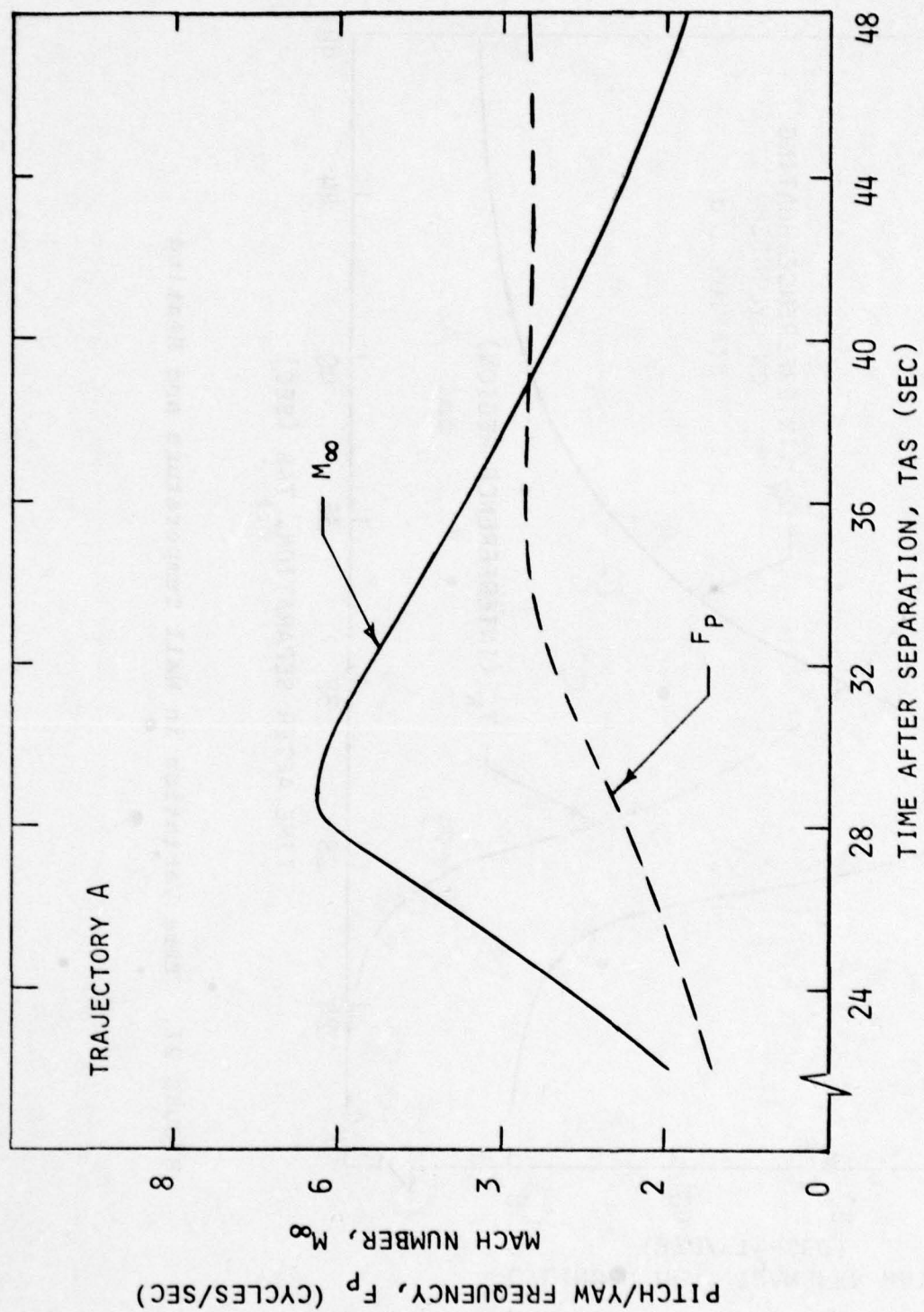


FIGURE 26. Time Variation in Mach Number and Pitch Frequency



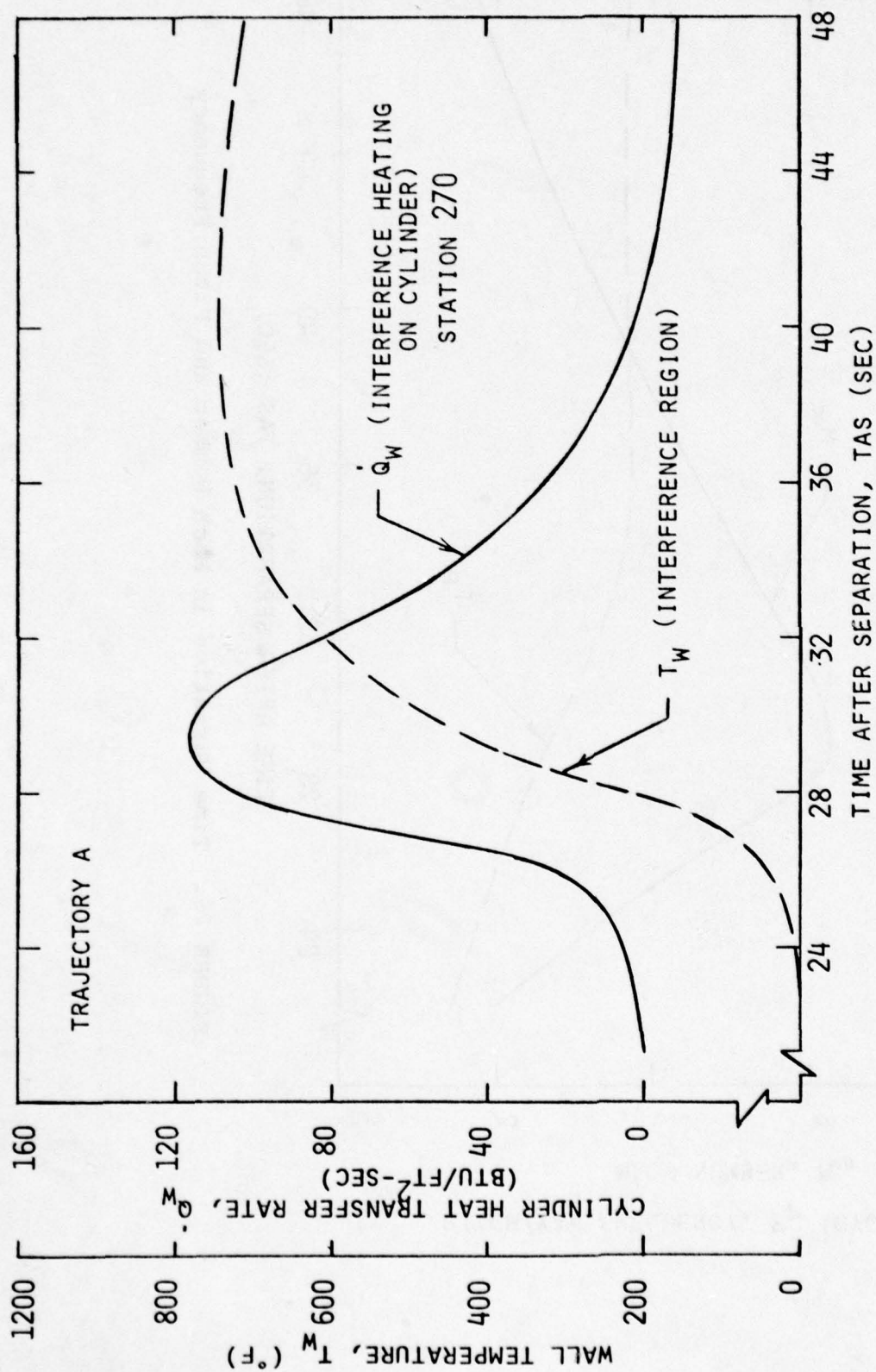


FIGURE 27. Time Variation in Wall Temperature and Heating

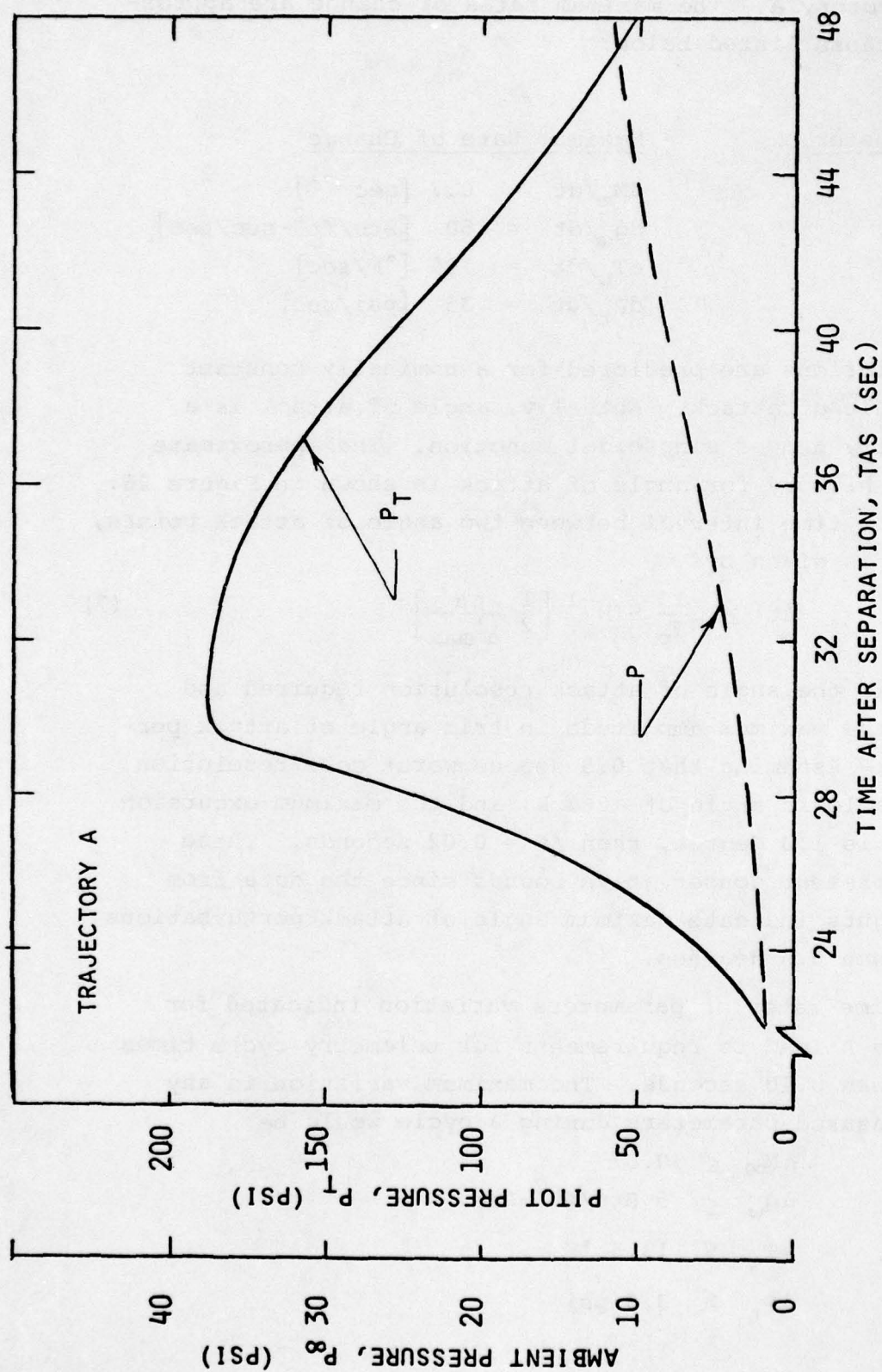


FIGURE 28. Time Variation in Pitot and Ambient Pressure

for Trajectory A. The maximum rates of change are approximately those listed below:

<u>Parameter</u>	<u>Maximum Rate of Change</u>
$M_\infty$	$dM_\infty/dt = 0.7 \text{ [sec}^{-1}\text{]}$
$\dot{q}_w$	$d\dot{q}_w/dt = 50 \text{ [Btu/ft}^2\text{-sec/sec]}$
$T_w$	$dT_w/dt = 135 \text{ [}^\circ\text{F/sec]}$
$P_t$	$dP_t/dt = 35 \text{ [psi/sec]}$

These variations are predicted for a nominally constant (zero) angle of attack. Actually, angle of attack is a very lightly damped sinusoidal function. The approximate frequency history for angle of attack is shown in Figure 26. The minimum time interval between two angle of attack points,  $\Delta\alpha$  apart, is given by

$$\Delta t \geq \frac{1}{\pi F_p} \sin^{-1} \left[ \frac{1}{2} \frac{\Delta\alpha}{\alpha'_{\max}} \right] \quad (7)$$

where  $\Delta\alpha$  is the angle of attack resolution required and  $\alpha'_{\max}$  is the maximum amplitude in trim angle of attack perturbation. Assuming that 0.5 degree worst case resolution is acceptable in angle of attack, and the maximum excursion from trim is 1.0 degree, then  $\Delta t = 0.02$  seconds. These should represent conservative bounds since the data from FLAME flights indicate maximum angle of attack perturbations smaller than 0.5 degrees.

The time rates of parameters variation indicated for Trajectory A lead to requirements for telemetry cycle times shorter than 0.10 seconds. The maximum variation in any of the measured parameters during a cycle would be:

$$\begin{aligned} \Delta M_\infty &\leq 0.07 \\ \Delta \dot{q}_w &\leq 5 \text{ Btu/ft}^2\text{-sec} \\ \Delta T_w &\leq 13.5 \text{ }^\circ\text{F} \\ \Delta P_t &\leq 3.5 \text{ psi} \end{aligned}$$



While faster cycle times may be desirable, it is doubtful that response capabilities of available instrumentation would be fast enough to derive benefit from attaining them. The telemetry system selected cycles approximately twice this fast, as described in Section V.

The fundamental response requirement for all instrumentation is that each measurement sampled during a data cycle reflects the magnitude, during the data cycle, of the quantity measured. The on-board angle of attack and Mach number measurements will associate flow conditions with each set of measurements recorded over a time interval of approximately 0.05 seconds. Consequently, instrumentation should respond in a time interval comparable to that cycle time. As will be discussed in Section V, which describes the instrumentation selection, the rapid response requirement and the requirement to survive the severe thermal environment are conflicting. In general, rapid response instruments tend to be more fragile.

#### 4.2 PRESSURE MEASUREMENT REQUIREMENTS

There will be 63 quasi-static pressure measurements made on the IFLEX vehicle. Two sets of static pressure measurements, undisturbed surface pressure and interference flow induced pressures, are associated with the experiment. The remaining three sets of surface static pressure, differential pressure and pitot pressure measurements are associated with the determination of angle of attack and Mach number. In addition to the quasi-static measurements, there will be three fluctuating pressure measurements. Two of these will be in the interference flow region and one will be in the undisturbed flow.

On a nominal trajectory, the undisturbed surface pressure on the aft cylinder is approximately the level of the ambient static pressure. This level is indicated, for Trajectory A, in Figure 29. The range of pressures anticipated is 2-15 psi.

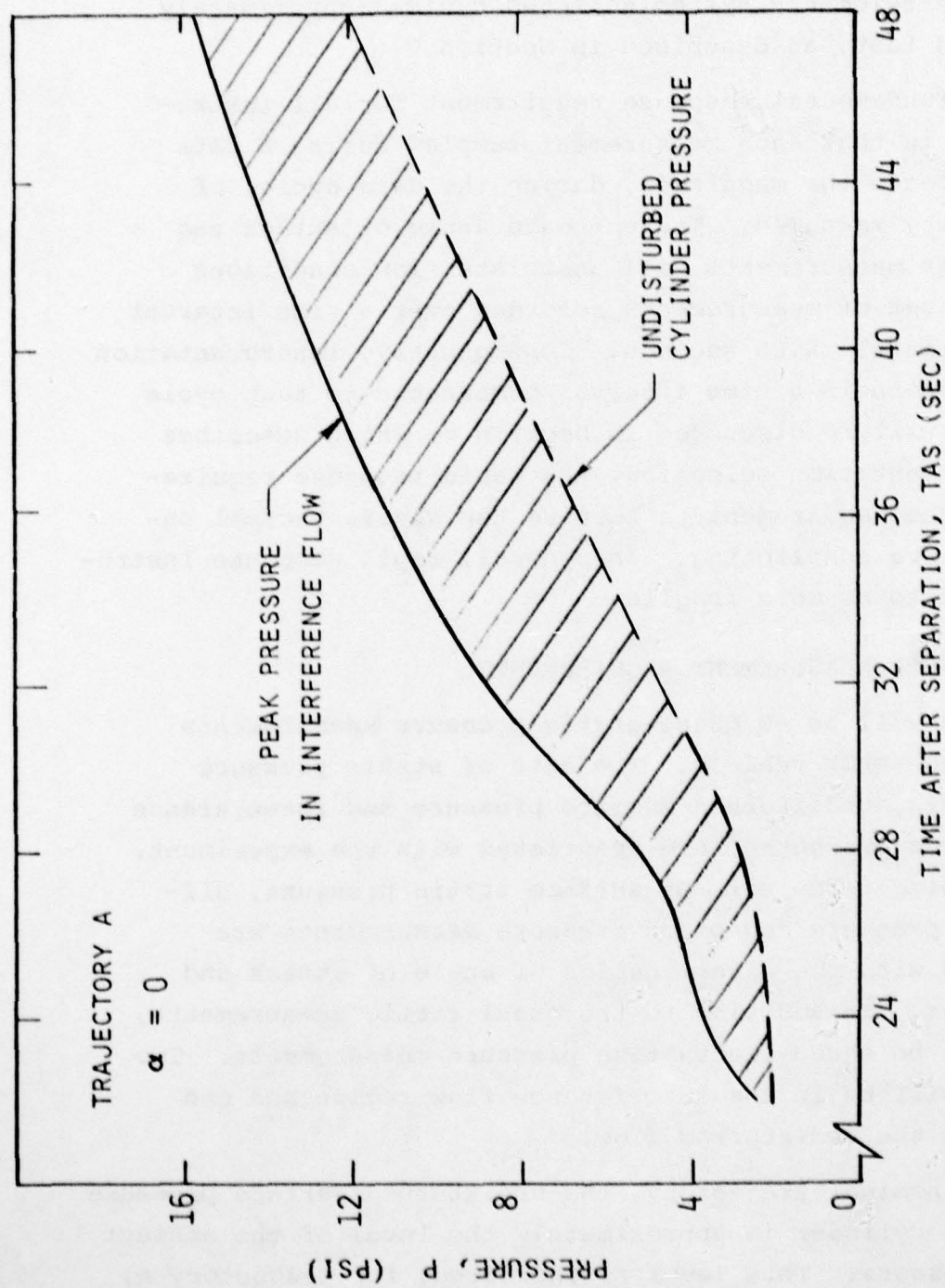


FIGURE 29. Nominal Interference Flow Pressure Levels



Peak pressure in the interference flow region on the aft cylinder is also illustrated in Figure 29. The principal objective of pressure measurements on IFLEX is to measure the difference between these pressures and to resolve the spatial variation of the pressure gradient between them. Since the maximum difference is approximately 4 psi, it is necessary to resolve pressure differences of less than 0.5 psi to accomplish the IFLEX objectives. The maximum pressures expected in the interference flow region are those on the fin wedge surface. These are illustrated for the nominal zero angle of attack and for 5 degree angle of attack perturbation, in Figure 30. The combination of requirements for pressure measurements in the interference flow region indicates a gage specification to provide:

Maximum Scale = 25 psi  
Resolution =  $\pm 0.25$  psi  
Response Time = 0.05 seconds

The angle of attack measurement system requires the measurement of quasi-static pressure levels on the forecone and forward cylinder of the IFLEX vehicle at 90 degree intervals about the periphery. In addition, differential pressures between the 180 degree opposing measurement pairs are to be measured in each case. The use of this data, with a pitot pressure to be measured, to derive angles of attack and sideslip is described in Section 4.5. These measurements will be made, at station 30 on the forecone and station 105 on the forward cylinder, on the geometry illustrated in Figure 3. The pressure levels at these stations are approximately cone pressure and free stream pressure, respectively, as indicated in Figure 14. The history of cone pressure level at the nominal (zero) trim angle of attack is illustrated in Figure 31. Also illustrated is the pressure difference due to 1 degree perturbation in angle of attack. For the system to resolve 0.5 degrees angle of attack, half this difference



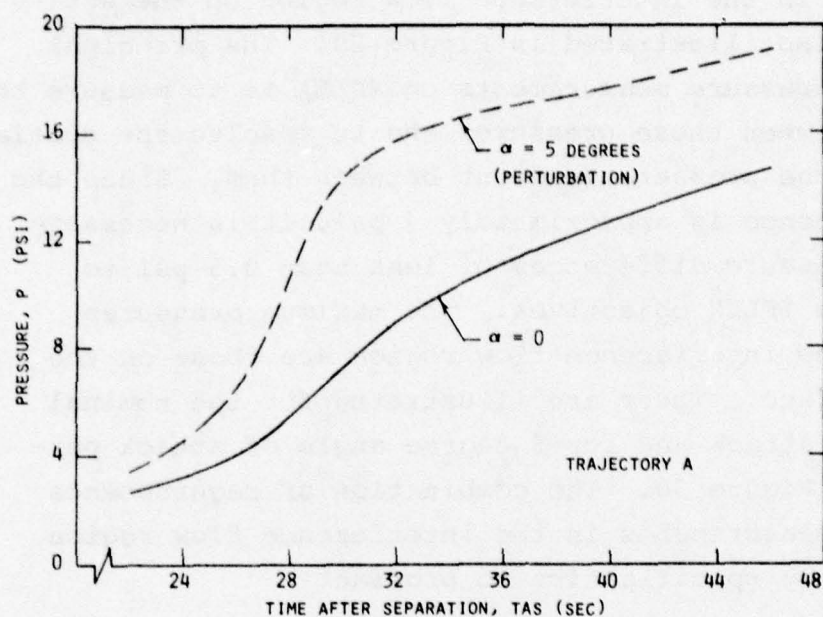


FIGURE 30. Fin Pressure Levels

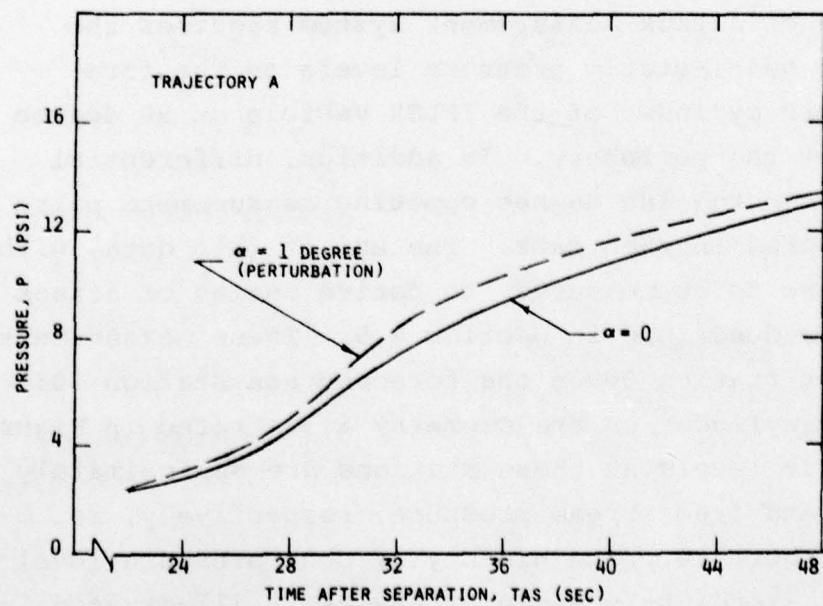


FIGURE 31. Cone Pressure Levels

of approximately 0.5 psi must be accurately resolved. These requirements are essentially those specified for the interference flow region quasi-static pressure gauges, above. In addition, the differential pressures should be accurately resolved to less than 0.25 psi.

The quasi-static pitot-pressure gage to be mounted in the nosetip is principally a Mach number measurement device. The scale for the gage is indicated by the nominal pitot pressure history illustrated in Figure 28 above. Maximum measurements approaching 300 psi should be accommodated, to provide off-nominal high Mach number resolution. A 25 psi error in pitot pressure at maximum Mach number corresponds to an error in implied Mach number of  $M_\infty = 0.5$ . Therefore, 2 to 5 percent of the 300 psi full scale pressure would provide adequate accuracy and resolution for this gauge.

Fluctuating pressure measurements will be made in two locations within the interference flow region and at a control location on the aft cylinder, outside the interference region. There is only limited information available to provide instrumentation selection criteria for these measurements. The criteria derived have been based on measurements reported in Reference 18 for two-dimensional shock/boundary layer interactions.

In Reference 18, Holden reports rms pressure fluctuations levels of 0.002 times the freestream dynamic pressure for attached turbulent boundary layers, and levels as high as 0.2 times the freestream dynamic pressure near reattachment in separated regions. Power spectrum of pressure and skin friction fluctuations indicate a peak power at a frequency corresponding to a Strouhal number of order  $10^{-3}$  (frequency non-dimensionalized by freestream velocity and boundary layer momentum thickness). The spectrum of the pressure fluctuation

near reattachment for a separation caused by a strong shock ( $M = 8.6$  and  $\theta_s = 20$ ) is shown in Figure 32. The absolute pressure scale is an interpretation of Holdens data giving an overall rms fluctuation of approximately 0.1 times the maximum freestream dynamic pressure for IFLEX Trajectory A. This large amplitude is characteristic of reattachment pressures in two-dimensional separated flows. It therefore is believed to represent a conservative upperbound for IFLEX interference flow where boundary layer separation is not anticipated. The frequency scale, which was also established using IFLEX maximum dynamic pressure conditions, indicates that the peak pressure fluctuation occurs at a few hundred Hertz.

In order to detect large scale fluctuations such as these, if they are experienced, the requirements for the fluctuating pressure gages in the interference flow region are: 1) the absolute pressure range is 0.2 to 20 psi, and 2) the frequency band width is 50 to 5000 Hz.

#### 4.3 HEAT TRANSFER MEASUREMENT REQUIREMENTS

Heat transfer rates will be measured in three environments on IFLEX. These measurements will be made on steel plates on the aft cylinder and on the fin. Locations of these plates are illustrated in Figure 24. One environment is on the fin surface at the base; the second is in the interference flow region on the cylinder; and the third is on the cylinder upstream of the interference flow region. The history predicted for these three levels is illustrated, for Trajectory A, in Figure 33. The critical heating rate measurement resolution involves the definition of the gradient in the region between the peak interference heating and the undisturbed surface heating on the cylinder. The maximum rise in that increment is approximately 60 BTU/FT<sup>2</sup>-sec. Late in the trajectory this difference is predicted to be



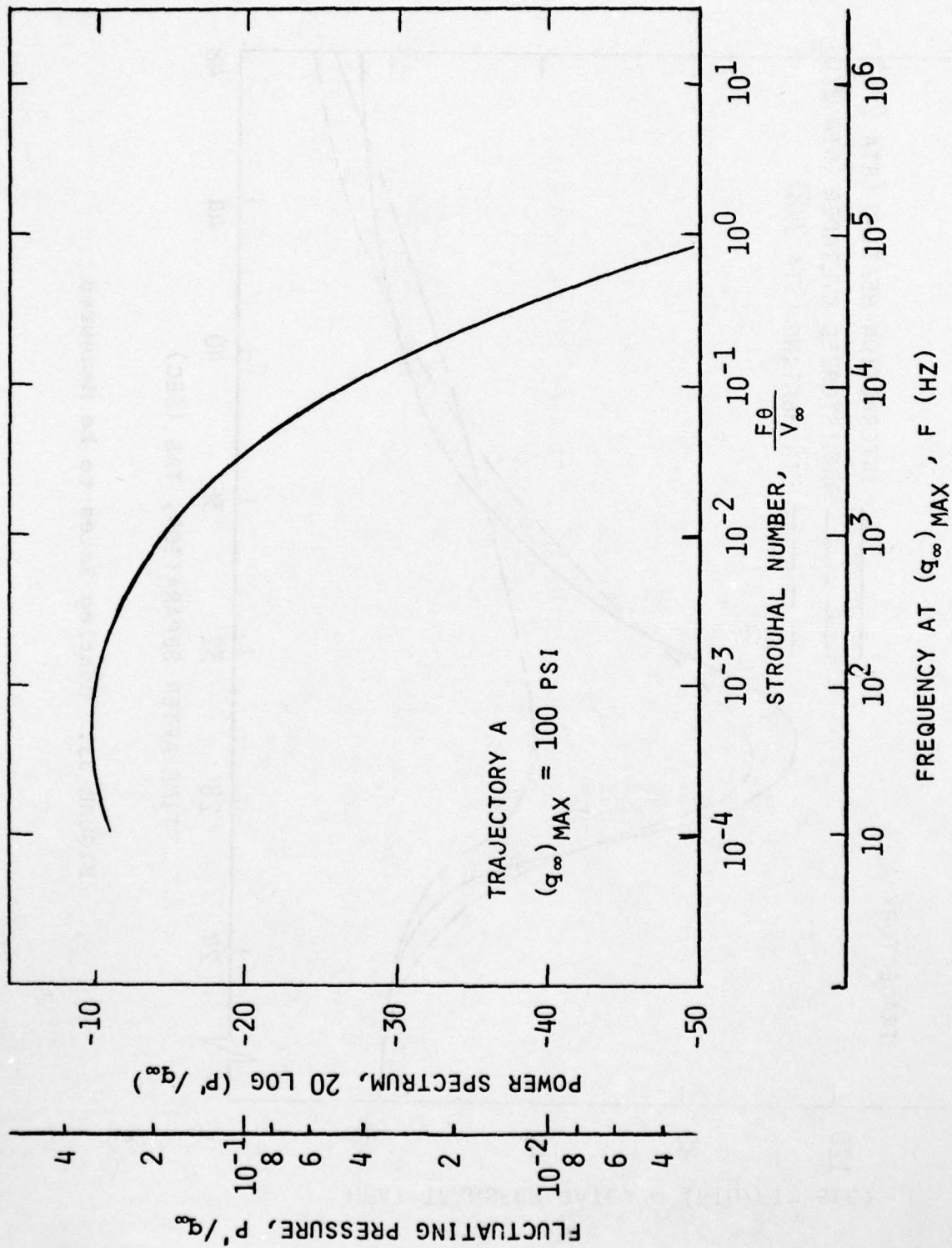


FIGURE 32. Fluctuating Pressure Scaling At Separated Boundary Layer Reattachment

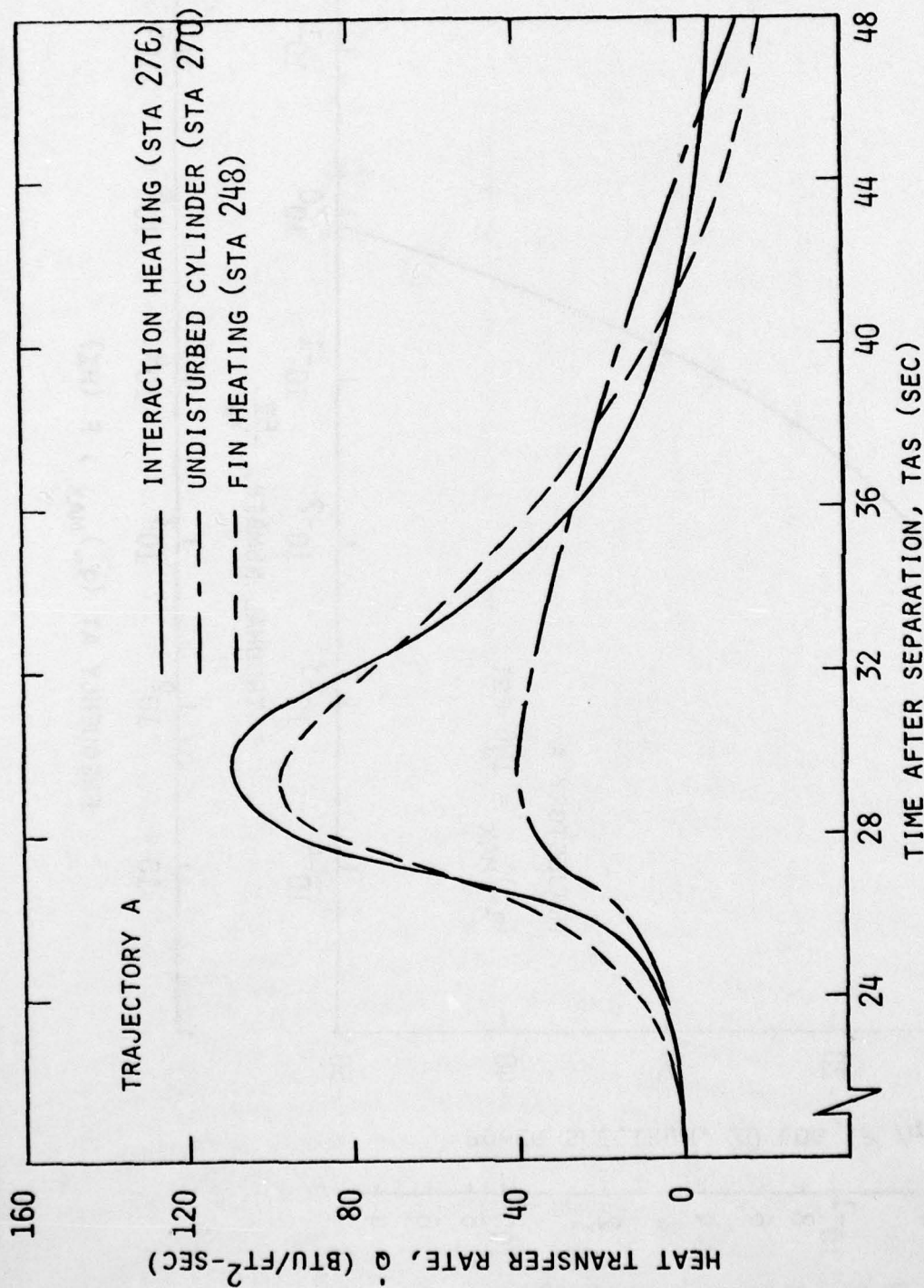


FIGURE 33. Heating Rates to be Measured

very small, with the heating rate in the interference flow region actually falling below that in the undisturbed flow. This is a result of higher wall to recovery temperature ratio in the interference flow region than in the undisturbed flow. The results shown in Figure 33 do not reflect the effects of lateral heat conduction through the 0.2 inch skin, so the effects of wall temperature differences are probably exaggerated at a fixed time point. The corresponding surface temperatures are shown in Figure 34.

Adequate definition of the gradients in heat transfer rate in the interference flow region appears to require a minimum measurement resolution of approximately  $5 \text{ BTU/FT}^2\text{-sec}$ . Accuracy to 1/5th that level would be desirable. On the fin, and in the interference flow regions, capability to measure heat transfer rates up to  $150 \text{ BTU/ft}^2\text{-sec}$  is required. In the undisturbed flow region, full scale capabilities of  $60 \text{ BTU/FT}^2\text{-sec}$  will be sufficient.

As discussed previously, the accuracy of estimation of Stanton number from measured heat transfer rates is limited by the accuracy with which wall-to-recovery temperature ratio can be determined. Consequently, wall temperature measurements are required if IFLEX heat transfer data is to be compared with data from other flight environments.

The wall surface temperature measurement requirements are defined in scale and response rate by the temperature histories illustrated in Figures 34 and 35. The capability to measure wall temperature up to  $1000^\circ\text{F}$  is required. Resolution of temperature differences of approximately  $10^\circ\text{F}$  would be desirable.

Calculations, described in Section VI, indicate the maximum difference between surface and backface temperatures on the 1020 steel plate selected for instrumentation mounting is approximately  $100^\circ\text{F}$ . Consequently, the wall-



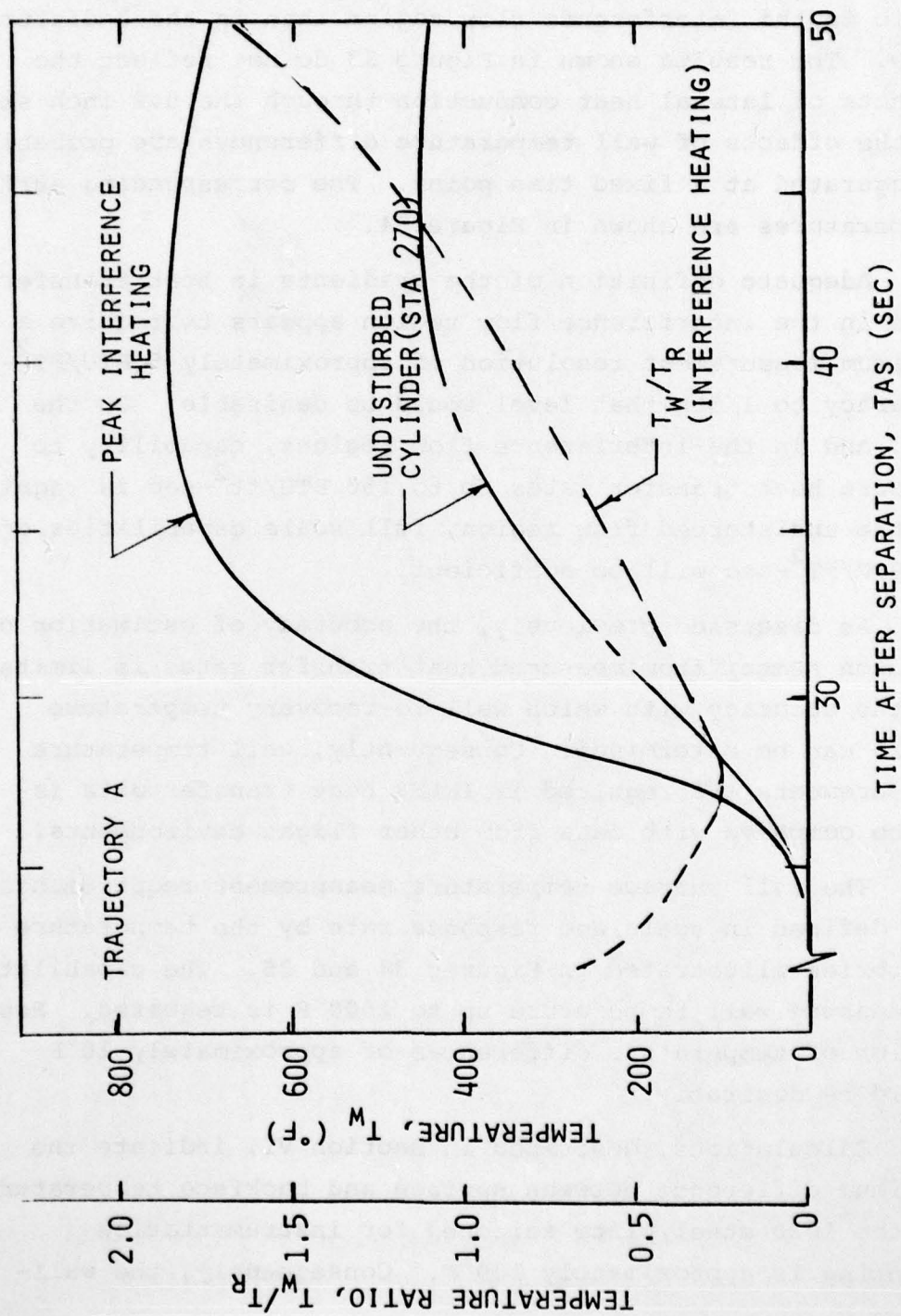


FIGURE 34. Surface Temperature History on Aft Cylinder

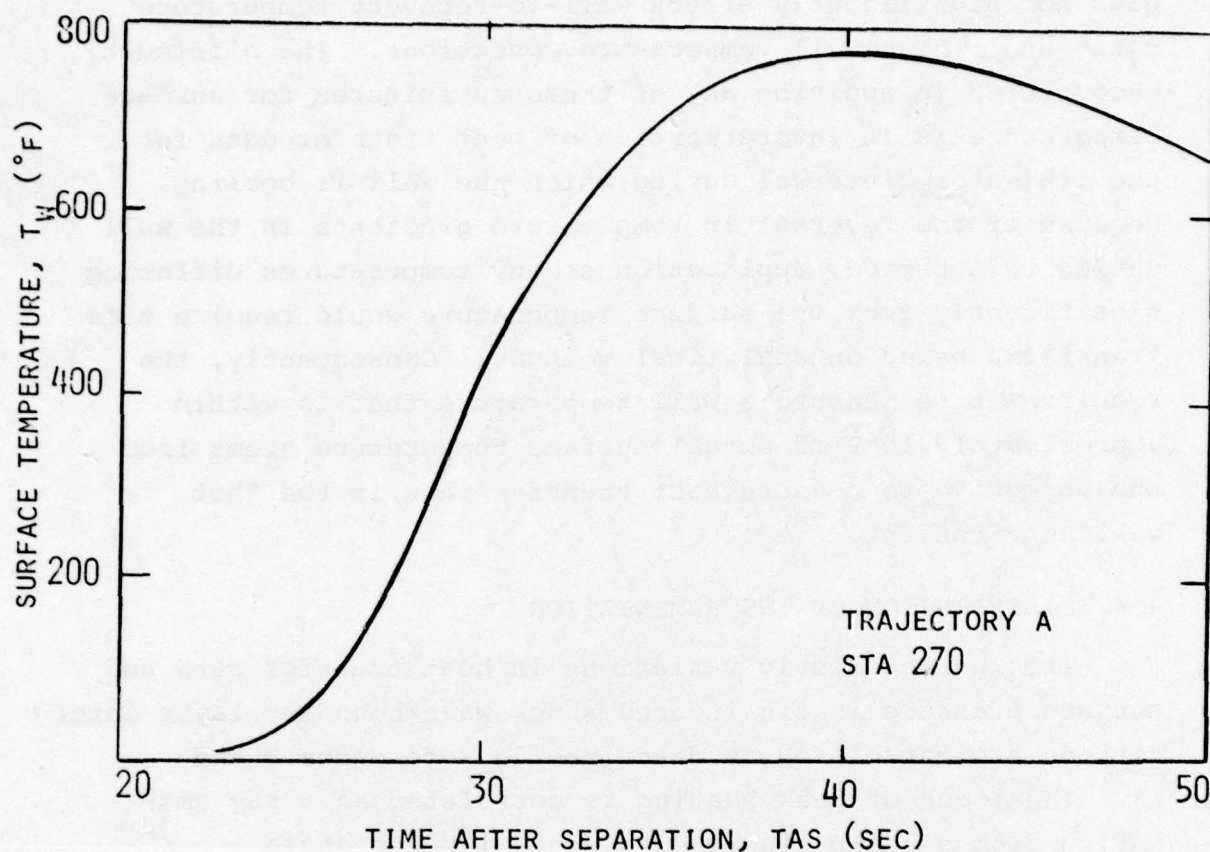


FIGURE 35. Fin Surface Temperature History

to-recovery temperature ratio illustrated in Figure 34 is not significantly effected, at high wall temperature, if backface temperature is used as surface temperature. A second possibility will be evident from the discussion of the Gardon Gage type heat transfer rate measurement instrument described in Section V. That is, the temperature of the reference ring on the gage must be measured to use in temperature dependent calibrations. Therefore, it could be used as a wall temperature measurement. Analysis indicates that this temperature differs by as much as 200 $^{\circ}\text{F}$  from instrumented plate surface temperature. Again, this difference

does not significantly effect wall-to-recovery temperature ratio under high wall temperature conditions. The difficulty encountered in applying any of these substitutes for surface temperature is in interpretation of heat transfer data for the trajectory interval during which the wall is cooling. Because of the reversal in temperature gradients in the wall during this period, application of any temperatures differing significantly from the surface temperature would require time transforms based on analytical methods. Consequently, the requirement to measure a wall temperature that is within approximately 10°F of actual surface temperature stems from the objective to measure heat transfer rate in the "hot wall" environment.

#### 4.4 DISTRIBUTION OF INSTRUMENTATION

The characteristic variations in heat transfer rate and surface pressure in fin induced shock wave/boundary layer interactions are correlated as described in References 3 and 13. The locus of peak heating is correlated as a ray emanating from a sharp fin leading edge with the angle

$$\lambda_H = 0.24(\theta_s - \theta_w) + \theta_w \quad (8)$$

where  $\theta_s$  is the wedge-induced shock angle relative to the undisturbed flow direction and  $\theta_w$  is the wedge surface angle from the same reference. The history of this angle and the shock angle are illustrated, for Trajectory A, in Figure 36. This correlation was derived from data taken on a flat plate. However, in Reference 3, it is shown to be reasonably valid for a fin-induced interference flow on a body of revolution. These correlations do not extend to definition of the maximum heating point along the locus defined. Some of the data suggest that it is a distance approximately 40 times the boundary layer thickness from the leading edge of the fin, measured in the direction of the undisturbed flow.



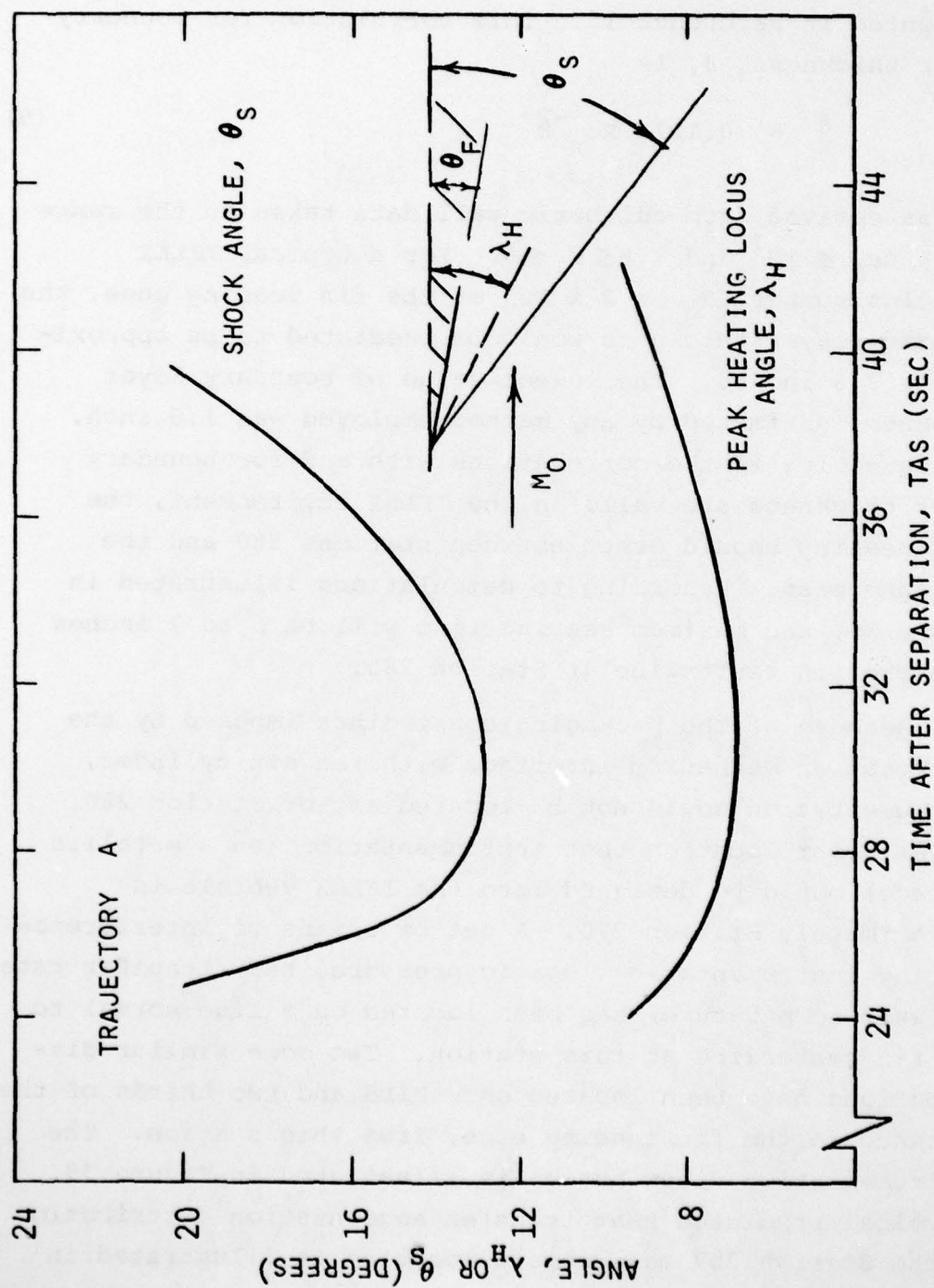


FIGURE 36. Fin Shock and Peak Heating Locus Angles

AD-A078 861

SCIENCE APPLICATIONS INC IRVINE CA

F/6 20/4

HYPERSONIC INTERFERENCE FLOW FLIGHT EXPERIMENT DESIGN.(U)

JUN 79 L A CASSEL , T C DUNCAN , E H LAHTI

F33615-77-C-3043

UNCLASSIFIED

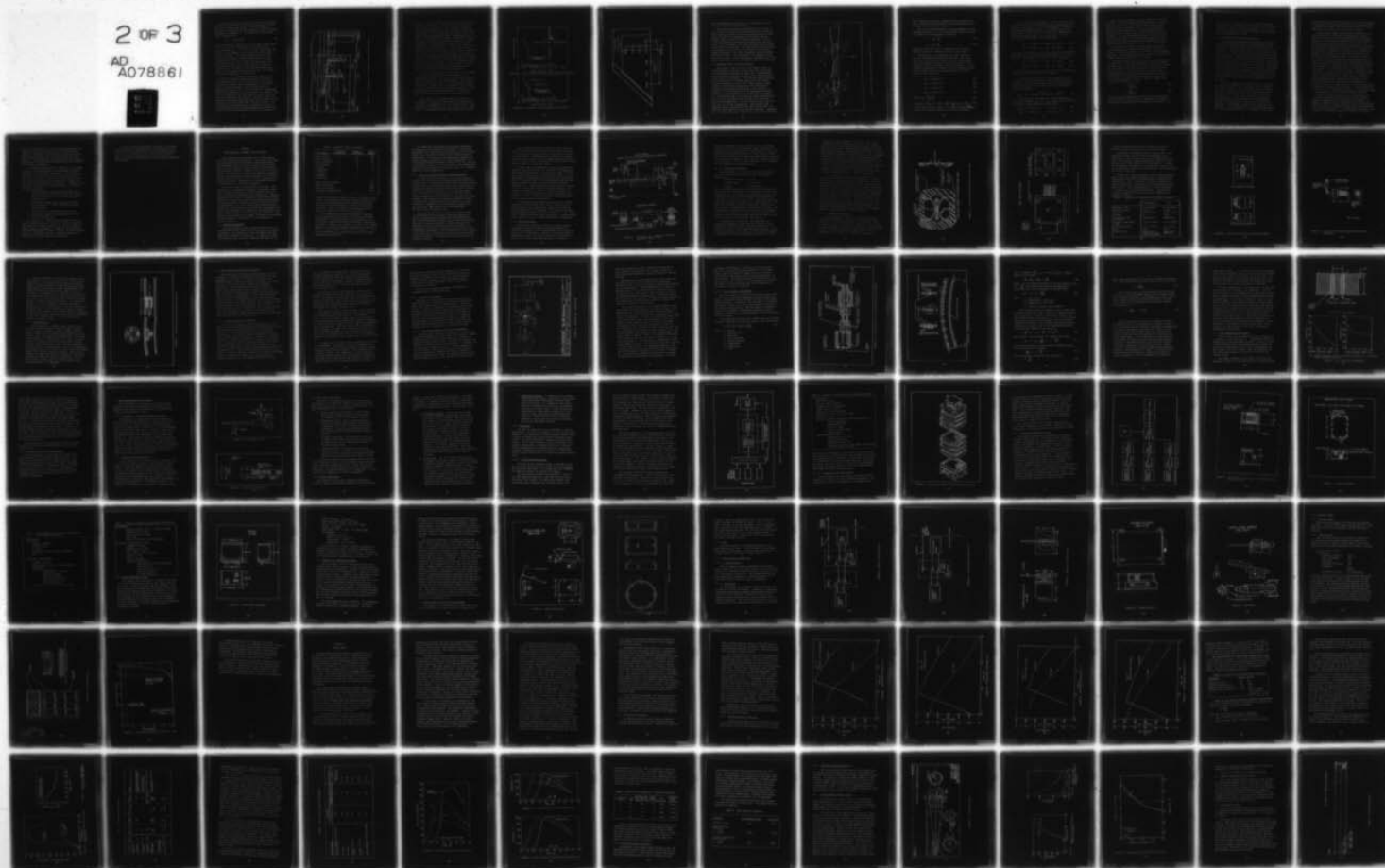
SAI-175-80R-008

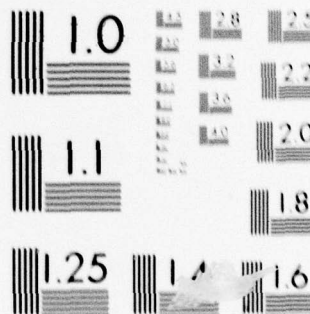
AFFDL-TR-79-3065

NL

2 OF 3

AD  
A078861





MICROCOPY RESOLUTION TEST CHART  
NATIONAL BUREAU OF STANDARDS-1963-A



Several methods were employed to estimate the turbulent boundary layer thickness on the IFLEX vehicle aft cylinder, at the fin leading edge station. The most reliable is believed to be based on the correlation by Roshko and Thomke, presented in Reference 15. This correlation for boundary layer thickness,  $\delta$ , is

$$\frac{\delta}{X} = 0.1215 \text{ Re}_x^{-\frac{1}{8}} \quad (9)$$

It was derived from adiabatic wall data taken in the range  $10^5 \leq \text{Re}_\delta \leq 10^7$  and  $1.8 \leq M_1 \leq 5$ . For a typical IFLEX Reynolds number,  $\text{Re}_e = 2 \times 10^8$  at the fin leading edge, the boundary layer thickness would be predicted to be approximately 2.5 inches. The lowest value of boundary layer thickness estimated by any method employed was 1.0 inch. Consequently, if the correlations with and for boundary layer thickness are valid in the IFLEX environment, the peak heating should occur between stations 280 and the cylinder base. According to calculations illustrated in Figure 36, the maximum heating line will be 5 to 7 inches from the fin centerline at Station 280.

Because of the packaging constraints imposed by the fin rotation mechanism interface with the aft cylinder, instrumentation could not be located aft of Station 280. The aft-most location that instrumentation (on a metallic surface) could be designed into the IFLEX vehicle is approximately Station 270. A set of triads of interference heating instrumentation (static pressure, heat transfer rate, and wall temperature) has been located on a line normal to the fin centerline at this station. Two more similar distributions have been located one third and two thirds of the distance to the fin leading edge, from this station. The instrumentation distribution is illustrated in Figure 37. A typical predicted heat transfer augmentation distribution at the Station 257 measurement location is illustrated in

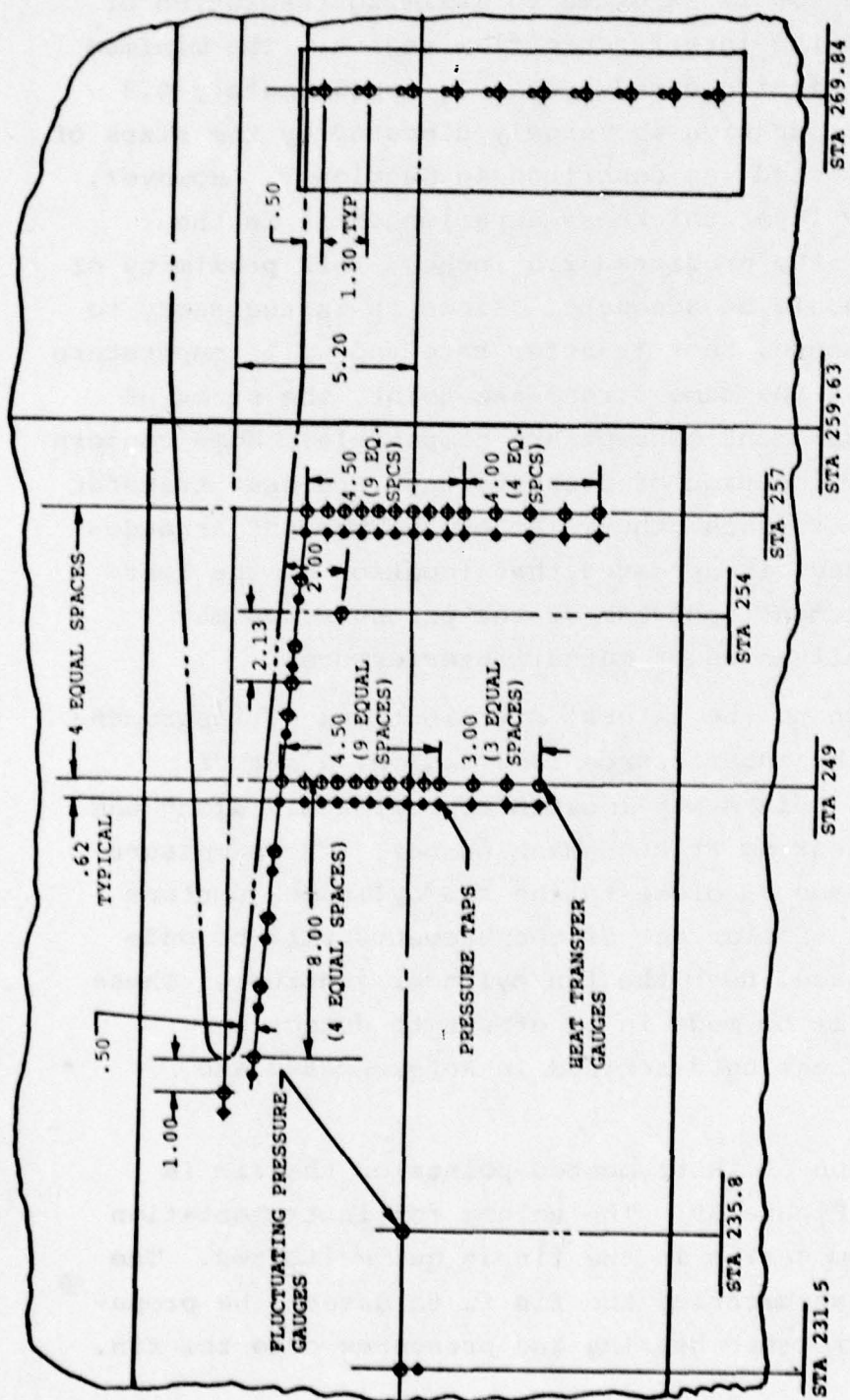


FIGURE 37. Distribution of Interference Heating Instrumentation



Figure 38a. The associated pressure amplification profile is shown in Figure 38b. These predictions are based on correlations in Reference 3. The transverse spacing of the instrumentation is selected to maximize resolution of the gradient in the interference flow region. The minimum spacing between instrumented points is approximately 0.5 inches. This separation is largely dictated by the sizes of instruments selected, as described in Section V. However, if the boundary layer thickness experienced is in the neighborhood of the predicted 2.5 inches, this proximity of measurements should be adequate. Since it is necessary to infer that pressure, heat transfer rate and wall temperature were measured at the same streamwise point, the sizes of gauges and measurement concept are compatible. Some concern exists over the location of pressure taps and heat transfer gauges relative to each other. After the present arrangement was designed, it appeared that location of the heat transfer measurement upstream of the pressure tap may minimize the influences of mutual interference.

In addition to the lateral distributions of instrumentation across the interference flow region, a set of instrumentation points was located approximately along the locus of peak heating at high Mach number. These measurements will be made as close to the fin/cylinder juncture as possible. A similar set of measurements will be made on the fin surface, near the fin/cylinder juncture. These measurements will be made in an effort to detect the vortex induced heating described in References 3 and 13.

The location of instrumented points on the fin is illustrated in Figure 39. The volume for instrumentation and access accommodation in the fin is quite limited. The objective of instrumenting the fin is to detect the propagation of interference heating and pressures onto the fin.



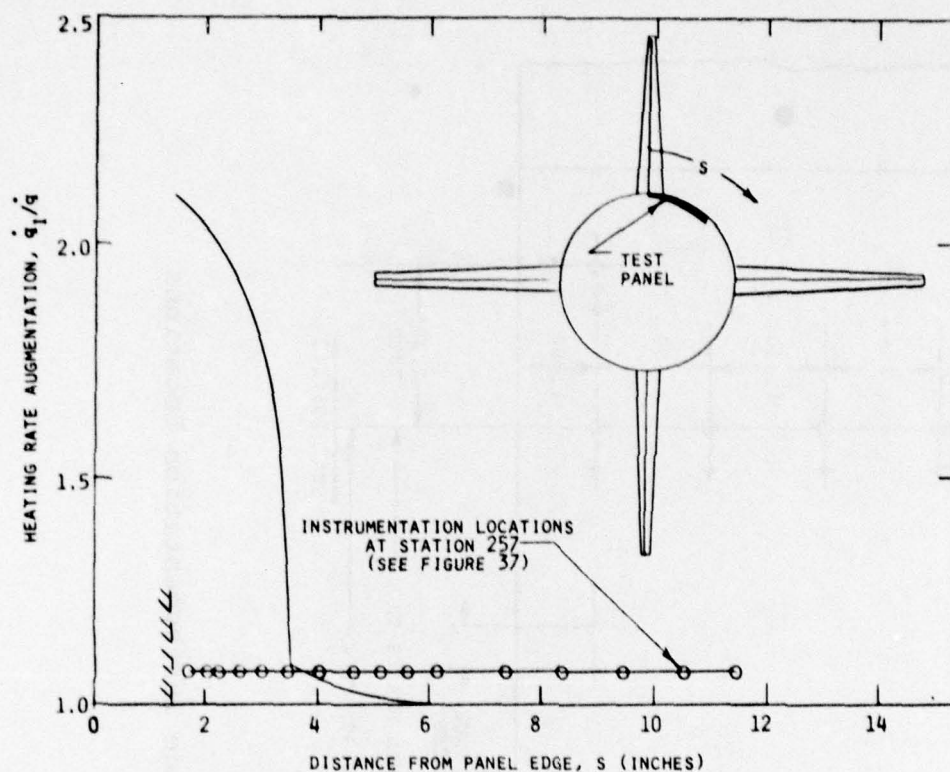


FIGURE 38a. Predicted Heat Transfer Rate Augmentation Profiles

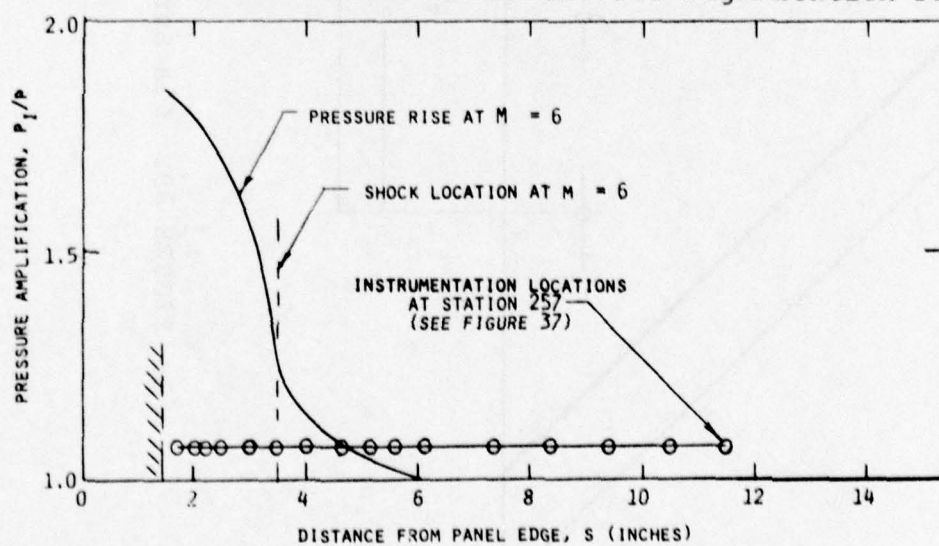


FIGURE 38b. Predicted Pressure Amplification Profiles

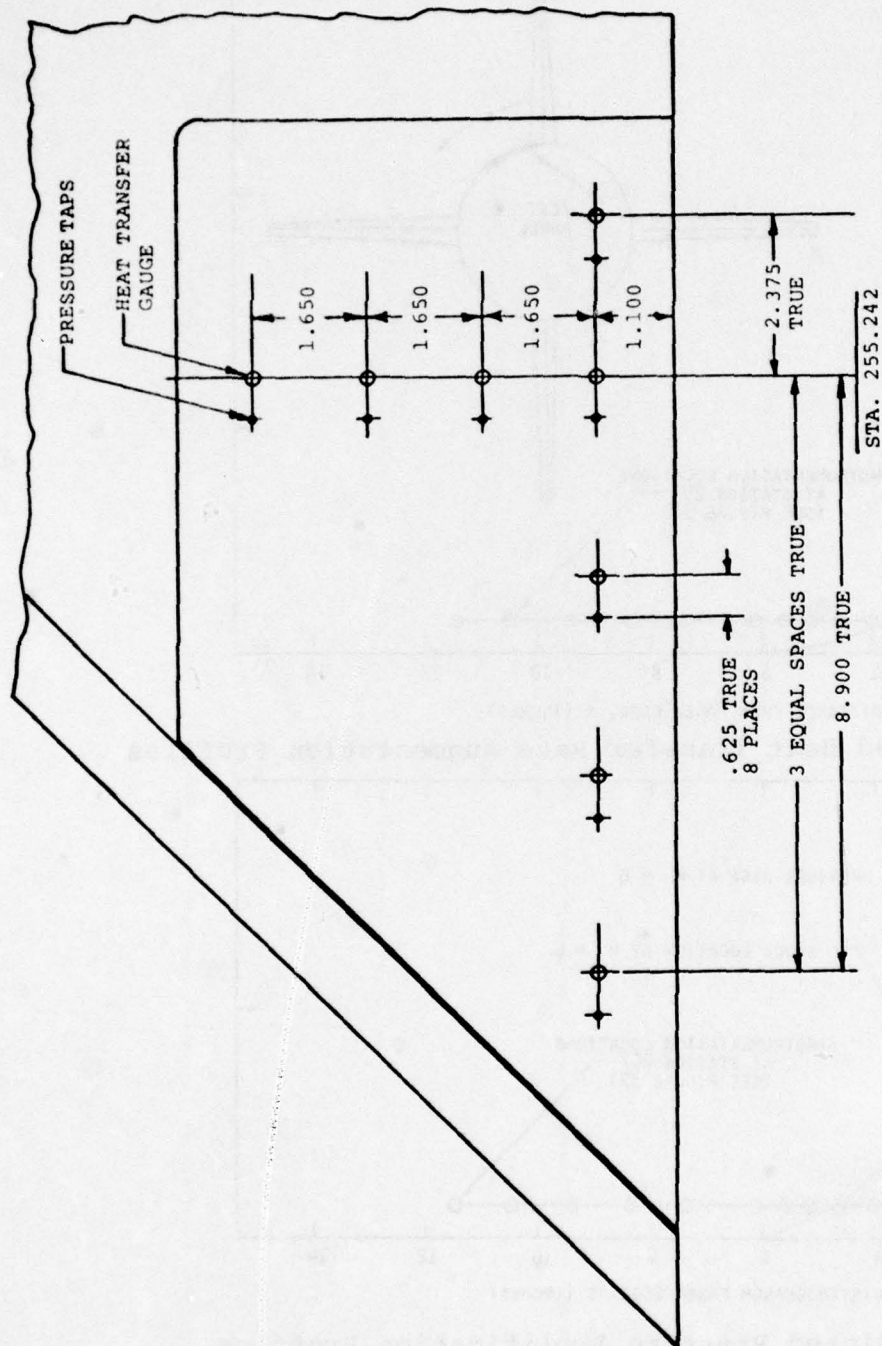


FIGURE 39. Fin Surface Instrumentation Locations

The instrumentation on the fin is not distributed in such a way as to resolve steep gradients.

The fluctuating pressure measurements will be made at the locations indicated by the hexagon symbols in Figure 37. Since there are no data available on distributions of fluctuating pressures in 3-dimensional interference heating regions, these locations are somewhat arbitrary. The two in the interference flow region are located near the circulating flow reattachment line, where fluctuations are likely to be largest in magnitude. They were placed where adjoining instrumentation provides the best definition of the quasi-steady environment. The third fluctuating pressure measurement will be made in the undisturbed flow, upstream of the interaction region. This will provide a reference point from which the influence of the interference flow can be measured.

#### 4.5 REFERENCE CONDITIONS DATA REDUCTION

Mach number, angle of attack, and sideslip angle will be determined from analysis of data from nine static pressure measurements indicated in Figure 40. One measurement will be the pitot pressure measured at the centerline stagnation point on the nosetip. A set of four static pressures will be measured at 90 degree intervals on the forward cylinder periphery at station 105. This station is downstream of the pressure expansion from the forecone and upstream of the pressure compression on the frustrum. A second set of four pressures will be measured at 90 degree intervals on the periphery of the forward cone at station 30. The pressure taps on the nose cone have been designated  $P1_z$ ,  $P3_z$ ,  $P2_y$ ,  $P4_y$  and  $P5_x$  for the yaw, pitch and longitudinal axes respectively. On the 9-inch cylinder they are  $P6_y$ ,  $P8_y$ ,  $P7_z$  and  $P9_z$  respectively. The pressure range required for all yaw and pitch axes will be 0-25 PSIA. The pressure range required for  $P5_x$  will be 0-300 PSIA. Pressures  $P1_z - P3_z$ ,  $P2_y - P4_y$ ,  $P6_z - P8_z$  and  $P7_y - P9_y$  will be measured



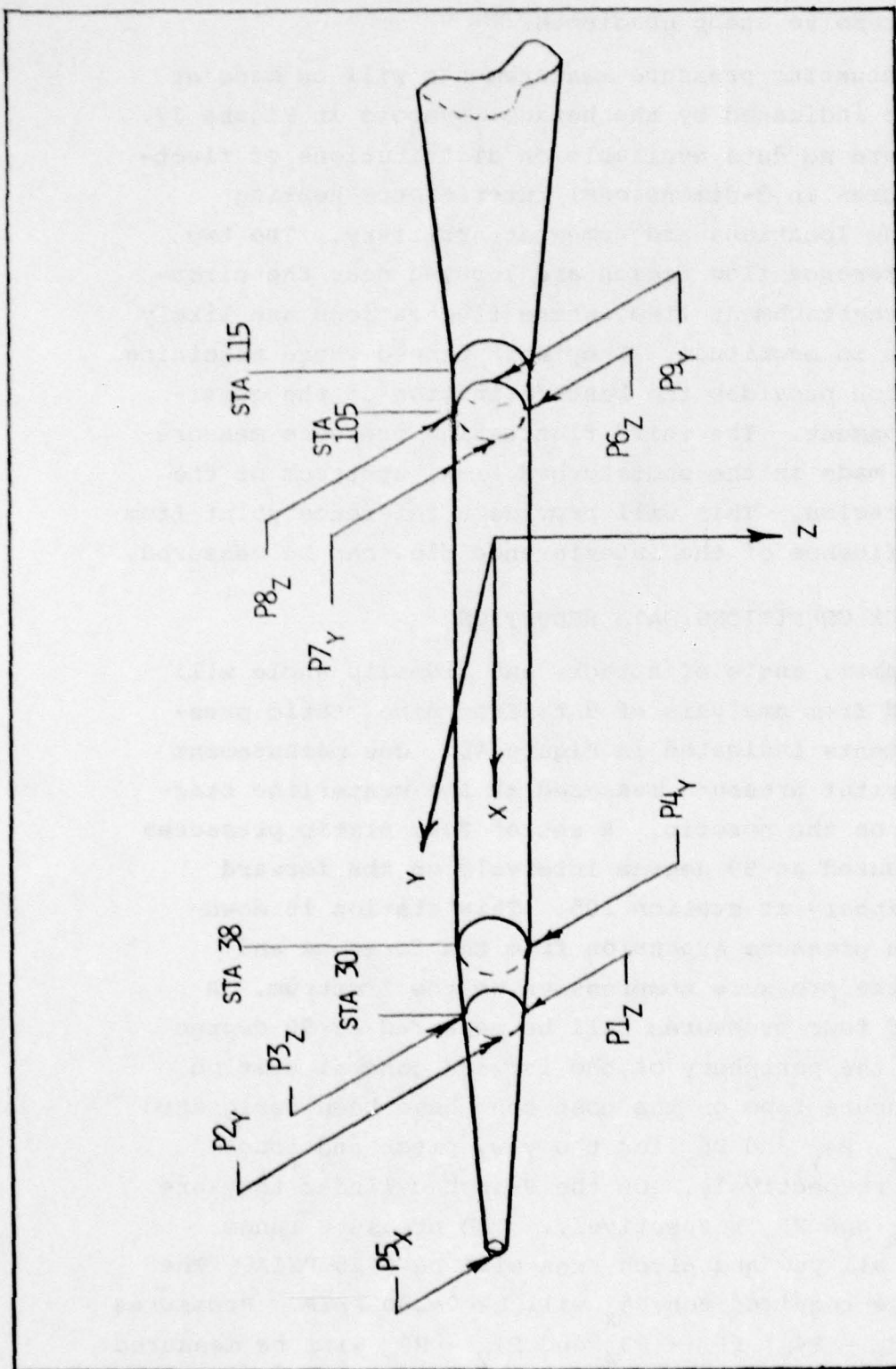


FIGURE 40. Reference Conditions Measurements Locations

with differential pressure transducers with a range of  $\pm 10$  PSID. These pressure ranges will provide measurements over a 5 degree range in angle of attack.

The axis system employed for these measurements is that defined in Figure 40. In this axis system, angles of attack and sideslip are conventionally defined as

$$\alpha = \tan^{-1} \frac{V_z}{V_x} \quad (10)$$

$$\beta = \sin^{-1} \frac{V_y}{\bar{V}} \quad (11)$$

where the subscripts refer to components of the missile velocity vector,  $\bar{V}$ , resolved on the x, y and z axes.

The procedure for determining the flight conditions from the pressure measurements is iterative. The semi-empirical correlations in Reference 19 are used to express the coefficients at stations 30 and 105 in terms of the angles of attack, Mach number and static pressure. For the pressure measurements at station 30 on the nosecone, where the zero angle of attack inclination angle is  $6^\circ$ , the pressure coefficients are

$$C_{p1} = R(\gamma, M_\infty, \alpha_0 + \alpha) \quad (12)$$

$$C_{p3} = R(\gamma, M_\infty, \alpha_0 - \alpha) \quad (13)$$

$$C_{p2} = R(\gamma, M_\infty, \alpha_0 + \beta) \quad (14)$$

$$C_{p4} = R(\gamma, M_\infty, \alpha_0 - \beta) \quad (15)$$

$$\text{where } C_{pi} = \frac{P_i - P_\infty}{\frac{\gamma}{2} P_\infty M^2} \quad (16)$$

$$\text{and where } R(\gamma, M_\infty, \theta) = \left( \frac{\gamma+7}{4} - \frac{\gamma-1}{4} \right) + \frac{6}{M_\infty} \sin^2 \theta + \frac{M_\infty^2 - 1}{M_\infty^4} \quad (17)$$

In this equation,  $\theta > 0$  and  $\gamma = 1.4$  since air behaves approximately as a thermally perfect gas in this environment.

For the pressure measurements at station 105 on the forward cylinder, only the windward pressure coefficients can be defined using Equation (17) since the equation is valid only for positive angles of attack. The windward side in the  $\alpha$  and  $\beta$  planes is determined by the sign of the measured differential pressures,  $dp_{68} = p_6 - p_8$  and  $dp_{79} = p_7 - p_9$ . The pressure coefficients in the  $\alpha$  plane are

$$C_{p6} = R(Y, M_\infty, \alpha) \quad \text{if } dp_{68} = p_6 - p_8 > 0 \quad (18)$$

$$C_{p8} = R(Y, M_\infty, \alpha) \quad \text{if } dp_{68} = p_6 - p_8 < 0 \quad (19)$$

When  $dp_{68}$  is zero, then  $p_6$  is equal to  $p_8$  within the measurement accuracy and both are direct measurements of the static pressure. The pressure coefficients in the  $\beta$  plane are

$$C_{p7} = R(Y, M_\infty, \beta) \quad \text{if } dp_{79} = p_7 - p_9 > 0 \quad (20)$$

$$C_{p9} = R(Y, M_\infty, \beta) \quad \text{if } dp_{79} = p_7 - p_9 < 0 \quad (21)$$

Again, when  $dp_{79}$  is zero, then  $p_7$  is equal to  $p_9$  and both are interpreted as static pressure measurements.

To begin the iteration, the static pressure is taken as the average of the pressures on the forward cylinder,  $p_6$  through  $p_9$ . The freestream Mach number is then estimated from the pressure on the nosetip,  $p_5$ , using the Rayleigh Pitot Tube equation,

$$\frac{p_5}{p_\infty} (Y, M_\infty) = \left( \frac{Y+1}{2} M_\infty^2 \right)^{\frac{Y}{Y-1}} / \left( \frac{2Y}{Y+1} M_\infty^2 - \frac{Y-1}{Y+1} \right)^{\frac{Y}{Y-1}} \quad (22)$$

By defining the differential pressure coefficient in the  $\alpha$  and  $\beta$  planes,  $C_{p31}$  and  $C_{p42}$ , respectively, the angles of attack in these planes can be determined.

$$\Delta C_{p31} = R(Y, M_\infty, \alpha_O - \alpha) - R(Y, M_\infty, \alpha_O + \alpha) \quad (23)$$

$$\Delta C_{p42} = R(Y, M_\infty, \beta_O - \beta) - R(Y, M_\infty, \beta_O + \beta) \quad (24)$$



With the  $\alpha$  and  $\beta$  angles of attack estimated, a better estimate of the static pressure can be obtained by solving Eqs. (18) or (19) in the  $\alpha$  plane when  $\alpha > 0$  or  $\alpha < 0$ , respectively; and by solving Eqs. (20) or (21) in the  $\beta$  plane when  $\beta > 0$  or  $\beta < 0$ , respectively. The new estimate of the static pressure is again taken as the average of these two estimates. The new Mach number estimate is obtained implicitly from Eq. (22). With the new Mach number and static pressure, the angle of attack may be recalculated by solving the differential pressure coefficient, Eqs. (23) and (24).

This iteration scheme converges rapidly because the flight conditions are sensitive functions of the data, the angles of attack are especially sensitive to the differential pressures. In two sample cases run to check out the iteration scheme, convergence occurred in two steps.

The second system for angle of attack and sideslip angle determination is based upon measurement of three components of acceleration in the body fixed axis. The angles of attack are then deduced from the normal and side force characteristics measured in wind tunnel testing, and the dynamic pressure derived from ground based measurements of velocity and altitude. As illustrated in Section III, the normal force characteristics are linear in angle of attack, over the range of interest, so that

$$\alpha = \frac{\eta_z W}{q_\infty S_R C_{N\alpha}} \quad (25)$$

$$\beta = \frac{\eta_y W}{q_\infty S_R C_{Y\beta}} \quad (26)$$

Given accurate atmosphere and trajectory data, the requirement to estimate vehicle weight is probably the governing uncertainty in this method of determining these angles. The

principal source of these errors is residual propellant uncertainties. These should introduce errors of less than 5 percent in angle of attack determination. The accuracy of the force coefficient slopes determined from wind tunnel data is approximately the same.

#### 4.6 INTERFERENCE FLOW DATA INTERPRETATION

The IFLEX objectives include derivation of high Mach and Reynolds number environment interference heating data for hypersonic vehicle design, and determination of the accuracy with which these measurements can be made in flight experiments. To satisfy these objectives, aerothermodynamic ground testing and computational analyses must parallel the flight experiment. The ground testing will provide data for comparison with flight test results, particularly for determining the sensitivity of interference heating to the Reynolds number difference between ground and flight test. This wind tunnel testing will also provide data in partial substitution for the boundary layer flow properties profile survey data, which will not be taken in flight. Based on this data and the measurements to be made in flight, computational models of the boundary layer approaching the experiment will be selected.

The direct comparison of IFLEX data with ground test data will be facilitated by obtaining data on a geometric scale model of IFLEX. With such data, direct comparison with IFLEX flight data can be made. Ground test data requirements should extend beyond the flight measurement requirements for IFLEX. They should include detailed characterization of interference flow and approaching boundary layer conditions as functions of the flowfield parameters. For example, surveys of total pressure and temperature in the interference flow and approaching boundary layer should be measured. At a minimum, the boundary



layer thickness and the velocity profile should be determined as functions of the flowfield parameters, including Reynolds number and Mach number. As wide a range of wall to recovery temperature ratio as possible should be simulated.

Since the Mach number range and some temperature ratio values encountered on IFLEX may be reproduced in existing ground test facilities, these parameters should be matched. However, since the Reynolds number range of IFLEX cannot be reproduced in ground test facilities, some range of the Reynolds number parameter should be obtained in ground tests. One significant Reynolds number effect is its influence on the location of transition. The proximity of transition is reflected in the shape of the boundary layer profile approaching the interference region. For IFLEX, transition will always begin on the nose cone (before station 30), in which case the running length to the interference region is almost an order of magnitude larger than the running length to the beginning of transition (the fin leading edge is at station 240). It is doubtful that early transition can be obtained in a ground test facility without resorting to some form of boundary layer trips. Therefore, the location of natural transition should be varied, perhaps by changing Reynolds number between locations just upstream of the interference region to a location as far upstream as is possible. Testing two model scales or in two test facilities is required to accomplish the variation. The variation will be useful only if a significant fraction of the boundary layer is turbulent under the high Reynolds number condition.

With the ground test data, a direct comparison with the flight test data can be obtained in which the Mach number and temperature ratio parameters are matched. For example, a somewhat cursory comparison of the maximum Stanton number increase as a function of Mach number and temperature ratio could be obtained. If the comparison is accurate, then it might be reasonably assumed that existing correlations



based on ground test data will have been approximately validated with flight test data obtained at flight Reynolds numbers. In addition, these correlations may then be used with increased certainty in the design of similar flight vehicles. If the comparison is not accurate, then a Reynolds number effect will have been documented and a more complete data analysis is required.

If a Reynolds number effect is observed, it is probably a result of the heat transfer rate and pressure variation dependence on the boundary layer profile. In this event, some representation of the state of the boundary layer on IFLEX will be required. The boundary layer characterization will be obtained through some combination of flight test data analysis and computational techniques. A number of computational techniques are available including, in order of increasing complexity:

- 1) integral boundary layer solutions coupled with a finite difference inviscid flowfield code (such as the code by Soloman, et. al. of NSWC, described in Reference 4-4);
- 2) differential boundary layer equations solutions, again coupled with a finite difference inviscid flowfield code;
- 3) viscous shock layer equations solutions; and
- 4) solutions to higher order approximations of the Navier Stokes equations

The selection of a computational technique should be based on several criteria. One is the ability to reproduce the ground test boundary layer data for the scale model of IFLEX, another is the ability to reproduce the undisturbed flow aeroheating data for IFLEX. Finally, the method selected should be sufficiently general in geometry applicability to be useful for other vehicle configurations.

With the selected computational technique, the boundary layer condition for IFLEX should be characterized and correlated with the corresponding interference flowfield measurements. This correlation would be narrower than the more general correlation obtained when no Reynolds number dependence was observed.



## SECTION V

### INSTRUMENTATION, TELEMETRY AND ELECTRONICS

The measurements requirements for the IFLEX program have been identified in Section IV. This section will identify instruments suitable for making these measurements, and equipment necessary for signal conditioning and telemetry to ground stations. Where necessary, the rationale for selecting a specific instrument over others will be presented. The criteria for selection of specific instruments has been strongly weighted toward candidates which reflect the performance history of like or similar instruments in a flight environment. Descriptions of instruments provided by manufacturers are included in Appendix II.

Three basic types of measurements will be made. The quantities to be measured are pressure, temperature (where heat transfer measurements are being viewed as a special case of temperature measurement) and acceleration. Pressure measurements fall into two categories: quasi-steady measurements which include wall pressures and pressure measurements to determine missile altitude and flight parameters, and unsteady pressures, i.e., time resolved fluctuating pressures. Temperature, heat transfer, and acceleration measurements are viewed as quasi-steady. In addition to the measurement functions, signal sources for missile operation indicators, event markers, and initiators for a number of events will be required. The distribution of data elements to be telemetered is listed in Table 1.

#### 5.1 PRESSURE MEASUREMENTS

The shock-boundary layer interaction regions will be instrumented with 250 steady and 3 fluctuating wall pressure transducers. The locations of these transducers and their ranges were discussed in Section IV. In addition to these wall pressure taps, 2 sets of 4 pressure taps each will be



TABLE 1. Telemetry Channel Assignments

MEASUREMENT	CHANNELS/ MEASUREMENTS	NUMBER/ MEASUREMENTS	TOTAL CHANNELS
Heat Transfer	2	50	100
Static Pressure	1	50	50
Wall Temperature	1	50	50
Cone Pressure	1	4	4
Cylinder	1	4	4
Differential Pressure	1	4	4
Stagnation Pressure	1	1	1
Acceleration	1	3	3
Total PCM Data Channels			216
Monitor Functions			TBD
Total PCM Channels			250
Fluctuating Pressures 1FM		3	3FM

located on the 6 degree conical section (at station 30) and on the 9 inch diameter cylindrical section (station 105) of the missile. Pressure taps will be spaced 90° circumferentially at each station and will serve as pitch and yaw indicators. Also, a stagnation point pressure will be measured as indicated in Figure 40 (Section IV).

All transducers and associated electronic equipment must be compatible with the missile pre-flight and flight environments. Peak accelerations were estimated to be 25 g's and the vibration environment requirements specified by MIL-STD-81 C, Method 514.2, category d.1 and d.2 are assumed adequate. The shock environment requirement was taken to be that of the same standard, Method 516.2, Procedure I. The actual environment is not known and analysis has not been accomplished to predict it.

The temperature environments for pressure transducers are dictated by the methods of installation. Quasi-steady measurements can tolerate longer lag times so that the transducers can be installed sufficiently far removed from the vehicle skin. Pre-flight ground temperatures represent the highest expected temperatures for these transducers. The fluctuating pressure measurements require very close coupling to the vehicle surface so as not to distort the frequency and amplitude of the pressure fluctuations. They will, therefore, experience higher temperatures.

#### 5.1.1 Vehicle Attitude and Flight Condition Sensors

The expected flight parameters and required sensitivities for the pitch and yaw transducers have been identified in Section IV. A conventional configuration has been selected for the location of the pressure taps, that is 90 degree circumferential spacing at two selected missile axial stations, as shown in Figure 40 (Section IV). The expected ranges are 0 - 15 psi for the cone pressures, 0 to 5 psi for the cylinder pressures, and 0 to 300 psi for the stagnation point pressure. The ranges for the cone and cylindrical section are practically identical and can be covered by the same transducer. Therefore, only two transducer ranges need to be considered: eight each in the 0 to 15 psi range and one in the 0 to 300 psi range.

The signs of the angle of attack and sideslip angles are determined from the pressure difference between two sensor locations separated 180 degrees circumferentially. When these differences are small, and the absolute pressures are large, it becomes desirable to measure the pressure difference directly using differential transducers. For convenience, this approach has been selected using 0-5 psid differential transducers. Little resolution is lost, however, if the difference is determined by subtracting one absolute pressure measurement from the other for the relatively low pressure expected.



The transducers required to measure vehicle attitude and flight performance are located in the forward sections of the missile where physical space constraints are not particularly severe. Transducers can be effectively isolated from the vehicle wall so that the temperature constraints are those of the pre-flight environment at the White Sands Missile Range, assumed to be less than 150°F.

A large number of transducers would meet the specified pressure range and acceleration, vibration, and temperature environmental constraints. The selection of specific transducers was therefore based on performance history in flight environments. Transducers well suited for this application, with a well established record, are capacitive-type general purpose transducers (Series 1332/1333) manufactured by Rosemount, Inc. These transducers exhibit excellent accuracy (0.1% Full Scale), have excellent long term stability, are rugged in construction, and have a high-level output (0 to 5 Volts DC). These transducers are fully temperature compensated to 150°F. Detailed description and specifications can be obtained from the manufacturer.

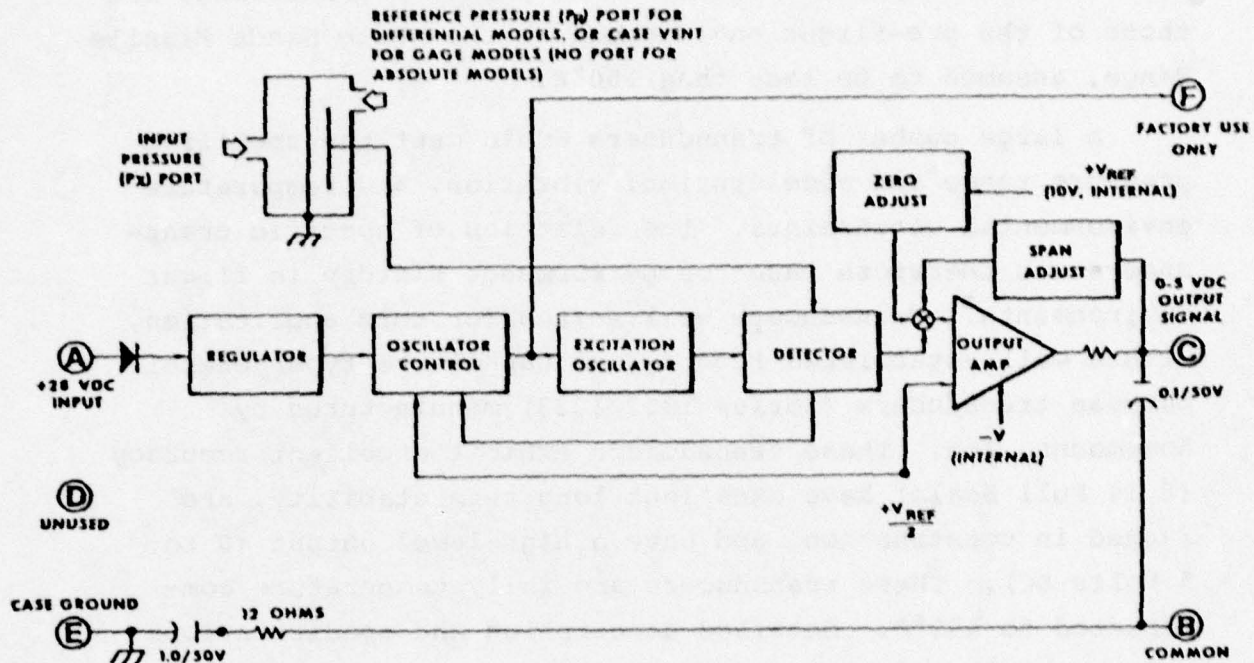
The specific models selected for the cone and cylinder pressures are Model 1332A, Code 4 with a range of 0 to 30 psia and Model 1332A, Code 8 with a range of 0 to 500 psi for the stagnation point pressure. The 4 differential pressure transducers selected are model 1332B Code 2. The transducer, together with some overall dimensions, is shown schematically in Figure 41 with a diagram describing its operation.

#### 5.1.2 Surface Pressures

A survey was conducted to identify candidate pressure transducers suitable for measuring the quasi-steady and fluctuating pressures in the shock-boundary layer interaction region of the IFLEX vehicle. Because of the large number of measurements required in a small region of the missile and because of the very limited physical space available to



# BLOCK DIAGRAM MODELS 1332/1333 CAPACITIVE PRESSURE TRANSDUCERS



## DIMENSIONAL DRAWINGS

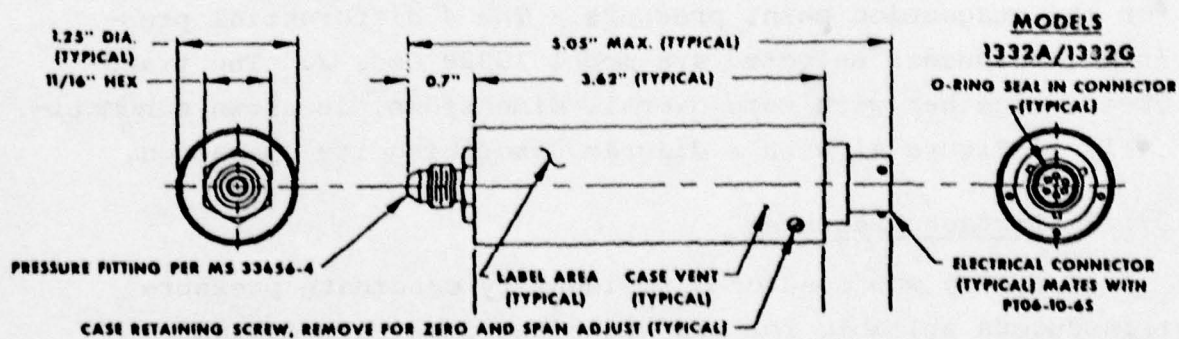


FIGURE 41. Rosemount, Inc., Capacitive Pressure Transducer (Model 1332A)

house the transducers, small transducer size is a primary selection criterion. The relatively rapid changes of the environment to be measured and the requirement to cycle 10-20 times per second preclude the use of Scanni-Valves. These devices were considered since they are used routinely in ground test facilities to sample a large number of pressure taps with a few transducers. For the IFLEX application, one transducer must be dedicated to each pressure tap.

#### 5.1.2.1 Quasi-Steady Pressures

The requirement for the quasi-steady pressure measurements were identified in Section IV, and are restated in summary here:

Frequency Response: 0 to 5 Hz

Pressure Range: 0 to 200 psia

Number: 50 transducers

The above requirements present no particular difficulty for a large number of transducers. The imposition of the flight environment and very limited available space eliminates all transducers that are vibration/acceleration sensitive, or those that are relatively large, and/or those which require elaborate circuitry for excitation or signal processing. The small size and simple circuitry requirement virtually dictates the use of semiconductor or piezoelectric devices. The semiconductor transducers are best suited for low frequency or quasi-steady applications while piezoelectric devices are ideally suited for high frequency applications (and not well suited for steady or quasi-steady applications).

A transducer well suited for this application is a Diffused Semiconductor Strain Gage (DSSG) device. This transducer is typically small, vibration insensitive, has small static error, and is among the lowest in price. A particularly attractive configuration of this type of transducer is manufactured by Kulite Semiconductor Products, Inc. and

is depicted in the schematic of Figure 42. This type of transducer has been incorporated by Kulite into compact housings for 25 to 36 transducers specifically for the purpose of facilitating a large number of independent pressure measurements in space limited applications. Such a completely self-contained transducer package which houses 36 transducers is depicted in Figure 43. A more complete description of the housing and detailed performance characteristics of the transducers can be obtained from the manufacturer. The transducers selected for this application cover two pressure ranges. The "low" pressure range will be measured using transducers applicable from 0 - 30 psi and the "high" pressure will be measured using 0 - 200 psi transducers.

The individual pressure ports are connected to the respective transducers through a combination of stainless steel tubing, installed in the hot missile skin, and high temperature flexible tubing. This method of connecting the pressure tubes and the mounting of the transducer package to the cold inner missile frame will assure a transducer temperature well below the maximum transducer operating temperature of 250 F. Average lag times for the proposed installation and the transducers selected was estimated (Reference 21) to be on the order of 0.2 seconds. The possibility of vapor, from cold air captured in the tubes during aircraft carry, condensing during the experiment has been suggested. An analysis of this phenomena and its effect on measurements should be completed prior to final selection.

#### 5.1.2.2 Fluctuating Pressures

The requirements for measuring the fluctuating pressures were established in Section IV and presented graphically in Figure 32. The frequency range of 10 Hz to 5 KHz is readily covered by a number of transducers. Unfortunately, the need to measure fluctuating pressures requires that each transducer be closely coupled to the orifice. This requirement in turn causes the transducer to be exposed



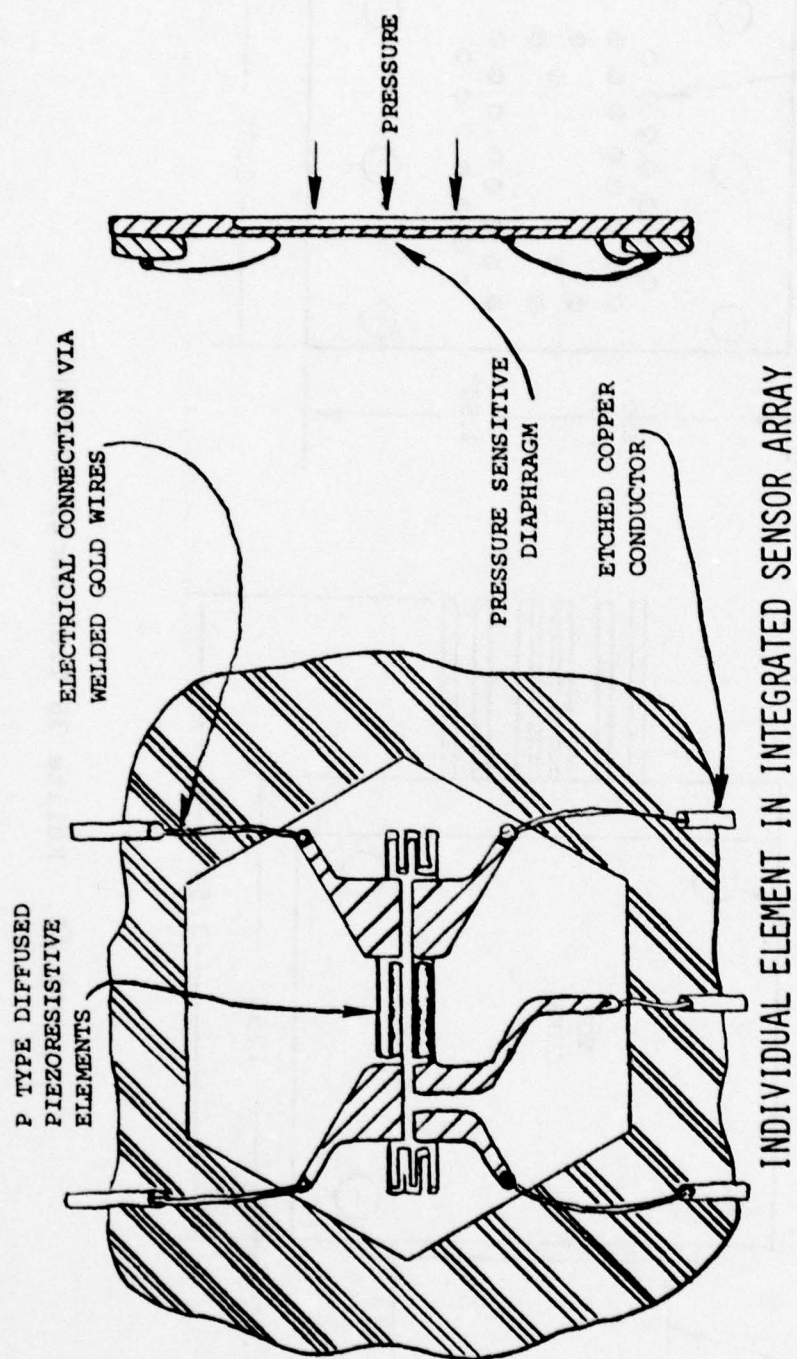


FIGURE 42. Kulite Diffused Semiconductor Strain Gage

# QUASI-STEADY PRESSURES

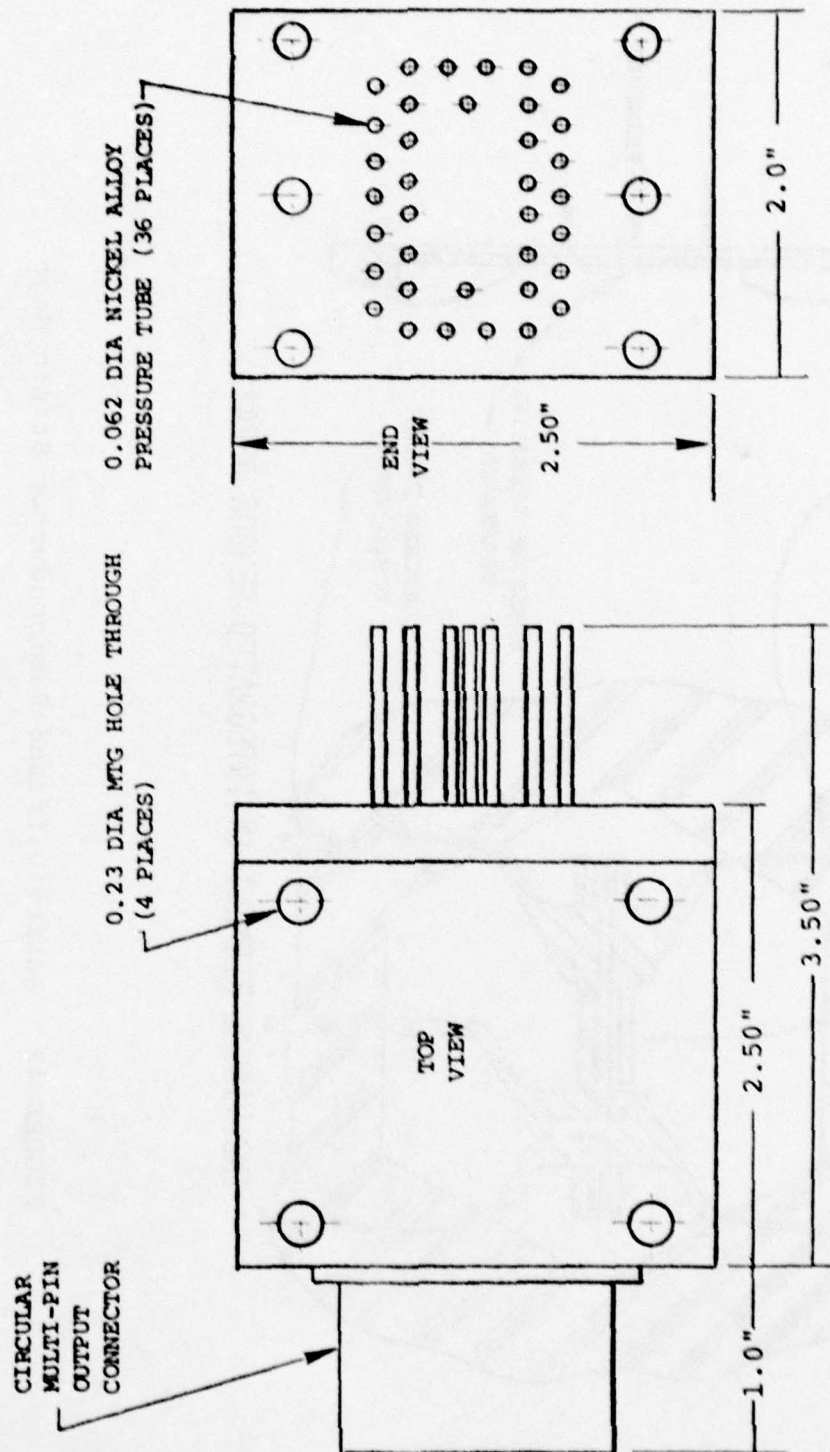


FIGURE 43. Kulite 36 Transducer Housing

to higher temperatures due to heat transfer from the hot vehicle skin and the hot gases of the boundary layer.

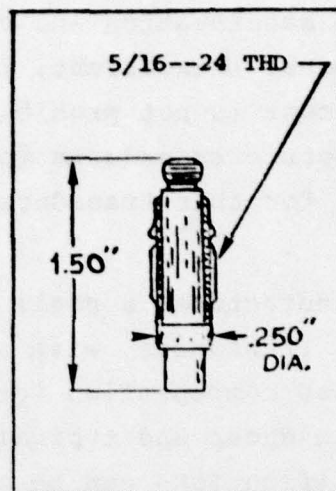
Piezoelectric transducers operate reliably over a wide temperature range, are small and are compensated to be insensitive to the missile acceleration and vibration environments. The frequency response is excellent, typically 1 Hz to greater than 100 KHz and cost is not prohibitive. A typical high temperature piezoelectric transducer and a flight rated charge amplifier required for this transducer (PCB Piezotronics) are shown in Figure 44.

Kulite, Inc. also manufactures a small Diffused Semiconductor Strain Gage (DSSG) transducer, with a wide operating temperature range which has compensation for vibration and acceleration. Such a transducer and typical dimensions are shown in Figure 45. Specifications can be obtained from the manufacturer. Either a piezoelectric or a DSSG transducer is suitable for the proposed measurements. Important performance parameters for the two types of transducers are compared in Table 2.

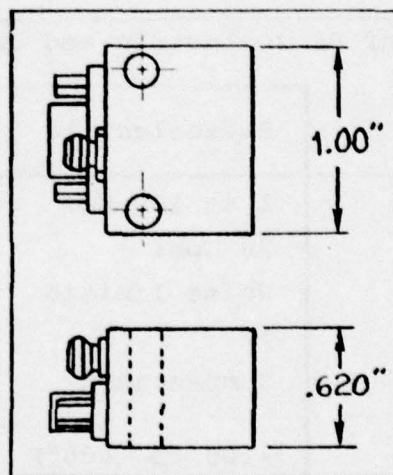
Table 2. Comparison of Piezoelectric and DSSG Transducers

	Piezoelectric	DSSG
Frequency range	1 to 100 KHz	DC to 50 KHz
Maximum pressure	50 Kpsi	5 Kpsi
Resolution	Noise limited	Noise limited
Accuracy	1%	0.25%
Acceleration and vibration	Compensated	Compensated
Operating temperature range	-100 to +600°F	-65 to +525°F
Compensated Range	-100 to +600°F	80 to 450°F
Size	Small	Small
Disadvantages	Needs charge amplifier. High output impedance.	Need signal amplifier



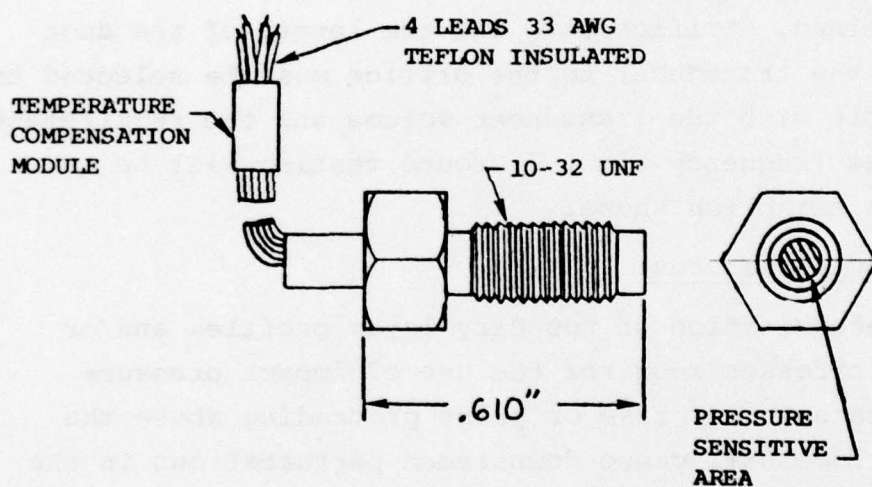


HIGH TEMPERATURE TRANSDUCER



FLIGHT RATED CHARGE AMPLIFIER

FIGURE 44. Typical Piezoelectric Pressure Transducer



MFG. BY KULITE

FIGURE 45. Typical Diffused Semiconductor Strain Gage Transducer

Neither transducer can tolerate the expected vehicle skin temperature or direct exposure to the boundary layer temperatures. The piezoelectric transducer has been selected for IFLEX application because its high temperature compensation range extends to higher temperatures. Also insulated shield cable leads are available for these instruments. Transducers will be thermally insulated from the vehicle skin and mounted in a heat sink of sufficient heat capacity to absorb excessive heat transferred through the gas or leaked through the insulation. An installation schematic for these transducers is shown in Figure 46. Dimensions and exact configuration of the heat sink have not been determined. Orifice size and the length of the duct connecting the transducer to the orifice must be selected to be compatible with the transducer volume and the requirement of the 5 KHz frequency limit. Ground testing will be required to establish these.

#### 5.1.3 Impact Pressures

The determination of boundary layer profiles and/or wall shear stresses requires the use of impact pressure probes or rakes. Any rake or probe protruding above the missile surface will cause downstream perturbations in the boundary layer. Measurements made downstream of such rakes will therefore be of questionable value. Also, the determination of boundary layer profiles from impact pressure rakes is greatly complicated if the local flow angularity is not known a priori or when boundary layers are 3-dimensional. The determination of wall shear from Preston tube measurements suffers from the same angularity problems. Skin friction balances are complicated devices, are usually bulky and do not have an established flight test reputation. For the above reasons, neither rakes nor Preston tubes or skin friction balances are recommended.



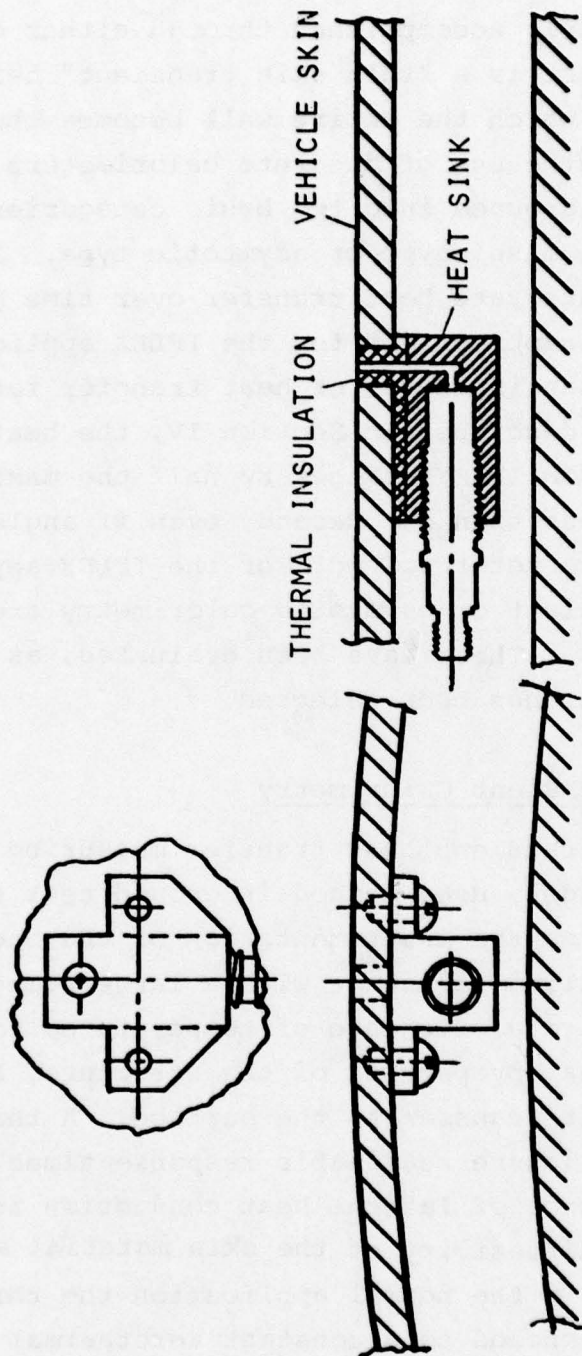


FIGURE 46. Fluctuating Pressure Transducer Mounting

## 5.2 HEAT TRANSFER/TEMPERATURE MEASUREMENTS

The measurement of convective heat transfer to solid boundaries is routinely accomplished through either of two approaches. The first is a "thin skin transient" heat transfer method, in which the entire wall becomes the sensor; the second involves the use of discrete calorimeters. Calorimeters can be grouped into two basic categories, namely slug (thermal mass) type or asymptotic type. Slug type calorimeters integrate heat transfer over time periods. They are therefore inappropriate for the IFLEX application where the rapidly changing level of heat transfer rate is to be resolved. As described in Section IV, the heat transfer rate to be measured on IFLEX changes by half the maximum scale to be measured in less than one second, even if angle of attack variations are not resolved. For the IFLEX application, only thin skin transient or asymptotic calorimetry are appropriate approaches. These have been evaluated, as described below, and the latter has been selected.

### 5.2.1 Thin Skin Transient Calorimetry

The thin skin transient heat transfer measuring technique is the most widely used method in ground test facilities. The technique involves the instrumentation of the back surface of a thin walled structure with a large number of thermocouples. The rate of change of temperature, together with the known thermal properties of the structure, becomes a measure of the heat transfer to the surface. A thin model wall is required to insure reasonable response times and to minimize the importance of lateral heat conduction in the skin. The thermal diffusivity of the skin material also plays an important role. In the normal application the thin skin model is suddenly exposed to a constant aerothermal environment. Ideally, the model wall temperature is much lower than recovery temperature so that temperature versus time data

can be recorded for long periods. The accuracy of the technique diminishes rapidly as the model wall approaches recovery temperature since the slope of the temperature versus time curve is required. The same statement applies for any case where the rate of change of temperature with time becomes small, that is when the net heat transfer to the wall becomes small.

The interpretation of thin skin heat transfer data is uncomplicated when model wall thicknesses are constant and no structural members or other heat sinks, such as pressure taps or transducers, are in contact with the model wall. The presence of such heat sinks complicates the required lateral heat conduction corrections and can render the technique ineffective for low heat transfer rates.

The principal concern in the selection of heat transfer rate measurement instrumentation for IFLEX is the resolution of the rapid changes in that quantity. The response time of the thin wall heat transfer model can be estimated from the solution of the one-dimensional conduction equation for constant material properties (i.e. temperature independent material properties). The time constant for a 0.100" thick wall thickness, and properties of 1020 steel selected for the IFLEX instrumented plates, is on the order of 0.2 seconds. This value is considered too large in light of the expected maximum rate of change of heat transfer rate of  $50 \text{ Btu/ft}^2/\text{sec}/\text{sec}$ .

For application to IFLEX, several alternatives in design were considered. A reduction of the wall thickness and/or use of a wall material of greater thermal diffusivity would obviously reduce the time constant. Other problems would be introduced, however. The temperature of the thinner wall would more rapidly approach and follow recovery temperature. This would lead to smaller net heat transfer, resulting in reduced resolution of the temperature versus time slope. A



second problem, which may even be important for the 0.100 inch wall thickness, results from differential thermal expansion of the thinner skin relative to the more massive, colder structure. Finally, as the wall becomes thinner and hotter its strength decreases. Then the possibility of buckling will increase.

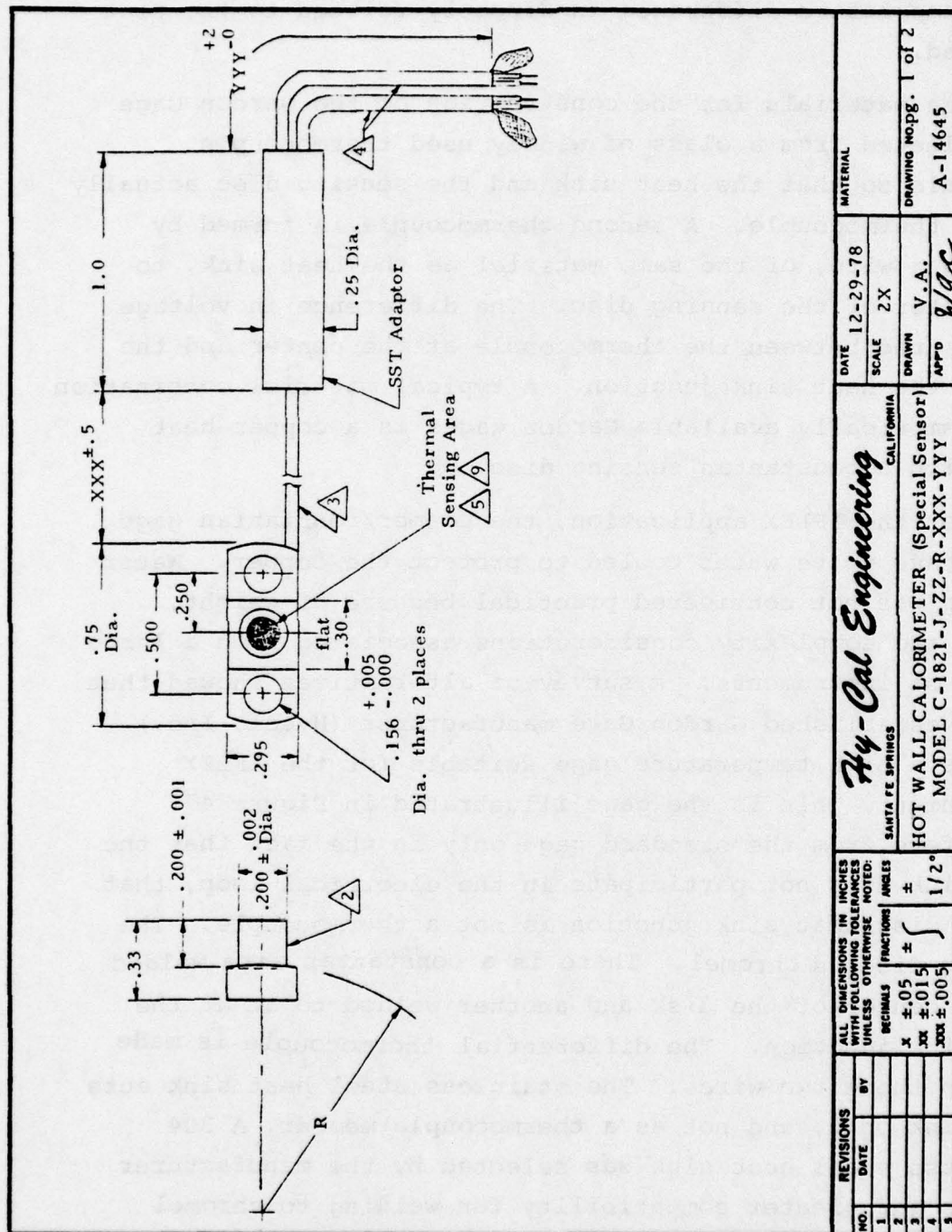
The thin skin transient technique is therefore not recommended for the IFLEX application.

#### 5.2.2. Asymtotic Calorimeters

Asymtotic calorimeters measure the conduction of heat within the sensor. The sensor is calibrated to measure the output signal proportional to the heat input to the calorimeter. Two types of asymtotic calorimeters have been used in reentry vehicle flight test applications (Reference 20). The Gardon type gage, which measures the lateral heat conduction in a thin film is the most common. An insulated rod type gage which measures heat conduction in depth has also been used. The insulated rod type of instrument has response characteristics similar to the thin skin transient technique and will therefore not be considered further.

##### 5.2.2.1 Gardon Type Asymtotic Calorimeter Description

The Gardon type asymtotic calorimeter is a mechanically robust heat transfer gage with a short time constant. Common designs yield electrical output suitable for recording or telemetry without amplification. No electrical excitation is required so that the gage is totally passive. A schematic of a Gardon Gage is shown in Figure 47. In the operation of the calorimeter, a heat flux is absorbed by the surface of the thin circular foil sensing disc which is welded to a massive cylindrical heat sink. The assumed uniform heating rate absorbed by the disc flows radially to the heat sink.



The radial conduction causes a temperature difference to exist between the center and the periphery of the foil. This temperature difference is directly related to the heat absorbed.

The materials for the construction of the Gardon Gage are selected from a class of widely used thermocouple materials so that the heat sink and the sensing disc actually form a thermocouple. A second thermocouple is formed by welding a wire, of the same material as the heat sink, to the center of the sensing disc. The difference in voltage is measured between the thermocouple at the center and the one at the heat sink junction. A typical material combination for commercially available Gardon gages is a copper heat sink with a constantan sensing disc.

For the IFLEX application, the copper/constantan gage would have to be water cooled to protect the copper. Water cooling was not considered practical because of weight, volume and complexity considerations associated with a large number of instruments. A survey of alternatives showed that a well established Gardon Gage manufacturer (Hycal, Inc.) markets a high temperature gage suitable for the IFLEX environment. This is the gage illustrated in Figure 47. It differs from the standard gage only in the fact that the heat sink does not participate in the electrical loop, that is, the disc/heat sink junction is not a thermocouple. The sensing disc is chromel. There is a constantan wire welded to the center of the disk and another welded to it at the heat sink junction. The differential thermocouple is made between these two wires. The stainless steel heat sink acts as a sink only, and not as a thermocouple member. A 304 stainless steel heat sink was selected by the manufacturer for its far greater compatibility for welding to chromel and its improved high temperature properties over copper. In addition to the differential thermocouple, a chromel



constantan thermocouple is welded to the stainless steel heat sink to monitor heat sink temperature. All thermocouple leads are changed to copper wires at a stainless steel housing, designed to assure constant temperature for all junctions. The design features are illustrated in the wiring diagram and schematic of the transducer in Figure 48. The method of installation and the overall appearance of the gage is depicted in Figure 49.

#### 5.2.2.2 Heat Transfer Gage Response

The Gardon Gage is an asymptotic calorimeter which senses a heat flux by means of a temperature difference which produces an electrical output (voltage) related to that temperature difference. In practice, the instrument is calibrated by imposing a known heat flux on the element and recording the output voltage directly. This procedure in essence bypasses the intermediate temperature measurement which is, however, required to gain an understanding of the functioning of the instrument.

The temperature response of the Gardon Gage was described by Gardon (Reference 22) using the radial conduction equation

$$\rho c \frac{\partial T}{\partial t} = \frac{\dot{q}}{s} + \frac{1}{r} \left[ \frac{\partial}{\partial r} (kr \frac{\partial T}{\partial r}) \right] \quad (27)$$

where

- $\rho$  = density
- $c$  = specific heat
- $q$  = heat flux
- $s$  = foil thickness
- $r$  = radius (variable)
- $k$  = conductivity
- $T$  = temperature
- $t$  = time

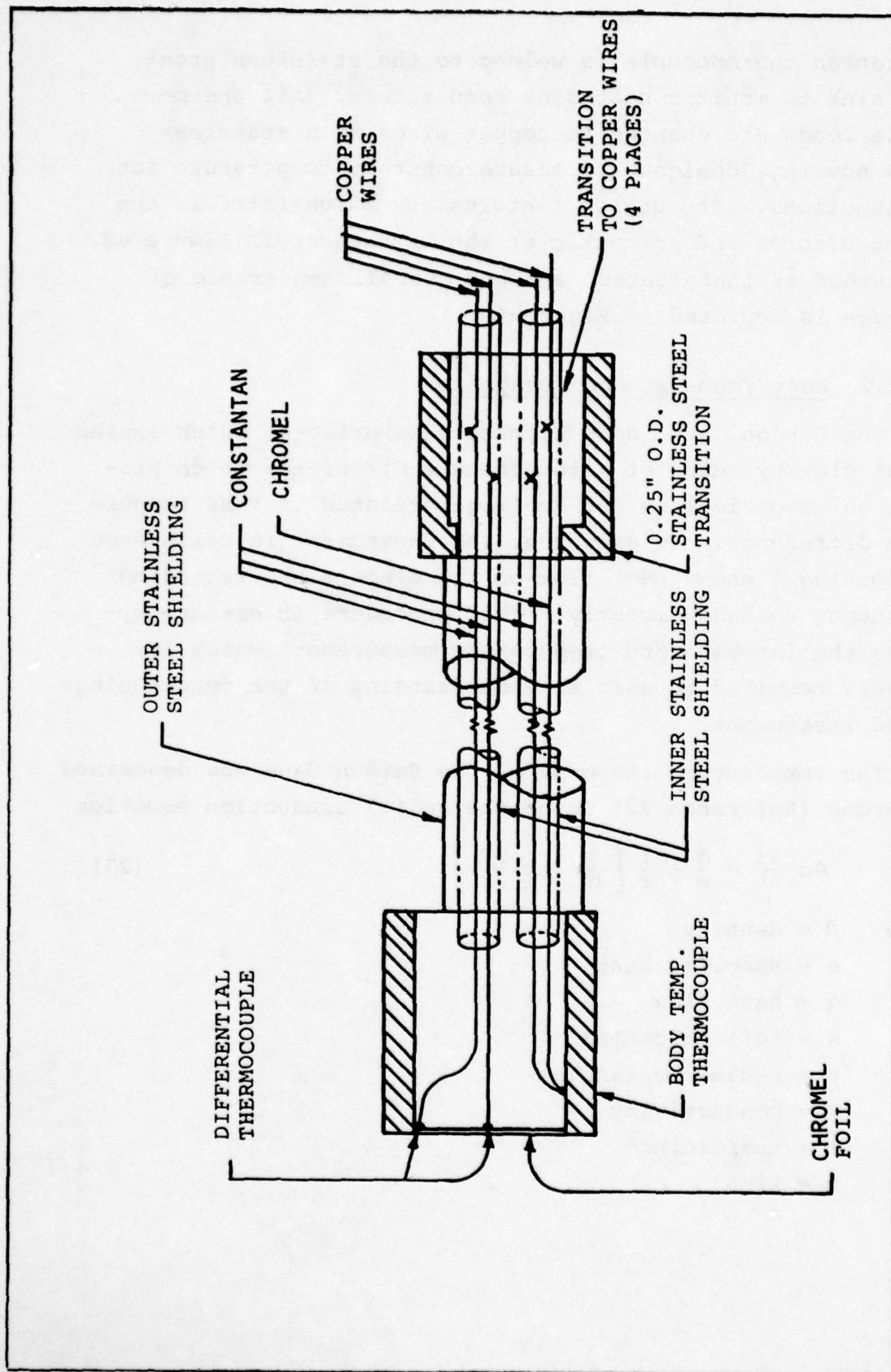


FIGURE 48. Wiring Diagram of the Chromel-Constantan Calorimeter

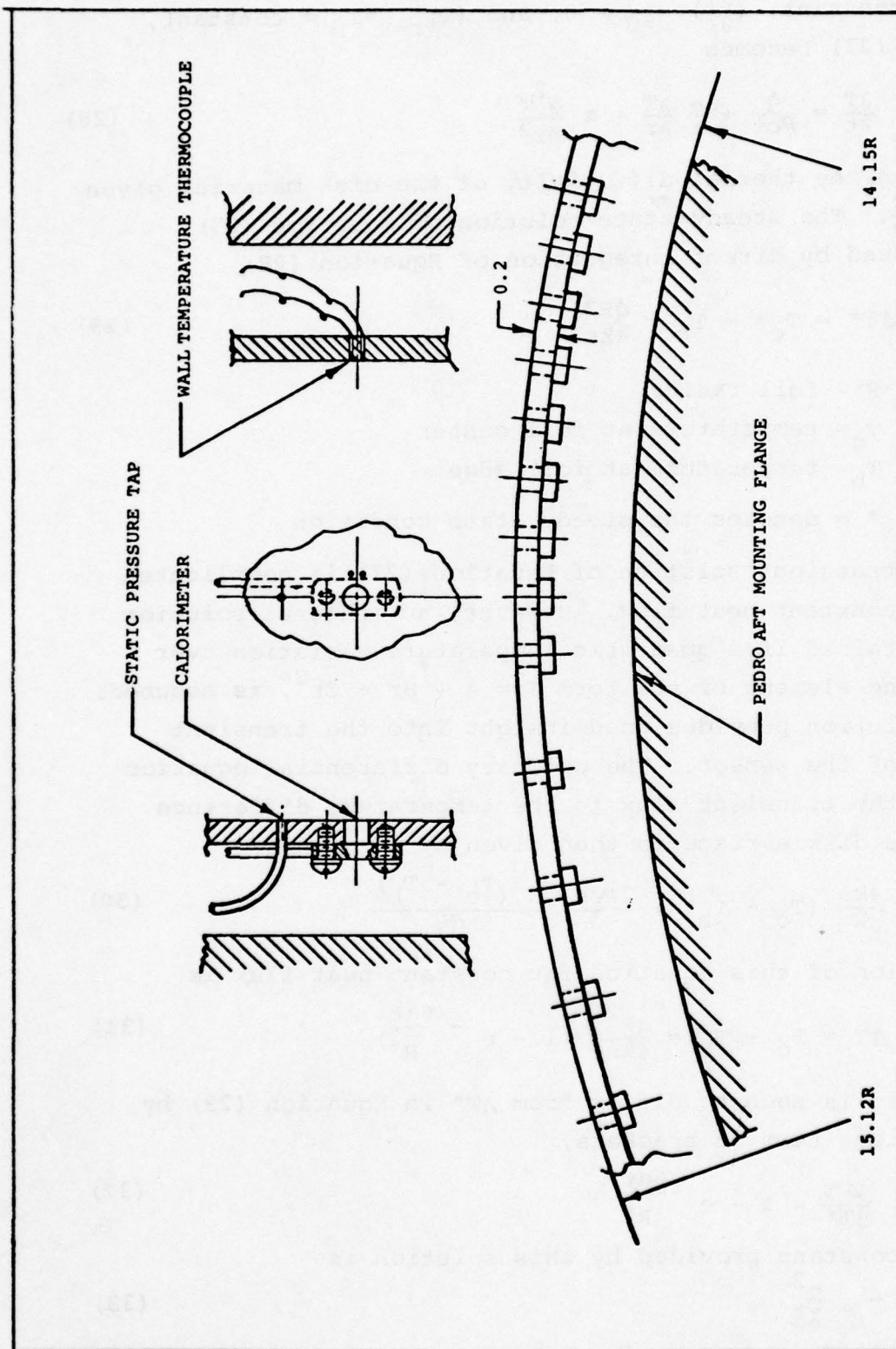


FIGURE 49. Cylinder Plate Instrumentation Schematic



For  $k = \text{constant}$ ,  $(\frac{\partial T}{\partial r})_{r=0} = 0$ , and  $(T)_{r=R} = T_b = \text{constant}$ , equation (27) becomes

$$\frac{\partial T}{\partial t} = \frac{\dot{q}}{\rho c_s} + \frac{\alpha}{r} \frac{\partial T}{\partial r} + \alpha \frac{\partial^2 T}{\partial r^2} \quad (28)$$

where  $\alpha$  is the thermal diffusivity of the disk material given by  $\alpha = \frac{k}{\rho c}$ . The steady state solution of Equation (27) was obtained by direct integration of Equation (28),

$$\Delta T^* = T_c^* - T_b = \frac{\dot{q} R^2}{4ks} \quad (29)$$

where  $R$  = foil radius  
 $T_c$  = temperature at foil center  
 $T_b$  = temperature at foil edge  
 $*$  = denotes the steady state condition

The transient solution of Equation (27) is complicated even for constant heat flux. However, an integral solution can be obtained if a quadratic temperature variation over the sensing element of the form  $T = A + Br + Cr^2$ , is assumed. Such a solution provides good insight into the transient response of the sensor. The ordinary differential equation relating the transient flux to the temperature difference across the disk surface is then given by

$$\dot{q} = \frac{4ks}{R^2} (T_c - T_b) + \frac{2\rho c_s}{3} \frac{d(T_c - T_b)}{dt} \quad (30)$$

The solution of this equation for constant heat flux is

$$\Delta T = T_c - T_b = \frac{\dot{q} R^2}{4ks} \left( 1 - e^{-\frac{6\alpha t}{R^2}} \right) \quad (31)$$

this result is seen to differ from  $\Delta T^*$  in Equation (29) by the transient term in brackets,

$$\frac{\Delta T}{\Delta T^*} = 1 - e^{-\frac{6\alpha t}{R^2}} \quad (32)$$

The time constant provided by this solution is

$$\tau = \frac{R^2}{6\alpha} \quad (33)$$

This result compares well with the exact solution of Equation (28), given in Reference 23, which results in the time constant

$$\tau = \frac{R^2}{5.65\alpha} \quad (34)$$

The hot wall Gardon gage manufactured by Hy-Cal Engineering has a 1/8 inch diameter sensing disc of chromel welded to a stainless steel body. The response time of this transducer is then given by the thermal diffusivity of chromel (0.175 ft<sup>2</sup>/hr at room temperature and the sensor geometry from equation 33

$$\tau = \frac{R^2}{6\alpha} = .09 \text{ sec.} \quad (35)$$

The time constant for the above instrument is seen to be adequate, even for the maximum rate of change of heat flux. The Gardon gage was originally developed for application in radiation environments (Reference 20). There the wall temperature difference between disc center and heat sink does not affect the net heat transfer, for reasonably low sensor temperatures. In the application to the convective environment, the sensor and heat sink temperatures become important in the determination of the film heat transfer coefficient, especially in the presence of heat transfer gradients. This effect has been termed the non-isothermal heating or non-isothermal wall effect. It has been treated extensively in the literature. Reference 24 presents a concise treatment of the non-isothermal wall effect for

steady heat transfer. It is shown that for small streamwise heat transfer gradients (small relative to the sensor dimensions), non-isothermal wall effects may be neglected. For the IFLEX application, where sensor dimensions are on the order of one tenth of the boundary layer dimensions, these non-isothermal wall effects can safely be neglected.

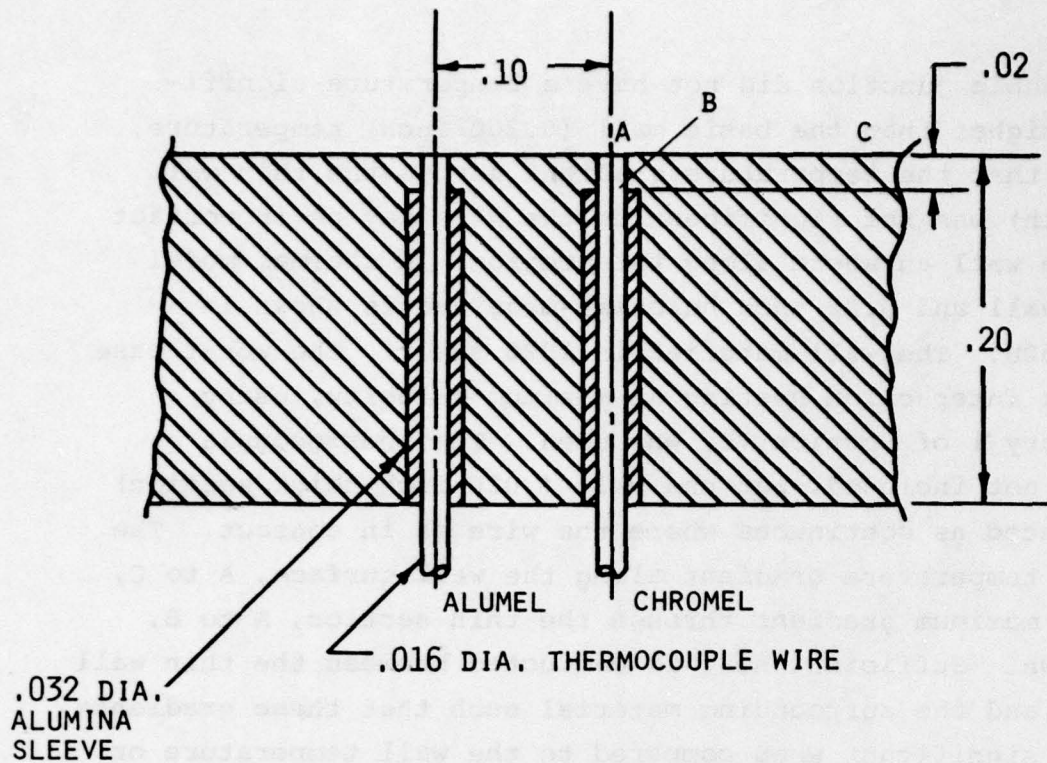
For ideal performance of the Gardon gage, the heat sink should remain near a constant, low temperature. For the hot wall calorimeter recommended, the low temperature requirement is removed. However, for the instrument selected, the sink temperature lags recovery temperature over all but the terminal segment of the flight trajectory. With this condition satisfied, the difference between the center temperature and the rim temperature only approaches zero near the trajectory end. Therefore, the heat transfer data will be accurately measured over most of the trajectory. Some resolution will be lost late in the trajectory, when heat transfer rates become small. At that time, the vehicle wall and sensor heat sinks approach recovery temperature by virtue of increased wall temperature and decreased recovery temperature. The absolute accuracy of the gauge, in the region of low heat transfer to hot walls, will require experimental determination.

### 5.2.3 Wall Temperature Measurement

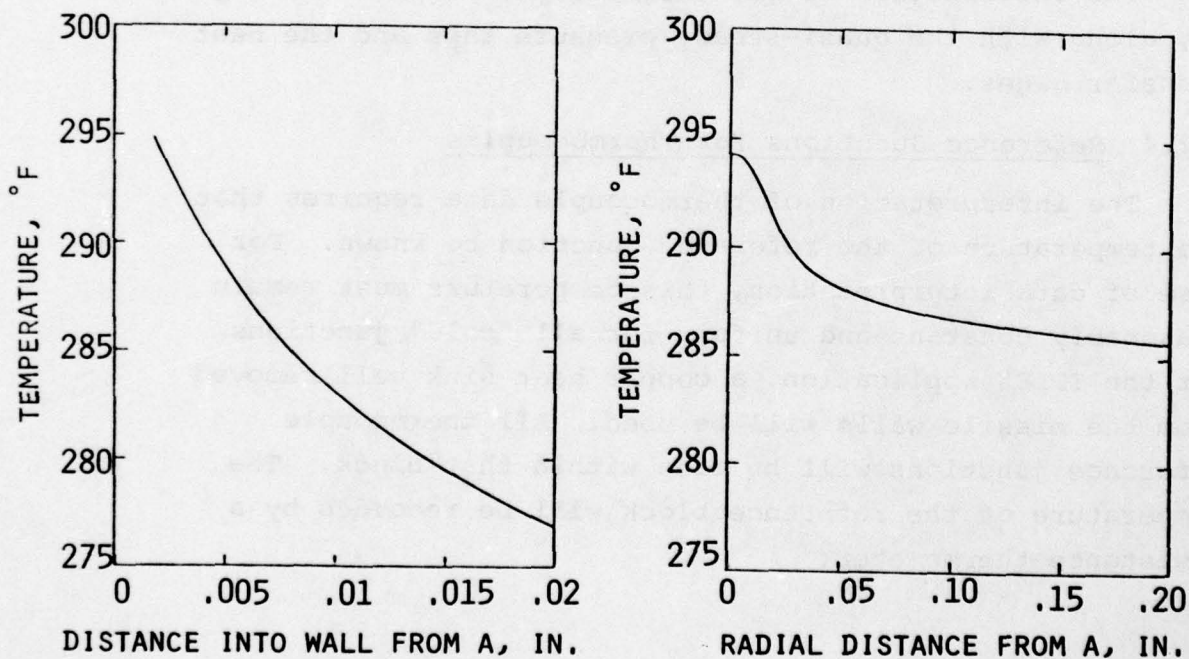
The wall outer surface temperature must be measured in the vicinity of the calorimeter without modifying the wall temperature by the measurement apparatus. This will be done by using chromel-alumel thermocouples mounted as shown in Figure 50A. Thermocouple wires (0.016 inch diameter) are spot welded at the wall surface. They are insulated from the cooler inner region of the wall by a 0.032 inch OD alumina sleeve.

The thermal response of this region of the wall was analyzed to insure (1) that the thin wall (.020 inch) at the





(A) Typical Installation



(B) Thermal Response of Wall Thermocouple (Trajectory 1, 34 Seconds, Shock interaction Heating)

FIGURE 50. Wall Temperature Thermocouple

thermocouple junction did not have a temperature significantly higher than the basic wall (0.200 inch) temperature, and (2) that the temperature gradient across the thin wall (in depth) was not significant as the wire may be in contact with the wall anywhere along this region. A thermal model of the wall and 0.32 inch hole was made and is shown in Figure 50B. The wall material is 1020 steel. The worst case of shock interaction heating at maximum velocity, using trajectory 1 of Section VI, was used. The thermocouple wire is not included, but the wall (.020 inch thick section) was treated as continuous where the wire is in contact. The maximum temperature gradient along the wall surface, A to C, and the maximum gradient through the thin section, A to B, are shown. Sufficient heat is conducted between the thin wall section and the surrounding material such that these gradients are not significant when compared to the wall temperature or the recovery temperature.

The installation of the thermocouple is shown in Figure 49, along with the quasi-steady pressure taps and the heat transfer gages.

#### 5.2.4 Reference Junctions for Thermocouples

The interpretation of thermocouple data requires that the temperature of the reference junction be known. For ease of data interpretation, this temperature must remain reasonably constant and uniform for all "cold" junctions. For the IFLEX application, a copper heat sink well removed from the missile walls will be used. All thermocouple reference junctions will be made within that block. The temperature of the reference block will be recorded by a resistance thermometer.



### 5.3 OTHER MEASUREMENTS AND INDICATORS

Three components of acceleration and various system operation indicators will be measured in addition to the pressure, heat transfer, and temperature measurements described in the previous sections.

#### 5.3.1 Acceleration - 3 Mutually Perpendicular Axes

Acceleration in 3 orthogonal axes will be measured to provide IFLEX vehicle dynamics data. These data will also be in the D.C. to 5 Hz data bandwidth with acceleration sensitivity ranges of 50, 10 and 10 g's for the longitudinal, pitch, and yaw axes respectively. The axes orientation are illustrated in Figure 51. The Entran Devices, Inc., Model EGC-240 series meets the requirements for this experiment (Figure 52). The standard temperature compensation range of this device is 80° to 180°F. This range is not adequate for the range of temperature expected in the thermally protected area (0 to 100°F). Entran Devices will provide a non-standard, temperature compensated unit, with similar characteristics. Output signal F.S. voltages will be +100 mV for the 10 g devices and +200 mV for the 50 g device.

#### 5.3.2 Missile Operation Indicators

Signal sources for the missile operation indicators will be from switch closures, battery voltage monitors, thermocouple or thermistor temperature indicators and others as needed. These indicators are purposely defined generally so that as the need for one is established it can easily be incorporated into the system. It has not yet been determined which are critical and which might be included on a space available basis. Specific flight operations requirements will dictate some installations. As indicated in Table 1, 34 channels of PCM telemetry are available for these indicators.



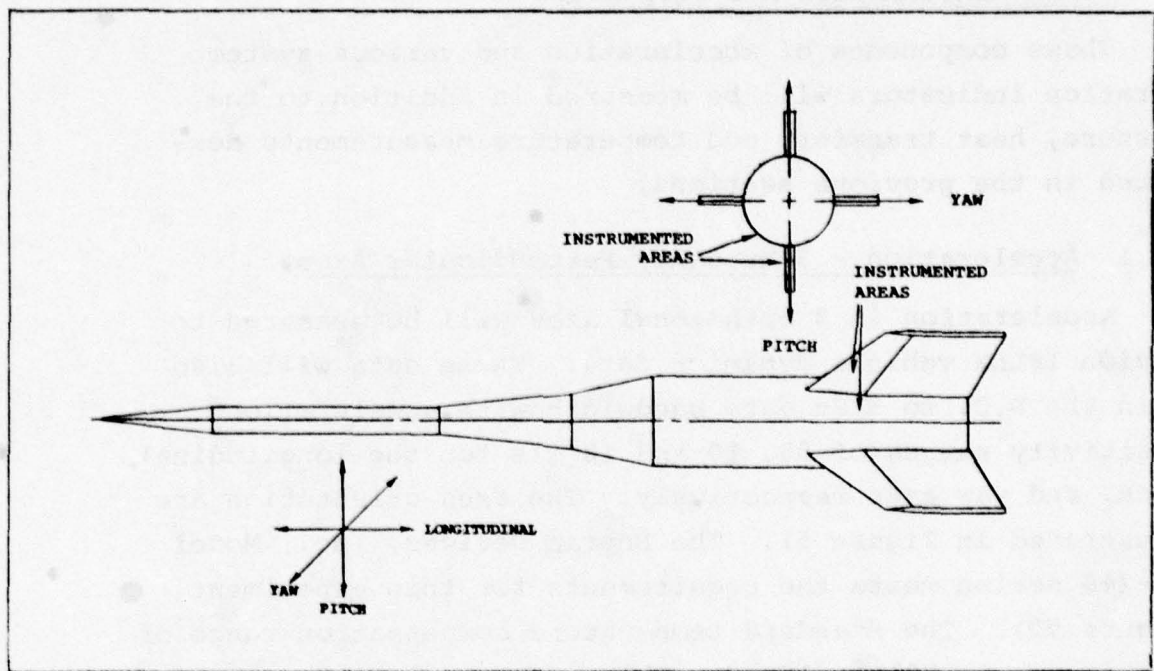


FIGURE 51. Accelerometer Axes

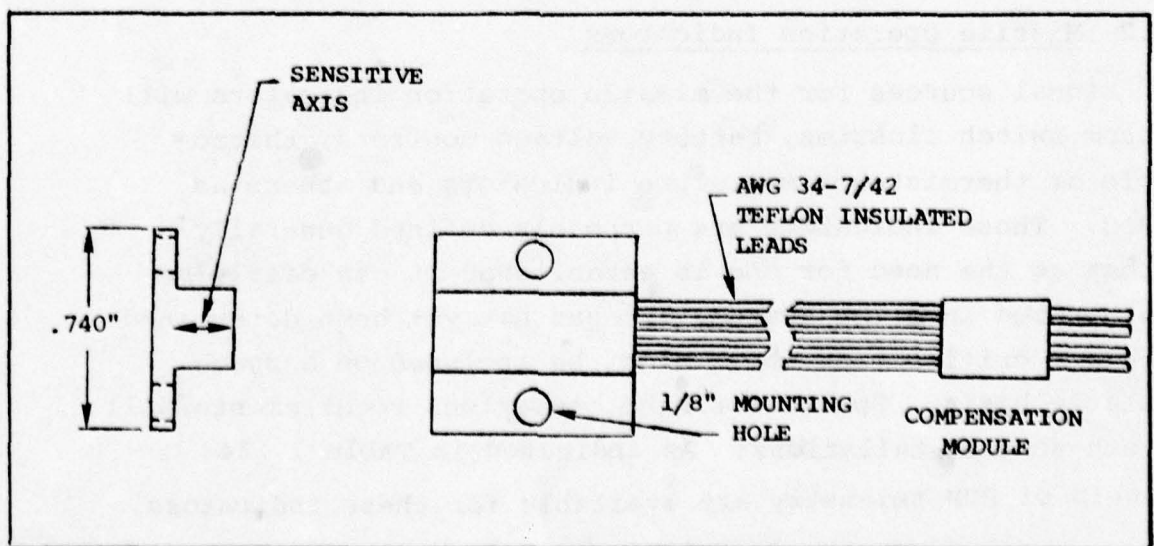


FIGURE 52. Accelerometer Dimensions

#### 5.4 DATA ACQUISITION SYSTEM

The task of the airborne portion of the data acquisition system is to combine the outputs of the various transducers and transmit them to a ground recording station. The basic subsystems consist of the following:

- 1) Signal conditioning electronics - These circuits convert the transducer outputs into forms which are compatible with the multiplexing subsystem.
- 2) Multiplexing system - This is the system used to combine all the modified transducer outputs into a form which can be used to modulate the telemetry transmitter. Several forms are available which are compatible with the ground telemetry receiving equipment.
- 3) Telemetry transmitter - The selection of this unit is based on the capabilities of the range receiving equipment as well as the requirements imposed by the multiplexing system.
- 4) Telemetry antenna - In addition to the pattern dictated by the relationship to the range receivers during the flight trajectory, the flight environment imposes severe restrictions on the physical design.

No cooling is planned for the equipment except for heat sinks. The most critical item for maximum allowed temperature is the telemetry transmitter (137°F). Except for the brief flight time, the maximum temperature that the IFLEX will be subjected to is that encountered on the ground prior to flight. Limiting this temperature to 120°F is recommended.

##### 5.4.1 Signal Conditioning

The outputs of the various transducers incorporated cannot, in general, be directly connected to the multiplexing

system. To implement a multiplexing system in a straightforward manner the inputs must be confined to a few ranges of voltages. In addition, different types of transducers impose special requirements on the conditioning electronics to obtain the required signal levels. Specifically, these are:

- a) Piezoelectric device. The piezoelectric element in a device generates an electrical charge when a mechanical input is applied. The resulting output voltage is inversely proportional to the capacity of the circuit. Since the cable connecting the device to a multiplexer forms a portion of this capacity, the output voltage is sensitive to cable length. Common practice is to use a charge amplifier to overcome this complication. A charge amplifier is merely a noninverting operational (servo) amplifier which drives the input to null and senses the feedback current required. The feedback required is thus only dependent on the charge generated. Units such as the Kistler Instrument Co. Model 553A, occupying less than one cubic inch volume, are readily available.
- b) Strain gages. All strain gages operate on the principle of measuring a change of resistance which accompanies imposing mechanical strain on an element. Since the resistance change does not in itself generate a signal, an excitation supply is required as a minimum. In this case, signal conditioning may incorporate amplification and filtering in addition to supplying the excitation for a bridge. The Aydin Vector multiplexer unit selected also contains strain gage excitation and low level amplifiers making external circuitry unnecessary.



- c) Thermocouple devices. In common practice, thermocouples have one element connected to a frame ground. Since many natural thermocouple junctions exist within an airframe, it is imperative that instrumentation thermocouple junctions not be connected directly to a common ground. Signal conditioning electronics for these devices consists of a differential input amplifier with good common mode rejection. Again, the Aydin Vector multiplexor package can incorporate low level signal amplifier with 80 dB common mode rejection.

#### 5.4.2 Multiplexer

Two types of multiplexing are incorporated in the proposed system. One type is a sampling, or time division multiplexing. It is applicable for slowly changing signals, where a series of discrete data points provide sufficient information. The second technique is frequency division multiplexing. Here a high frequency carrier (as compared to the signal to be measured) is frequency modulated. Upon subsequent demodulation the original signal is continuously recorded. Frequency division multiplexing is reserved for rapidly varying signals such as fluctuating pressure measurements.

##### 5.4.2.1 Time-Division-Multiplexer

The time division multiplex system is designed to process up to 250 data points at a minimum rate of 20 samples per second per data point. This system must also determine the sampling sequence and identify each sample.

Two time division systems were considered. They are the Pulse Amplitude Modulation (PAM) and the Pulse Coded Modulation (PCM) systems. The PAM system requires less transmitted signal bandwidth and has lower initial cost,

but its limiting factor is that the successful reception of amplitude data is proportional to the signal-to-noise ratio at the receiver. PCM is essentially the same as PAM with the exception that the signal is digitized prior to transmission. PAM is also digitized, but after it has been received and demodulated. The PCM signal is essentially a go or no-go signal. Because of this it is virtually immune to error generated by noise. The PCM system has a disadvantage compared to the PAM system in that it requires more bandwidth to carry the same information. After analyzing the IFLEX requirements it was concluded that the PCM system is compatible with the mission. The PCM system was therefore selected. All quasi-steady data will be telemetered through the PCM system.

The basic elements of a PCM system are shown in Figure 53. The analog channels that the PCM system will handle are all the quasi-steady state measurements (250 inputs). The multiplexer is an electronic switching device that turns on one channel at a time and is controlled by the PCM system programmer and sync generator. As each channel is turned on, the analog amplifier and sample/hold circuit samples that signal amplitude and holds it at that amplitude. The sample/hold circuit holds that value while the analog to digital converter (ADC) converts the signal from an analog amplitude to a binary number. This number is fed to the mixer amplifier. The PCM programmer then repeats the whole process for the next channel sampled. The PCM programmer determines the sequence of sampling, generates a frame sync code and generally controls the entire signal conditioning process.

The Aydin-Vector MMP-600 PCM system appears most adaptable to IFLEX objectives. Table 3 depicts some of the features of this system. Resolution can be selected from 7, 8, 9, or 10 bits; 8 bits has been selected. The reason for this selection is that 8 bits represent 256 steps ( $2^8$ )

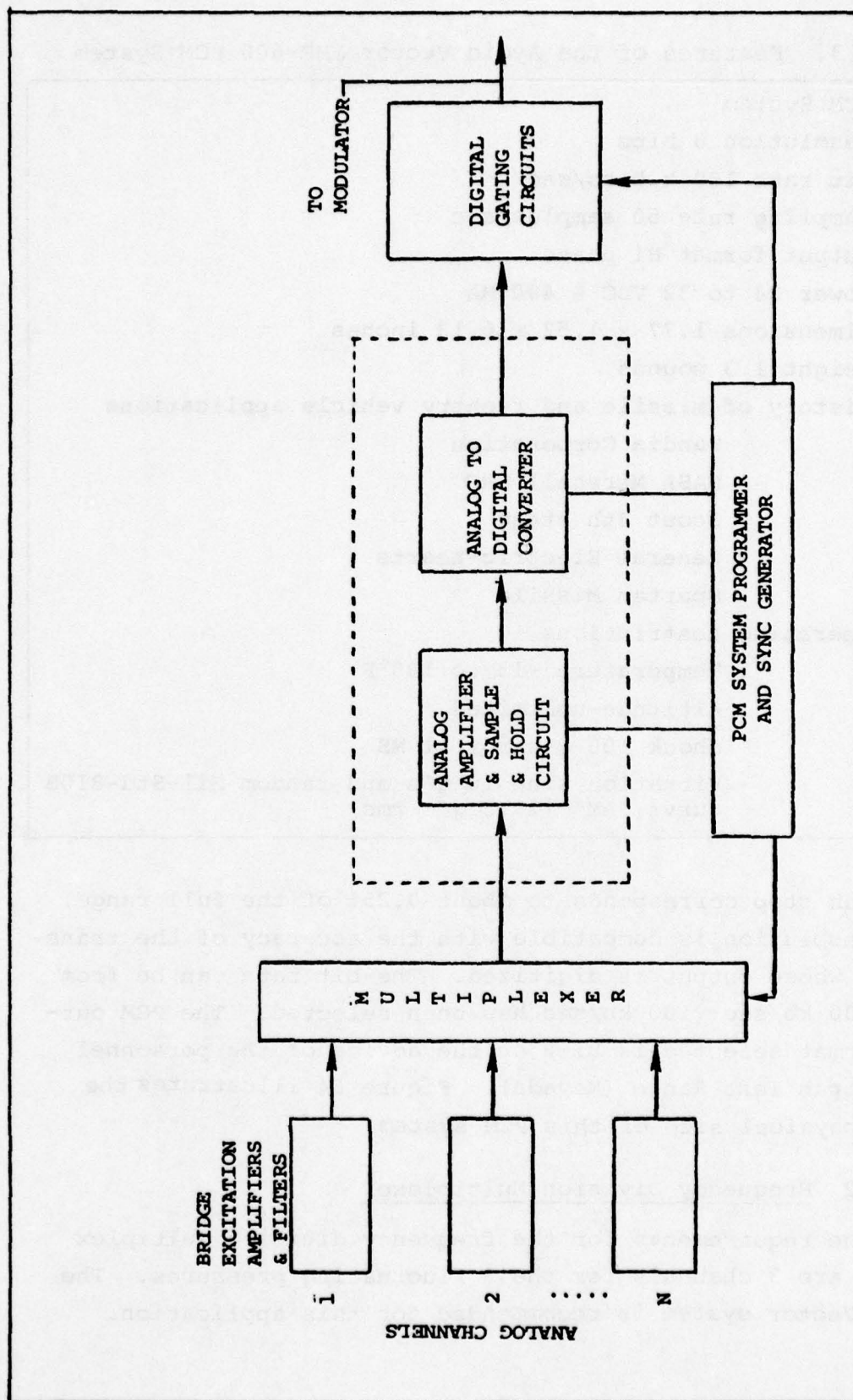


FIGURE 53. Basic Elements Of A PCM System



Table 3. Features of the Aydin Vector MMP-600 PCM System

PCM System
Resolution 8 bits
Bit rate 100 k bits/sec
Sampling rate 50 samples/sec
Output format Bi phase
Power 24 to 32 VDC @ 400 MA
Dimensions 1.77 x 1.52 x 6.13 inches
Weight 1.3 pounds
History of missile and reentry vehicle applications
Sandia Corporation
NASA Marshall SRC
Scout 4th stage
General Electric-hearts
Spartan Missile
Operating Restrictions
Temperature -13 to 185°F
Altitude-unlimited
Shock 100 g's for 11 MS
Vibration sine 10 g's and random Mil-Std-810B curve "AM" (29.3 g's rms)

and each step corresponds to about 0.25% of the full range. This resolution is compatible with the accuracy of the transducers whose output is digitized. The bit rate can be from 1 to 500 kb/sec; 100 kb/sec has been selected. The PCM output format selected is Bi-Ø on the advice of the personnel at Tonopah Test Range (Nevada). Figure 54 illustrates the small physical size of this PCM system.

#### 5.4.2.2 Frequency Division Multiplexer

The requirements for the frequency division multiplex system are 3 channels for the 3 fluctuating pressures. The Aydin-Vector system is recommended for this application.

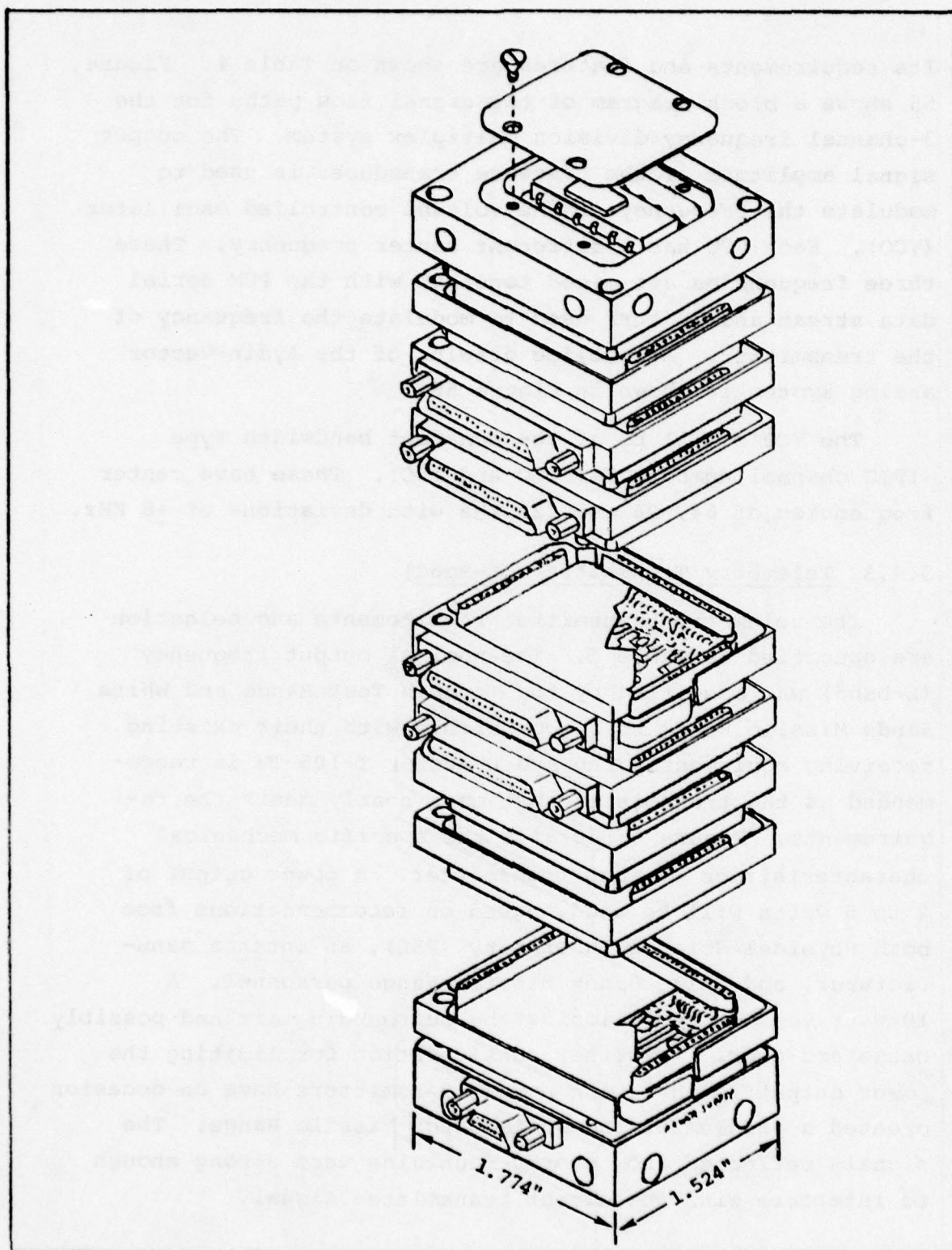


FIGURE 54. Aydin Vector MMP-600 PCM System Illustration

Its requirements and features are shown on Table 4. Figure 55 shows a block diagram of the signal flow path for the 3-channel frequency division multiplex system. The output signal amplitude of the pressure transducer is used to modulate the frequency of the voltage controlled oscillator (VCO). Each VCO has a different center frequency. These three frequencies are mixed together with the PCM serial data stream and in turn used to modulate the frequency of the transmitter. An outline drawing of the Aydin-Vector analog system is shown in Figure 56.

The VCO's will be of the constant bandwidth type (IRIG channel numbers 7C, 11C and 15C). These have center frequencies of 64, 96 and 128 KHz with deviations of  $\pm 8$  KHz.

#### 5.4.3 Telemetry Transmitter (L-Band)

The telemetry transmitter requirements and selection are specified in Table 5. The nominal output frequency (L-band) was specified by the Tonopah Test Range and White Sands Missile Range to be compatible with their existing receiving equipment. The Aydin-Vector T-105-TV is recommended as the transmitter that most nearly meets the requirements. Figure 57 details the specific mechanical characteristics of this transmitter. A power output of 2 to 5 watts will be used, based on recommendations from both Physical Science Laboratory (PSL), an antenna manufacturer, and White Sands Missile Range personnel. A 10-watt version could ionize the surrounding air and possibly cause arc-over. A further consideration for limiting the power output is that high power transmitters have on occasion created a problem at the White Sands Missile Range. The signals reflected from nearby mountains were strong enough to interfere with the direct transmitted signal.



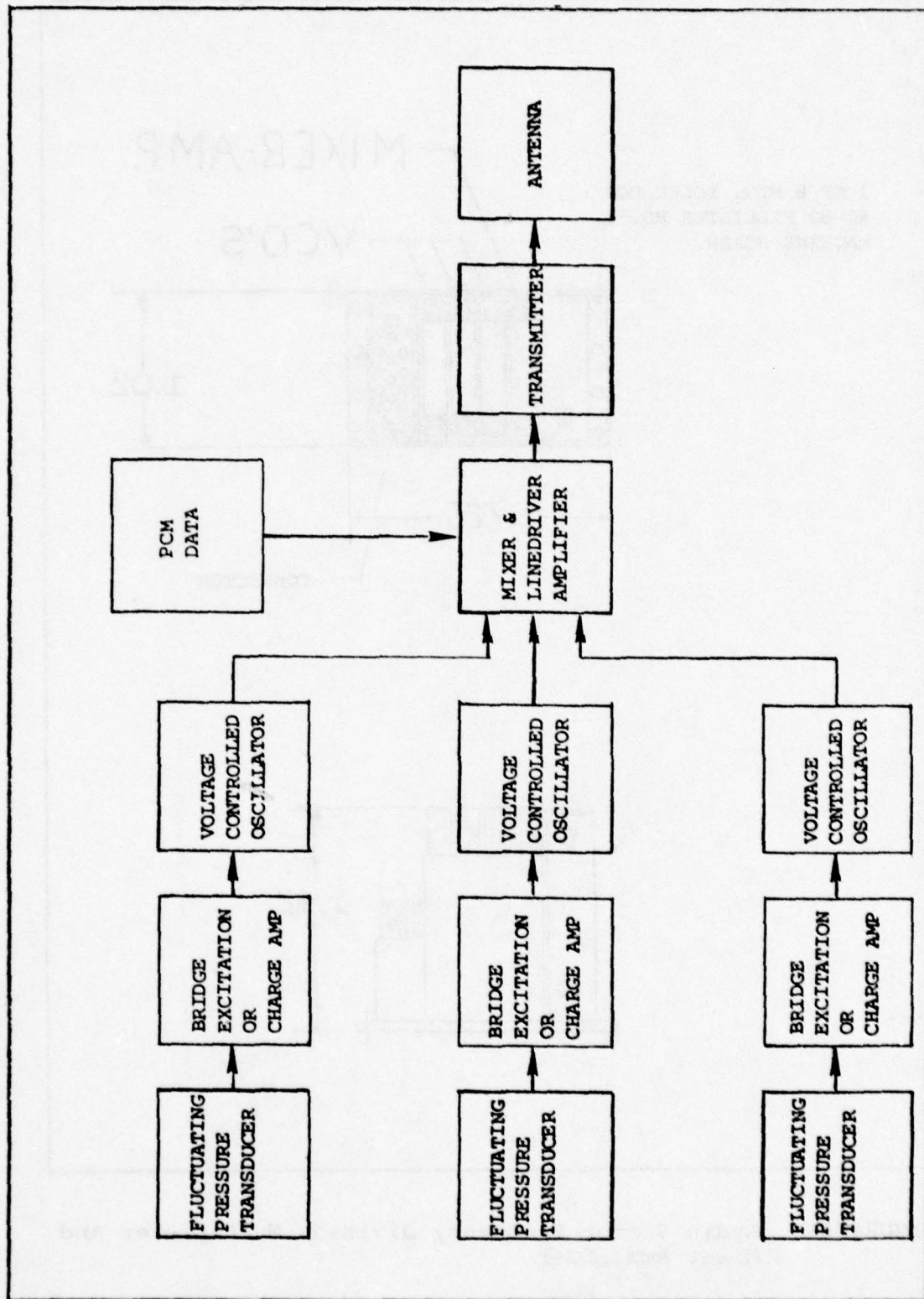


FIGURE 55. Fluctuating Pressure Data Flow Chart

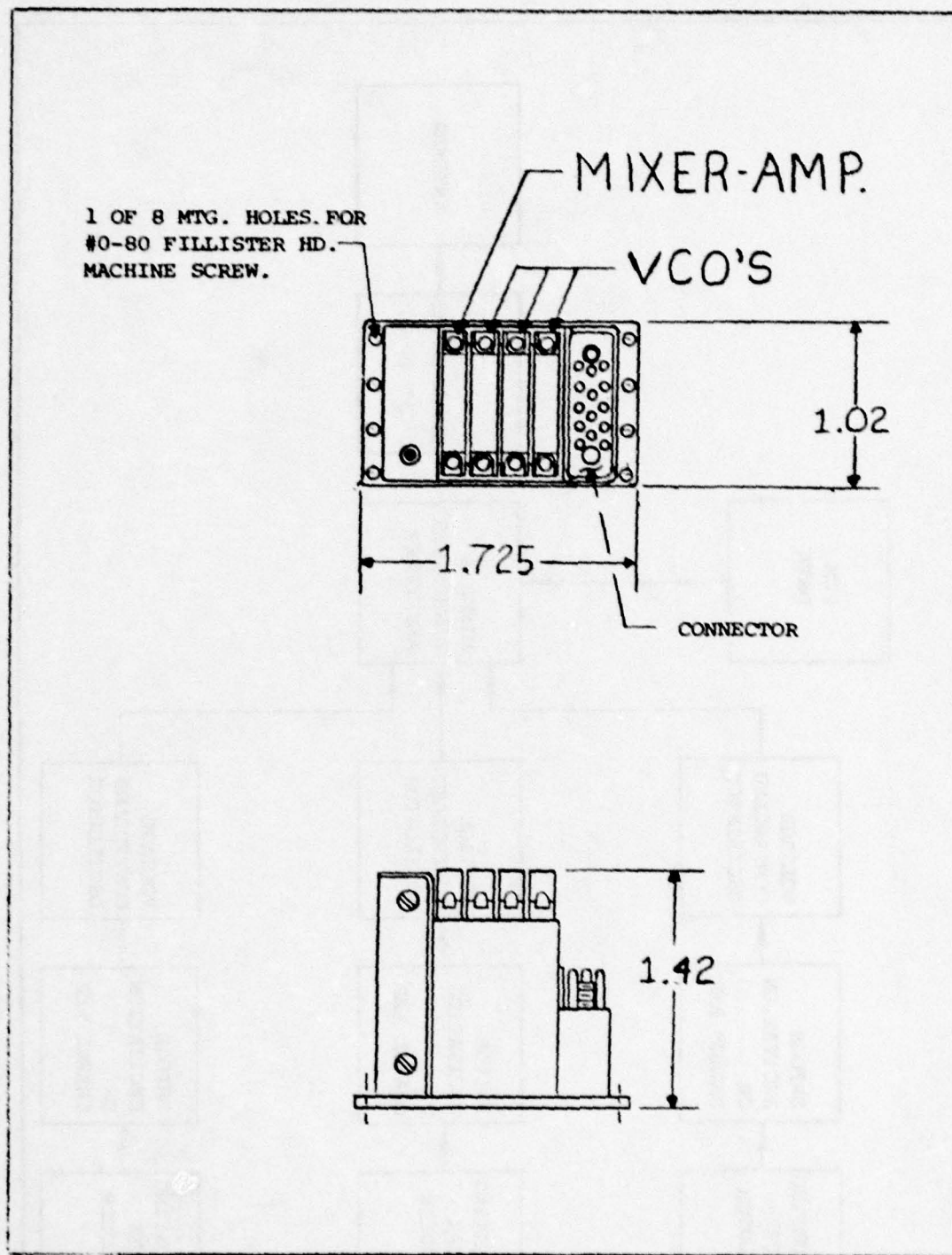


FIGURE 56. Aydin Vector Frequency Division Multiplexer And Mixer Amplifier

## AYDIN VECTOR T-105 TV SERIES

INPUT VOLTAGE:  $28 \pm 4$  VOLTS INPUT CURRENT: 2.0 A MAXIMUM

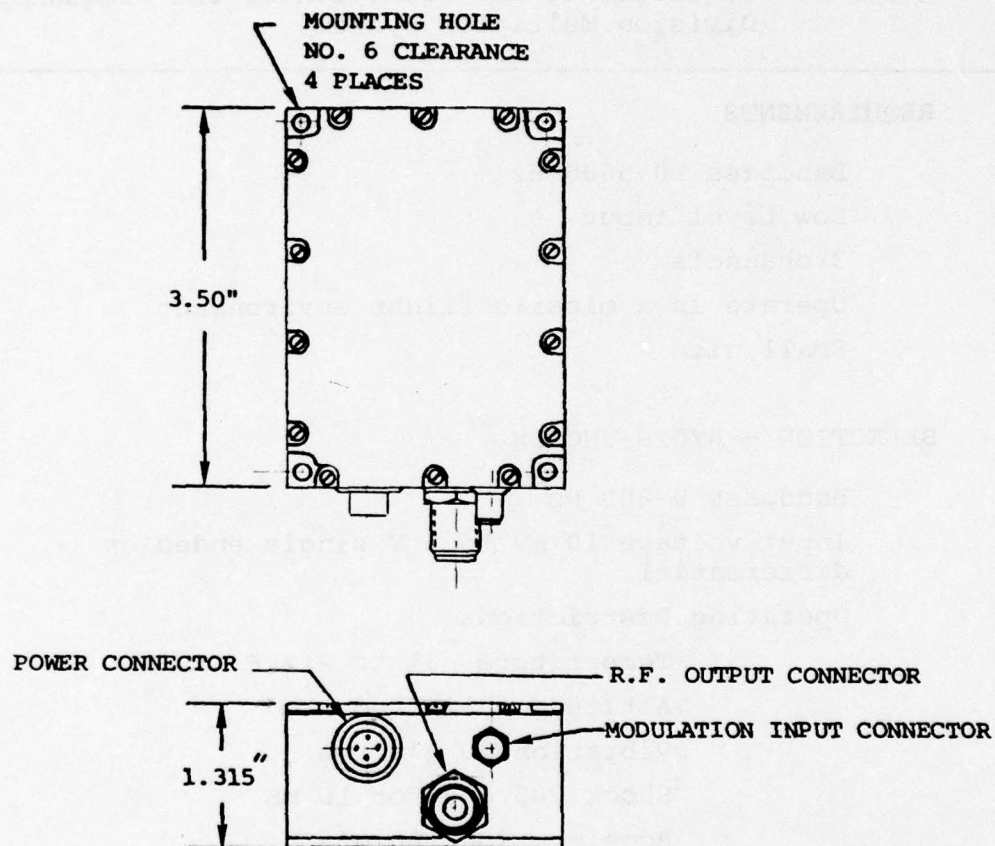


FIGURE 57. L-Band Transmitter



Table 4. Requirements and Selection of the Frequency Division Multiplex System

REQUIREMENTS

Bandpass 10-5000 Hz

Low Level input

3 channels

Operate in a missile flight environment

Small size

SELECTION - AYDIN-VECTOR

Bandpass 0-800 Hz

Input voltage 10 mV to 5 V single ended or differential

Operating Restrictions

Temperature -31 to 212°F

Altitude unlimited

Vibration 30 g's rms

Shock 200 g's for 10 mS

Acceleration 100 g's

Size h x w x d = 1.42 x 1.72 x 1.02 inch

Table 5. Telemetry Transmitter Requirements and Selection

REQUIREMENTS

Frequency output 1.435 to 1.540 GHz (L-Band)  
Bandwidth 10 Hz to MHz  
Power output 2 to 5 watts  
Small size  
Operate in missile flight environment

SELECTION - AYDIN-VECTOR t-105-tv

Frequency = L-Band  
Bandwidth 10 Hz to MHz  
Power output 5 watts  
Size 2.50 x 3.50 x 1.32 inches  
Volume 16.5 in<sup>3</sup>  
Weight 1.0 pounds  
Operating Restrictions  
    Temperature 2 to 137°F (base plate)  
    Vibration 20 g's  
    Shock 100 g's for 11 ms  
    Acceleration 100 g's  
    Altitude unlimited

5.5 RADAR TRANSPONDER (C-BAND)

The frequency band specified by the Tonopah Test Range and the White Sands Missile Range is the C-Band (5.690 to 5.765 GHz). A high pulse power (100 watts minimum) output was specified by the Tonopah Test Range (TTR) so that the IFLEX vehicle could be acquired and tracked prior to launch. Because of the intermittent operation, higher power levels are acceptable on the transponder than on the transmitter. A Motorola SST-271C was selected as the radar transponder for this experiment. An outline drawing of this transponder is shown in Figure 58. Its size and performance are summarized as follows:

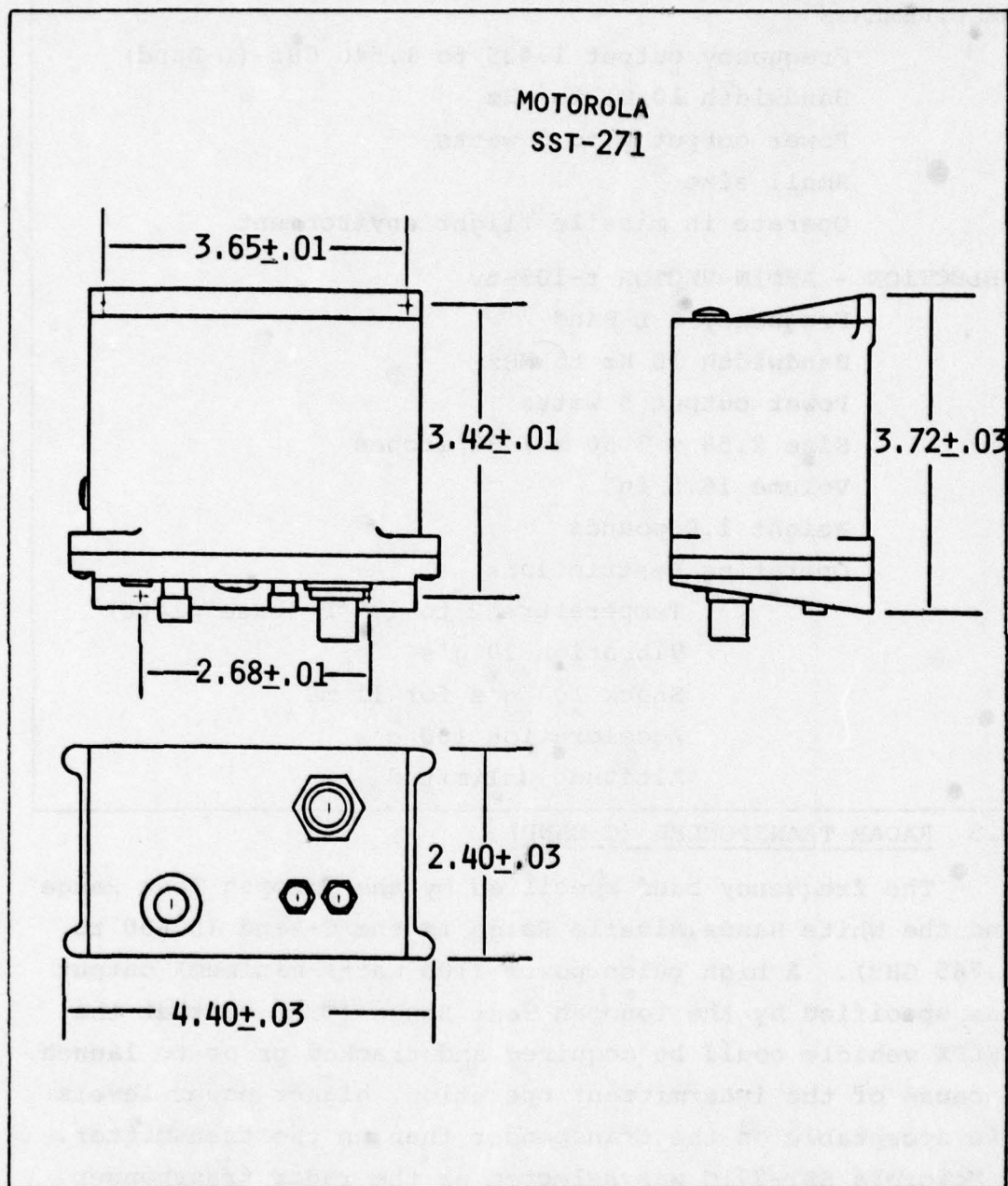


FIGURE 58. C-Band Radar Transponder



Output frequency - 5.728 GHZ

Peak pulse power output - 400 watts

Size L x W x D - 4.40 x 2.40 x 3.72 inches

Weight - 3.2 pounds

Input power at 24 - 30 VDC - 0.7 amps maximum

Environmental

Vibration - 25.4 g's

Shock - 100 g's for 11 ms

Acceleration - 100 g's

Temperature - 65 F to 167°F

The SST-271C is no longer in quantity production (as of March 26, 1979) and that it should be replaced with a Motorola standard model which is the SST 171. This device occupies slightly more volume, 39 in<sup>3</sup> instead of 33 in<sup>3</sup>, and has otherwise similar specifications as the SST 271C.

#### 5.6 TELEMETRY AND TRANSPONDER ANTENNAS

Since the vehicle will be rolling during the flight, omnidirectional antenna patterns for the telemetry and radar transponder would be desirable. However, the flight profiles reveal there is no real requirement for a signal to be transmitted directly forward. Absence of this requirement allows consideration of a flush-mounted antenna configuration. Further, it was determined that the vehicle will be in view by at least two ground-based antennas during the entire flight. Thus, notches in the airborne antenna pattern are unlikely to result in signal dropouts. It is desirable that both antennas be combined into one 9-inch diameter structure that will be attached at Location 36.89 on the IFLEX vehicle. Also, surface flow disturbance due to the antenna must be held to a minimum.

Two design approaches were considered. The recommended approach is the Physical Science Laboratory of New Mexico State University (PSL) quadra-loop design. The L-Band

antenna consists of four PSL quadra-loop radiators spaced 90° apart on a 9-inch diameter bolt-in section. This bolt-in section will also accommodate the transponder (C-Band) antenna system. One PSL quadra-loop radiator is illustrated in Figure 59, and Figure 60 shows the bolt-in section with both the L-Band and C-Band antenna systems in their proposed locations. Energy is radiated through the flush quartz windows.

An alternative approach is to employ a wrap-around antenna design either by PSL or Vega Precision Laboratories (VPL). In this approach both L and C-Band antennas are combined in one package; the L-Band antenna is a 4-element array, while the C-Band is a 24-element array. The quartz windows are not compatible with the wrap-around antenna, so non-uniform ablation is not a consideration. However, the antenna radiator must be thermally insulated. In this design the Dyna-Therm DE-350 insulator would be used over the antenna radiators. The disadvantage is that the electrical transmission characteristics of DE-350 in the L and C bands are unknown. Therefore, they would have to be determined before this system could be recommended. This would require measuring the radiation pattern when transmitting through the DE-350. DE-350 was formulated to eliminate the presence of alkali metals so that an ionized layer would not form during ablation. However, preliminary experiments conducted on DE-350 at SAI, at the intermediate S-Band frequency of 2.450 GHz, indicate the induced power losses may be excessive. The opinion of PSL is that the quadra-loop antenna will be adequate if surface recession of the Dynatherm DE-350 in the vicinity of the quartz windows is sufficiently small as it is predicted to be.

#### 5.7 ROCKET MOTOR IGNITION AND FIN DEPLOYMENT

The sequence of fin deployment and rocket motor ignition is initiated by a lanyard which is attached to the

PHYSICAL SCIENCES LAB  
MODEL 6.063

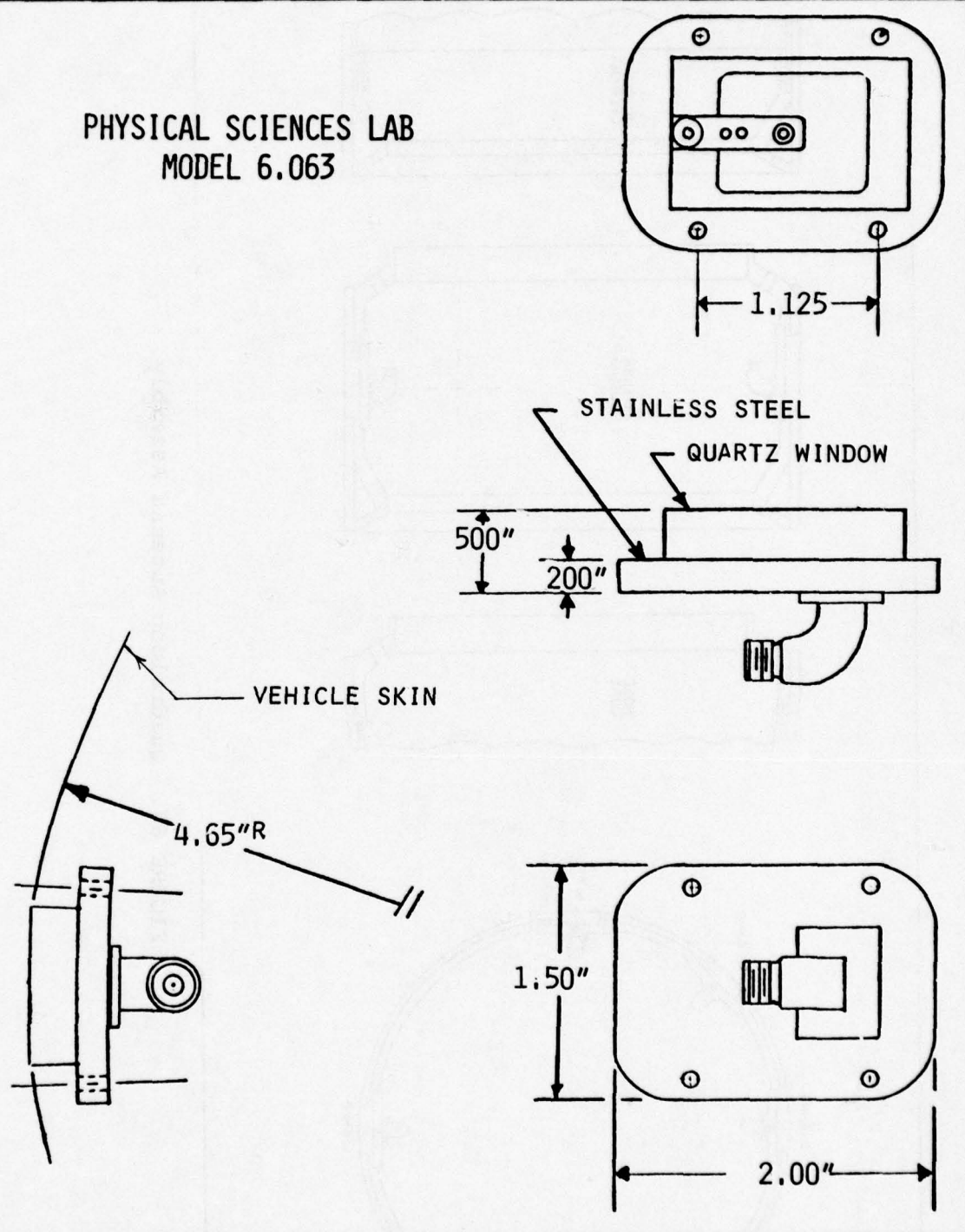


FIGURE 59. Quadraloop Radiator



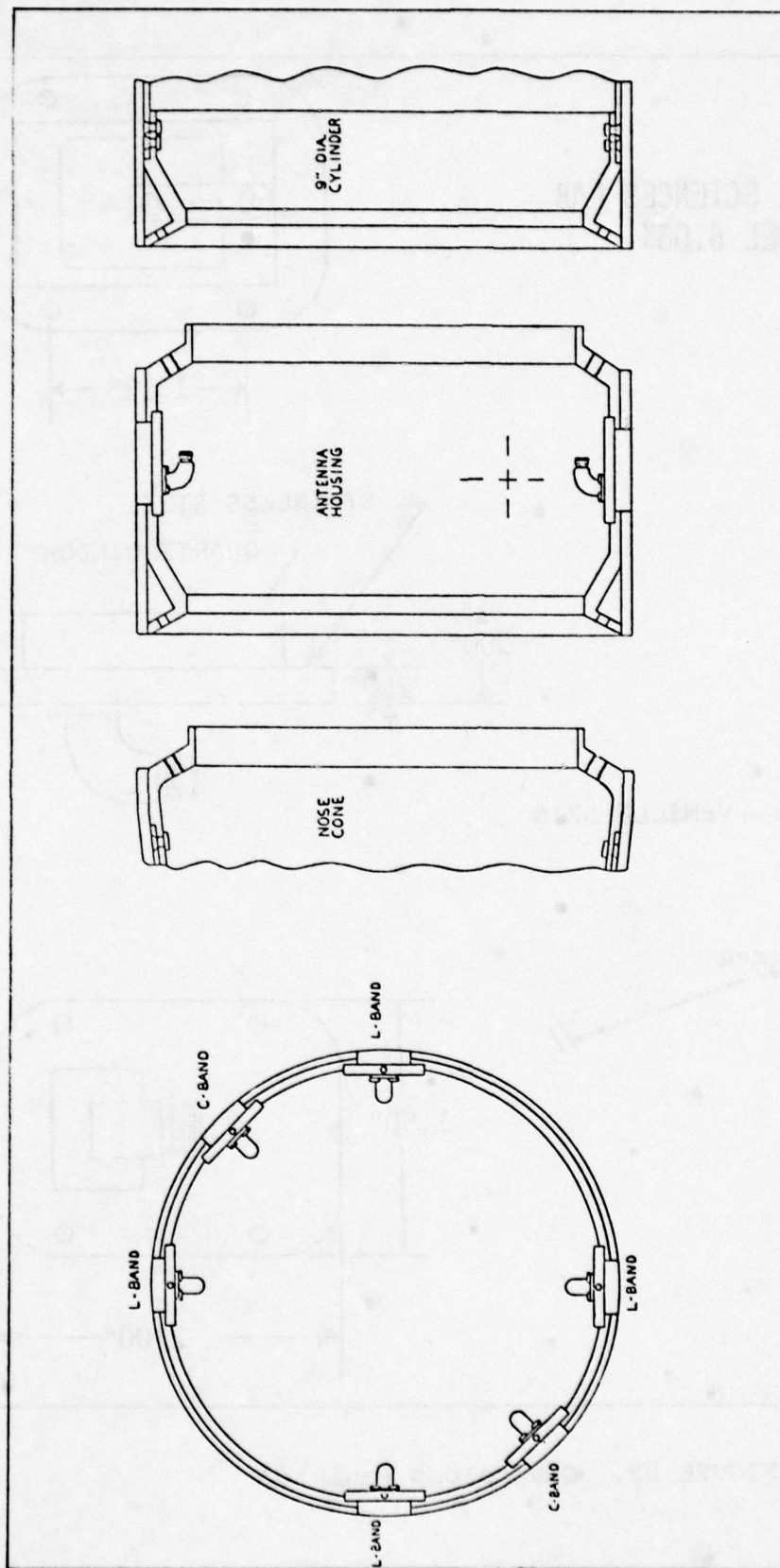


FIGURE 60. Quadraloop Antenna Assembly

launcher. When the IFLEX vehicle clears the launcher, the lanyard releases two mechanical timers. One is for the motor, the other is for fin deployment. The fin deployment timer connects an actuating squib-directly to a battery. This squib deploys the fins. The timer for the rocket motor arms the ignitor squib so that a UHF command receiver is able to fire the motor. The circuits for these functions are shown in Figures 61 and 62.

#### 5.7.1 Timer

The timer selected is the Raymond Engineering, Inc. Model 1060 interval timer. It will be used for both applications with a difference in the time interval setting. An outline drawing of the timer is shown in Figure 63.

#### 5.7.2 Motor Ignition Command Link

##### 5.7.2.1 Command Receiver

The UHF command receiver recommended by White Sands Missile Range for use in the IFLEX vehicle to initiate rocket ignition is a Cincinnati Electronics Corp., Model CR-110 (1). It is illustrated in Figure 64. This command receiver has the capability to command up to four total events, so if other applications arise the system is expandable.

##### 5.7.2.2 UHF Antenna

The UHF antenna for the command receiver does not have to survive the flight environment. Therefore, a relatively inexpensive spike antenna supplied by PSL (Model 23020) was selected for this function. As shown in Figure 65, two elements mounted 180 degrees apart insure coverage by the command transmitter. The location was selected so that the flow upstream of the experiment region will not be affected.

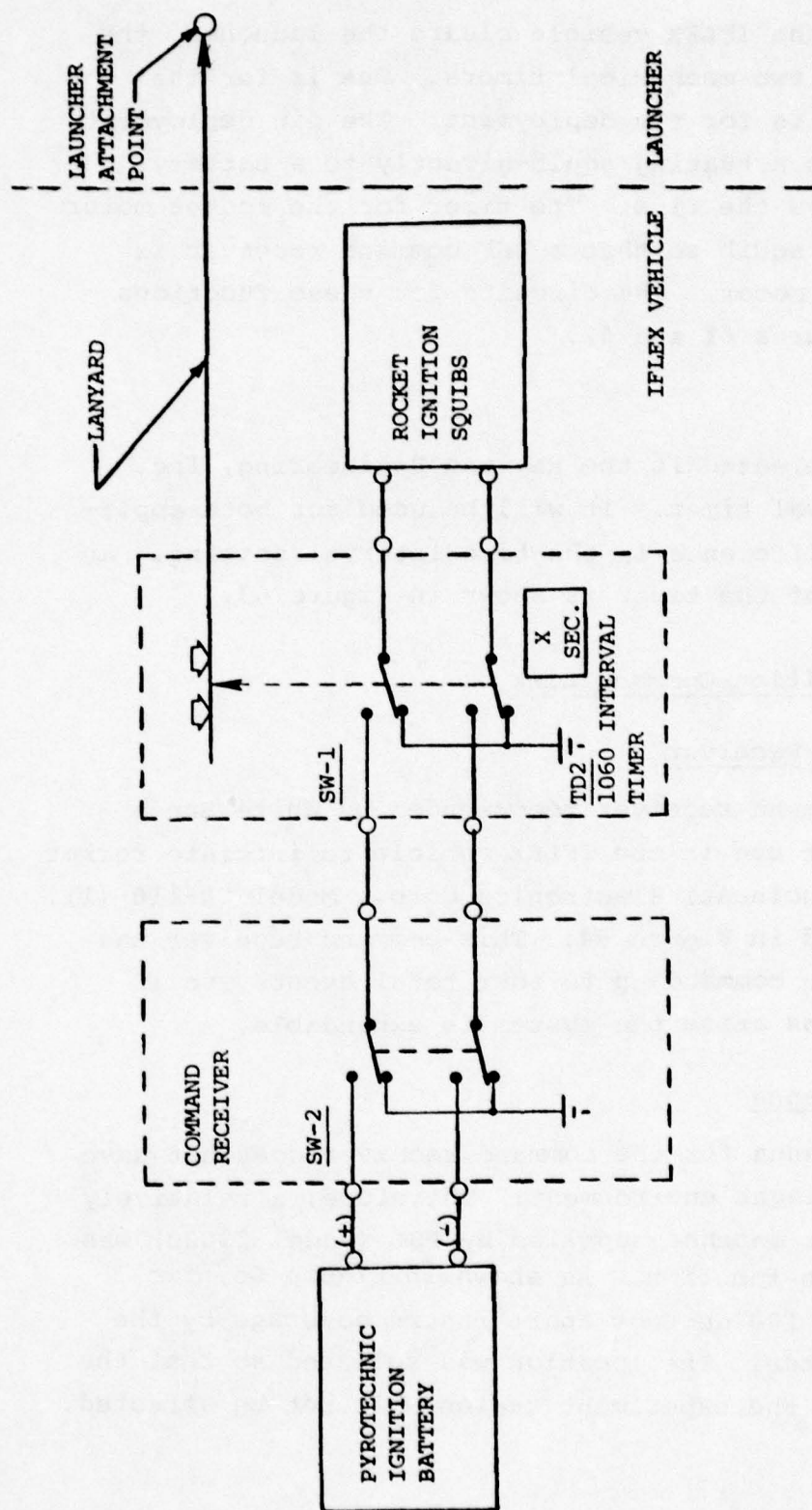


FIGURE 61. Rocket Ignition Circuit



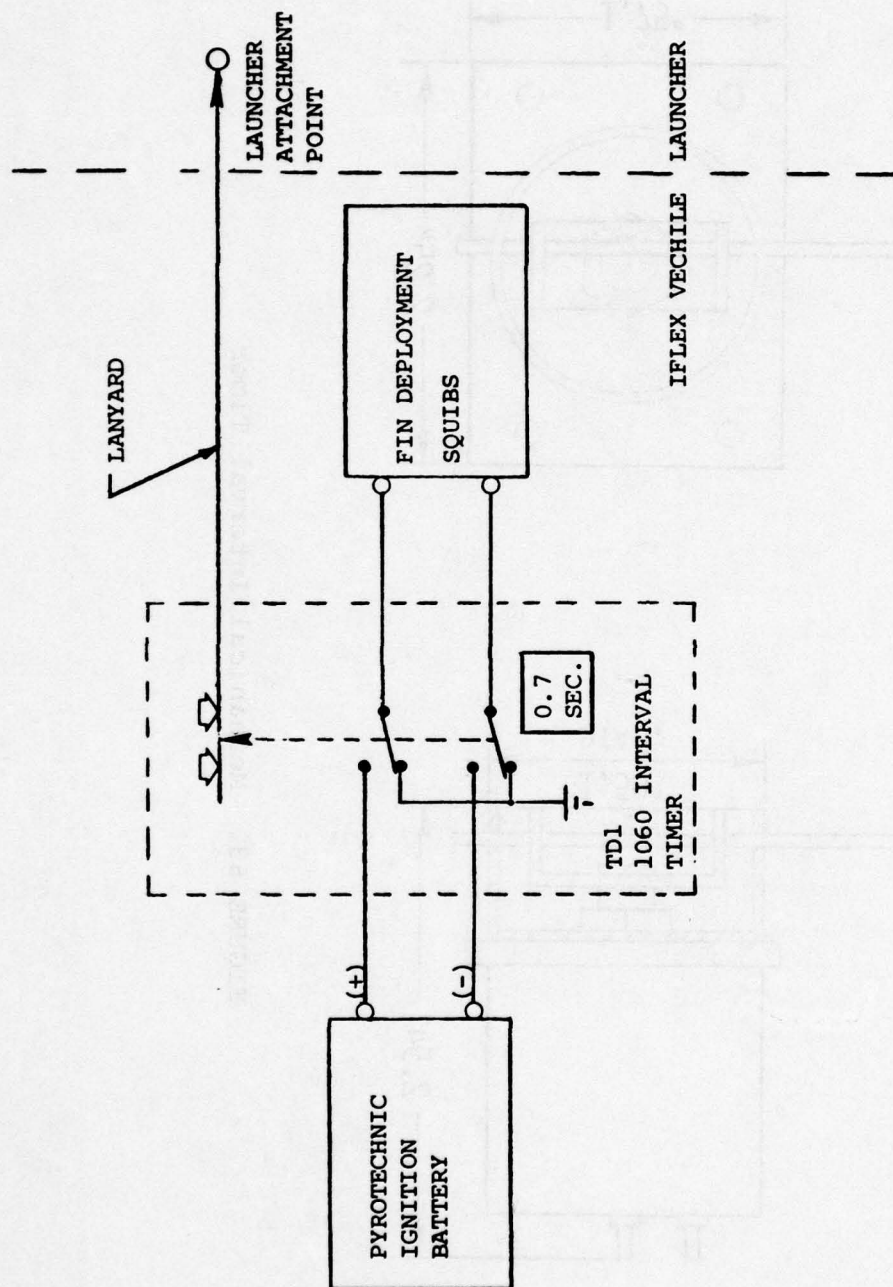


FIGURE 62. Fin Deployment Timer Circuit

RAYMOND ENGINEERING, INC.

P/N 1060

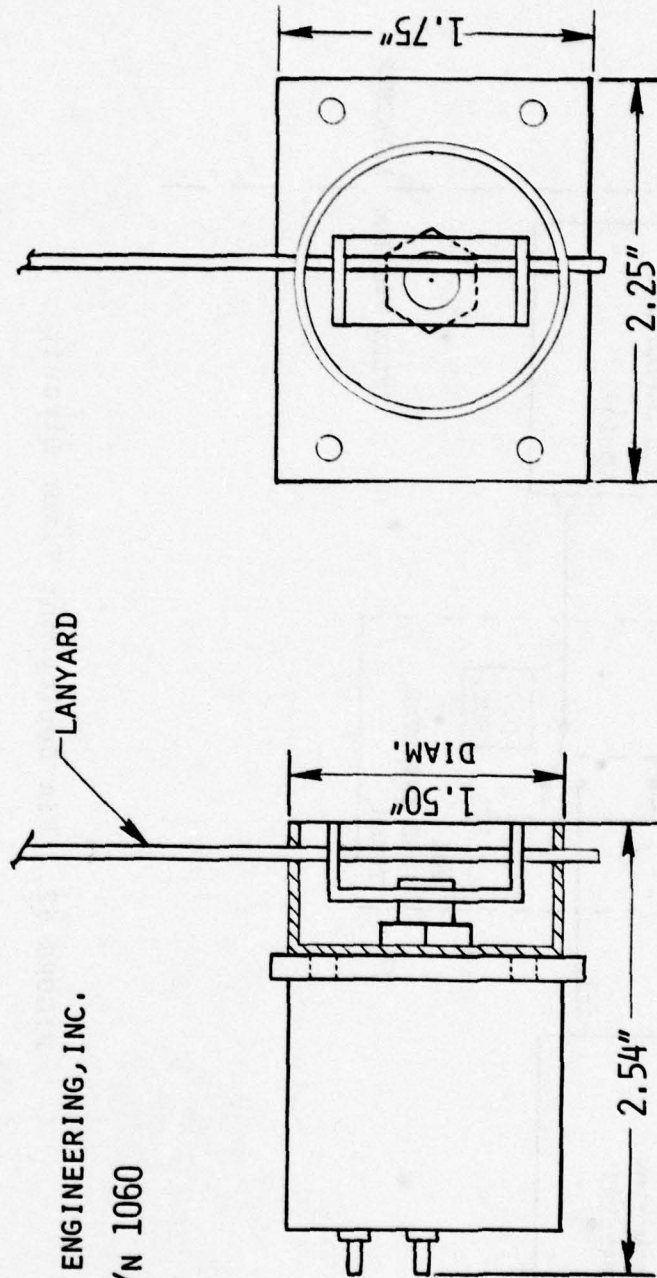


FIGURE 63. Mechanical Interval Timer

CINCINNATI ELECTRONICS  
MODEL CR-110

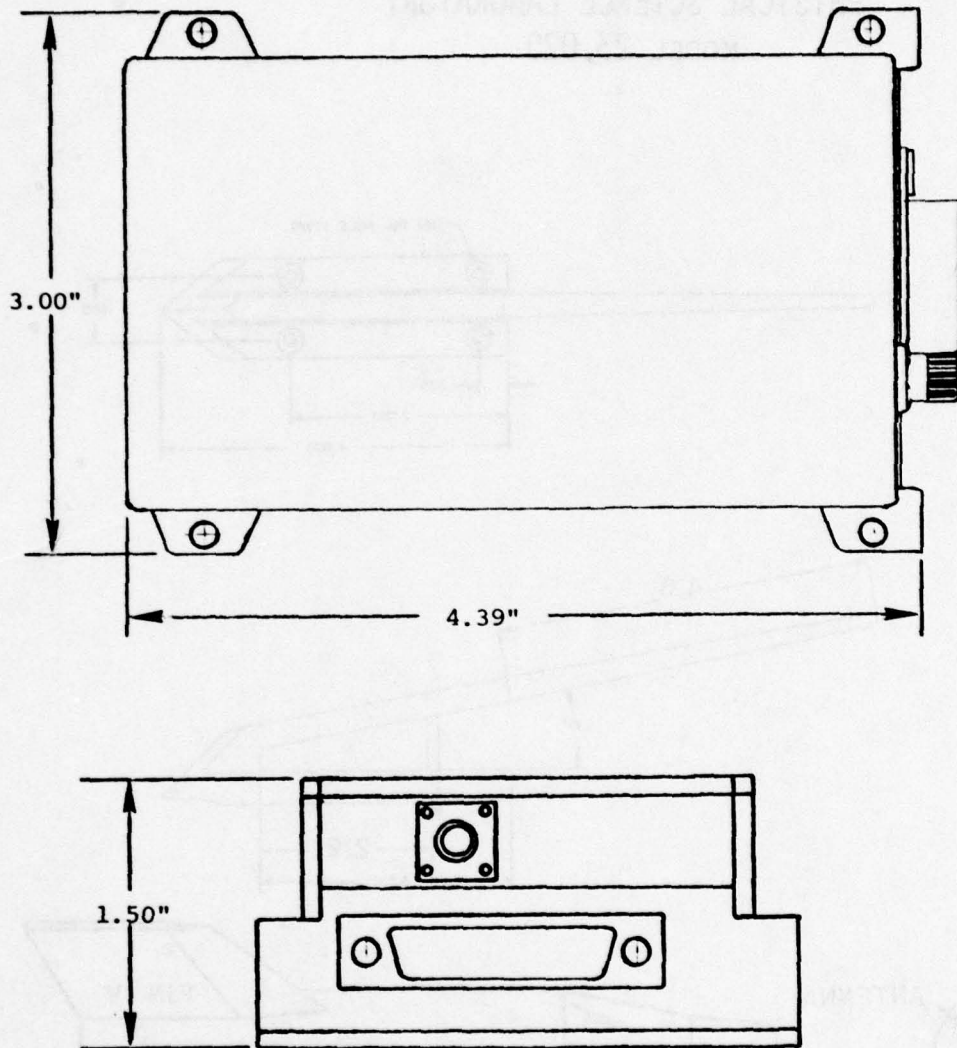


FIGURE 64. Command Receiver



PHYSICAL SCIENCE LABORATORY  
MODEL 23,020

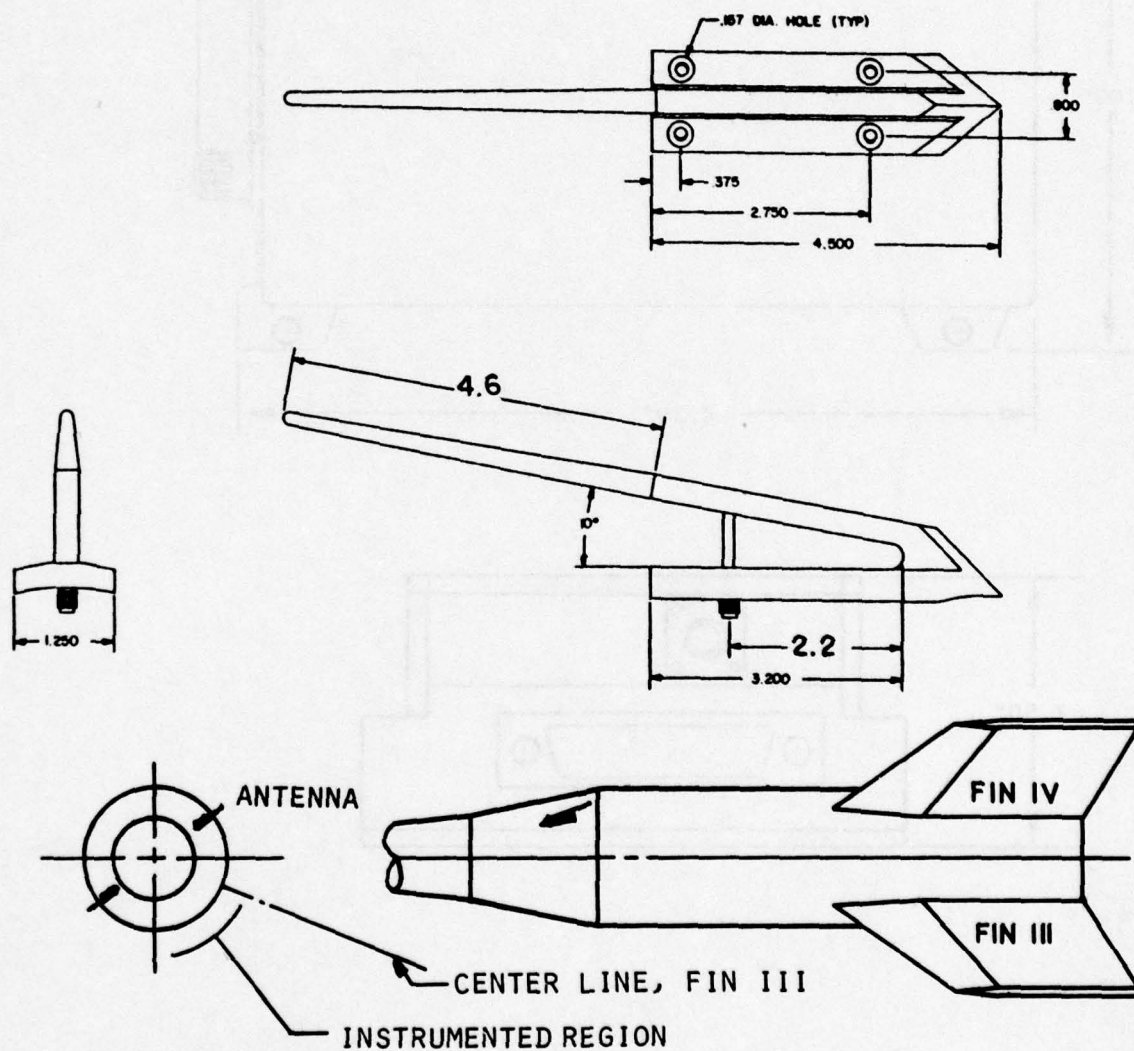


FIGURE 65. UHF Antenna

## 5.8 ELECTRICAL POWER

### 5.8.1 External Power

While the IFLEX vehicle is attached to the launching aircraft it will draw 28 VDC power from the aircraft. This power will be used for electronics, heaters and battery charging.

### 5.8.2 Internal Power

When the IFLEX vehicle is launched, all systems will be operated by battery power except that there will no longer be heater or battery charging power. The internal missile electrical power requirements are listed as follows:

Voltage - 24 to 30 VDC

Current drain

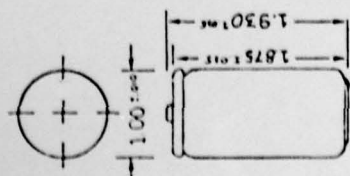
Telemetry transmitter	4000 MA
Radar transponder	700
PCM system	400
Transducer excitation	300
Unassigned	100

---

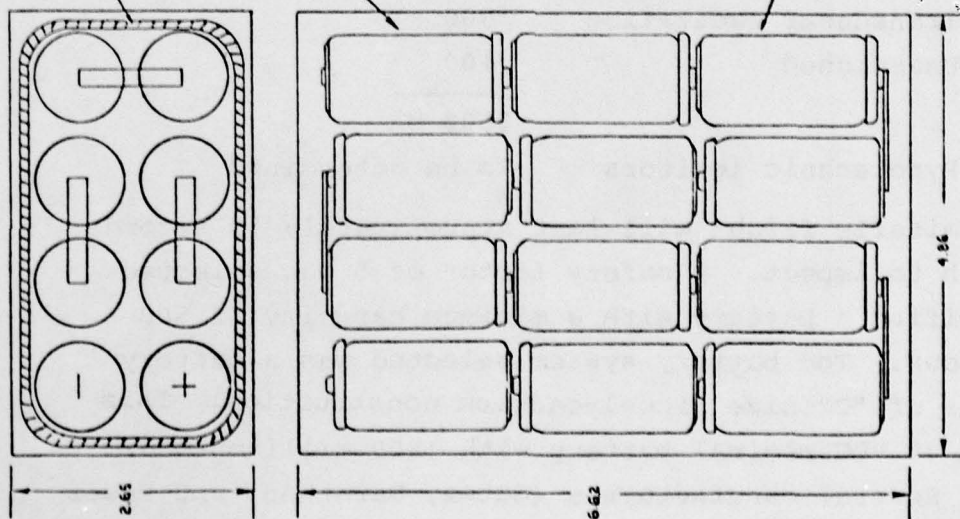
5500 MA

Pyrotechnic ignitors      To be determined

A typical missile flight will last approximately 50 seconds from launch to impact. A safety factor of 5 was selected which specified a battery with a minimum capacity of 500 milliamp-hour. The battery system selected was a battery of 24 cells of "C" size nickel-cadmium construction. This produces a 30 VDC nominal battery with 1800 milliamp-hour capacity. Several manufacturers (Gates, Marathon, and Power Sonic) produce cells of this geometry, shown in Figure 66. Performance of the battery pack is illustrated in Figure 67. The total package weighs four pounds and occupies 50 cubic inches.



DIMENSIONS FOR  
A SINGLE CELL



WEIGHT ..... 2.6 oz (73.7 Gms.)  
POLARITY ..... Case-Bag; Cover-Pos.  
VOLTAGE ..... 1.25 Volts  
AVERAGE CAP. TO 1.0 VOLT ..... 1.65 AH @ 1 Hr. Rate  
1.80 AH @ 5 Hr. Rate  
RECOMMENDED CHARGE ..... 0.19 Amps - 14 Hours  
FAST CHARGE RATE ..... 0.45 Amps - 4.5 Hours  
INTERNAL IMPEDANCE (8 1,000 Cycles) ..... 0.016 Ohms

Cell is equipped with a pressure relief vent.

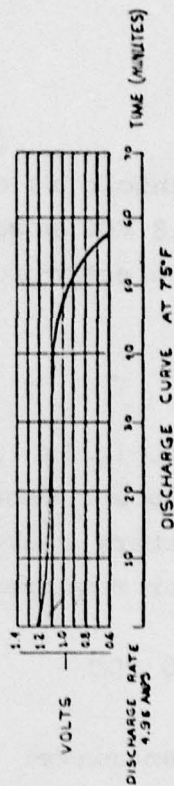


FIGURE 66. Battery Schematic



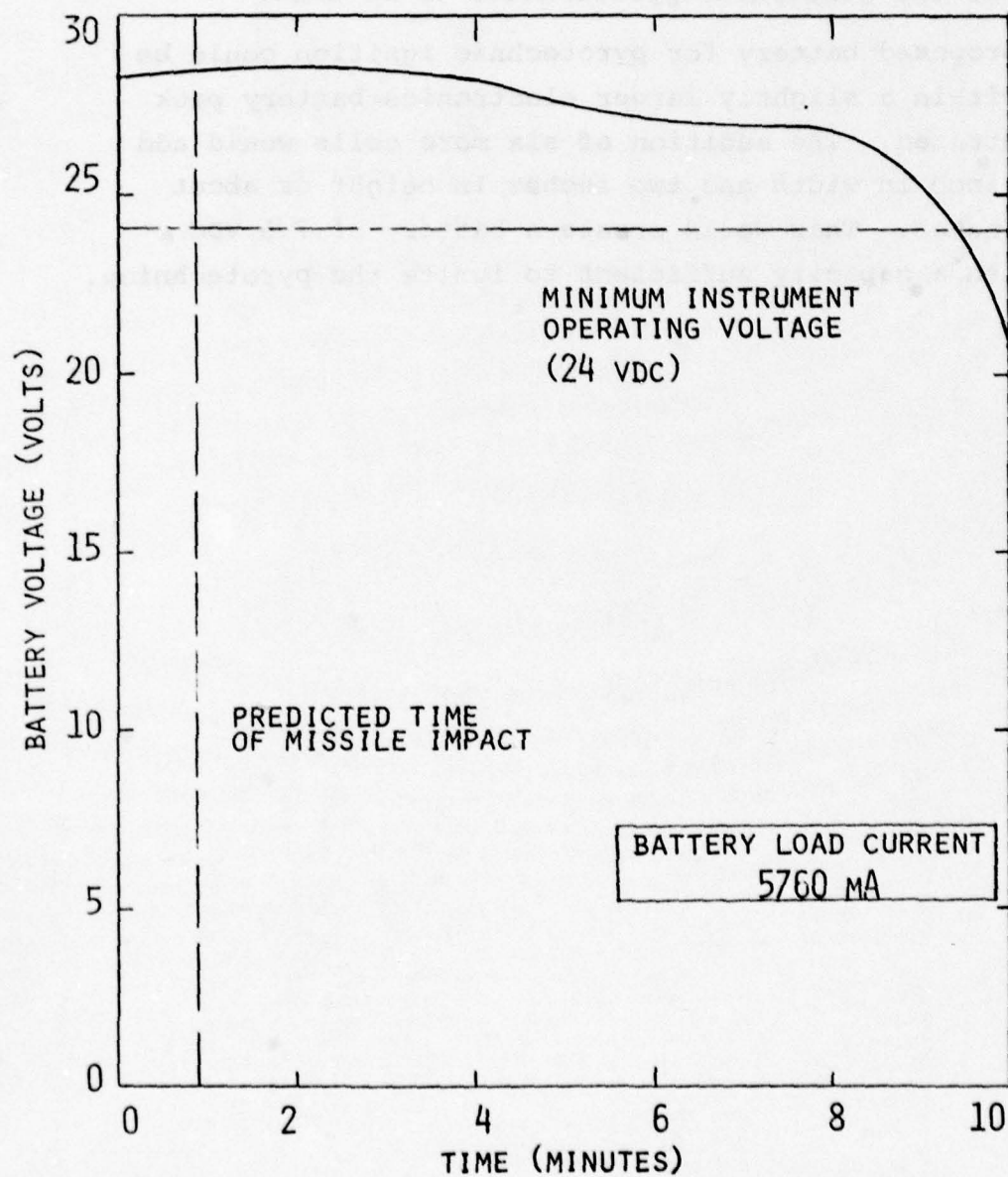


FIGURE 67. Instrumentation Battery Voltage Vs. Time

A separate power source is required to initiate pyrotechnic devices (i.e., fin deployment and rocket ignition) because of possible shorts and transients that may be impressed into the electronic power source if they were not independent. The specific requirements for the ignition of the pyrotechnics remain to be established after final selection of the particular pyrotechnics to be used.

The proposed battery for pyrotechnic ignition could be enclosed within a slightly larger electronics battery pack than illustrated. The addition of six more cells would add about one inch in width and two inches in height or about 13 cubic inches. This would create a battery of 7.5 VDC nominal with a capacity sufficient to ignite the pyrotechnics.

## SECTION VI

### VEHICLE DESIGN

The principal design constraints for IFLEX result from the necessity to maintain the aircraft compatibility qualification of the FLAME launch vehicle. This constraint requires maintenance of the FLAME launch vehicle external geometry and mass properties. The fundamental difficulty imposed by this constraint results from the necessity to fly IFLEX through a significantly more severe thermal environment than was encountered by the FLAME launch vehicle first stage. The FLAME launch vehicle dropped the first stage after achieving maximum Mach number. The IFLEX vehicle continues flight of this complex configuration for 10 to 15 seconds of heat soak, into a lower altitude, higher density environment.

The IFLEX vehicle configuration was shown compared to the FLAME launch vehicle first stage in Figure 3 (Section II). Both are cone-cylinder-flare-frustum-cylinder configurations of nearly identical dimensions. The axially symmetric external surface inclinations (6 degrees, 6 degrees, 11.75 degrees for the cone, flare, frustum) have been maintained identically. The aft cylinder on the IFLEX vehicle has a slightly larger dimension to accommodate experiment instrumentation between the Pedro rocket case and the external surface. The fin geometry of the two vehicles is the same.

The IFLEX vehicle structure has been designed to be aeroelastically as stiff or stiffer than the FLAME vehicle structure. Regions that are different structurally than FLAME are the larger diameter fin support ring, the non-insulated forward stainless steel cone, and the carbon steel and



stainless steel panels that serve as the experiment surfaces. These regions have been analyzed extensively in regard to strength, thermal stress, and thermally induced distortion, and designed accordingly. The results of these analyses are presented in this section.

The FLAME launch vehicle employed an ablative insulator coating called FIREX RX-2376A for external thermal protection. As described in Reference 25, FIREX has a relatively low ablation temperature (280°F) and a moderate heat of ablation (1800 Btu/lb). These were adequate for the relatively short flight times of the FLAME first stage. However, the relatively long flight time to decreasing altitude, which is characteristic of the IFLEX trajectories, results in about four times the total cold wall heating experienced by the FLAME first stage. The amount of FIREX coating required to provide thermal protection on the IFLEX mission was judged prohibitive for two reasons. First, the thermal response of the material in the flight environment is not sufficiently well characterized to provide confidence that uniform ablative performance would be expected. Second, the large volume of ablation would result in downstream interference between the ablation products and the aeroheating experiment instrumentation.

A wide range of candidates were considered for the IFLEX vehicle external surface thermal protection system (TPS). These ranged from complete metallic (non-ablative) to complete ablator coatings. The experiment requirements are best met if ablators are not employed. Ablating surfaces invariably result in gaseous and particulate material in the boundary layer, as well as surface roughness and varying degrees of shape change. These all result in variable boundary layer characteristics and flow contamination which will change the character of the viscous/inviscid flow interactions to be investigated in the experiment.

The problem associated with designing a metallic TPS were assessed in some detail during the IFLEX design effort. They are principally associated with the thermal expansion resulting from the high surface temperatures for the IFLEX mission and the large linear dimensions associated with the vehicle components. Considering stainless steel or titanium walls with thicknesses varying from .075 to 0.20 inches, and depending on the location on the vehicle, metal surface temperatures were predicted to be on the order of 800° to 1400°F for the IFLEX design trajectory discussed below. These temperatures eliminate the use of titanium, and require the metal to be either stainless steel, or a super-alloy such as Inconel. (The declining strength of titanium with temperature, in this temperature range, is unacceptable.) A pre-design effort showed that such a vehicle was feasible from the stand points of total weight, strength, cost, and manufacturing. However, the mass distributions appeared likely to differ significantly from that of the FLAME first stage. It would at least require a significant increase in design effort to insure a satisfactory c.g. location to maintain aircraft compatibility. In addition, employment of a hot metal structure greatly increases the design effort necessary to evaluate thermal expansion, thermal stress, and thermal protection of interior components. The principal problems appeared associated with the design of joints in which thermal expansion must be accommodated. The loss of strength, disruption of the flow surface, and possible leakage of hot air into the vehicle interior would have to be analyzed. Design of the metallic skin requires consideration of buckling due to thermal stress and pressure loads, and surface dynamic stability. Augmented heating and higher skin temperatures must be considered in the shock interaction areas near the lugs and



fins. Many of these design problems require adaption and extension of the state-of-the-art in high temperature structural design.

Advancement of the state-of-the-art in structural design is not an IFLEX program objective. Consequently, the likely cost and risk associated with design and manufacture of a metallic TPS was judged beyond the scope of the IFLEX design program. In consideration of the aeroheating experiment requirement to minimize ablative TPS interaction with the vehicle flowfields, a hybrid external surface TPS was selected. A metallic surface is employed in the immediate vicinity of instrumentation and in less critical heating areas upstream of the experiment. The remainder of the external surface is protected by an insulator with a high decomposition temperature (approximately 850°F). This approach reduces the linear dimensions of metallic surfaces to minimize total expansion at joints and permits insulation at joints. The hybrid TPS approach by no means eliminates the joint and thermal stress design problems, but it greatly reduces their scope and number.

In the following paragraphs, the thermal and structural design analysis of each section and subsystem of the IFLEX vehicle is described. Some of the more than 50 design drawings prepared to specify the structure manufacture and assembly requirements are included for illustrative purposes. These detailed design drawings are catalogued in Appendix I and are available from AFFDL/FXG.

#### 6.1 TPS MATERIAL EVALUATION

The thermal protection system consists primarily of an insulative/ablative coating protecting the steel, aluminum, and magnesium structure. Experiment regions are



made of either stainless steel or 1020 steel which is insulated from the inner structure. These steel surfaces have been designed to allow for thermal expansion and to minimize thermal warpage.

The trajectories used in the thermal analysis are presented in Figure 68, 69, 70 and 71. These trajectories differ from trajectory A of Section 3.3 in that they are based on preliminary aero data, which had a lower drag coefficient. This results in a lower velocity decay rate. Hence, these trajectories have a higher coast velocity, relative to the peak Mach number, resulting in a more severe thermal environment. Trajectory 1, Figure 68, has a 26 second ignition time and a maximum Mach No. of 6.0. It represents the highest heating rate and was used in the thermal analysis where ablation rate and thin skin response was of concern. Trajectory 2, Figure 69, has a 20 second ignition time and the maximum Mach No. of 6.0. Its maximum heating rate is less than that of Trajectory 1; however, its total integrated cold wall heating is about the same and its flight duration is longer. Thus, it was used in the analyses where in-depth thermal response was critical, such as the insulated magnesium skin.

Trajectories 3 and 4 of Figures 70 and 71 have a lower maximum Mach number of 5.0. They are being considered as alternate flight trajectories in an effort to reduce the rate of ablation.

#### 6.1.1 Insulator Material Evaluation

The material selected for the body surface is Dyna-Therm DE-350, and Dyna-Therm DE-370 for the fin surfaces. Dyna-Therm DE-350 is a room temperature curing, silicone

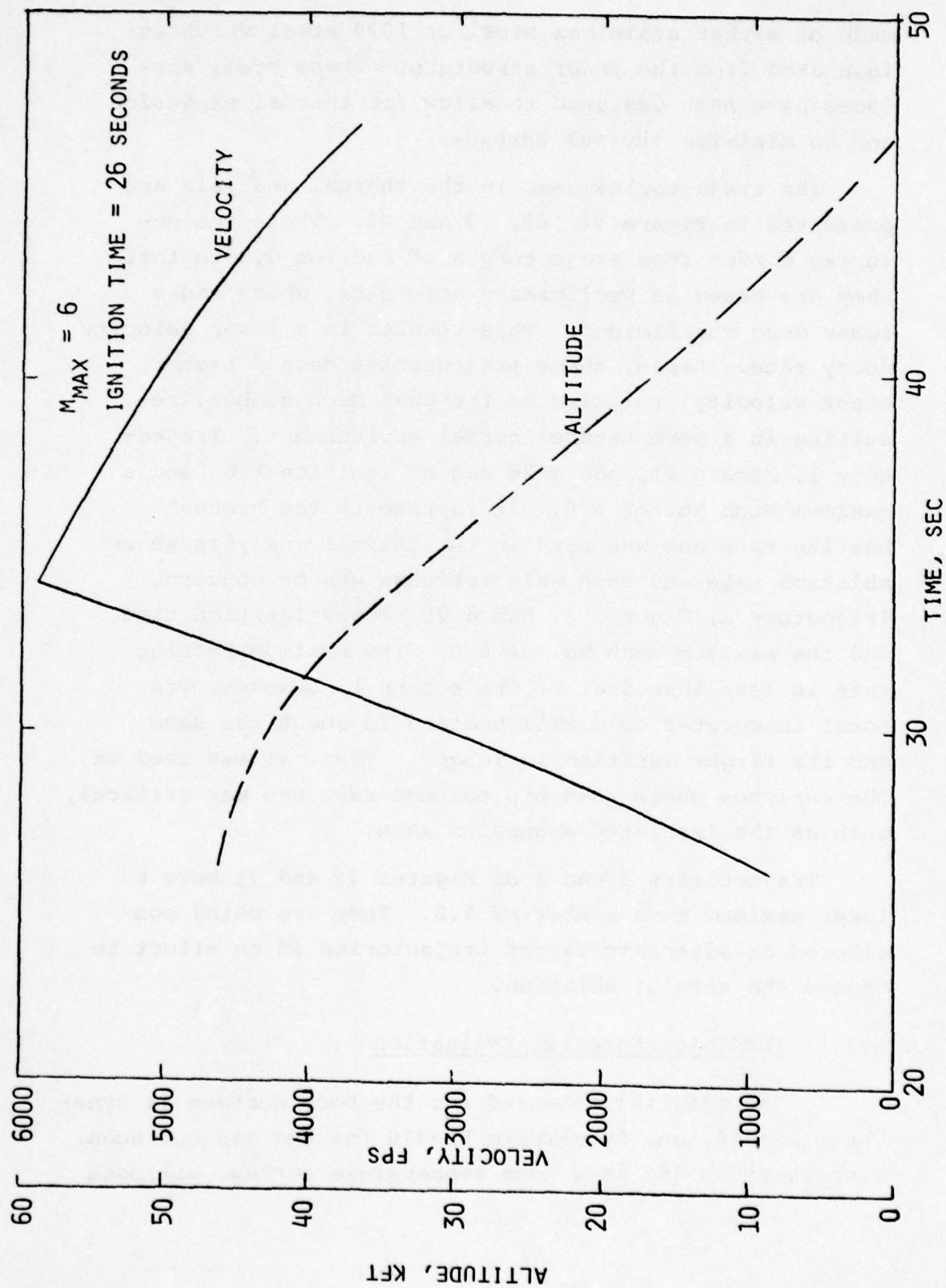


FIGURE 68. IFLEX Design Trajectory No. 1

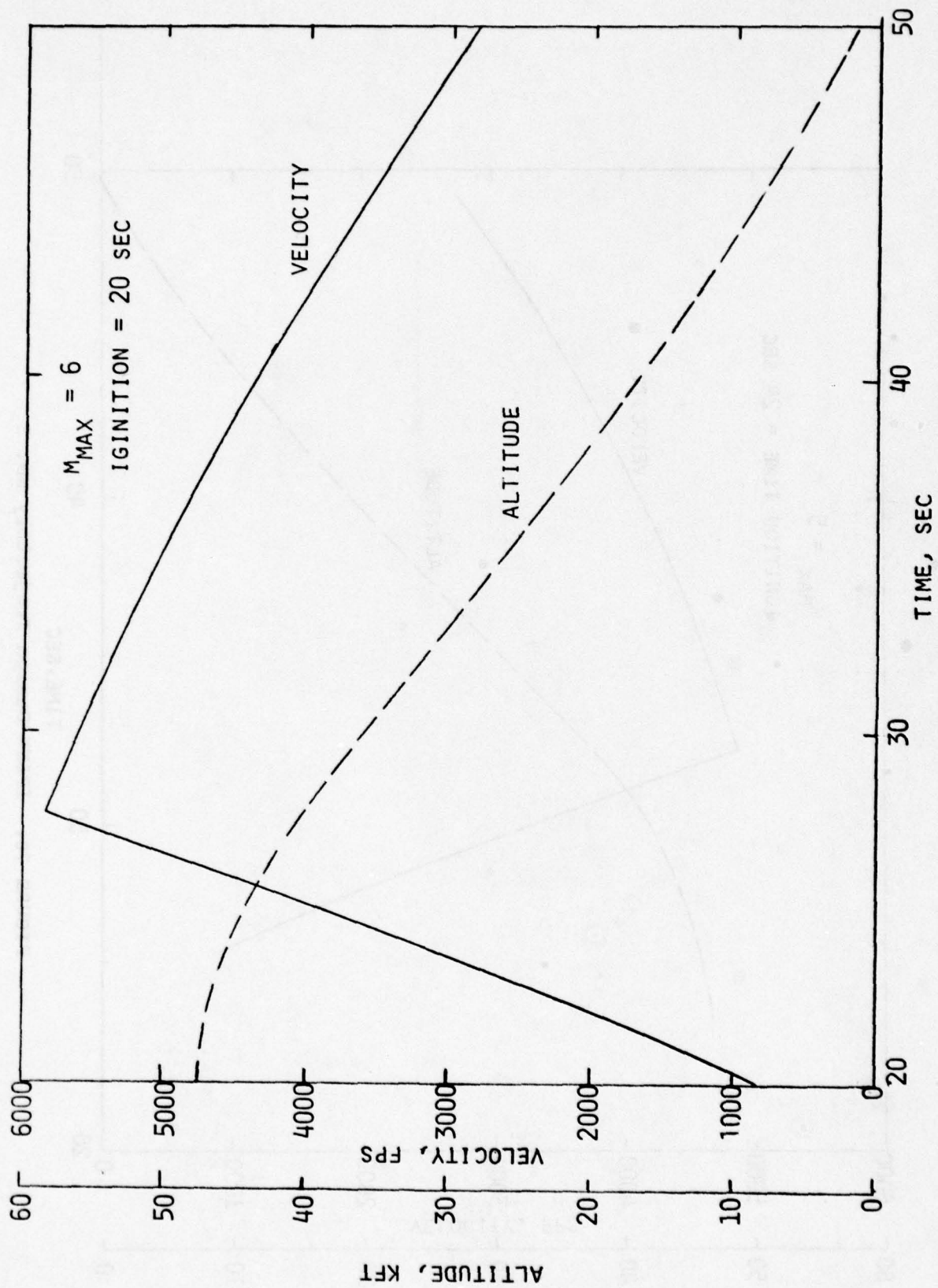


FIGURE 69. IFLEX Design Trajectory No. 2



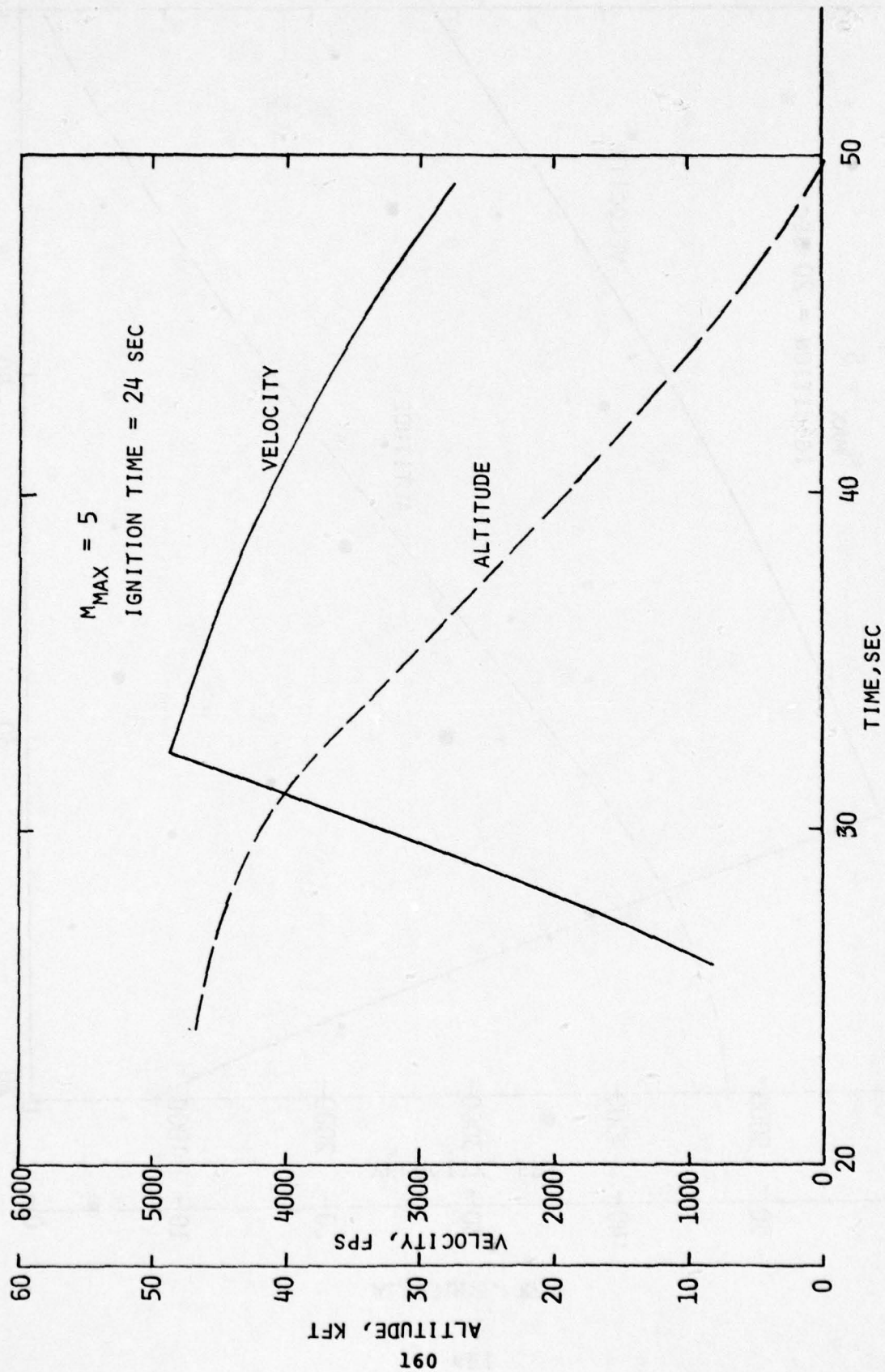


FIGURE 70. IFLEX Design Trajectory No. 3

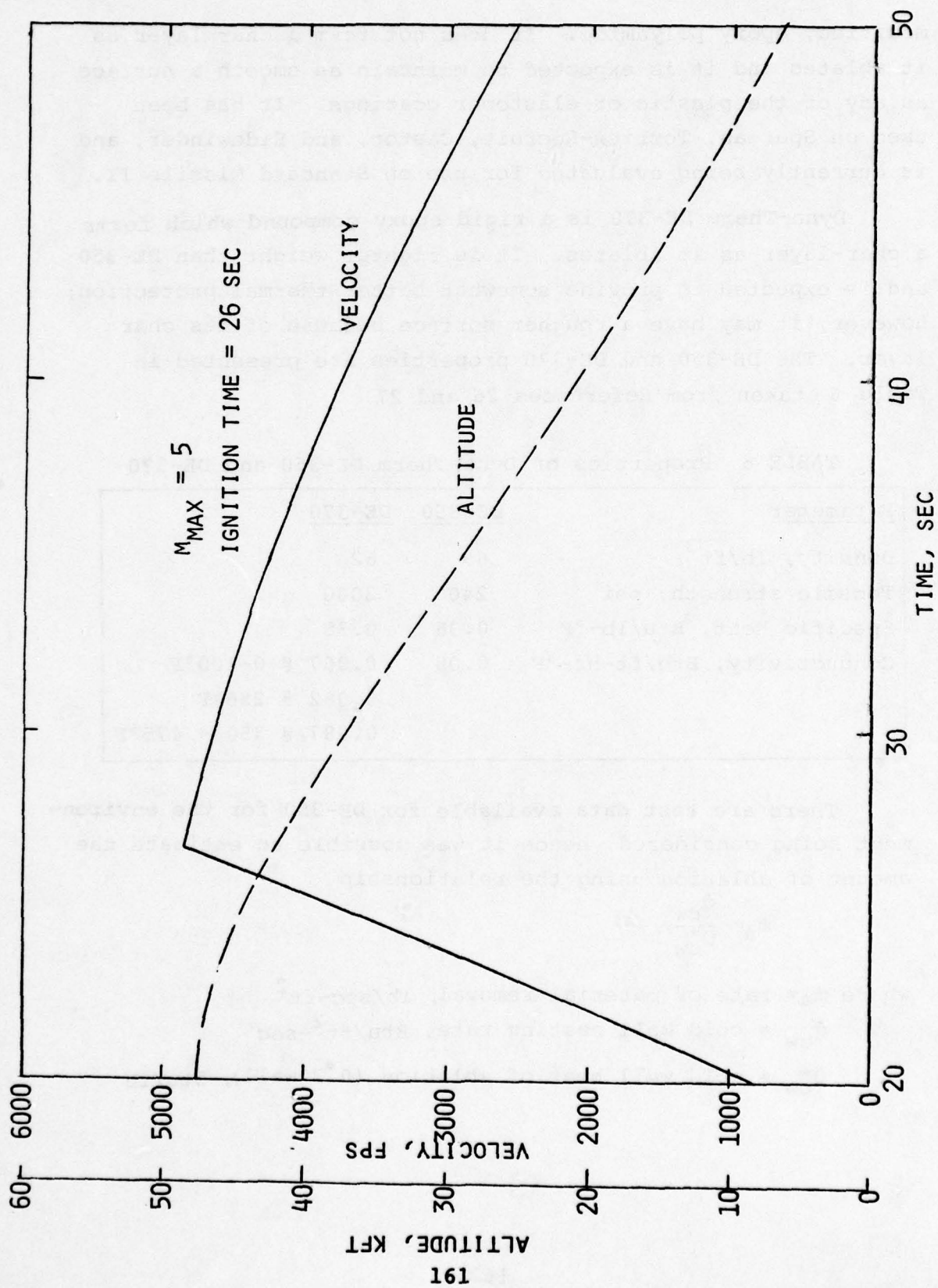


FIGURE 71. IFLEX Design Trajectory No. 4

modified, epoxy polyamide. It does not form a char layer as it ablates and it is expected to maintain as smooth a surface as any of the plastic or elastomer coatings. It has been used on Spartan, Terrier-Recruit, Castor, and Sidewinder, and is currently being evaluated for use on Standard Missile II.

Dyna-Therm DE-370 is a rigid epoxy compound which forms a char-layer as it ablates. It is lighter weight than DE-350 and is expected to provide somewhat better thermal protection; however, it may have a rougher surface because of its char layer. The DE-350 and DE-370 properties are presented in Table 6 taken from References 26 and 27.

TABLE 6 Properties of Dyna-Therm DE-350 and DE-370

Parameter	DE-350	DE-370
Density, lb/ft <sup>3</sup>	69	62
Tensile strength, psi	240	3000
Specific Heat, Btu/lb-°F	0.36	0.38
Conductivity, Btu/ft-hr-°F	0.08	0.067 @ 0-100°F 0.082 @ 250°F 0.087 @ 350 - 475°F

There are test data available for DE-350 for the environment being considered, hence it was possible to estimate the amount of ablation using the relationship

$$\dot{m}_a = \frac{\dot{q}_{cw}}{Q_{cw}^*}$$

where  $\dot{m}_a$  = rate of material removal, lb/sec-ft<sup>2</sup>

$\dot{q}_{cw}$  = cold wall heating rate, Btu/ft<sup>2</sup>-sec

$Q_{cw}^*$  = cold wall heat of ablation (0°F wall), Btu/lb



The cold wall heating rate was determined using the computer code described in Reference 28. This code computes the aerodynamic heating using local similarity with the surface being represented as a cone, flat plate, wedge, sphere, etc.

The cold wall heating of the IFLEX 11.75 degree frustum and the aft cylinder are presented in Figure 72 based on trajectory 1. The frustum environment is representative also of the heating on the forward cone near the nose tip and on the 5 degree ramp on the fins. The aft cylinder is the low end of the heating regime, and other sections fall between these two. The maximum shear stress was calculated to be  $30 \text{ lb/ft}^2$  on the frustum, and  $16 \text{ lb/ft}^2$  on the aft cylinder.

A summary of the available ablation data for DE-350 is presented in Table 7, along with representative requirements of the IFLEX vehicle. The Flamemaster Data Sheet is taken from tests which formed the Material Specification 11244452, Reference 29. The  $Q_{cw}^*$  values were computed from the ablation rates presented in Reference 26 and 29. The hot air test of Reference 29 consisted of placing the samples at a  $10^\circ$  angle of attack in a Mach 2.0 air stream with a cold wall ( $0^\circ\text{F}$ ) heat flux of  $170 \pm 10 \text{ Btu/ft}^2\text{-sec}$ , an aerodynamic shear force of  $21 \pm 3 \text{ lbs/ft}^2$ , and an enthalpy of  $1000 \pm 50 \text{ Btu/lb}$  for 10 seconds. The ablation depth was 0.08 inches. This test environment is very similar to the IFLEX Mach 6 trajectory environment for the frustum, except that the maximum aerodynamic shear on the IFLEX vehicle is slightly larger, and the maximum total enthalpy is less.

The aerodynamic shear also affects the  $Q_{cw}^*$  values, as can be seen in Table 7. The low shear environments of References 28 and 29 resulted in quite high values of  $Q_{cw}^*$ . Figure 73 presents the effect of shear on  $Q_{cw}^*$  based on data

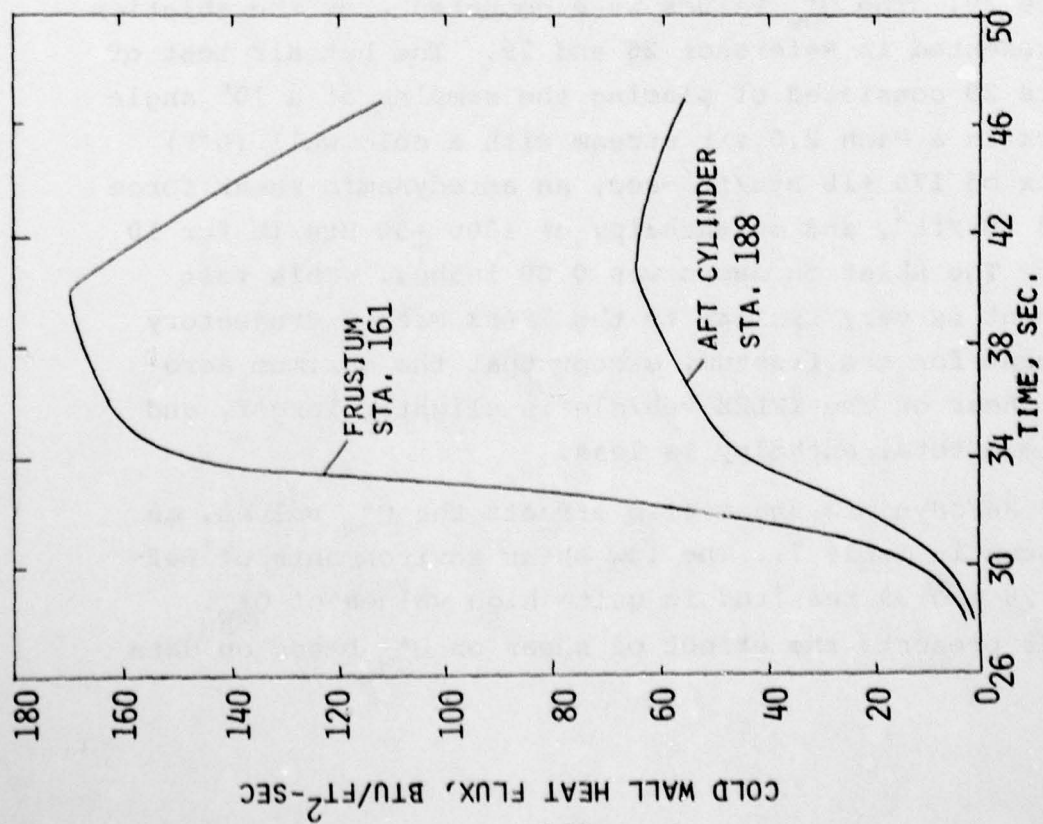


FIGURE 72. IPLEX Design Heating Environment, Trajectory 1

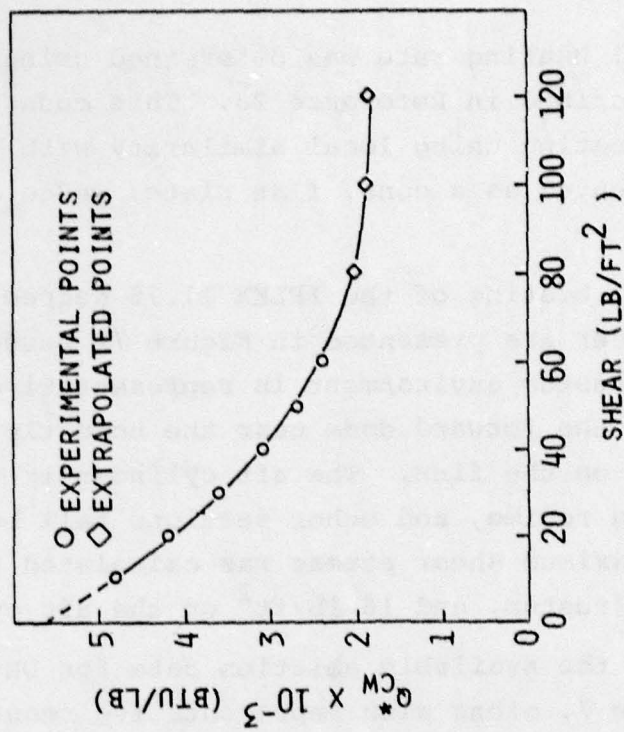


FIGURE 73. Aerodynamic Shear Effects on  $Q_{CW}^*$ , Dyna-Therm DE-350

Table 7. Ablation Data For DE-350

Reference	Total H (Btu/lb)	$\dot{q}_{cw}$ (Btu/ft <sup>2</sup> -sec)	T <sub>surface</sub> (°F)	Shear Stress (lb/ft <sup>2</sup> )	Q* Cw (Btu/lb)	Remarks
<u>TEST DATA</u>						
Flamemaster Data Sheet	1000	170	2000		3715	Data obtained by Flamemaster from Specification 11244452 below.
US Army Spec. 11244452	1000	170		21	3715	Douglas SPARTAN hot air tests M=2, 10° wedge.
US Army Spec. 11244452	1000 1000	80 60			3547 @ 5 atm 6857 @ 3 atm	Douglas SPARTAN, Plasma jet, M=3.
SANDIA Report SAND77-0469		283 647 997	3740 4400 4700	low ~5 max.	8054 6402 5340	Sandia Laboratories arc-jet subsonic flow.
<u>IFLEX ENVIRONMENT</u>						
Prustum, Sta 161	775 (max)	170 (max)	<1700	30 (max)	3500	
Aft Cylinder	775 (max)	65 (max)	<1300	16 (max)	4600	



published in Reference 30. These values are in agreement with the published data of References 26 and 29 and will be used in this study.

The amounts of ablation of DE-350 on all surfaces were computed using equation 38 and the environment of Trajectory 1. A  $Q_{cw}^*$  of 3500 Btu/lb, based on the maximum shear stress on the frustum, was used for all sections. This is conservative for regions other than the frustum and fin ramp. The insulative coating thickness selections, substructure temperature rise (predicted using trajectory 2 and the code described in Reference 28) and the amounts of ablation are presented in Table 8. The amounts of ablation should be conservative since the air enthalpies and shear stresses are less than the test conditions during much of the flight and the mass loss is based on the total heat to a cold wall. The temperature difference between the freestream recovery temperature and the wall temperature is expected to be less than that in the test, and the average heat input is lower, although over a longer time period, resulting in more conduction into the coating.

The ablation rate can be reduced by using the less severe Mach 5 trajectories and/or earlier ignition times. This was investigated by calculating the cold wall heating on the frustum for trajectories 1, 2, 3, and 4. The results are shown in Figure 74. The cold wall heat flux for the less severe trajectories is much lower. The surface temperatures of the Dyna-Therm insulator, without material ablation, were also calculated, and are shown in Figure 75. The surface temperature for the Mach 5 flight are still high enough that some material degradation will occur, but it should be small.

For the heat transfer experiments, the rate of ablation is the major parameter of concern. To investigate this and to compare the different trajectories, the rate of ablation

TABLE 8 TPS Coating Thickness Requirements

VEHICLE REGION	DYNATHERM MINIMUM THICKNESS (in)	MAXIMUM SUBSTRUCTURE TEMPERATURE RISE (°F)	MAXIMUM ABLATION (in)
30 in. diameter aft cylinder STA 185 to 308	0.12	65	.04/.06 in shock region
Fin ramp	0.20	10	0.13
Fin flat	0.14	92	0.06
Frustum, STA 161 to 185	0.2	8	0.11
6° Flare, STA 115 to 161	0.15	57	0.08
9 in. diameter forward cylinder, STA 37 to 115	0.15	52	0.05

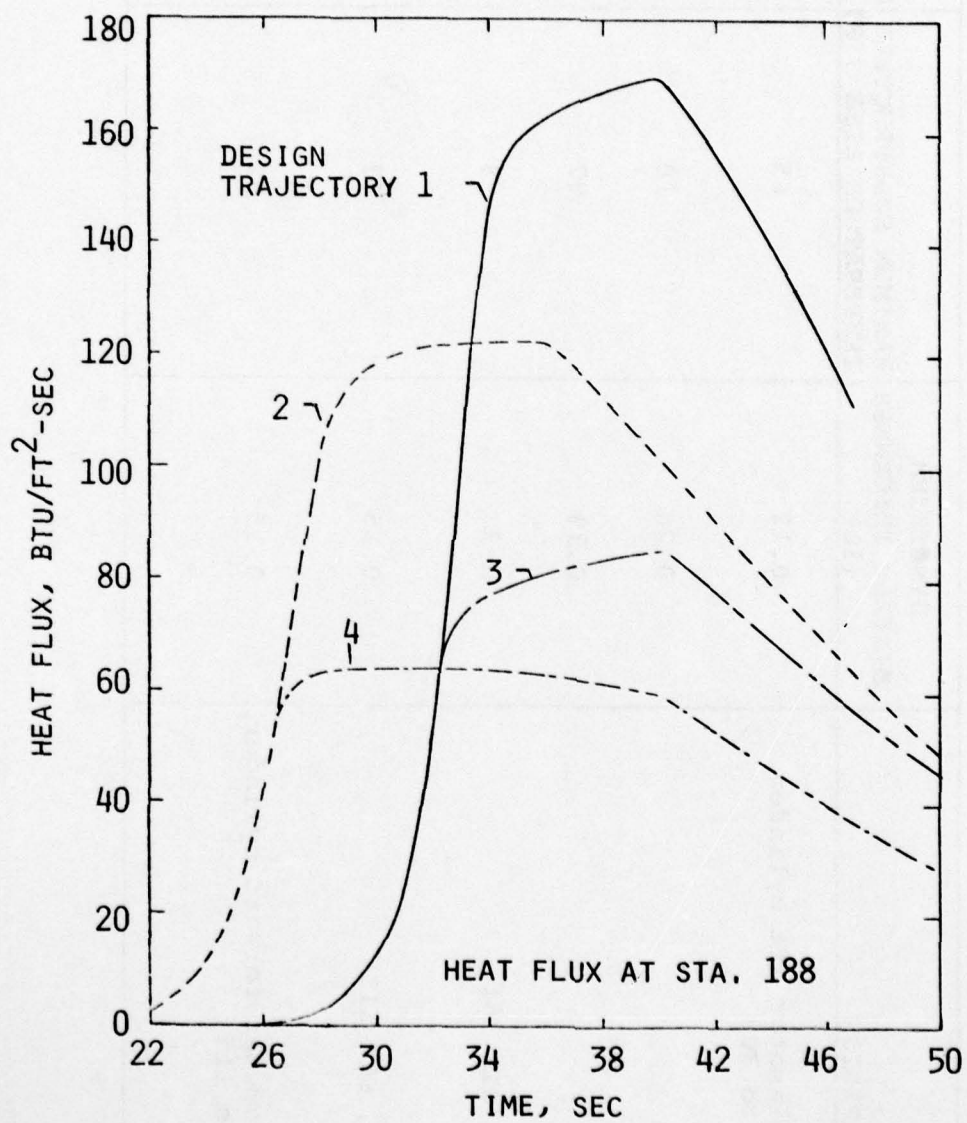


FIGURE 74. Cold Wall Heat Flux to the Frustum



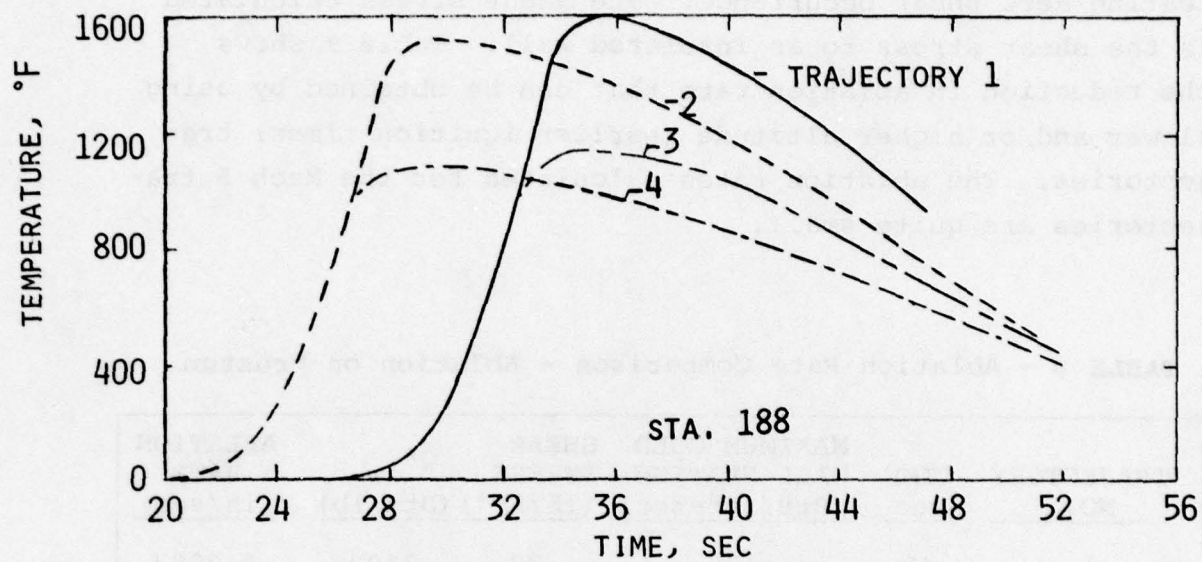


FIGURE 75. Frustum Insulation Surface Temperature

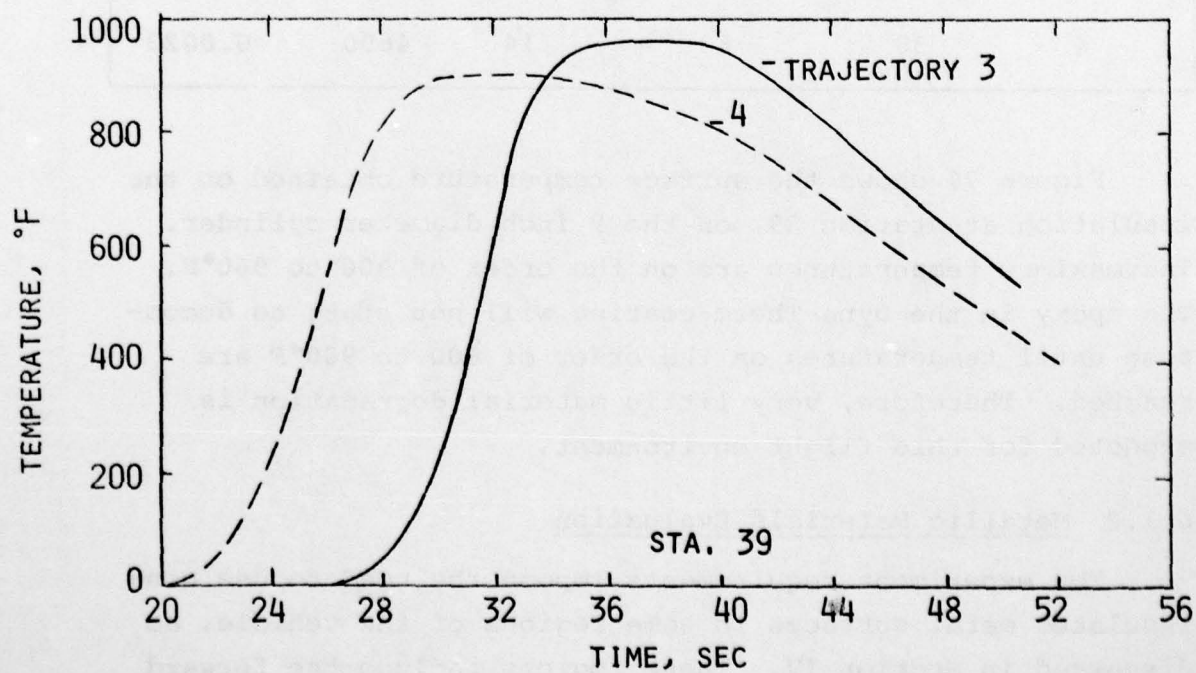


FIGURE 76. Forward Cylinder Insulation Surface Temperature

was predicted at the flight time corresponding to maximum heating/aero shear occurrence. The shear stress calculated is the shear stress to an insulated wall. Table 9 shows the reduction in ablation rate that can be obtained by using slower and/or higher altitude (earlier ignition times) trajectories. The ablation rates calculated for the Mach 5 trajectories are quite small.

TABLE 9 - Ablation Rate Comparison - Ablation on Frustum

TRAJECTORY NO.	TIME sec	MAXIMUM COLD WALL HEATING (Btu/ft <sup>2</sup> -sec)	SHEAR STRESS (lb/ft <sup>2</sup> )	Q* <sub>cw</sub> (Btu/lb)	ABLATION RATE (in/sec)
1	40	170	30	3500	0.0083
2	36	122	23	4000	0.0052
3	40	85	19	4200	0.0035
4	36	63	14	4600	0.0023

Figure 76 shows the surface temperature obtained on the insulation at station 39, on the 9 inch diameter cylinder. The maximum temperatures are on the order of 900 to 960°F. The epoxy in the Dyna-Therm coating will not start to decompose until temperatures on the order of 800 to 900°F are reached. Therefore, very little material degradation is expected for this flight environment.

#### 6.1.2 Metallic Materials Evaluation

The experiment requirements impose the need to use non-insulated metal surfaces in some regions of the vehicle, as discussed in Section IV. These regions include the forward cone and instrumented plates on the aft cylinder and fin.

Two materials are being used, stainless steel and 1020 steel. The stainless steel provides high temperature capability in regions where it is required and low carbon 1020 steel is utilized where required because its higher thermal conductivity reduces warpage. The 1020 steel is limited to a maximum temperature of 900°F to prevent rapid oxidation and surface scaling. A thorough thermal analysis was performed in order to facilitate the investigation of thermal expansion, thermal stress, shape retention, heat conduction into the substructure, attachment requirements, and surface temperature environment for the experiment.

The analyses were performed using AISI 301 stainless steel and AISI 1020 low carbon steel. The property data are presented in Table 10.

TABLE 10. Steel Material Properties

<u>PROPERTY</u>	<u>301 STAINLESS STEEL</u>	<u>1020 STEEL</u>
Density, lb/ft	501	491
Specific Heat, Btu/lb-°F		
@ 0°F	0.1	0.11
@ 1600°F	0.16	0.20
Thermal Conductivity, Btu/ft-hr-°F		
@ 0°F	9.3	30.0
@ 1600°F	11.8	19.5



### 6.1.3 Internal Insulation Materials

The hot metal panels being used on the structure must be insulated from the magnesium structure. The insulation material being used is Fiberfrax 970 Paper, described in Reference 31. It consists of alumina and silica fibers. It has a thermal conductivity of 0.032 Btu/ft-hr-°F at 500°F, and 0.049 at 1000°F. When sandwiched between 2 metal plates, it is compressed; however, it must not be compressed by more than a factor of 2.5. The minimum thickness presented in the drawings must be maintained at all times.

### 6.2 Forward Conical Section Design

The forward cone, shown in Figure 77, replaces the FLAME payload section. It has a metal surface to insure a smooth, non-receding flow surface to facilitate the pressure measurements for the angle of attack determination. It will contain ballast for center-of-gravity control.

The cone shell, from station 6 to station 38, is made from 0.2 inch thick AISI 321 stainless steel annealed sheet. It has no external thermal insulation. The surface temperature profile during flight and the temperature gradient for the time of flight at which the maximum temperature differential from outside to inside occurs are shown in Figures 78 and 79, respectively. Thermal strains and stresses were calculated from these temperatures and are shown in Figure 80. Both the thermal compressive stress at the outer surface and the thermal tension stress at the inner surface are below the corresponding allowable yield stresses for the material at the respective temperatures. The compressive stress from external pressure is small. The 0.2 inch thick skin is gradually tapered to the thicker cooler material at station 37.1 to avoid any excessive thermal stresses. The maximum radial deflection, at station 38, at the time of maximum skin temperature (874°F, Figure 78), is 0.032 inches.

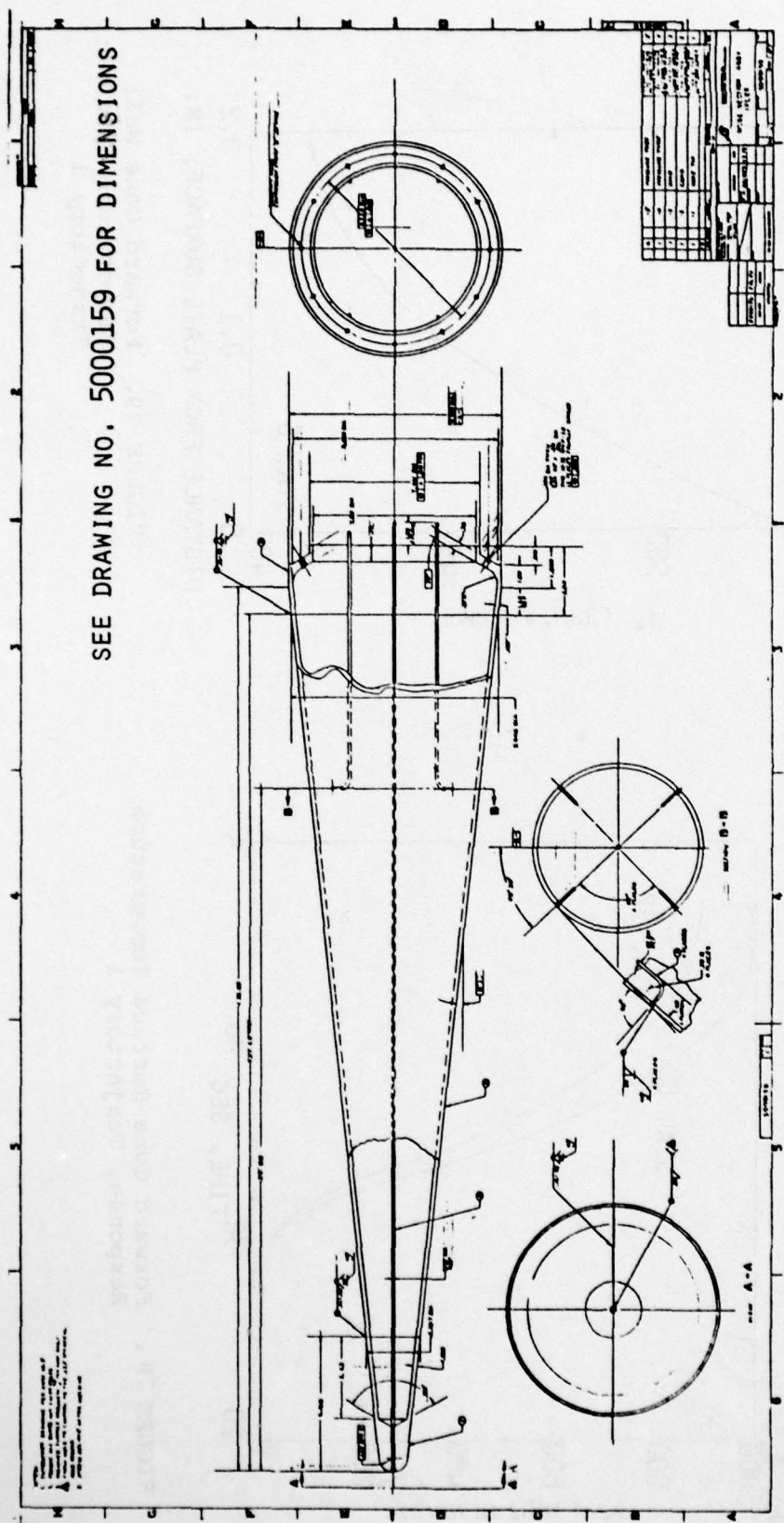


FIGURE 77. Forward Cone Design

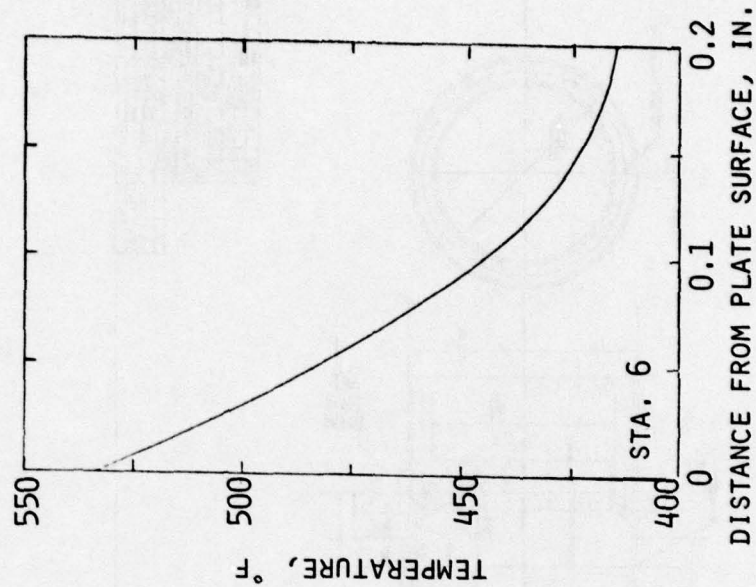


FIGURE 79. Forward Cone Wall Temperature Gradient, Trajectory 1

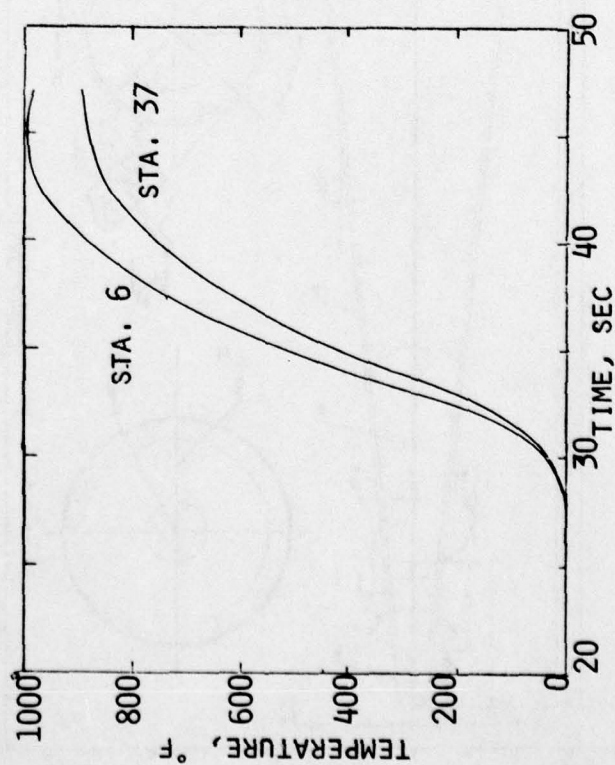


FIGURE 78. Forward Cone Surface Temperature Response, Trajectory 1



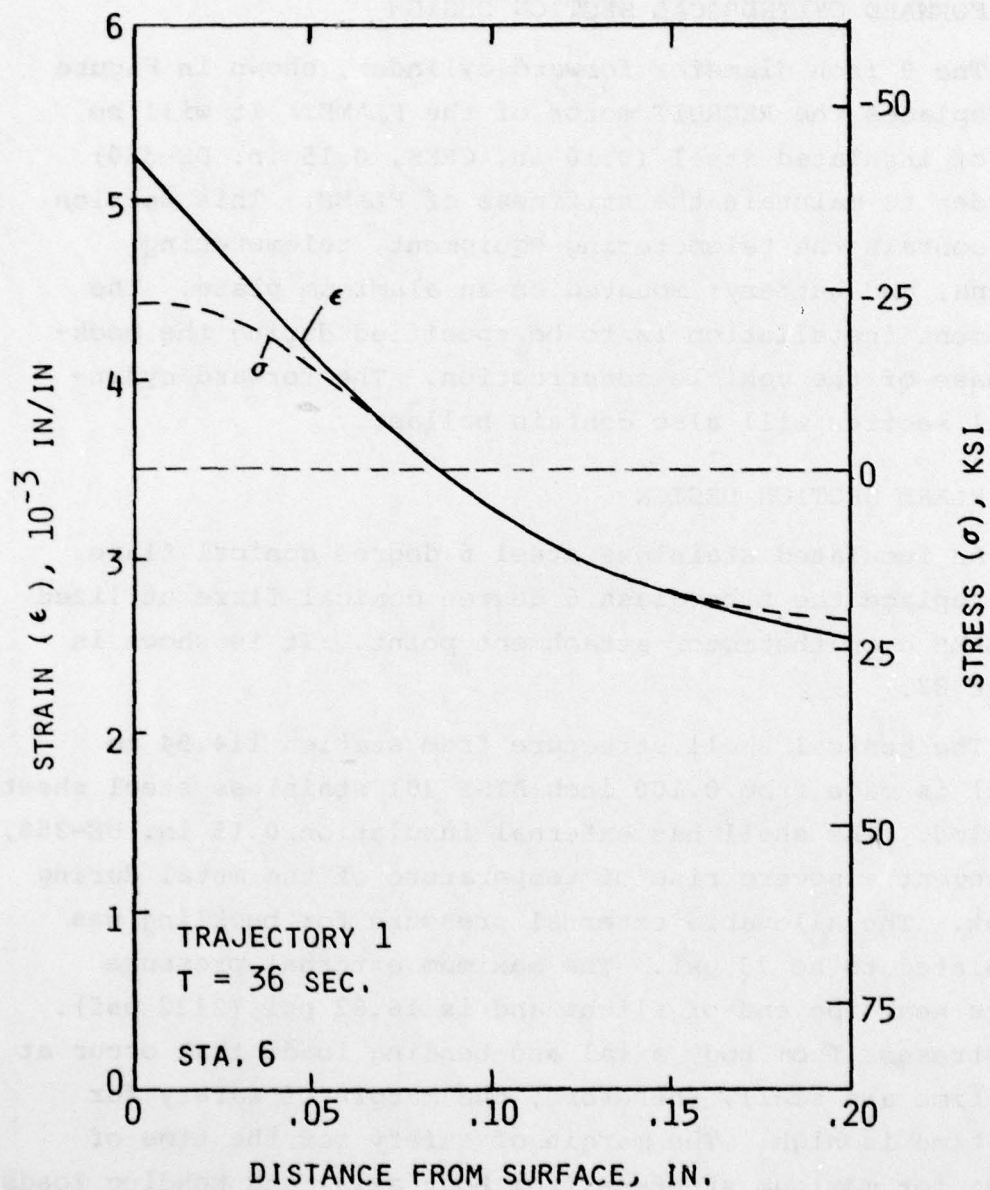


FIGURE 80. Forward Cone Thermal Stress and Strain

Therefore, the material and thicknesses for the shell are acceptable for strength and deflection.

Station 0 to 6 will be a stainless steel plug.

### 6.3 FORWARD CYLINDRICAL SECTION DESIGN

The 9 inch diameter forward cylinder, shown in Figure 81, replaces the RECRUIT motor of the FLAME. It will be made of insulated steel (0.10 in. CRES, 0.15 in. DE-350) in order to maintain the stiffness of FLAME. This section will contain the telemetering equipment, telemetering antenna, and battery; mounted on an aluminum plate. The equipment installation is to be specified during the mock-up phase of the vehicle construction. The forward cylindrical section will also contain ballast.

### 6.4 FLARE SECTION DESIGN

An insulated stainless steel 6 degree conical flare will replace the fiberglass 6 degree conical flare utilized on FLAME over the motor attachment point. It is shown in Figure 82.

The conical shell structure from station 114.94 to 160.61 is made from 0.100 inch AISI 301 stainless steel sheet annealed. The shell has external insulation, 0.15 in. DE-350, to prevent a severe rise of temperature of the metal during flight. The allowable external pressure for buckling was calculated to be 73 psi. The maximum external pressure occurs near the end of flight and is 16.82 psi (2422 psf). The stresses from body axial and bending loads that occur at this time are small, therefore, the margin of safety for this time is high. The margin of safety for the time of flight for maximum stresses from body axial and bending loads is also high. Therefore, the 0.1 inch thick stainless steel shell provides satisfactory strength.

SEE DRAWING NO. 5000162 FOR DIMENSIONS



FIGURE 81. Forward Cylinder Design



AD-A078 861

SCIENCE APPLICATIONS INC IRVINE CA

F/6 20/4

HYPERSONIC INTERFERENCE FLOW FLIGHT EXPERIMENT DESIGN.(U)

JUN 79 L A CASSEL , T C DUNCAN , E H LAHTI

F33615-77-C-3043

UNCLASSIFIED

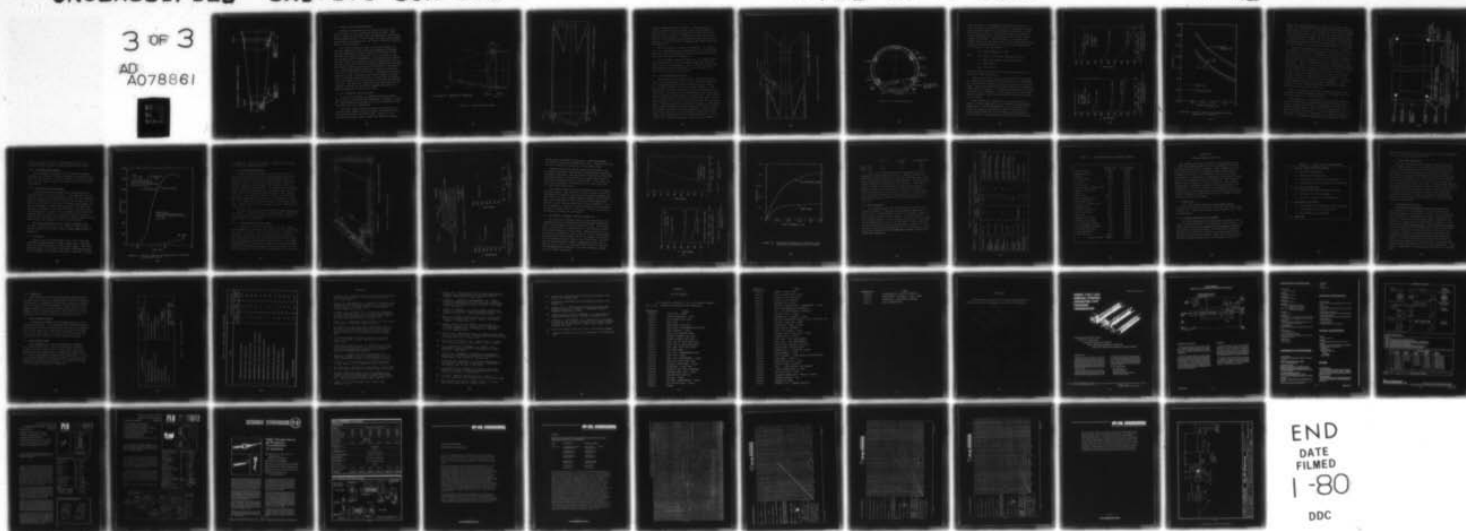
SAI-175-80R-008

AFFDL-TR-79-3065

NL

3 OF 3

AD  
A078861



END  
DATE  
FILMED  
1-80  
DDC



SEE DRAWING NO. 5000158 FOR DIMENSIONS

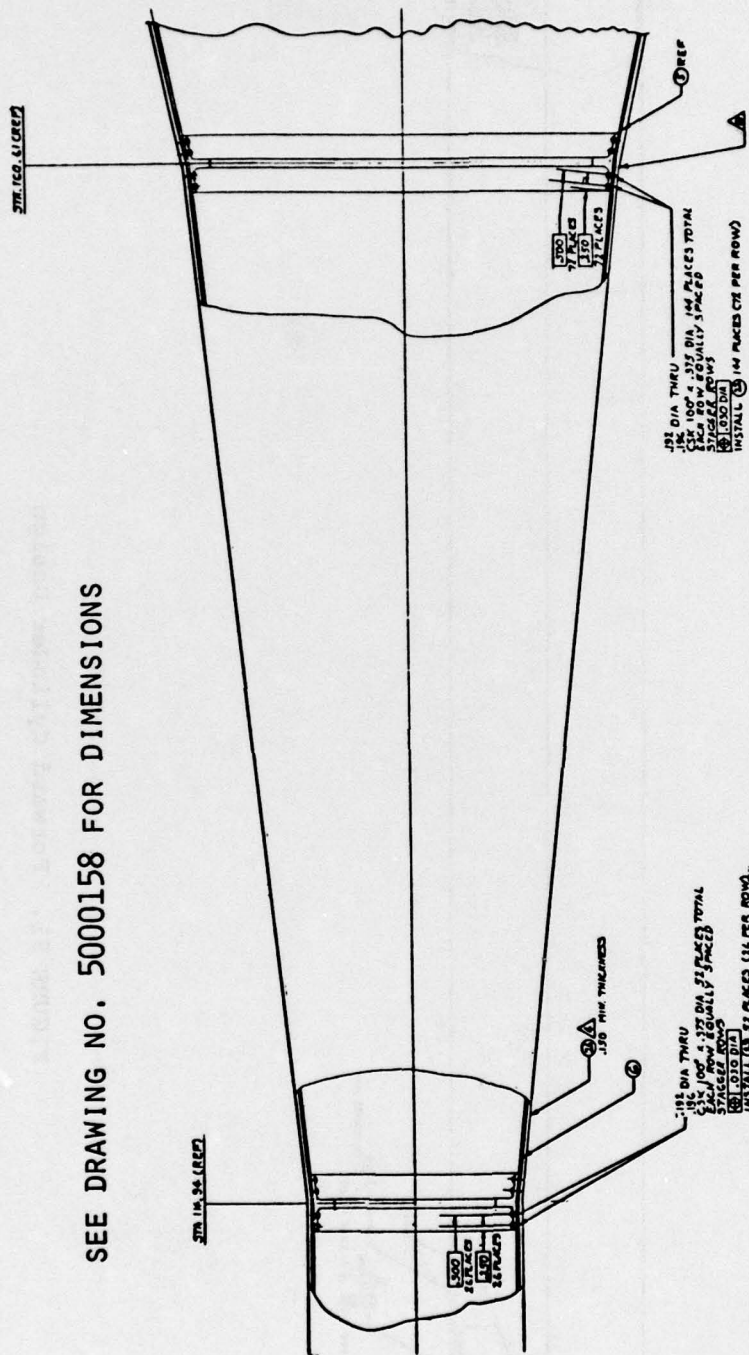


FIGURE 82 . Six Degree Flare Design



## 6.5 CONICAL FRUSTUM SECTION DESIGN

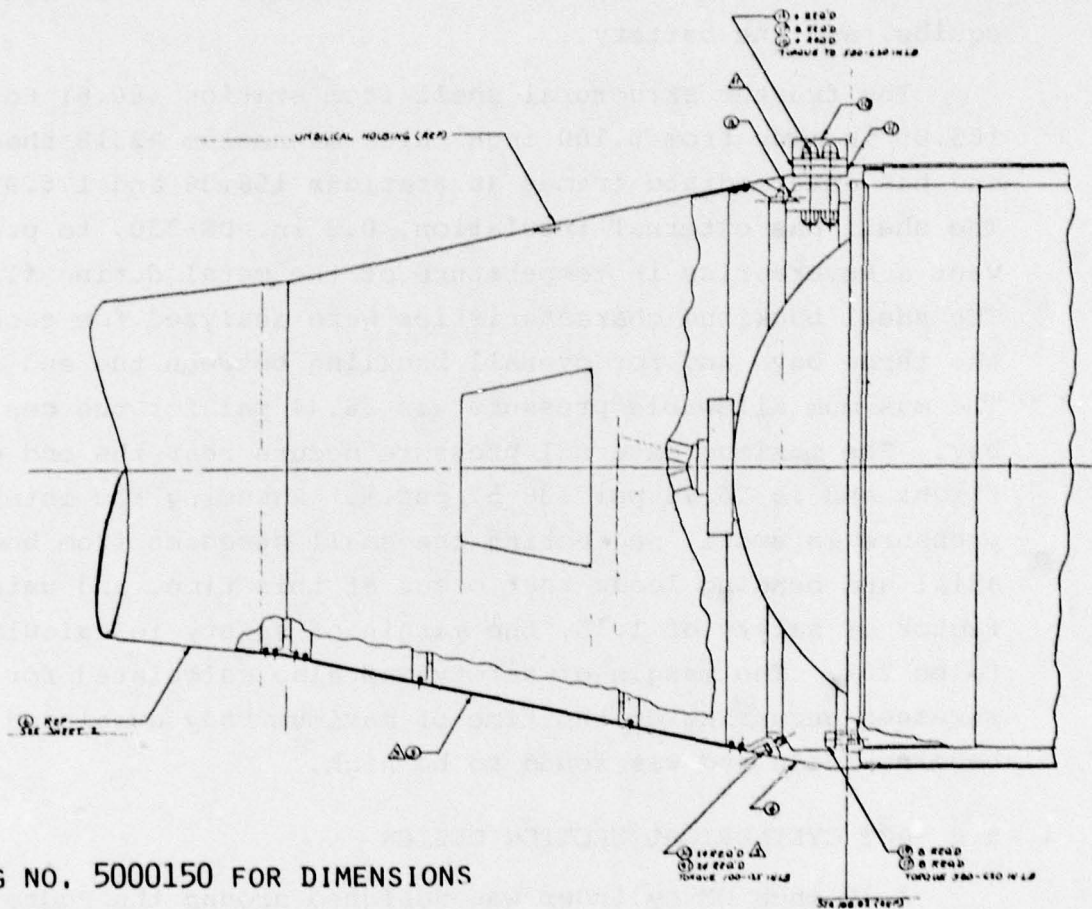
Between the 6 degree conical flare and the aft cylindrical section is an 11.75 degree conical frustum. This section, shown in Figure 83, will be identical to the corresponding FLAME section. It will house the signal conditioners, heat transfer instrumentation, the timers, the motor ignition squibs, and the battery.

The frustum structural shell from station 160.61 to 185.05 is made from 0.100 inch thick magnesium A231B sheet and has intermediate frames at stations 168.36 and 176.99. The shell has external insulation, 0.2 in. DE-350, to prevent a severe rise in temperature of the metal during flight. The shell buckling characteristics were analyzed for each of the three bays and for overall buckling between the end frames. The maximum allowable pressure was 38.44 psi for the center bay. The maximum external pressure occurs near the end of flight and is 26.78 psi (38 57.psf.). Assuming the internal pressure is small, neglecting the small stresses from body axial and bending loads that occur at this time, and using a factor of safety of 1.15, the margin of safety is calculated to be 25%. The margin of safety was also calculated for the stresses occurring at the time of maximum body axial and bending loads and was found to be high.

## 6.6 AFT CYLINDRICAL SECTION DESIGN

A 30 inch OD cylinder was designed around the Pedro rocket motor to facilitate the experiment, as shown in Figure 84. This section will be made of 0.10 inch magnesium alloy, insulated with 0.12 inch DE-350.

Two steel rings, which can slide on the motor case, provide radial support for the cylinder in addition to the end rigid mounting to the motor case. There is a non-insulated 1020 steel plate on which the pressure and heat



SEE DRAWING NO. 5000150 FOR DIMENSIONS

FIGURE 83. Conical Frustum Design

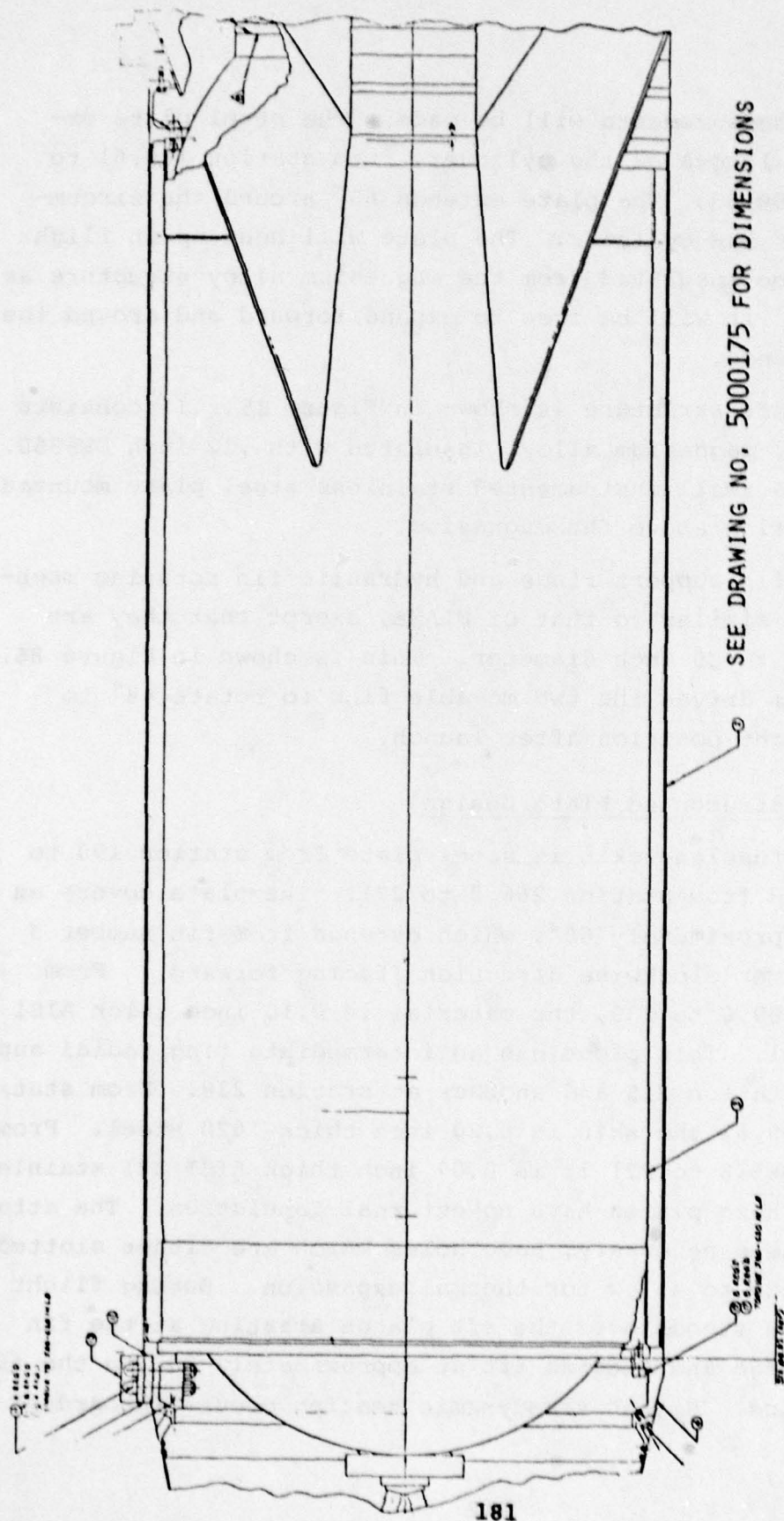


FIGURE 84. Aft Cylinder Design



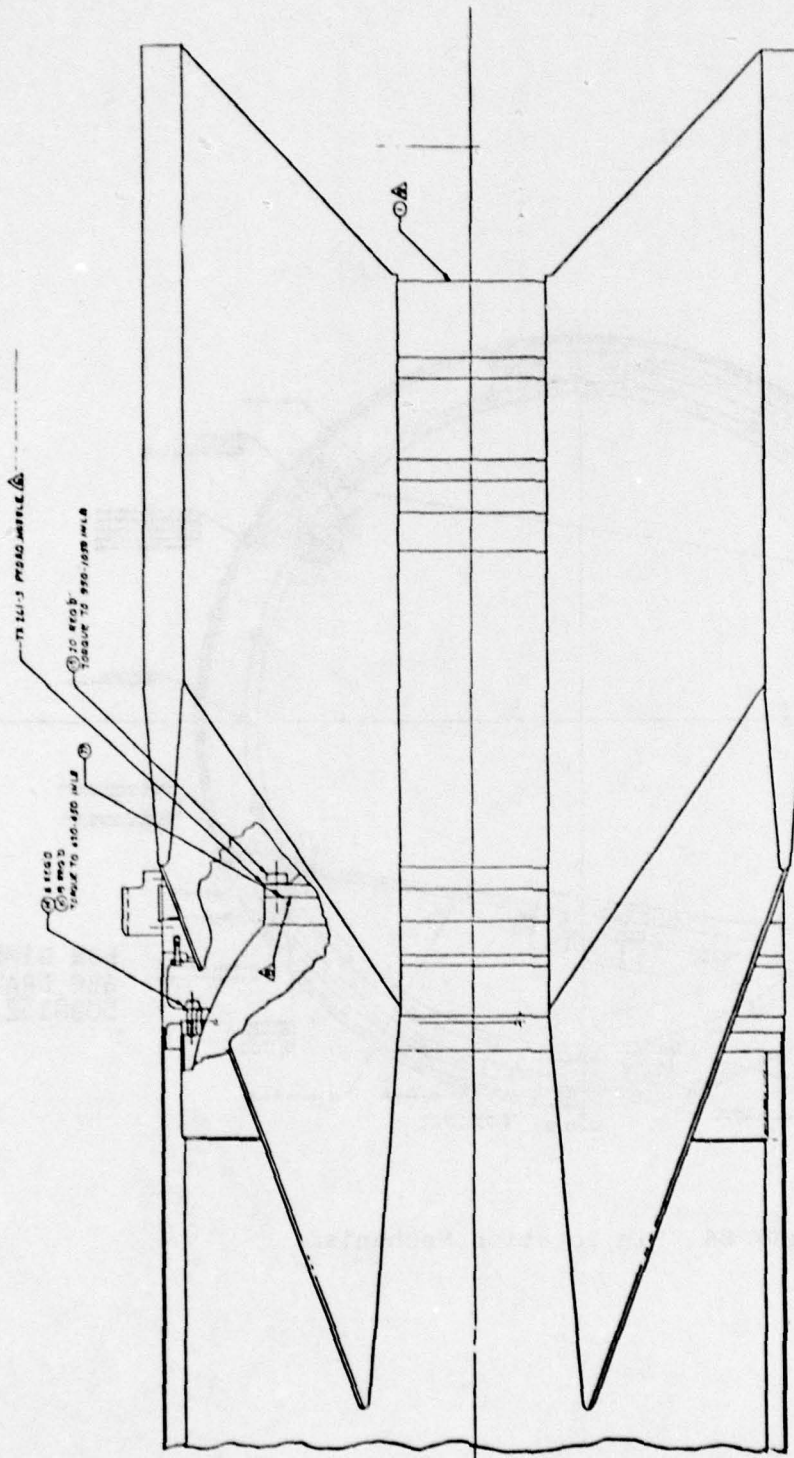
transfer measurements will be made. The steel plate extends the length of the cylinder, from station 189.61 to station 259.63. The plate extends  $60^\circ$  around the circumference of the cylinder. The plate will heat up in flight and will be insulated from the magnesium alloy structure as required. It will be free to expand forward and around the circumference.

The aft structure is shown in Figure 85. It consists of 0.1 in. magnesium alloy, insulated with .12 inch DE-350. There is a small instrumented stainless steel plate mounted on insulation above the magnesium.

The fin support rings and hydraulic fin rotating mechanism are similar to that of FLAME, except that they are scaled up to 30 inch diameter. This is shown in Figure 86. The system drives the two movable fins to rotate  $48^\circ$  to their flight position after launch.

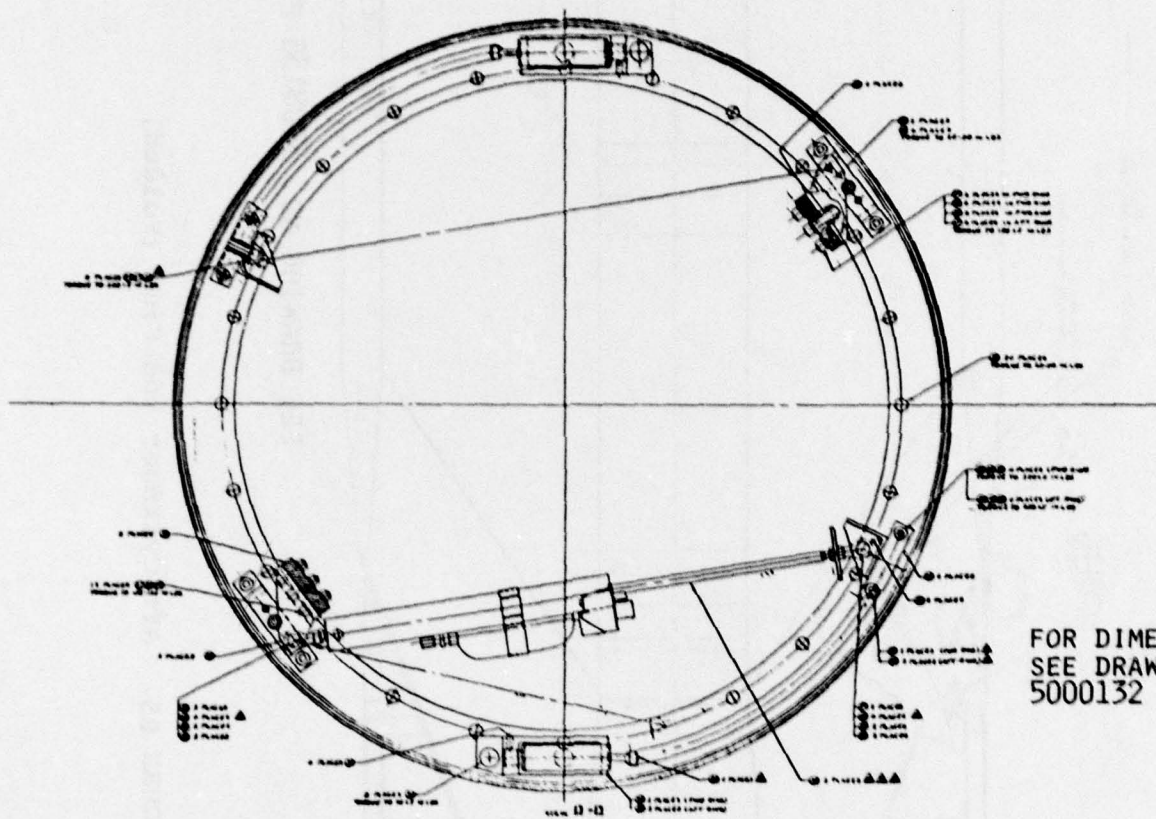
#### 6.6.1 Instrumented Plate Design

The fuselage skin is steel plate from station 190 to 259.63 and from station 266.8 to 271. The plate covers an arc of approximately  $60^\circ$ , which extends from fin number 3 in a counter clockwise direction (facing forward). From station 189.6 to 238, the material is 0.10 inch thick AISI 1020 steel. This piece has an intermediate ring radial support at station 215 and another at station 238. From station 238 to 259.63 the skin is 0.20 inch thick 1020 steel. From station 266.8 to 271 it is 0.07 inch thick AISI 321 stainless steel. These plates have no external insulation. The attachments, where necessary, have holes which are either slotted or oversize to allow for thermal expansion. During flight a shock wave stands over the aft plates starting at the fin leading edge and extends aft at approximately  $20^\circ$  to the fin center line. Higher aerodynamic heating occurs inboard of



SEE DRAWING NO. 5000156 FOR DIMENSIONS

FIGURE 85. Aft Cylinder and Fins (Folded)



FOR DIMENSIONS,  
SEE DRAWING NO.  
5000132

FIGURE 86. Fin Rotation Mechanism



this shock wave. The temperature gradients through the skin are shown in Figures 87 and 88, for the time in flight where maximum temperature differential between the outside and inside skin occurs. These calculations are shown for various thickness AISI 321 stainless steel and AISI 1020 carbon steel plates. They are shown for locations both forward and aft of the shock wave. In the shock interference region, the augmented heat flux is calculated through use of correlations from (Reference 3).

$$\dot{q}_I = \dot{q} \left[ 5(M \sin \theta_s - 1) + 0.75 \right]$$

where

$\dot{q}_I$  = heat flux in shock interaction region

$\dot{q}$  = heat flux without shock interaction

$M$  = Mach number

$\theta_s$  = shock angle

Figure 89 shows the plate surface maximum temperatures as a function of plate thickness.

Thermal strains and radial deflections were calculated for these plates considering the location of the attachments and conservatively assuming no warping restraint at the free edges. These radial deflections were found to be acceptable (less than 0.14 inches). The thermal stresses were calculated and found to be acceptable. These plates do not carry body axial or bending loads, and the stresses from external pressure are small.

These plates will experience significant thermal expansion. These expansions were calculated at maximum plate temperature. For the forward plate (0.10 inch thick 1020 steel) the maximum temperature is 800°F, from which the longitudinal deflection is 0.29 inches and the tangential is 0.08 inches. Considering the 0.20 inch thick 1020 steel

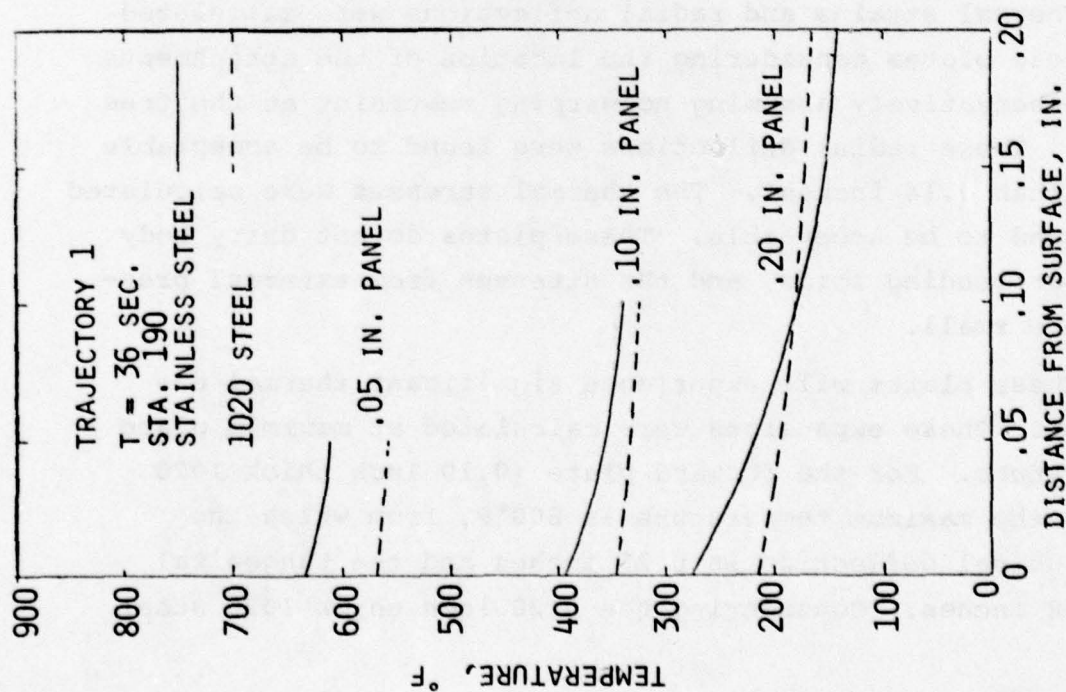


FIGURE 87. Fuselage Steel Plate Maximum Temperature Gradient in Undisturbed Flow

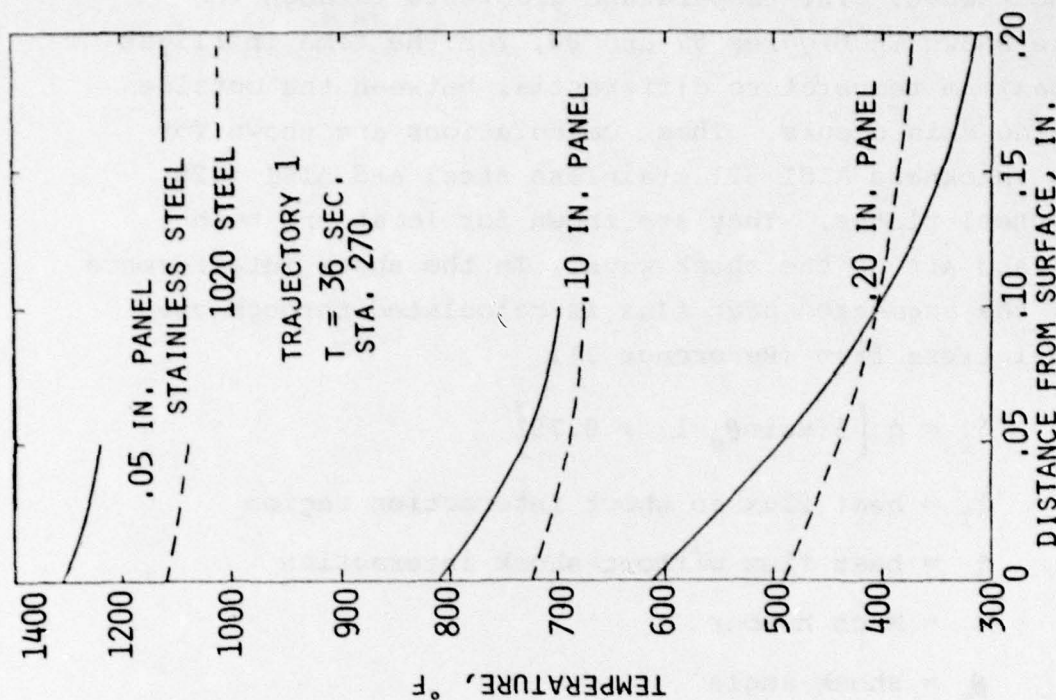


FIGURE 88. Fuselage Steel Plate Maximum Temperature Gradient in Interaction Region

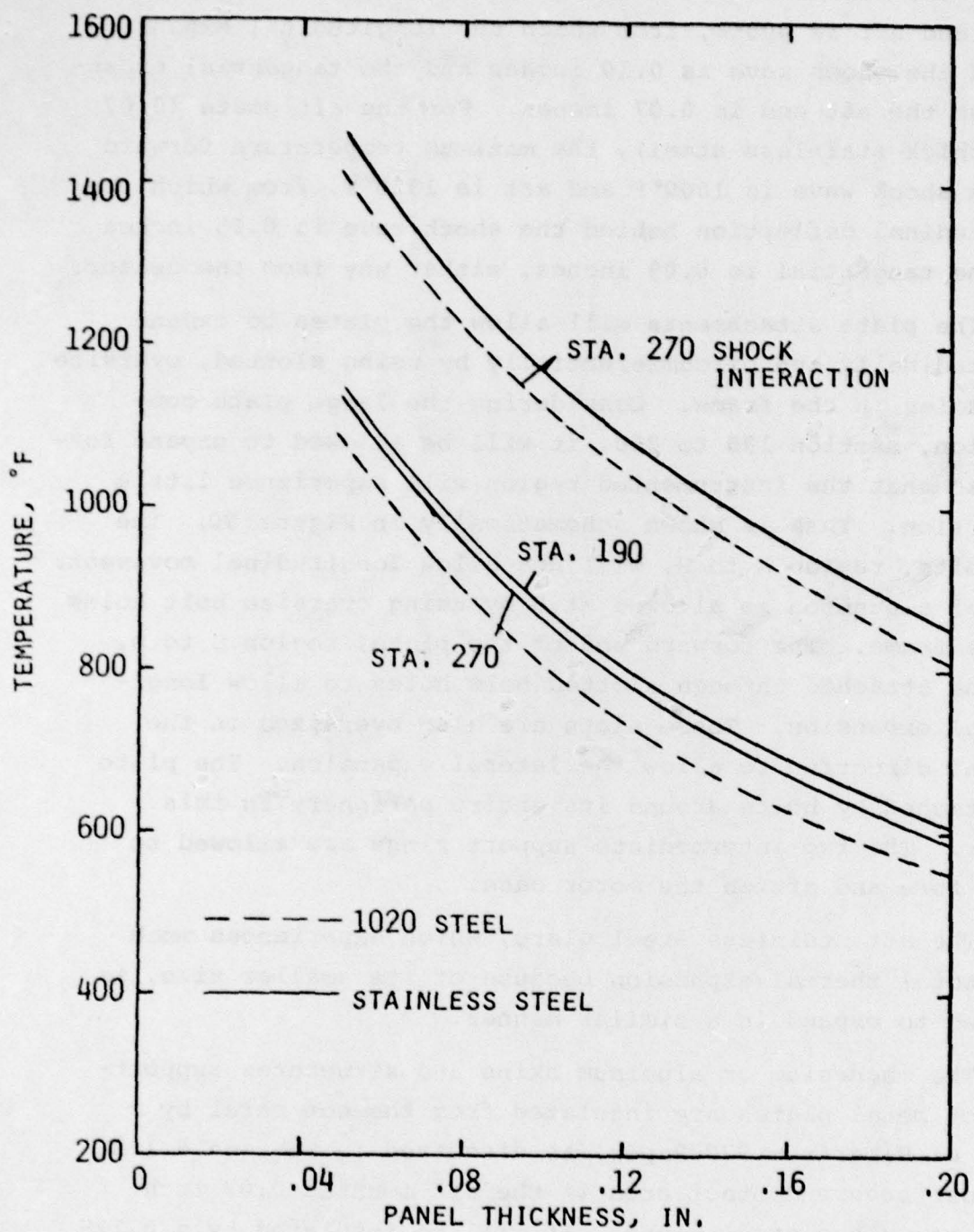


FIGURE 89. Fuselage Steel Plate Maximum Surface Temperature Trajectory 1



plate, the maximum temperature forward of the shock wave is 540°F and aft is 805°F, from which the longitudinal expansion behind the shock wave is 0.10 inches and the tangential expansion at the aft end is 0.07 inches. For the aft plate (0.07 inch thick stainless steel), the maximum temperature forward of the shock wave is 1000°F and aft is 1320°F, from which the longitudinal deflection behind the shock wave is 0.05 inches and the tangential is 0.09 inches, either way from the center.

The plate attachments will allow the plates to expand longitudinally and circumferentially by using slotted, oversize bolt holes in the frame. Considering the large plate combination, station 190 to 260, it will be allowed to expand forward so that the instrumented region will experience little distortion. This is shown schematically in Figure 90. The aft bolts, region A to B, will not allow longitudinal movement. Lateral expansion is allowed at B by using oversize bolt holes in the frame. The forward end of the plate, region C to D, will be attached through slotted bolt holes to allow longitudinal expansion. These slots are also oversized in the lateral direction to allow the lateral expansion. The plate is attached by bolts around its entire periphery in this manner. The two intermediate support rings are allowed to slide fore and aft on the motor case.

The aft stainless steel plate, which experiences much less total thermal expansion because of its smaller size, is allowed to expand in a similar manner.

The magnesium or aluminum skins and structures supporting hot metal plates are insulated from the hot metal by a layer of Fiberfrax 970 Paper, as discussed in Section 6.1.3. the most severe contact area is the aft mounted 0.07 inch thick stainless steel plate. It will be insulated by a 0.125 inch layer of Fiberfrax, compressed to a minimum thickness of 0.05 inch. The predicted magnesium skin temperature rise,

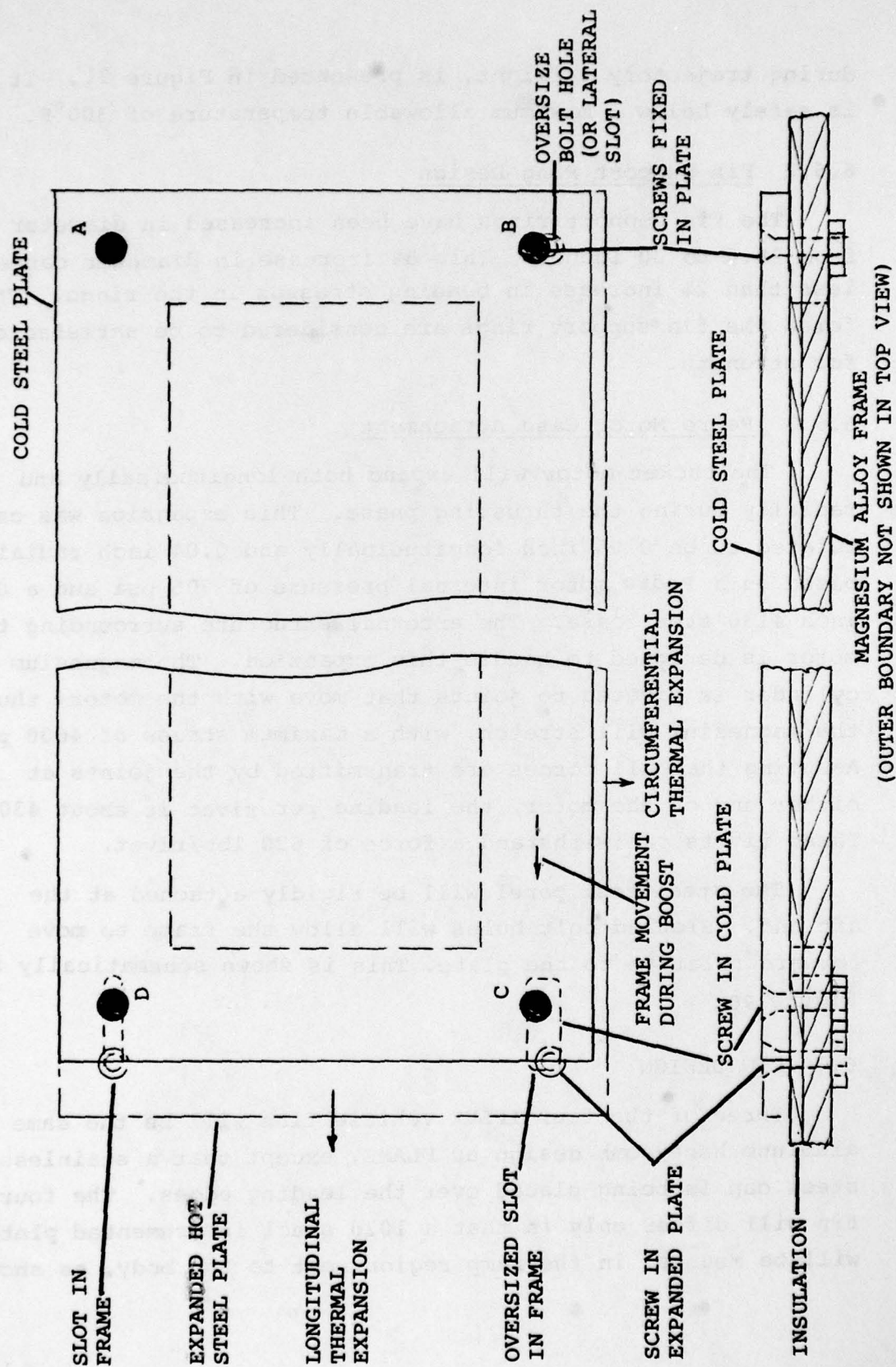


FIGURE 90. Schematic of Steel Plate Thermal Expansion



during trajectory 1 flight, is presented in Figure 91. It is safely below a maximum allowable temperature of 300°F.

#### 6.6.2 Fin Support Ring Design

The fin support rings have been increased in diameter from 28.6 to 30 inches. This 5% increase in diameter causes less than 2% increase in bending stresses in the rings. Therefore, the fin support rings are considered to be satisfactory for strength.

#### 6.6.3 Pedro Motor Case Attachment

The rocket motor will expand both longitudinally and radially during the thrusting phase. This expansion was calculated to be 0.05 inch longitudinally and 0.04 inch radially, based on a Pedro motor internal pressure of 705 psi and a 0.11 inch 4130 steel case. The external structure surrounding the motor is designed to handle this expansion. The magnesium cylinder is riveted to joints that move with the motor; thus, the magnesium will stretch, with a maximum stress of 4600 psi. Assuming that all forces are transmitted by the joints at either end of the motor, the loading per rivet is about 430 lbs. These rivets can withstand a force of 620 lbs/rivet.

The steel test panel will be rigidly attached at the aft end. Slotted bolt holes will allow the frame to move forward relative to the plate. This is shown schematically in Figure 90.

### 6.7 FIN DESIGN

Three of the four IFLEX vehicle fins will be the same aluminum honeycomb design as FLAME, except that a stainless steel cap is being placed over the leading edges. The fourth fin will differ only in that a 1020 steel instrumented plate will be mounted in the ramp region next to the body, as shown



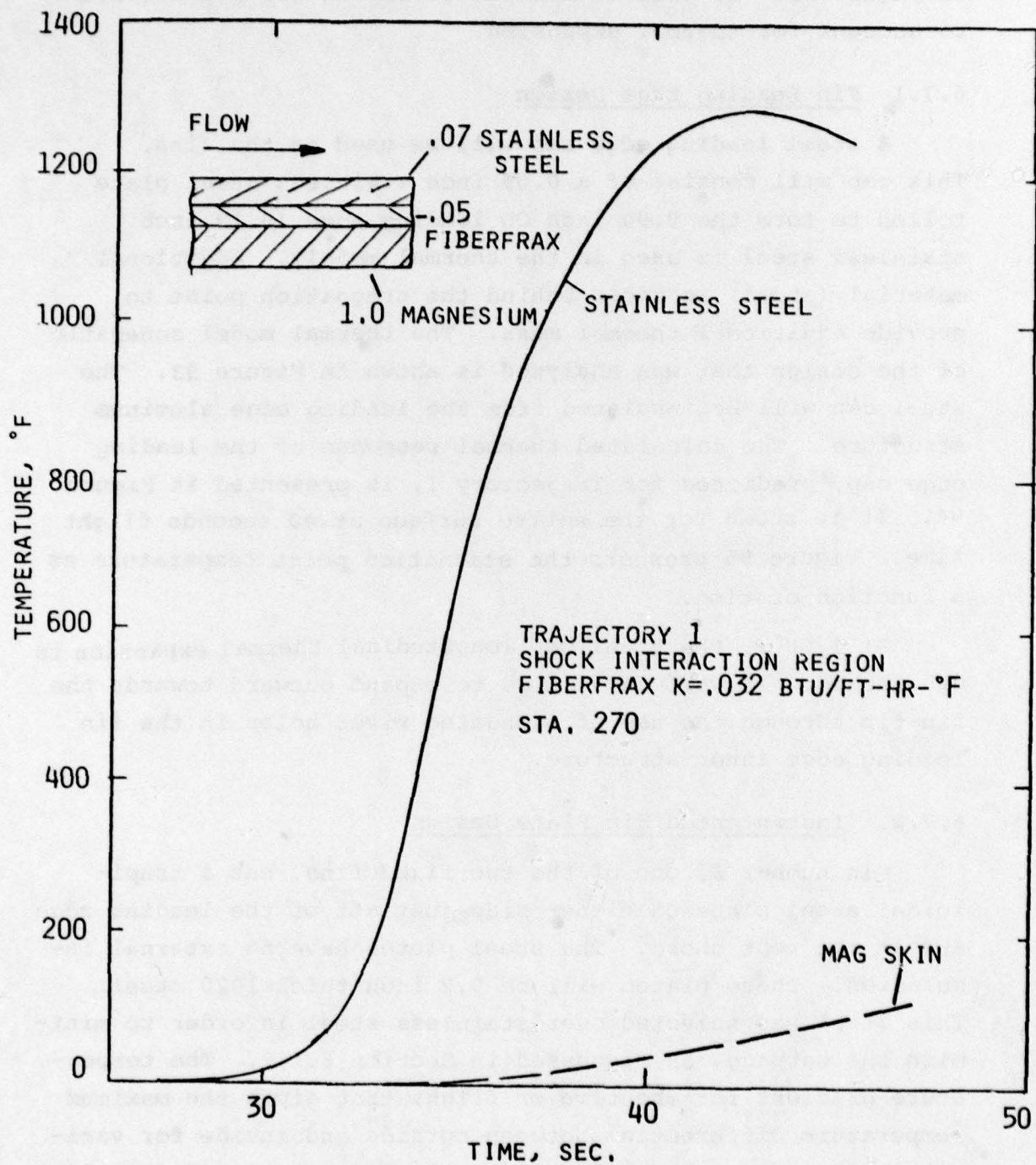


FIGURE 91. Thermal Response of Magnesium Skin Insulated from Aft Test Panel

in Figure 92. It will be allowed to expand aft and outward to account for thermal expansion.

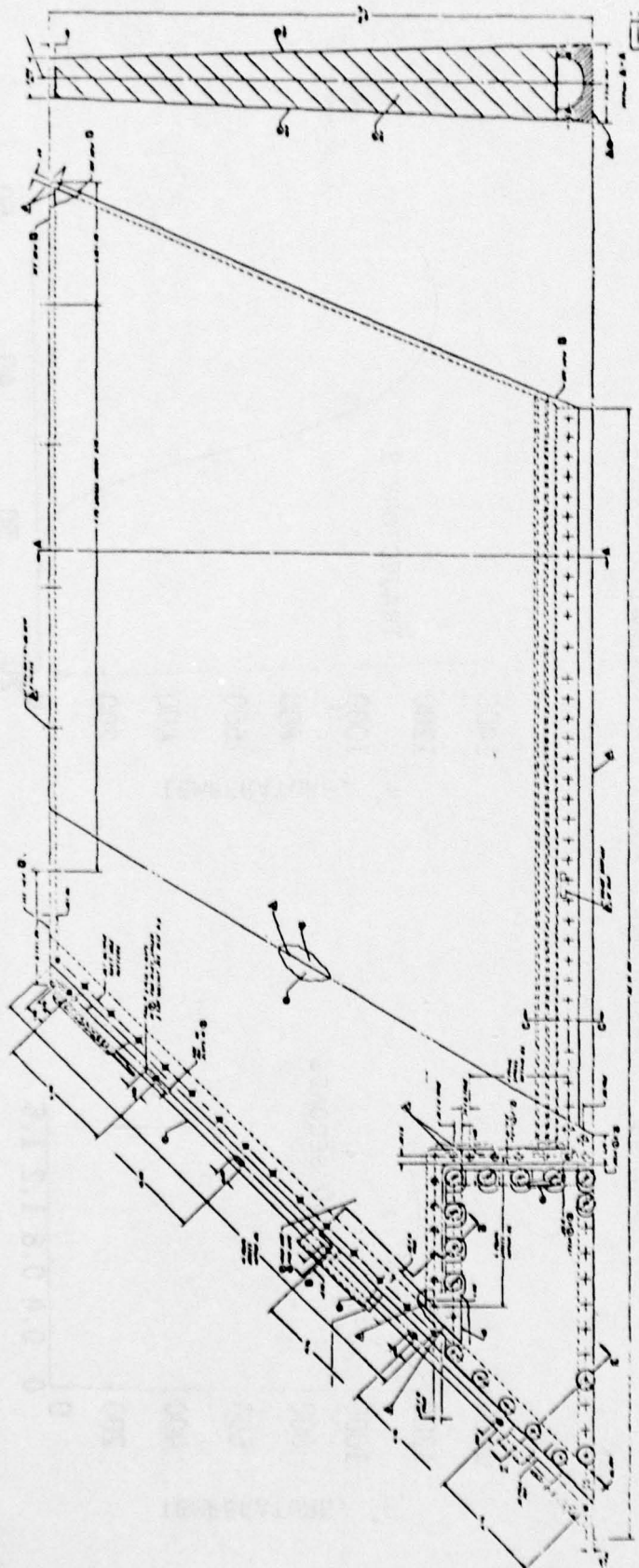
#### 6.7.1 Fin Leading Edge Design

A steel leading edge cap will be used on the fins. This cap will consist of a 0.09 inch stainless steel plate rolled to form the 0.90 inch OD leading edge (0.10 inch stainless steel is used in the thermal model). Additional material (steel) is added behind the stagnation point to provide additional thermal mass. The thermal model schematic of the design that was analyzed is shown in Figure 93. The steel cap will be insulated from the leading edge aluminum structure. The calculated thermal response of the leading edge cap, predicted for Trajectory 1, is presented in Figure 94. It is shown for the entire surface at 40 seconds flight time. Figure 95 presents the stagnation point temperature as a function of time.

At 1200°F, the steel cap longitudinal thermal expansion is 0.5 inches. It will be allowed to expand outward towards the fin tip through the use of elongated rivet holes in the fin leading edge inner structure.

#### 6.7.2. Instrumented Fin Plate Design

Fin number 3, one of the two fixed fins, has a trapezoidal steel plate on either side just aft of the leading edge and at the root chord. The steel plates have no external insulation. These plates will be 0.2 inch thick 1020 steel. This steel was selected over stainless steel in order to minimize the warpage, as discussed in Section 6.1.2. The temperature gradient for the time of flight that gives the maximum temperature differential between outside and inside for various thicknesses of both AISI 321 stainless steel and AISI 1020



INSTRUMENTED PLATE

SEE DRAWING NO. 5000131 FOR DIMENSIONS

FIGURE 92. Instrumented Fin Design



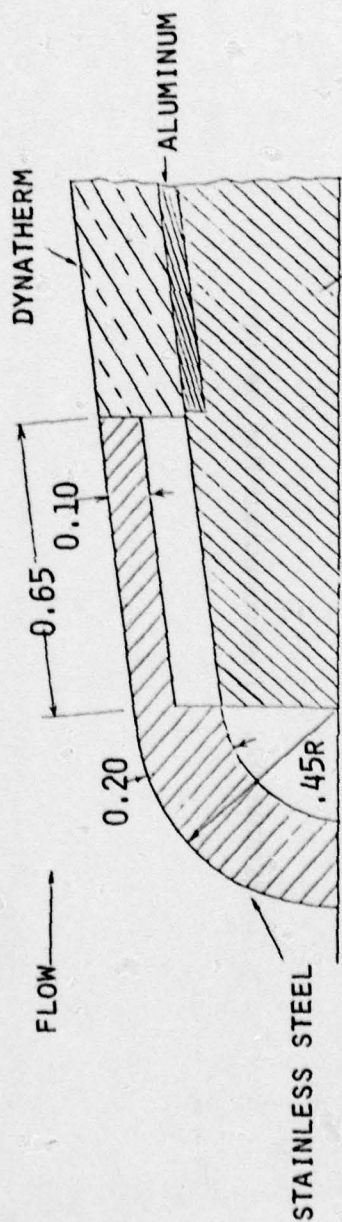


FIGURE 93. Leading Edge Model for Thermal Analysis

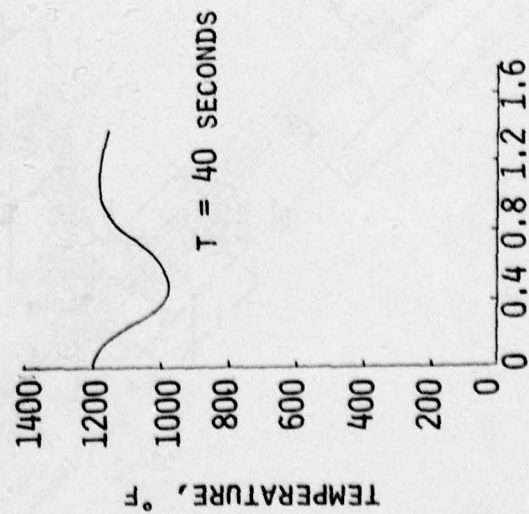


FIGURE 94. Leading Edge Temperature Profile

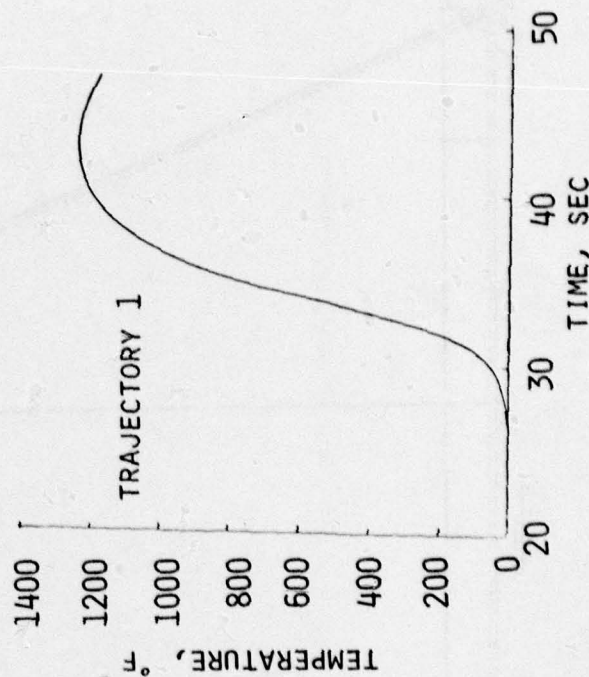


FIGURE 95. Leading Edge Stagnation Point Temperature

carbon steel are shown in Figure 96. Figure 97 presents the surface temperature response with time. These predictions are for a location 6 inches aft of the leading edge.

Thermal strains and normal deflections (warpage) were calculated from these temperatures, conservatively assuming no warping restraint. The deflections are shown in Figure 98. The results show a large reduction in normal deflection in going from stainless steel to carbon steel. Also, there is very little increase in deflection for 0.2 inch thick over 0.1 inch thick carbon steel.

The thermal stresses from the nonlinearity of the temperature gradient, when the plate is free to warp, are small. The bending stresses of the plate from external pressure are less than 30% of the allowable bending stress of the material. The lateral expansion of the plate at maximum temperature (880°F) is 0.10 inch chordwise and 0.04 inch spanwise. All of the attachments, except the forward inboard one, have either slotted or oversize holes in the plate. Thus, the plate will be allowed to expand aft and outward.

#### 6.8 ELECTRONICS COMPONENTS THERMAL PROTECTION

The electronic equipment used for data acquisition and telemetering must be maintained within specified temperature limits during captive carry and missile flight. This equipment is mounted on an aluminum plate in the forward cylinder and on wall brackets in the frustum. These sections are insulated from aeroheating during missile flight, and the plate has significant thermal mass; hence, the thermal environment can be determined by the captive carry conditions. The minimum and maximum vehicle internal temperature limits during captive carry are set at -60°F and +60°F, based on cold and hot atmospheres per Reference 32 and the following assumed aircraft flight conditions:

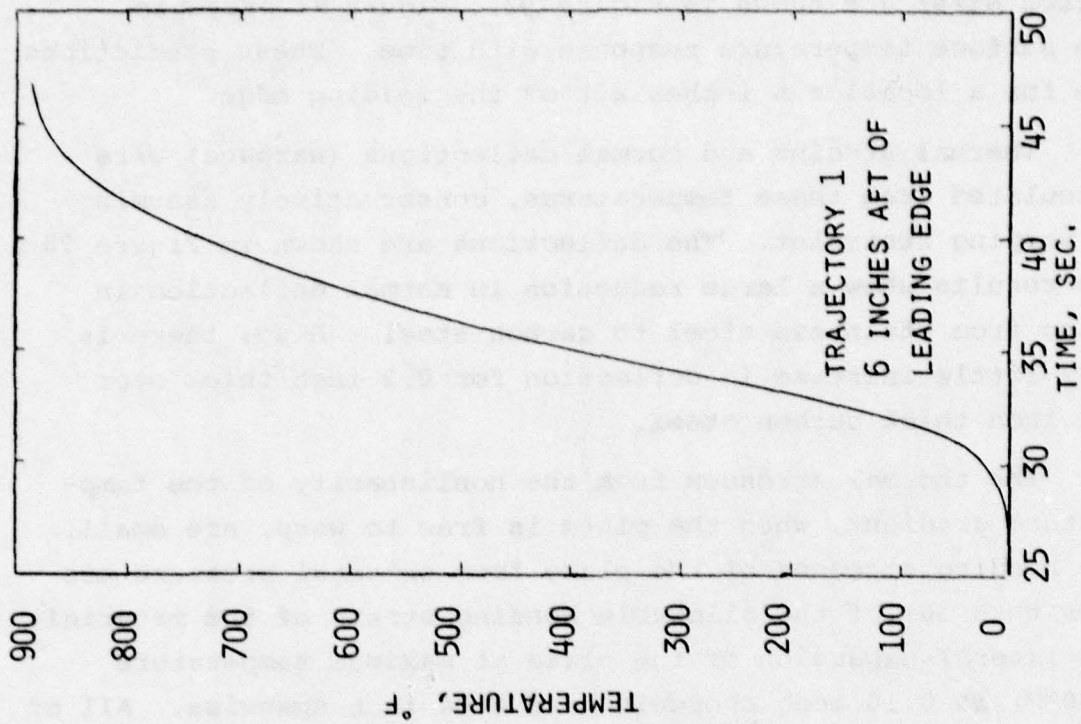


FIGURE 96. Fin Plate Maximum Temperature Gradients, Trajectory 1

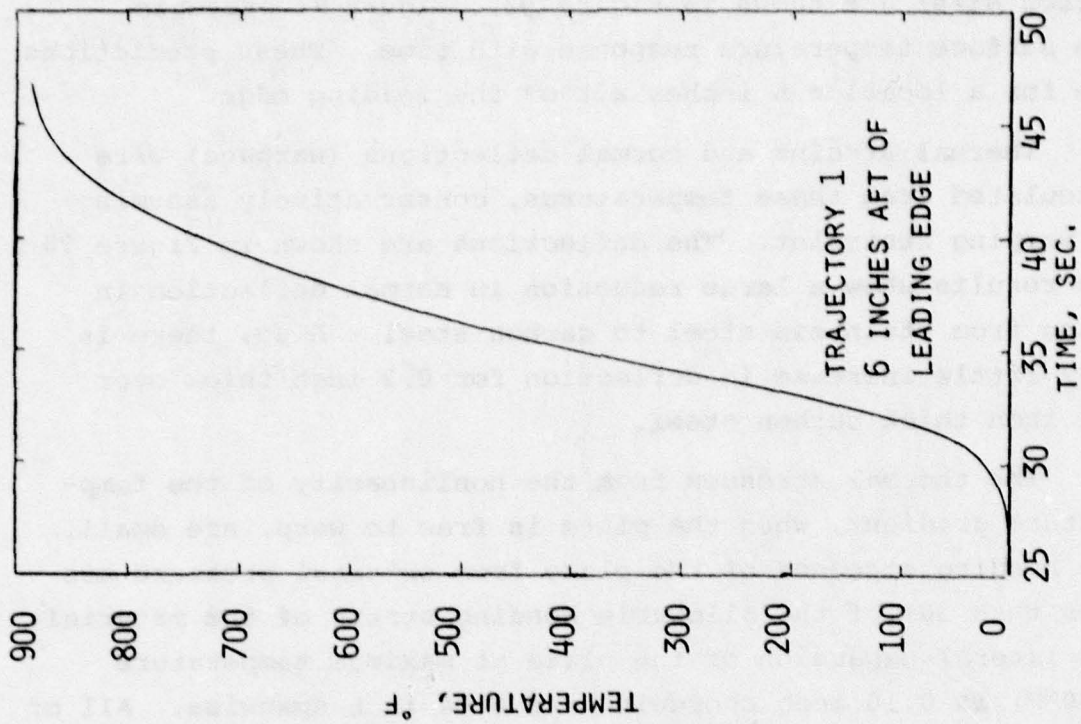


FIGURE 97. Fin Plate Surface Temperature



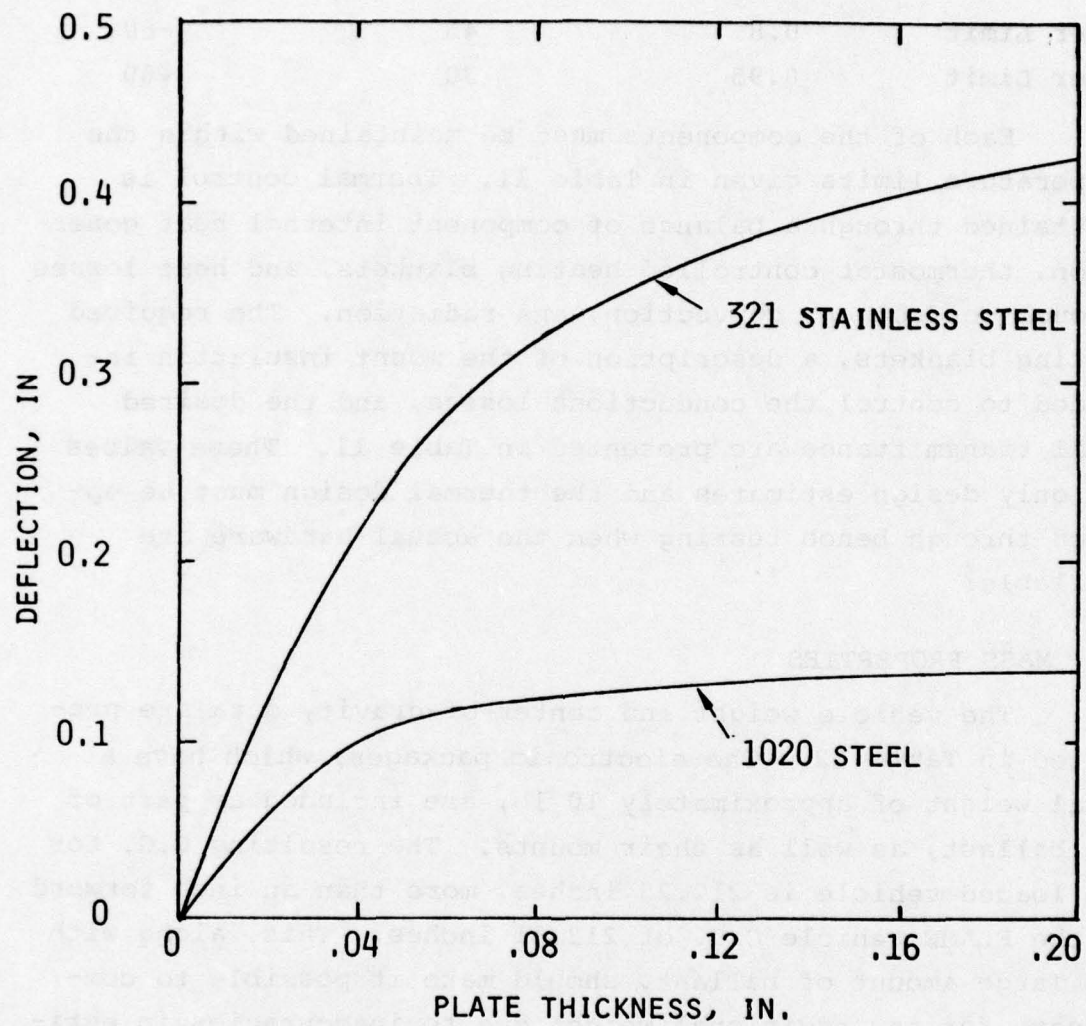


FIGURE 98. Thickness and Material Influence on Fin Plate Normal Deflection Due to Heating

	Mach No.	Altitude (kft)	Recovery Temp. (°F)
Lower Limit	0.8	45	-60
Upper Limit	0.95	30	+60

Each of the components must be maintained within the temperature limits given in Table 11. Thermal control is maintained through a balance of component internal heat generation, thermostat controlled heating blankets, and heat losses through conduction, convection, and radiation. The required heating blankets, a description of the mount insulation intended to control the conduction losses, and the desired total transmittance are presented in Table 11. These values are only design estimates and the thermal design must be updated through bench testing when the actual hardware are available.

#### 6.9 MASS PROPERTIES

The vehicle weight and center-of-gravity data are presented in Table 12. The electronic packages, which have a total weight of approximately 10 lb, are included as part of the ballast, as well as their mounts. The resulting C.G. for the loaded vehicle is 212.23 inches, more than an inch forward of the FLAME vehicle C.G. of 213.51 inches. This, along with the large amount of ballast, should make it possible to compensate for any additional weight due to inaccuracies in estimating the weight of the instrumentation wiring, tubing, and additional insulation.

TABLE 11. Electrical Component Thermal Requirements

Component	Temperature Limits (°F)	Power Consumption (watts)	Heater Size (watts)	Transmittance (Btu/hr-°F)	Mount Insulation
Transmitter	2 to 137	100	200	8.0	.25 thick x 5 in <sup>2</sup> stainless steel 4 No. 6 screws.
Signal Conditioner MMP-600	-13 to 185	13	0	1.0	.25 thick insulative washers, 4 No. 6 screws.
Signal Conditioner Freq. Div.	-31 to 212	5	0	1.0	.25 thick insulative washers, 4 No. 6 screws.
Radar Transponder	-65 to 167	21	0	1.0	.25 thick insulative washers, 4 No. 6 screws.
KPM-2-25	0 to 200	1	30	1.1	.25 thick insulative washers, 4 No. 6 screws.
Telemeter Battery	-4 to 113	-	150	0	Battery will be insulated
Fluctuating pressure	-65 to 450	.3/transducer	0	-	No requirement.
Quasi-Steady Heat Transfer	-65 to 100	0	0	-	No requirement.



TABLE 12. IFLEX Vehicle Mass Properties Summary

	<u>WEIGHT (LB)</u>	<u>C.G. (INCHES)</u>
Nose Section	38.2	26.22
Antenna Section	15.0	42.89
Ballast	300.0	47.00
9 Inch Section	74.9	76.88
6° Flare	73.5	138.72
11°44' Cone	44.0	175.11
Pedro Forward Adapter Ring	23.7	187.60
Forward Launch Lug	6.0	187.40
Bolts	2.0	188.00
Pedro Motor	2870.0	229.00
Shell Around Pedro	108.9	226.50
Aft Launch Lug	2.0	265.00
Pedro Aft Adapter Ring	18.1	261.35
5000110 Ring	23.5	264.66
Forward Slide Ring	21.8	265.42
Aft Slide Ring	21.8	285.84
Tail Can	30.5	274.53
5000126 Tail Skirt	23.6	287.88
4000127 Tail Skirt	4.4	294.35
Fin Deployment Beams	4.5	275.63
Fin Deployment Hardware	6.0	275.66
Instrumented Plate	1.2	268.93
Instrumented Fin	71.1	281.69
Basic Fins (3)	181.1	282.89
VEHICLE TOTAL	<u>3965.8</u>	<u>212.23</u>

## SECTION VII

### PROGRAM PLANNING AND COSTS

The scheduling and costs likely to be associated with a flight test program such as the one described in the previous chapters have been evaluated. Both schedule and cost have been estimated in an objective fashion since bids to accomplish the efforts involved have not been solicited.. The schedule is postulated on appropriate contractors, ranges, aircraft and components timely availability. The costs are based on SAI estimates of likely contractor rates and SAI projections of manpower required of those contractors, yet unidentified. The cost estimates for components such as electronics and instrumentation have been based upon candidate vendors estimates for the FY80 time period. Again, no binding bids have been solicited.

#### 7.1 PROGRAM PLAN

The flight program defined in this report can be organized in four major task areas with the sub-tasks listed in Table 13. Each task function is described in the following paragraphs.

##### 7.1.1 Vehicle Fabrication and Assembly

The IFLEX vehicle will be fabricated according to the design drawings provided in the appendix to this report. The Pedro rocket motor must be acquired with propellant loading appropriate for the performance characteristics selected. Telemetry and electronics systems for signal conditioning must be acquired and integrated. These systems include the antenna and power systems such as described in Section V.

TABLE 13 . IFLEX Program Task Breakdown

- |     |   |
|-----|---|
| 1.0 | VEHICLE FABRICATION AND ASSEMBLY            |
| 1.1 | Airframe Fabrication                        |
| 1.2 | Rocket Motor Acquisition                    |
| 1.3 | Electronics Acquisition and Assembly        |
| 1.4 | Instrumentation and Electronics Integration |
| 2.0 | FLIGHT TEST OPERATIONS                      |
| 2.1 | Range Safety and Flight Qualification       |
| 2.2 | Logistics and Field Assembly                |
| 2.3 | Aircraft Flight and Range Operations        |
| 3.0 | AEROHEATING EXPERIMENT                      |
| 3.1 | Instrumentation Acquisition and Calibration |
| 3.2 | Data Acquisition and Coordination           |
| 3.3 | Data Reduction and Analysis                 |
| 4.0 | REPORTING                                   |



The electronics systems and instrumentation must be integrated into the airframe during fabrication.

#### 7.1.2 Flight Test Operations

Both the contractors and government agencies involved in the IFLEX program will participate in flight test operations. The satisfaction of range safety and aircraft compatibility and flight qualification requires coordination and direction from the program sponsoring organization, the organization responsible for flight clearance, the organization providing flight operations (aircraft and pilot) and the organization providing the range. In the program scenario employed for planning purposes, these government organizations are identified in Section III. The role of the contractor is to provide the data necessary to obtain range and flight operations clearances. Then the contractor provides the necessary logistics and field operations to load the IFLEX vehicle on the aircraft.

#### 7.1.3 Aeroheating Experiment

The aeroheating experiment begins with acquisition and calibration of instrumentation. In most cases, the candidate suppliers identified in Section V will accomplish some calibration of instruments provided. Sufficient calibration to meet IFLEX requirements must be specified uniformly to all suppliers or accomplished in addition to that provided with the instrumentation. Data acquisition requirements and formats must be coordinated with the flight range to assure appropriate telemetry reception, recording and formatting. Finally, the instrumentation calibrations and telemetry data must be combined through a data reduction program. The data reduction will transform the telemetry recovered into appropriate descriptions of aeroheating parameters measured as functions of the flight environment. This requires combination of telemetry data and vehicle trajectory data.

#### 7.1.4 Reporting

The contractors reporting requirements should include periodic status reports, a comprehensive flight test planning review prior to shipping the first vehicle from its assembly point, pre and post flight reports for each flight, a final summary review of the flight program operations and a final summary review of aeroheating data. The latter two reviews should be integrated to form the program final report.

#### 7.2 IFLEX PROGRAM SCHEDULE

A functional schedule for the IFLEX program is illustrated in Figure 99. It is assumed that a two month separation between flights will provide the flexibility of modification to the latter two flight plans based upon the outcome of the first two flights. The early initiation of the data analysis task will provide the data reduction program.

#### 7.3 IFLEX PROGRAM COSTS

Costs estimated for the IFLEX program, by subtask, are listed in Table 14. These are based upon estimates by SAI of prices contractors are likely to be able to perform the various functions for, assuming the availability of trained, knowledgeable engineers and technicians. In most cases these estimates have been confirmed as reasonable by candidate contractors and suppliers, for a FY80 time frame, given the above availability assumptions.



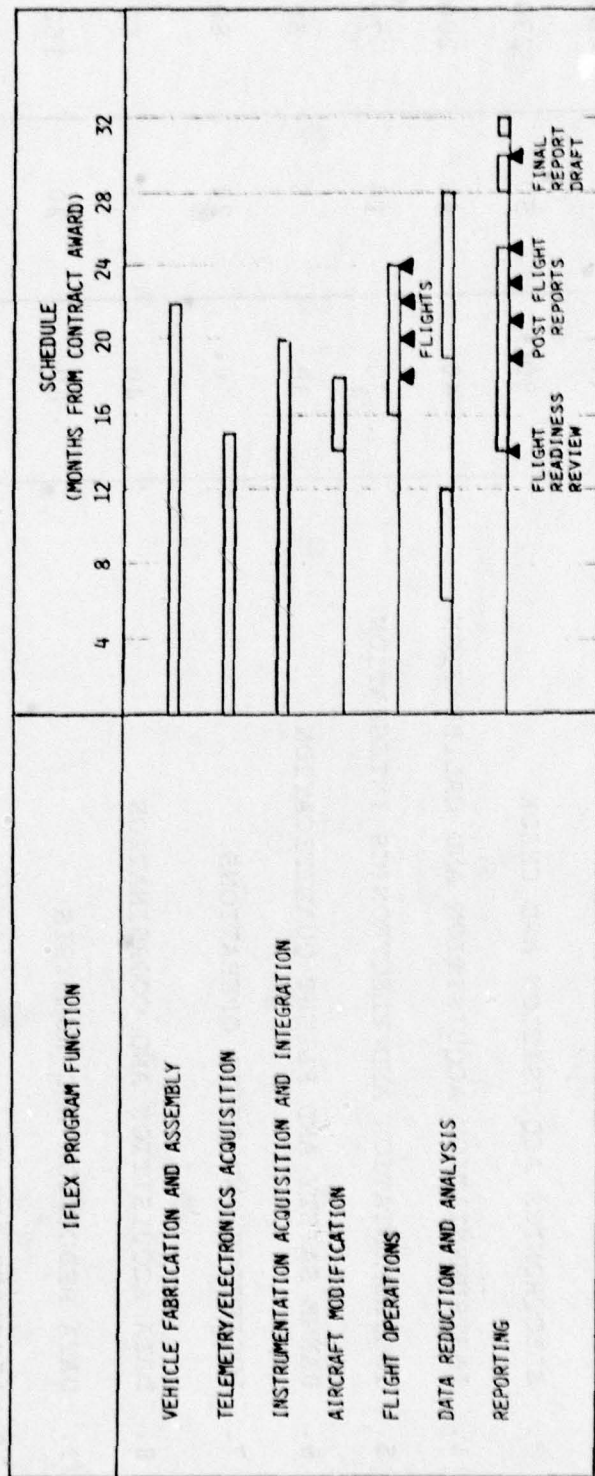


FIGURE 99. IFLEX Program Schedule



TABLE 14. IFLEX Program Cost Estimates

TASK	ESTIMATED COSTS (K\$)		
	NON RECURRING	PER FLIGHT	4 FLIGHT TOTAL
1. AIRFRAME MANUFACTURE AND ASSEMBLY	80	100	480
2. PEDRO ROCKET MOTOR ACQUISITION	40	110	480
3. ELECTRONICS ACQUISITION AND CHECK	30	50	230
4. INSTRUMENTATION ACQUISITION AND CALIBRATION	40	40	200
5. INSTRUMENTATION AND ELECTRONICS INTEGRATION	30	10	70
6. RANGE SAFETY AND FLIGHT QUALIFICATION	30	5	50
7. LOGISTICS AND FIELD OPERATIONS	0	20	80
8. DATA ACQUISITION AND COORDINATION	40	5	60
9. DATA REDUCTION AND ANALYSIS	80	20	160
10. AIRCRAFT AND RANGE OPERATIONS	40	35	180
11. REPORTING	60	15	120
TOTAL EXPERIMENT	470	410	2,110

#### REFERENCES

1. Korkegi, R.H. "Survey of Viscous Interactions Associated with High Mach Number Flight", AIAA Journal Vol. 9, pp 771-784, 1971.
2. Shang, J.S. and Hankey, W.L., "Numerical Solution of the Compressible Navier-Stokes Equations for a Three-Dimensional Corner", AIAA Paper 77-169, 15th Aerospace Sciences Meeting, January 1977.
3. Neumann, R.D. and Hayes, J.R., "Prediction Techniques for the Characteristics of the 3-D Shock Wave-Turbulent Boundary Layer Interaction", AIAA Paper 77-46, 15th Aerospace Sciences Conference, January 1977.
4. Fryer, J.R., "FLAME Test Vehicle 1976 Flight Test Series Final Report", DNA 4222F, February 1977.
5. Mattasits, G.R. and Cunningham, "Wind Tunnel Tests to Evaluate Store Separation and Aircraft Stability for the F-4J Aircraft and Pedro Recruit Missile at Mach Numbers from 0.6 to 2.0", AEDC-772-74-120, November 1974.
6. "F-4J/PEDRO RECRUIT Interface Analysis for Project Flame", MDC A3008, Contract DNA 001-74-C-0279, 16 August 1974.
7. Wolcott, H.D. and Cruce, A.C., "Integration of a Two Stage PEDRO/RECRUIT Rocket with the F-4J Aircraft for the Fighter Launched Advanced Materials Equipment (FLAME)", NAVAIRTESTCEN Document.
8. Dunn, J.L. "Fighter Launched Advanced Materials Experiment (FLAME) Utilizing F-4J Aircraft and a Two Stage PEDRO/RECRUIT Rocket", NAVAIRTESTCEN Document.
9. Lanham, D.L., "Documentation of the AFFDL FLAME Test at Mach Numbers 2 to 5", AEDC-TSR-78-V8, June 1978.
10. Phillips, W.H., "Effects of Steady Rolling on Longitudinal and Directional Stability", NACA TN No. 1627, 1948.
11. Marconi, Frank and Yaeger, Larry, "Development of a Computer Code for Calculating the Steady Super/Hypersonic Inviscid Flow Around Real Configurations, Volume III - Code Description", NASA CR-2676, May 1976.
12. Hoener, S.F., "Fluid-Dynamic Drag, Hoener Fluid Dynamics," 1965.

13. Token, K.H., "Heat Transfer Due to Shock Wave Turbulent Boundary Layer Interactions on High Speed Weapons Systems", AFFDL-TR74-77, April 1974.
14. Solomon, J., Ciment M., and Ferguson, R.E., "Three-Dimensional Supersonic Inviscid Flowfield Calculations on Reentry Vehicles with Control Surfaces", AIAA Paper 77-84, January 1977.
15. Roshko, A., Thomke, G.J., "Flare-Induced Interaction Lengths in Supersonic Turbulent Boundary Layers", AIAA Journal, Vol. 14, No. 7, July 1976, pp 873-879.
16. Berg, D., "Surface Roughness Effects on the Hypersonic Turbulent Boundary Layer", Ph.D. Thesis, California Institute of Technology, 1977.
17. Browne, L.W.B. and R.A. Antonia, "Calculation of a Turbulent Boundary Layer Downstream of a Step Change in Surface Temperature", Transactions of the ASME, Vol. 101, February 1979.
18. Holden, M.S., "Shock Wave Turbulent Boundary Layer Interaction in Hypersonic Flow", 10th Aerospace Science Meeting, AIAA Paper No. 72-74, January 1972.
19. Simon, W.E. and Walter, "L.A., Approximation for Supersonic Flow Over Cones", AIAA J. Vol. 1, No. 7, 1963.
20. P.J. Legendre, W.R. Grabowsky, R.G. Fowler, "The Challenge of Reentry Vehicle Instrumentation", SAMSO-TR-78-99, 31 May 1978.
21. Volluz, R.J., "Handbook of Supersonic Aerodynamics: Section 20, Wind Tunnel Instrumentation and Operation", NAVORD Report 1488 (Volume 6), January 1961.
22. R. Gardon, "An Instrument for the Direct Measurement of Intense Thermal Radiation", The Review of Scientific Instruments, Vol. 24, No. 5, May 1953.
23. L.W. Woodruff, L.F. Hearne, T.J. Keliher, "Interpretation of a Symbolic Calorimeter Measurements", AIAA Journal Vol. 5, No. 4, April 1967.
24. R.L. Ash, "Response Characteristics of Thin Foil Heat Flux Sensors", AIAA Journal, Vol. 7, No. 12, Dec 1969
25. Firex RX2376A Data Sheet, TR-186-5, Pfizer, 235 East 42nd Street, New York, N.Y. 10017, 1973.



26. Flamemaster Dyna-Therm DE-350 Technical Bulletin, Sun Valley, Ca., August 1977.
27. Flamemaster Dyna-Therm DE-370 Technical Bulletin, Sun Valley, Ca.
28. O'Neil, et.al., "The Variable Boundary Transient Heat Conduction Program", Report No. AY63-0065, General Dynamics/Astronautics, 1963.
29. "Material Specification 11244452", U.S. Army Material Command Redstone Arsenal, Alabama, 12 January 1973.
30. Auerbach, I. and McAlees, Jr., "Evaluation of the Heats of Ablation and Insulation Properties of Several Ablative Coatings for Rocket Motors", SAND77-0469, Sandia Laboratories, May 1977.
31. Fiberfrax Ceramic Fiber Data Sheet, Carborundum Company.
32. "Climatic Extremes for Military Equipment", MIL-STD-210A, 1957.

## APPENDIX A

### LIST OF DRAWINGS

This appendix presents a list of all drawing numbers and titles. Drawings are available from AFFDL/FXG.

<u>DRAWING NO.</u>	<u>TITLE</u>
4000098	SLIDE RING - IFLEX
4000099	LUG-FWD LAUNCHING - IFLEX
4000100	LUG: LAUNCH, AFT IFLEX
5000110	RING, TAIL
5000111	BASE PLATE, FIN-IFLEX
5000112	BASE PLATE, INSTRUMENTED FIN-IFLEX
5000113	RING, ADAPTER - IFLEX
5000114	RING, TAIL ADAPTER-IFLEX
4000115	DOUBLER, FORWARD LUG-IFLEX
4000116	SPACER, FORWARD LUG-IFLEX
4000117	RING, FWD CYL ASSY-IFLEX TAIL
4000118	RING, AFT CYL ASSY-IFLEX TAIL
4000119	RING, FWD, SKIRT ASSY-IFLEX
5000120	FIN, SKIN-IFLEX
5000121	FIN, SKIN, INSTRUMENTED-IFLEX
5000122	CORE, FIN - IFLEX
5000123	CORE, FIN, INSTRUMENTED - IFLEX
4000124	RING, AFT SKIRT-IFLEX TAIL
4000125	CYLINDER, SKIRT ASSY - IFLEX
4000126	SKIRT ASSY - IFLEX TAIL
4000127	FAIRING, IFLEX TAIL STRUCTURE
5000128	CYLINDER ASSY, TAIL - IFLEX
4000129	LEADING EDGE IFLEX FIN
5000130	FIN ASSY, IFLEX
5000131	FIN ASSY, INSTRUMENTED - IFLEX
5000132	TAIL SECTION ASSY - IFLEX
2000133	SPACER

<u>DRAWING NO.</u>	<u>TITLE</u>
2000134	INSERT, SLIDING RING
2000135	PLATE, SLIDING RING, IFLEX
4000136	CYLINDER, IFLEX ACTUATOR
4000137	PISTON, IFLEX ACTUATOR
5000138	ACTUATOR ASSY, IFLEX
4000139	CAP ASSY, LEADING EDGE, INSTRUMENTED - IFLEX
4000140	IFLEX INSTRUMENTATION SCHEMATIC
3000141	KPM -2 -25 MULTICHANNEL TRANSDUCER
5000142	CYLINDER, TAIL - IFLEX
3000143	TRANSMITTER, TELEMETRY, L-BAND
3000144	HOT WALL CALORIMETER MODEL C-1821-J-ZZ-R-XXX-YYY
3000145	ANTENNA, C-BAND AND L-BAND
3000146	TRANSPONDER, RADAR, C-BAND
3000147	POWER SUPPLY, INTERNAL
4000148	DOOR, TAIL ACCESS - IFLEX
4000149	DOUBLER, TAIL ACCESS DOOR - IFLEX
5000150	FORWARD SKIRT - IFLEX
4000151	PLATE ASSY - AFT INSTRUMENTED
4000152	PANEL ASSY - AFT INSTRUMENTED
3000153	MULTIPLEXER, FREQUENCY DIVISION
3000154	MULTIPLEXER, TIMER DIVISION
4000155	ANTENNA ASSY - C-BAND AND L-BAND
5000156	MAIN ASSEMBLY - IFLEX
5000157	PLATE ASSEMBLY - IFLEX MOTOR SECTION FAIRING
5000158	FLARE ASSY - IFLEX 6°
5000159	NOSE SECTION ASSY - IFLEX
4000160	ADAPTER FRAME Z SECTION
4000161	RING - 9 INCH SECTION, FWD ADAPTER
5000162	9 INCH SECTION ASSY - IFLEX
5000163	FWD SKIRT ASSY - IFLEX
3000164	PRESSURE TRANSDUCERS - ANGLE OF ATTACK
3000165	COMMAND RECEIVER - UHF
3000166	MECHANICAL TIMER
3000167	ANTENNA, UHF - COMMAND RECEIVER



DRAWING NO.

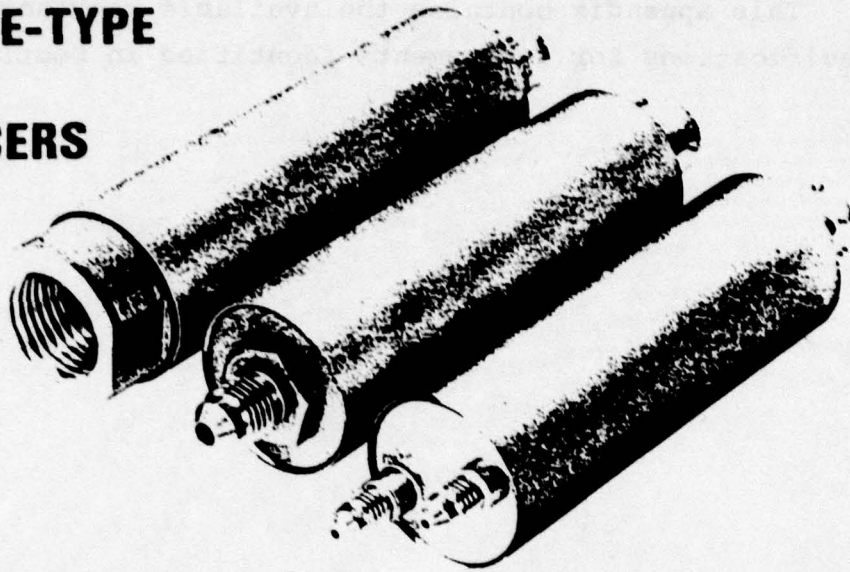
TITLE

3000168	ACCELEROMETER, FLIGHT DIAGNOSTICS
3000169	TRANSMITTER, TELEMETRY L-BAND 5 WATT
3000170	TRANSDUCER, FLUCTUATING PRESSURE
2000171	SLUG, PRESSURE TAP

## APPENDIX B

This appendix contains the available manufacturer's specifications for instruments identified in Section V.

## **SERIES 1332/1333 GENERAL-PURPOSE CAPACITIVE-TYPE PRESSURE TRANSDUCERS**



*High-level 0-5 VDC output*

*0.1% F.S. accuracy*

*Excellent long term stability*

*Many standard ranges for absolute,  
gage and differential pressure measurements*

### **INTRODUCTION**

Rosemount's 1332 and 1333 Series of Capacitive Pressure Transducers\* offer high accuracy in a compact size and a price competitive with many less accurate devices. The common feature of 28 VDC input and 0-5 VDC output for each of the many standard ranges available can greatly simplify the design of systems where a large number of measurements over a wide range of absolute, gage and differential pressure spans are required.

Series 1332/1333 Transducers utilize Rosemount's proven capacitive sensor technology in a design particularly suitable for high-volume production. The construction of these transducers offers the user high

reliability performance where moderate levels of vibration, shock and acceleration are present. The use of high quality and military grade electronic components further ensures dependable, low maintenance operation. If necessary for total system integration, the 0-5 VDC output can be specially calibrated over specified pressure ranges.

### **TYPICAL APPLICATIONS**

Engine Test Stands  
Flight Test Instrumentation  
Fuel Control Systems  
Barometric and Air Data Measurements  
Industrial Control Systems

---

**Rosemount**

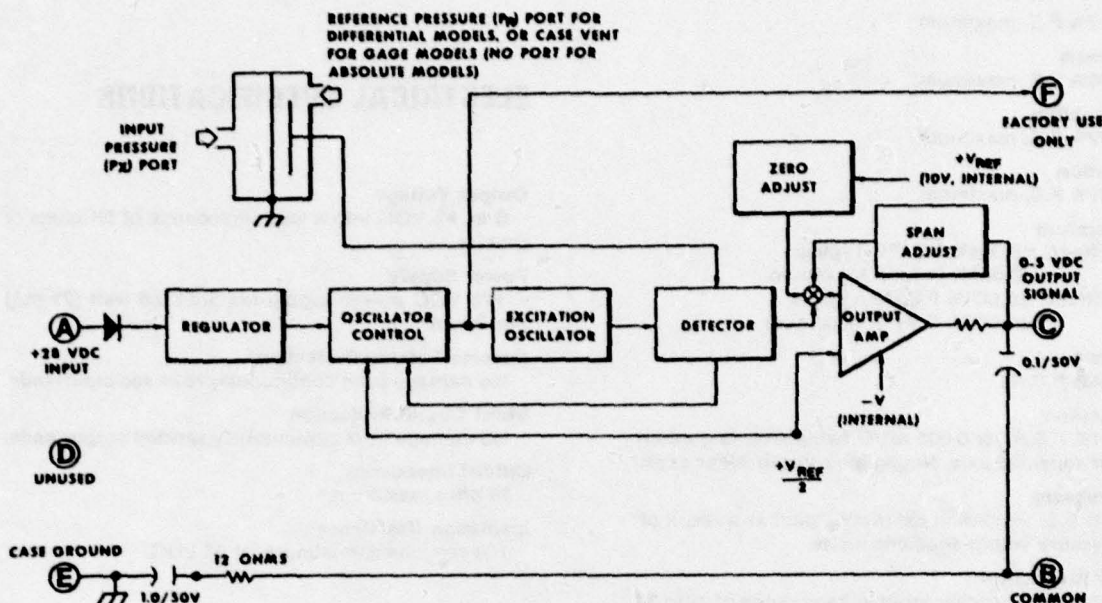
---

©Rosemount Inc., 1978

\*U.S. Patents No. 3,193,020; 3,271,009 and 3,318,153



## BLOCK DIAGRAM MODELS 1332/1333 CAPACITIVE PRESSURE TRANSDUCERS



### PRINCIPLE OF OPERATION

All Series 1332 and 1333 Transducers feature Rosemount's patented capacitive pressure sensor design. The unique low-stress diaphragm and precision capacitance measuring circuit provide high-accuracy performance.

As shown in the Block Diagram, the sensor capsule generates a capacitance signal directly proportional to the pressure sensed. A controlled product oscillator — consisting of an oscillator, a feedback network and a control amplifier — excites the sensing capsule such that the signal current from the detector is a linear function of the sensed pressure. The signal is scaled by an output amplifier to provide a low-impedance, high-level 0-5 VDC output signal.

### ACCURACY

The static error band of the Series 1332/1333 Transducer is 0.10% of full scale output. This error includes the effects of hysteresis, repeatability, resolution and non-linearity. The effect of environmental factors can be Root-Sum-Squared (RSS method) with the static error band to give the overall operating accuracy for the specific application.

Temperature is the most significant error source in any pressure transducer. The Series 1332/1333 transducers are compensated with computer-selected electronic components to optimize transducer performance over the range of 0° to 150°F.

## PERFORMANCE SPECIFICATIONS

### Non-Linearity

±0.09% F.S. maximum.

### Hysteresis

±0.04% F.S. maximum.

### Repeatability

±0.02% F.S. maximum.

### Resolution

±0.01% F.S. maximum.

### Temperature

Zero Effect: ±0.004% F.S./°F Typical

±0.007% F.S./°F Maximum

Span Effect: ±0.004% F.S./°F Typical

±0.007% F.S./°F Maximum

### Vibration

±0.04% F.S./G

### Acceleration

±0.04% F.S./G or 0.005 psi/G (whichever is greater) in most sensitive axis. Negligible error in other axes.

### Overpressure

±0.1% F.S. maximum calibration shift as a result of overpressure within specified limits.

### Supply Regulation

±0.02% F.S./volt over input voltage range of 22 to 32 VDC.

### Response Time

5 ms for 63% response

### Long Term Stability (6 months)

±0.15% F.S. maximum calibration drift during a six month operating period.

### Adjustments

Zero: ±2% F.S.

Span: ±2% F.S.

## ENVIRONMENTAL SPECIFICATIONS

### Pressure Media

Any media compatible with Ni-Span-C\* and stainless steel.

### Reference Media (differential or gage)

Dry, non condensing gas.

### Overpressure Limits

300% full-scale pressure for ranges up to 15 psi.

200% full-scale pressure for ranges up to 50 psi.

150% full-scale pressure for ranges over 50 psi, and for 22-32" Hg range.

### Operating Temperature Range

0° to 150°F compensated (-18° to 65°C)

-65° to 200°F uncompensated/storage (-54° to 93°C)

### Vibration

0.1 inch double amplitude or 10 g's peak from 5 to 2000 Hz.

\*Ni-Span-C is a trademark of International Nickel Co.

### Acceleration

±10 g's

### Shock

15 g's, 11 ms

## ELECTRICAL SPECIFICATIONS

### Output Voltage

0 to +5 VDC into a load impedance of 5K ohms or greater.

### Power Supply

+28 VDC power supply required 0.6 watt (21 mA) maximum.

### Reverse Polarity Protection

No damage from continuously reversed input leads.

### Short Circuit Protection

No damage from continuously shorted output leads.

### Output Impedance

10 ohm maximum.

### Insulation Resistance

100 megohms, minimum, at 50 VDC.

## PHYSICAL SPECIFICATIONS

### Weight

8 ounces maximum.

### Materials

Stainless steel case silicone rubber "O" rings.

### Labeling

Each transducer will be permanently marked with the following minimum information.

Model No.

Pressure Range

Electrical Connections

Serial No.

Input Voltage

Output Voltage

## OPTIONS

### Special Calibration

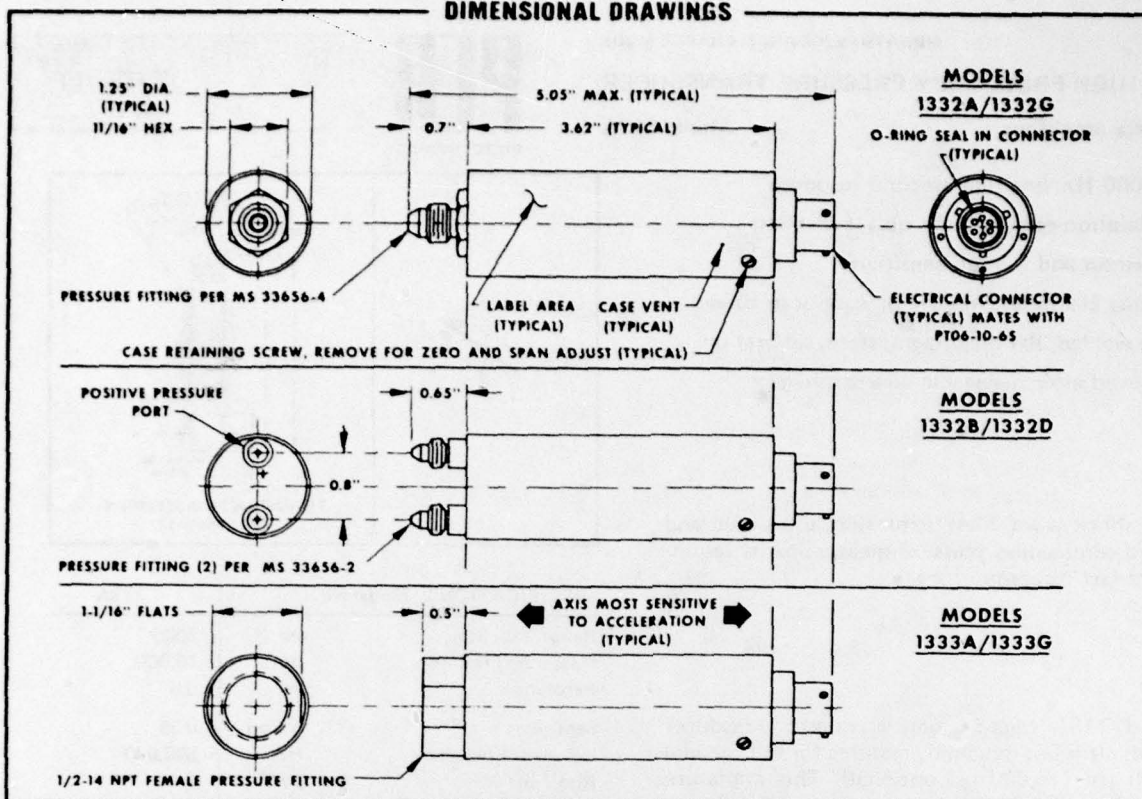
The standard 0-5 VDC output can be calibrated for many non-standard pressure ranges if required. Contact your local Rosemount Field Sales Office for further information.

### Mating Connector

Features cable strain relief; specify Rosemount P/N C10071-1006-0256 (Bendix P/N PT08A10-6S(SR) or equivalent).



## DIMENSIONAL DRAWINGS



## ORDERING INFORMATION

MODEL	
1332A	ABSOLUTE PRESSURE TRANSDUCER
1332B	BI-DIRECTIONAL DIFFERENTIAL PRESSURE TRANSDUCER
1332D	UNI-DIRECTIONAL DIFFERENTIAL PRESSURE TRANSDUCER
1332G	GAGE PRESSURE TRANSDUCER
1333A	ABSOLUTE PRESSURE TRANSDUCER (HIGH PRESSURE)
1333G	GAGE PRESSURE TRANSDUCER (HIGH PRESSURE)

CODE	PRESSURE RANGE				
	MODEL 1332A	MODEL 1332B	MODEL 1332D	MODEL 1332G	MODEL 1333A/G
1	0-5 psia	±2.5 psid	0-5 psid	0-5 psig	0-500 psia/psig
2	0-10 psia	±5.0 psid	0-10 psid	0-10 psig	0-750 psia/psig
3	0-15 psia	±7.5 psid	0-15 psid	0-15 psig	0-1000 psia/psig
4	0-30 psia	±15.0 psid	0-30 psid	0-30 psig	0-1500 psia/psig
5	0-50 psia	—	0-50 psid	0-50 psig	0-2000 psia/psig
6	0-100 psia	—	0-100 psid	0-100 psig	0-2500 psia/psig
7	0-250 psia	—	0-250 psid	0-250 psig	0-3500 psia/psig
8	0-500 psia	—	—	0-500 psig	0-5000 psia/psig
9	3-15 psia	—	—	3-15 psig	0-10000 psia/psig
10	22-32" HgA	—	—	—	—

1332A    2    ← TYPICAL MODEL NUMBER

# Rosemount Inc.

POST OFFICE BOX 35129 MINNEAPOLIS, MINNESOTA 55435

PHONE: (612) 941-5560 TWX: 910-576-3103 TELEX: 29-0183 CABLE: ROSEMOUNT



MINIATURE, QUARTZ, CHARGE MODE

## HIGH-FREQUENCY PRESSURE TRANSDUCER

for charge amplifiers

Model 113A

**PCB**  
PIEZOTRONICS

**PRESSURE**

- 500,000 Hz, one microsecond response
- acceleration-compensated quartz element
- low strain and motion sensitivity
- floating clamp nut; metric or American thread
- flush welded, flat diaphragm; static calibration
- improved interchangeable quartz minigage

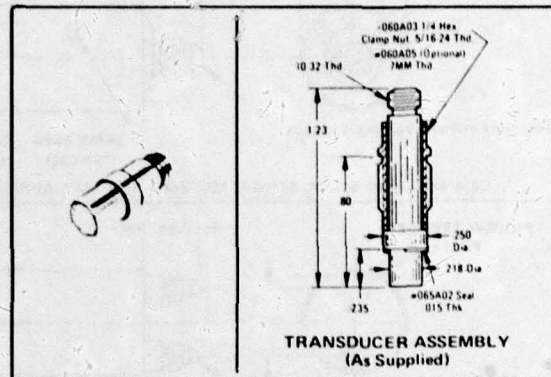
For shock wave, blast, explosion, ultrasonic and dynamic combustion pressure measurements requiring ultra-fast response.

Model 113A high-frequency, quartz transducer measures ultra-fast dynamic pressures for full vacuum to 3000 psi (15,000 psi optional). This miniature transducer measures transient or repetitive phenomena relative to the initial or average pressure level; over wide amplitude and frequency ranges under the most adverse environmental conditions. System voltage sensitivities range from 0.01 mV/psi to 300 mV/psi depending upon the amplifier involved. The electrostatic charge signal from this conventional piezoelectric transducer is converted into a voltage signal in a PCB similar charge amplifier.

The structure of this sophisticated instrument contains a super-rigid compression-mode quartz element with an integral compensating accelerometer to reduce vibration sensitivity and partially suppress internal resonance effects. The net result is unmatched dynamic response from a transducer that installs interchangeably in existing systems.

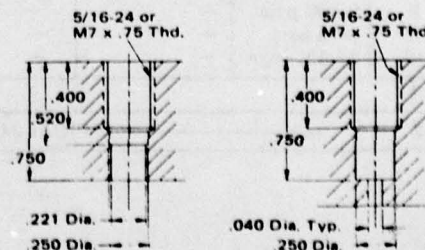
Miniature quartz transducers install flush or recessed in existing or new mini-gage ports directly in the test object or in a variety of threaded mounting adaptors, as illustrated. A floating nut, with either a 5/16-24 or M7 x 0.75 thread clamps the transducer in place, isolates against strain and facilitates installation and removal of the sealed transducer assembly.

To order a typical system, specify: the transducer model number (113A), low-noise transducer cable (003A 10' or other length); laboratory charge amplifier (model 462A); output cable (002A03') and mounting adaptor (60 Series), if required. For the metric threaded version (M7 x .75 clampnut), add the suffix "M" after the model number.



SPECIFICATIONS: Model No.		113A
Range, Full Scale	psi	3000
Maximum Pressure	psi	10,000
Resolution	psi	0.5
Sensitivity	pC/psi	0.35
Resonant Frequency	Hz	500,000
Rise Time	μsec	1
Linearity, B.S.L.	% F.S.	1
Resistance	ohms	10 <sup>12</sup>
Capacitance	pF	12
Acceleration Sensitivity	psi/g	0.002
Temperature Coefficient	%/°F	0.01
Temperature Range	°F	± 400
Flash Temperature	°F	3,000
Vibration/Shock	g	2000/20,000
Thread, Clamp Nut	UNF	5/16-24
Polarity		Neg.
Model No. (Optional Ranges)		
Low-Range	100 psi	113A02
High-Range	10,000 psi	113A03

### INSTALLATION: MOUNTING PORTS



## AIRBORNE CHARGE AMPLIFIER

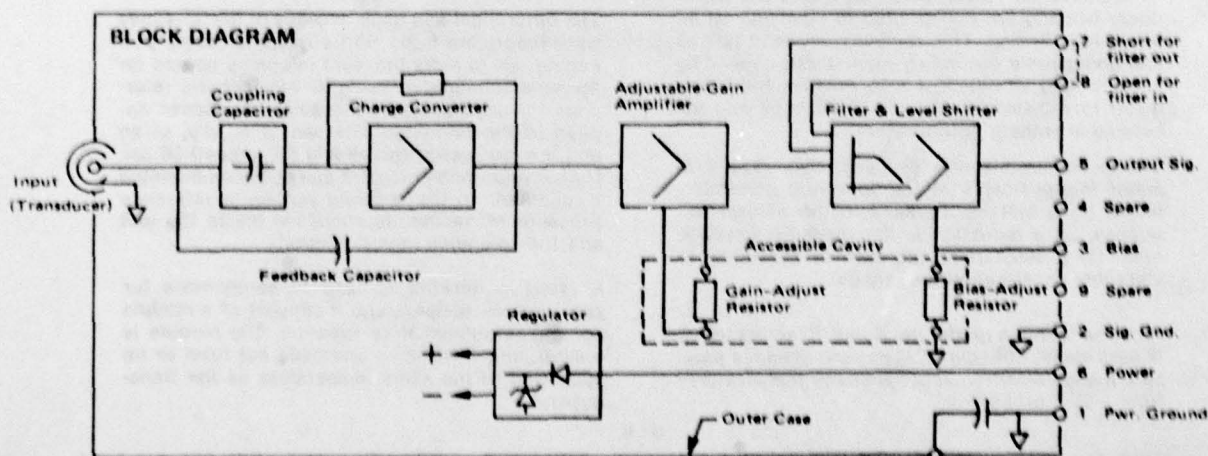
**Model 423B**

## ELECTRONIC

- 

SPECIFICATIONS	Model No.	4238
Input Range (for 4.5V output)	$\mu$ C	150 to 15000
Gain (Adjustable)	mV/ $\mu$ C	0.3 to 30
Linearity	% F.S.	$\pm 0.2$
Frequency Response ( $-3$ db) <sup>(1)</sup>	Hz	1 to 8000
Frequency Response (filter out, $-3$ db)	Hz	1 to 70000
Discharge Time Constant	sec	0.16
Output Signal	volt	0.5 to 5.0
Output Limits	volt	0 to 5.8
Output Bias (Adjustable)	volt	0.5 to 5.0
Bias Stability (Over temp. range)	mV	$\pm 50$
Output Impedance (less than)	ohm	500
Noise (pk. to pk.)	mV	20
Temperature Range	$^{\circ}$ F	$-40$ to $+200$
Vibration (pk. to pk.)	g	5000
Shock (200 $\mu$ sec, half sine)	g	20000
Power (reverse polarity protected)	VOC; mA	$+28 \pm 4$ ; 20
Isolation (min. case to power gnd)	megohm	10 @ 50 VOC
Input Connector	micro	10-32
Output Connector		MDM9SH001B
Size (length x width x height)	in	0.75 x 1.0 x 0.62
Weight	gm	15
Mounting Screws (8-32 length)	in	0.87

Options include factory-tailored ranging, biasing and filtering.

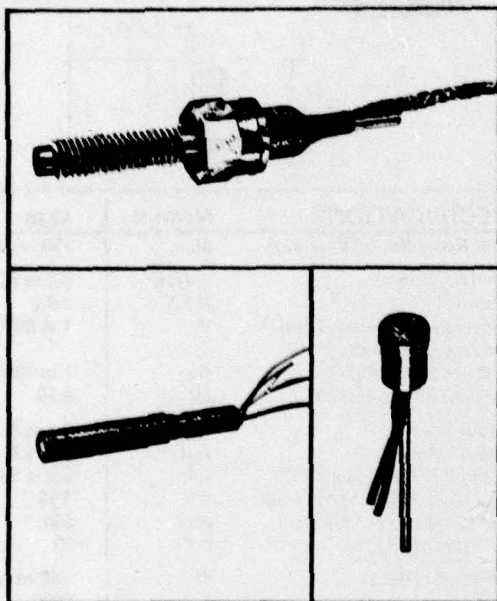


B-7





# KULITE SEMICONDUCTOR



## High Temperature IS Pressure Transducers 'E' SERIES

- Wide Temperature Capability  
-65°F to 525°F
- Flight Qualified
- Integrated Sensing (IS)<sup>®</sup>
- High Natural Frequency
- No Internal Lead Flexing
- Extremely Low G Sensitivity

The heart of the 'E' series transducer is the new Kulite dielectrically isolated epitaxial sensing element. It consists of a miniature silicon diaphragm on which a fully active four arm Wheatstone bridge has been atomically bonded, with isolation provided by a silicon dioxide dielectric. This monolithic construction affords excellent thermal characteristics in operation to high temperatures.

In addition, the silicon diaphragm and the transducer housing are constructed to eliminate all internal lead flexing. This removes any lead fatigue and undesirable secondary resonances caused by internal lead vibration. It also enables the transducer to withstand extremely high shock and acceleration without deterioration.

The subminiaturization process also results in major improvements in the following characteristics: (1) a marked increase in the natural frequency, (2) a reduction in the pressure sensitive area, (3) a substantial decrease in sensitivity to vibration, acceleration and shock.

All these features render the Kulite 'E' series transducers ideally suitable for static and dynamic pressure measurement in applications at temperatures from -65°F to +525°F.

The high temperature pressure transducer has been flight qualified both for use on supersonic aircraft engine-intake systems and also for measurement of surface pressure in missile re-entry vehicle studies. Another application, which utilizes the unique basic characteristics of the transducer, is the measurement of acoustic noise in close proximity to jet engine exhaust.

The differential and gage versions of the 'E' series transducers are fitted with a reference tube, permitting use of a dry pressure reference source for  $\Delta p$  measurements or using an atmospheric reference for gage pressure measurement. Gases applied to the reference side should be dry, clean and non-corrosive, and should not exceed 30 psi. Higher reference pressures can be accommodated if specified. In the absolute version, a reference pressure or vacuum is contained inside the unit and the reference tube is omitted.

A resistive network is used to compensate for zero shift vs. temperature. It consists of a module containing subminiature resistors. The module is temperature insensitive and does not have to be subjected to the same temperature as the transducer.

B-8

KULITE SEMICONDUCTOR PRODUCTS, INC., 1039 HOYT AVENUE, RIDGEFIELD, N.J. • TEL 201-945-3000  
EUROPEAN SUBSIDIARY: KULITE SENSORS LTD., 20 WOTE STREET, BASINGSTOKE, HANTS ENGLAND • TEL 0256-61646

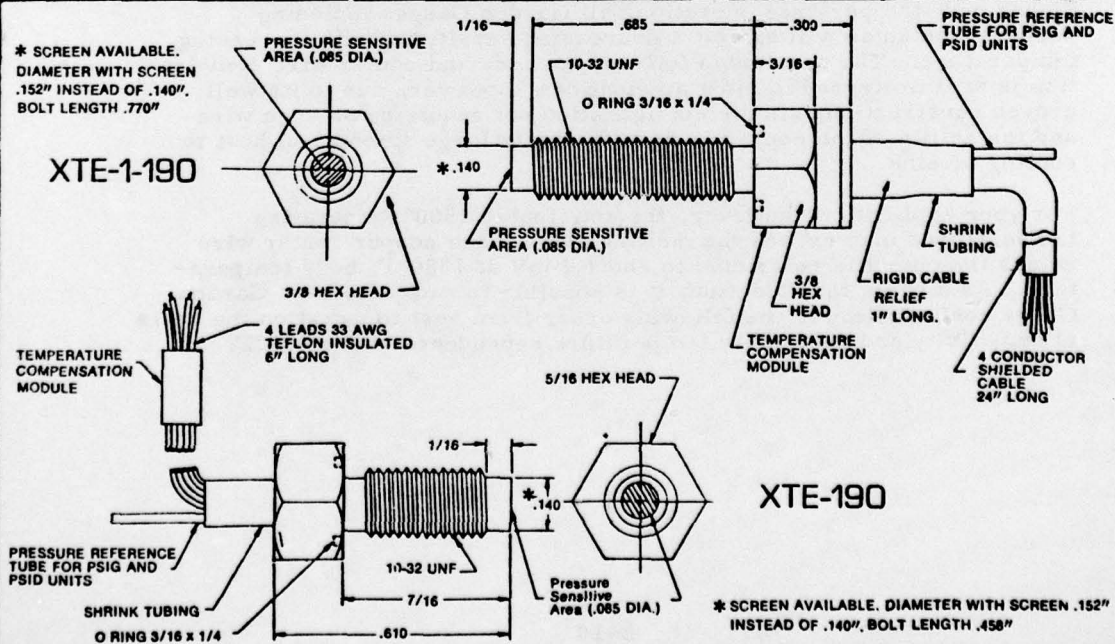


## Gage & Differential Transducers

### Specifications

Bridge Type	fully active four arm Wheatstone Bridge					
Rated Pressure	10 psi	25 psi	50 psi	100 psi	200 psi	300 psi
Maximum Pressure	20 psi	50 psi	100 psi	200 psi	300 psi	450 psi
Full Scale Output, Nominal	35mV	50 mV	100 mV	100 mV	100 mV	100 mV
Excitation (V AC Or DC)	30V	15V	15V	10V	10V	10V
Input Impedance	1000 ohm min.					
Output Impedance	2000 ohm max.					
Zero Balance	±15% FS	±10% FS	±5% FS	±5% FS	±5% FS	±5% FS
Combined Non-Linearity and Hysteresis	±1.0% FS max.					
Repeatability	0.5% FS					
Compensated Temperature Range (Standard)	80°F to 450°F (25°C to 235°C)					
Operating Temperature Range	-65°F to 525°F (-55°C to 273°C)					
Change of Sensitivity with Temperature	within 10% over compensated range					
Change of No-Load Output with Temperature	within 20% over compensated range					
Thermal Set of Zero	5% FS					
Thermal Set of Sensitivity	1% FS					
Natural Frequency (Minimum)	70 kHz	100 kHz	100 kHz	130 kHz	200 kHz	270 kHz
Acceleration Sensitivity						
Perpendicular	.001 % FS/g	.0005% FS/g	.00025% FS/g	.0002 % FS/g	.0002 % FS/g	.0001 % FS/g
Transverse	.0002% FS/g	.0001% FS/g	.00005% FS/g	.00004% FS/g	.00004% FS/g	.00002% FS/g

### XTE-1-190/XTE-190 Series Outline



# HY-CAL ENGINEERING

12105 Los Nietos Rd. • Santa Fe Springs, Ca. 90670 • (213) 698-7785 • Telex 67-4494

## TECHNICAL DISCUSSION

### FOR: SCIENCE APPLICATIONS

The sensor configuration we are proposing is shown in Drawing No. A-14645. This sensor employs a chromel-constantan Gardon Gauge with chromel as the foil and constantan edge and center wires in all welded construction on a stainless steel body. This construction is proven, and preferred as discussed below for high temperature application.

The standard copper-constantan Gardon Gauge embodies the correct balance of thermophysical and thermoelectric properties for low temperature dependence of the output up to 400°F body temperature. For temperatures above 200°F, experimental data shows a maximum temperature dependence (negative) of  $-.03\%/^{\circ}\text{F}$  for the copper-constantan gauge, with typical results as shown on GA-1165 in the lower temperature regions. It can be seen on GA-1165 that the temperature dependence of copper-constantan is first positive and then negative at low body temperature so that the error does not deviate significantly from average value obtained in low body temperature calibrations. For higher body temperature operation, all Gardon Gauges including copper-constantan will exhibit a decreasing sensitivity with increasing temperature. The constantan foil-copper body and center wire combination is still preferred in most applications, however, due to its well proven construction, simple configuration not requiring an edge wire and the ability of the copper body to dissipate large amounts of heat to cooling or sink.

For your application, however, the anticipated 1500°F operating temperatures may exceed the melting point of the copper center wire unless the output is restricted to about 4 mV at 1500°F body temperature. As a basis for selection, it is possible to rank alternate Gardon Gauge configuration in the following order from best to worst on the basis of sensitivity and sensitivity temperature dependence above 400°F.



# HY-CAL ENGINEERING

12105 Los Nietos Rd. • Santa Fe Springs, Ca. 90670 • (213) 698-7785 • Telex 67-4494

TABLE 1

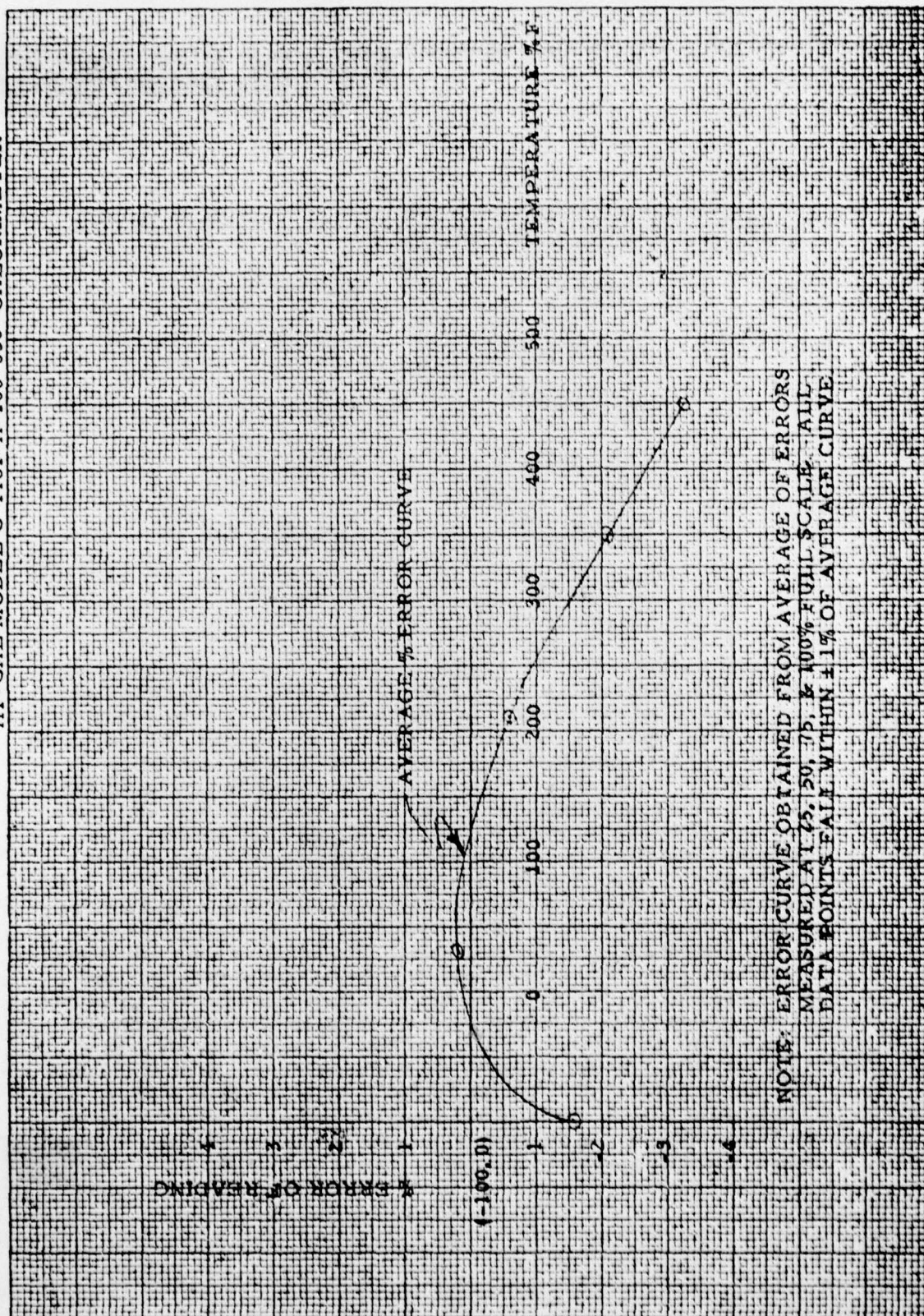
RELATIVE PERFORMANCES OF GARDON GAUGE DESIGNS HAVING  
SAME FOIL DIAMETER AND THICKNESS

<u>Rank</u>	<u>Sensitivity</u>	<u>Negative Tempco</u>
1 (highest)	<u>Chromel foil (highest)</u> <u>Constantan wire</u>	<u>Chromel foil (lowest)</u> <u>Constantan wire</u>
2	<u>Constantan foil</u> <u>Chromel wire</u>	<u>Constantan foil</u> <u>Copper wire</u>
3	<u>Constantan foil</u> <u>copper wire</u>	<u>Chromel foil</u> <u>Alumel wire</u>
4	<u>Chromel foil</u> <u>Alumel wire</u>	<u>Constantan foil</u> <u>Chromel wire</u>
5	<u>Alumel foil</u> <u>Chromel wire</u>	<u>Alumel foil</u> <u>Chromel wire</u>

The combination ranked No. 1 on both bases of comparison is proposed. Hy-Cal has produced this type sensor previously for use by NASA-Langley and others in hot wall heat flux measurements for space shuttle insulation tests. Four typical calibrations for Model C-1861-E-200 Calorimeters are attached. These units have copper bodies and are kept cool during calibration. Temperature dependent calibrations on the constantan foil/chromel wire combination, 4th ranked for tempco in Table 1, are shown on four attached calibrations for Model C-1821-G calorimeters. These units have stainless steel bodies like the units proposed, and are the same units for which raw data was provided during your meeting at Hy-Cal. The results illustrate the type of temperature calibrations you require, and also illustrate by their similarity that temperature dependence can be well established on a sampling basis. The proposed units will theoretically have about 70% of the temperature dependence shown. Perhaps more importantly, they will have 20 to 30% higher sensitivity, and almost twice the sensitivity at high temperature of the standard constantan/foil copper wire combination. This means that reasonable outputs can be obtained without having to drive excessive temperature gradients in the foil; on the order of 10 millivolts for 300°F  $\Delta T$  from center to edge. Lower  $\Delta T$  reduces any effect of the foil temperature rise on the intended convective heating measurements. It also allows smaller diameter foils and faster time constants for given constraints on output and  $\Delta T$ .



OUTPUT ERROR AS A FUNCTION OF BODY TEMPERATURE FOR  
HY-CAL MODEL C-1181-A-100-036 CALORIMETER



NOTE: ERROR CURVE OBTAINED FROM AVERAGE OF ERRORS  
MEASURED AT 25, 50, 75, & 100% FULL SCALE. ALL  
DATA POINTS FELL WITHIN  $\pm 1\%$  OF AVERAGE CURVE

CERTIFICATE OF CALIBRATION



DATE 10-27-77

CUSTOMER Gen. Appl. Science

P. O. NO. 5781

INST. TYPE Calorimeter

MODEL C-1861-200-072-036

ABSORPTIVITY .89

CERTIFIED RECORD OF CALIBRATION  
DATA ON THE INSTRUMENT DESCRIBED  
ABOVE. THE DATA WAS OBTAINED IN  
HY-CAL ENGINEERING'S THERMAL FLUX  
FACILITY.

REFERENCE STANDARD 14355

TESTED BY [Signature]

Q. C. APPROVAL [Signature]

OFFICIAL SEAL  
ALICE E. BOWMAN  
NOTARY PUBLIC - CAL  
LOS ANGELES COUG. 11  
My Comm. Expires Mar. 23, 1978

SUBSCRIBED AND SWORN TO  
BEFORE ME THIS 27 DAY  
OF October 19. 77

[Signature]



☒ ABSORBED ☐ INCIDENT



CERTIFICATE OF CALIBRATION

DATE November 3, 1978

CUSTOMER NASA Lewis

P. O. NO. C-17448-D

INST. TYPE Calorimeter

MODEL C-1821-C-100-024-072

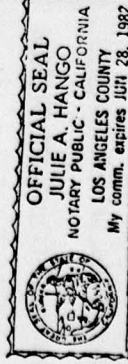
ABSORPTIVITY .764

CERTIFIED RECORD OF CALIBRATION DATA ON THE INSTRUMENT DESCRIBED ABOVE. THE DATA WAS OBTAINED IN HY-CAL ENGINEERING'S THERMAL FLUX FACILITY.

REFERENCE STANDARD

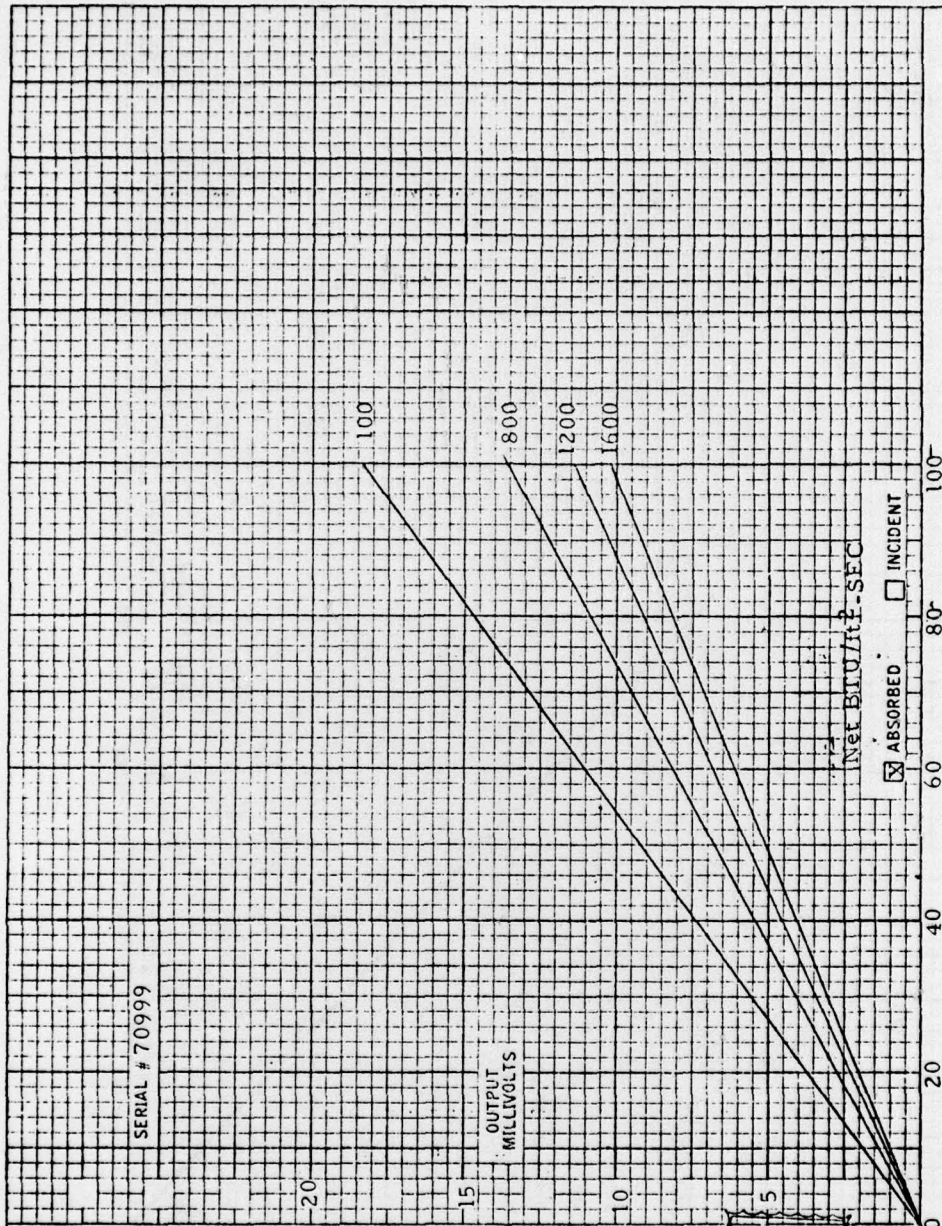
TESTED BY [Signature]

O. C. APPROVAL



SUBSCRIBED AND SWORN TO BEFORE ME THIS 3<sup>rd</sup> DAY OF Nov 1978

[Signature]



☒ ABSORBED ☐ INCIDENT



CERTIFICATE OF CALIBRATION



DATE 11-3-78

CUSTOMER NASA-Lewis

P. O. NO. C-17448-D

INST. TYPE Calorimeter

MODEL C-1821-G-100-024-072

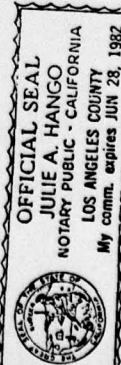
ABSORPTIVITY .790

CERTIFIED RECORD OF CALIBRATION  
DATA ON THE INSTRUMENT DESCRIBED  
ABOVE. THE DATA WAS OBTAINED IN  
HY-CAL ENGINEERING'S THERMAL FLUX  
FACILITY

REFERENCE STANDARD

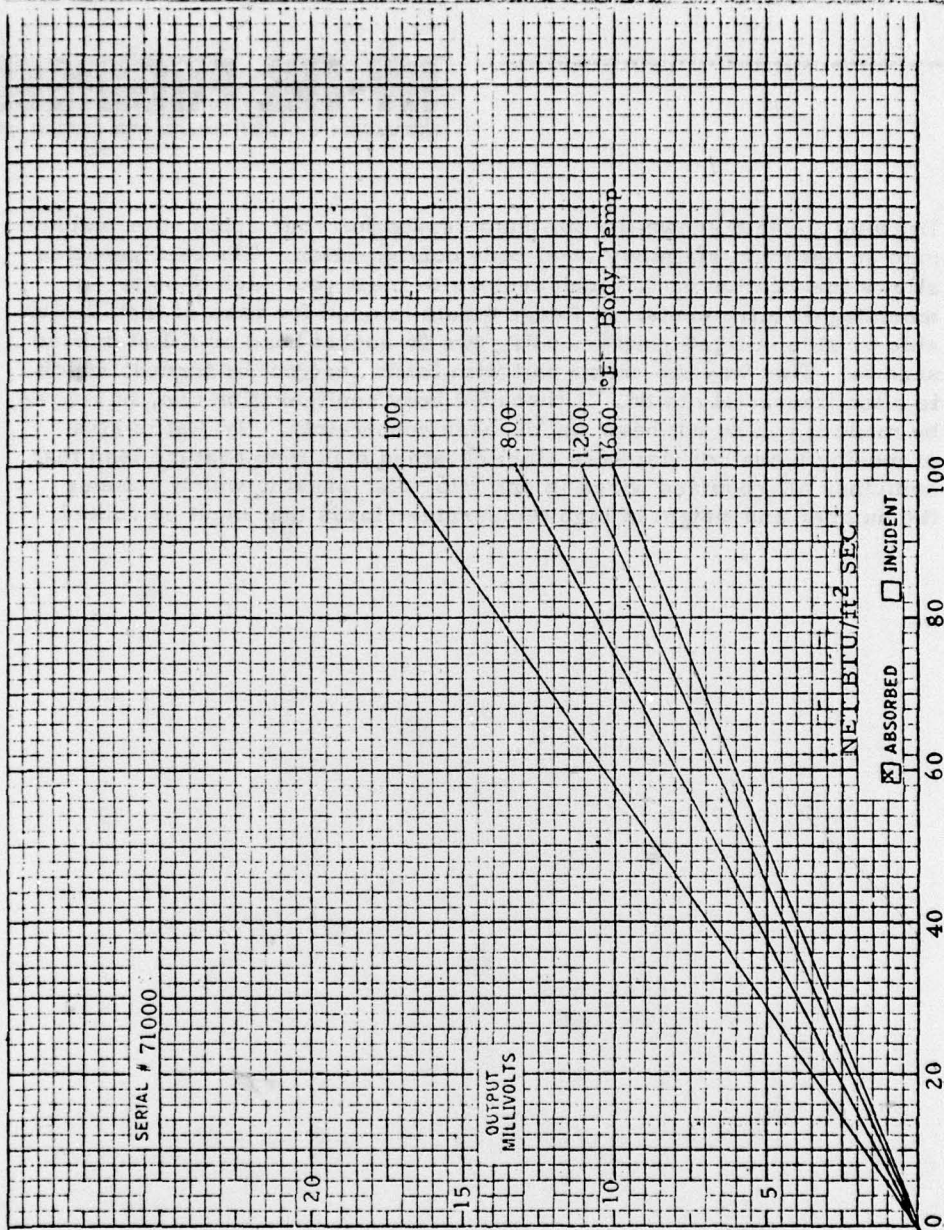
TESTED BY T. H. Hays

Q. C. APPROVAL



SUBSCRIBED AND SWORN TO  
BEFORE ME THIS 3rd DAY  
OF Nov. 1978

Julie A. Hango



---

## **HY-CAL ENGINEERING**

12105 Los Nietos Rd. • Santa Fe Springs, Ca. 90670 • (213) 698-7785 • Telex 67-4494

Drawing A-14615 shows the optimum sensor for your application welded onto an optimum stainless steel body configuration. The configuration allows installation on 0.3 inch centers to meet your high density mounting requirements. A flange mount is used for ease of installation side by side in tight quarters using two #6 socket head or fillister head screws. This way the entire unit with leads need not be turned, which is often impossible to do. A threaded body configuration can, of course, be made if you do not have any of these constraints. Hy-Cal is also proposing a custom stainless steel sheathed high temperature lead that combines all required wires in one 1/16" dia. sheath, which reduces the number and weight of high temperature leads that must be routed.





★U.S. Government Printing Office: 1979 — 657-084/266